Analysis of Buckled and Pre-bent Columns Used as Vibration Isolators

by

Jenny E. Sidbury

Thesis submitted to the Faculty of the
Virginia Polytechnic Institute and State University
In partial fulfillment of the requirements for the degree of

Master of Science
in
Civil Engineering

APPROVED BY:

_____

Dr. Raymond H. Plaut, Chairman

_____ _____

Dr. W. Samuel Easterling Dr. Thomas M. Murray

December 4, 2003
Blacksburg, VA

Keywords: Vibration isolator, passive vibration isolation, buckled structures, dynamic response, vibration

Analysis of Buckled and Pre-bent Columns Used as Vibration Isolators

By

Jenny E. Sidbury

Dr. Raymond H. Plaut, Chairman

Charles E. Via, Jr. Department of Civil and Environmental Engineering

(ABSTRACT)

Vibrations resulting from earthquakes, machinery, or unanticipated shocks may be very damaging and costly to structures. To avoid such damage, designers need a structural system that can dissipate the energy caused by these vibrations. Using elastically buckled struts may be a viable means to reduce the harmful effects of unexpected vibrations. Post-buckled struts can support high axial loads and also act as springs in a passive vibration isolation system by absorbing or dissipating the energy caused by external excitation. When a base excitation is applied, the buckled strut may act to reduce the dynamic force transmitted to the system, thus reducing the structural damage to the system.

Several models of buckled and pre-bent struts are examined with different combinations of parameters and end conditions. The models include pinned or fixed columns supporting loads above their buckling load, and columns with an initial curvature supporting various loads. The varying parameters include external damping, internal damping, and stiffness. The columns will be subjected to simple harmonic motion applied at the base or to a multi-frequency base excitation. The response of each model is measured by the deflection transmissibility of the supported load over a large range of frequencies. Effective models reduce the motion of the supported load over a large range of frequencies.

Acknowledgements

I would like to extend my sincere gratitude to everyone involved in making this research possible. First, I must thank Dr. Raymond Plaut for the opportunity to learn and work under his advisement, and for his constant support and helpfulness through every aspect of this research. I would also like to thank Dr. Thomas Murray and Dr. Samuel Easterling, not only for serving as my committee members, but also for encouraging my education during my time at Virginia Tech. I must also recognize the National Science Foundation for providing financial support of this research through Grant No. CMS-0301084.

In addition, I want to thank my parents for their constant love and tireless support throughout my education and my life. I am grateful to my father, Jim, for his encouraging words and for always being proud of my achievements. Also, thanks so much to my mother, Lorraine, and her unparalleled friendship and support. I could not have made it through this time without both of you in my life. Lastly, I would like to thank Michael Schultz for his undying love, support, and friendship for the past five years.

Table of Contents

Chapter 1: Introduction and Literature Review 1

1.1 Introduction 1

1.2 Literature Review 2

1.2.1 Isolators versus Absorbers 2

1.2.2 Vibration Isolation Models 5

1.2.3 Buckled Columns 7

1.3 Objective of Research 8

1.3.1 Overview 8

1.3.2 Description of models 9

Chapter 2: Pinned-end Buckled Column under Forced Harmonic Axial Excitation 12

2.1 Introduction 12

2.2 Basic Assumptions and Formulations 13

2.3 Numerical Solution of a Pinned-end Buckled Strut in Static Equilibrium 16

2.4 Forced Vibration of Pinned-end Buckled Strut due to Harmonic Base Motion 17

2.5 Numerical Solution of a Pinned-end Buckled Strut Under Forced Vibrations 23

2.6 Results for Forced Vibrations of the Pinned-end Buckled Strut 24

2.7 Conclusions 34

Chapter 3: Fixed-end Buckled Column under Forced Harmonic Axial Excitation 36

3.1 Introduction 36

3.2 Basic Assumptions and Formulations 36

3.3 Numerical Solution of a Fixed-end Buckled Strut in Static Equilibrium 37

3.4 Forced Vibration of Fixed-end Buckled Strut due to Harmonic Base Motion 38

3.5 Numerical Solution of a Fixed-end Buckled Strut Under Forced Vibrations 40

3.6 Results for Forced Vibrations of the Fixed-end Buckled Strut 41

3.7 Conclusions 49

Chapter 4: Pinned-end Column with Initial Curvature under Forced Harmonic Axial Excitation 51

4.1 Introduction 51

4.2 Basic Assumptions and Formulations 51

4.3 Numerical Solution of a Pinned-end Column with Initial Curvature in Static Equilibrium 52

4.4 Forced Vibration of a Pinned-end Strut with Initial Curvature due to Harmonic Base Motion 56

4.5 Numerical Solution of a Pinned-end Buckled Strut with Initial Curvature Under Forced Vibrations 57

4.6 Results for Forced Vibrations of the Pinned-end Strut with Initial Curvature 58

4.7 Conclusions 73

Chapter 5: Fixed-end Column with Initial Curvature under Forced Harmonic Axial Excitation 75

5.1 Introduction 75

5.2 Basic Assumptions and Formulations 75

5.3 Numerical Solution of a Fixed-end Column with Initial Curvature in Static Equilibrium 76

5.4 Forced Vibration of a Fixed-end Strut with Initial Curvature due to Harmonic Base Motion 79

5.5 Numerical Solution of a Fixed-end Buckled Strut with Initial Curvature Under Forced Vibrations 80

5.6 Results for Forced Vibrations of the Fixed-end Strut with Initial Curvature 81

5.7 Conclusions 95

Chapter 6: Fixed-end Buckled Column Under Forced Two-frequency Axial Excitation 96

6.1 Introduction 96

6.2 Basic Assumptions and Formulation 96

6.3 Numerical Solution of a Fixed-end Buckled Strut in Static Equilibrium 97

6.4 Forced Vibration of Fixed-end Buckled Strut due to a Two-frequency Excitation 98

6.5 Numerical Solution of a Fixed-end Buckled Strut Under Forced Two-frequency Axial Excitation 100
6.6 Results for a Fixed-end Buckled Strut Under Forced Two-frequency Axial Excitation 102
6.7 Conclusions 111
Chapter 7: Summary and Conclusions 112
7.1 Summary of Models 112
7.2 Summary of Analysis Procedure 112
7.3 Conclusions 113
7.4 Recommendations for Future Research 115
References 117
Appendix A 119
A.1 Pinned-end Strut, Static Equilibrium 119
A.2 Pinned-end Strut Dynamic Analysis 121
A.3 Additional Results for Forced Vibrations of the Pinned-end Buckled Strut 123
Appendix B 127
B.1 Fixed-end Strut, Static Equilibrium 127
B.2 Fixed-end Strut, Dynamic Analysis 129
B.3 Additional Results for Forced Vibrations of the Fixed-end Buckled Strut 132
Appendix C 141
C.1 Pinned-end Strut with Initial Curvature; Static Equilibrium 141
C.2 Deflected Shapes due to Load 143
C.3 Pinned-end Strut with Initial Curvature; Dynamic Analysis 145
C.4 Additional Results for Forced Vibrations of the Pinned-end Strut with Initial Curvature 147
Appendix D 150
D.1 Fixed-end Strut with Initial Curvature; Static Equilibrium 150
D.2 Deflected Shapes due to Load 152
D.3 Fixed-end Strut with Initial Curvature; Dynamic Analysis 154
D.4 Additional Results for Forced Vibrations of the Fixed-end Strut with Initial 157

Curvature 157
Appendix E 161
E.1 Fixed-end Strut in Static Equilibrium 161
E.2 Fixed-end Strut; Dynamic Analysis for Two-frequency Axial Excitation..... 163
Vita 167

List of Figures

Figure 1.2.1: Single-degree-of-freedom vibration isolator....3
Figure 1.2.2: Vibration absorber....4
Figure 1.3.1: Vibration Isolator with Pinned Buckled Strut....9
Figure 2.1.1: Undeformed Pinned-end Strut....12
Figure 2.2.1: Pinned-end Buckled Strut....13
Figure 2.2.2: Free-Body Diagram of Element of Pinned-end Buckled Strut....14
Figure 2.2.3: Pinned-end Element Components....15
Figure 2.4.1: Pinned Strut Under Forced Vibration....17
Figure 2.4.2: Free-Body Diagram of Element of Pinned-end Buckled Strut Under Forced Vibrations....18
Figure 2.5.1: Free-Body Diagram of Element of Pinned-end Buckled Strut Under Forced Vibrations with Damping....22
Figure 2.6.1: Transmissibility vs. Frequency for p_o=10, c=0, γ=0....25
Figure 2.6.2: Transmissibility vs. Frequency for p_o=11, c=0, γ=0....26
Figure 2.6.3: Transmissibility vs. Frequency for p_o=10, c=0.1, γ=0....27
Figure 2.6.4: Transmissibility vs. Frequency for p_o=10, r=0.1, γ=0....28
Figure 2.6.5: Transmissibility vs. Frequency for p_o=10, c=0.1, γ=0.001....29
Figure 2.6.6: Transmissibility vs. Frequency for p_o=10, c=0.1, γ=0.001....30
Figure 2.6.7: Transmissibility vs. Frequency for c=1, γ=0, r=5....31
Figure 2.6.8: Resonant Frequency vs. Supported Load for c=0, γ=0....32
Figure 2.6.9: Resonant Frequency vs. Stiffness Parameter for c=0, γ=0....32
Figure 2.6.10: $\omega\sqrt{r}$ vs. r for Pinned Strut....33
Figure 2.6.11: Transmissibility vs. Scaled Frequency for p_o=10, c=1, γ=0....34
Figure 3.1.1: Undeformed Fixed-end Strut....36
Figure 3.2.1: Fixed-end Buckled Strut....37
Figure 3.4.1: Fixed-end Strut under Forced Vibration....39
Figure 3.6.1: Transmissibility vs. Frequency for p_o=40, c=0, γ=0....42
Figure 3.6.2: Transmissibility vs. Frequency for p_o=41, c=0, γ=0....42

Figure 3.6.3: Transmissibility vs. Frequency for p_o=41, c=0.1, γ=0.....43
Figure 3.6.4: Transmissibility vs. Frequency for p_o=40, c=0.1, γ=0.....44
Figure 3.6.5: Transmissibility vs. Frequency for p_o=41, c=0.1, γ=0.....45
Figure 3.6.6: Transmissibility vs. Frequency for p_o=40, c=0.1, γ=0.01.....45
Figure 3.6.7: Transmissibility vs. Frequency for p_o=40, γ=0, r=0.1.....46
Figure 3.6.8: Transmissibility vs. Frequency for c=1, γ=0, r=1.....47
Figure 3.6.9: Peak Frequency vs. Stiffness Parameter for c=1, γ=0.....48
Figure 3.6.10: Maximum Transmissibility vs. Stiffness Parameter for c=1, γ=0.....49
Figure 4.1.1: Undeformed Strut with Initial Curvature.....51
Figure 4.2.1: Initial Shape of Pinned-end Buckled Strut with Initial Curvature.....52
Figure 4.3.1: Deflected Shape of Pinned-end Strut with do=0.05.....54
Figure 4.3.2: Nondimensional Load vs. Midspan Deflection.....55
Figure 4.3.3: Nondimensional Load vs. End Shortening.....56
Figure 4.6.1: Transmissibility vs. Frequency for p_o=10, c=1, γ=0, d_o=0.05.....58
Figure 4.6.2: Transmissibility vs. Frequency for po=10, c=1, γ=0, r=1.....59
Figure 4.6.3: Maximum Transmissibility vs. Stiffness Parameter for p_o=10, c=1, γ=0, d_o=0.05.....60
Figure 4.6.4: Resonant Frequency vs. Stiffness Parameter for p_o=10, c=1, γ=0, d_o=0.05 61
Figure 4.6.5: Transmissibility vs. Frequency for p_o=10, γ=0, r=1, d_o=0.05.....61
Figure 4.6.6: Transmissibility vs. Frequency for p_o=10, γ=0, r=1, c=0.1.....62
Figure 4.6.7: Maximum Transmissibility vs. Damping Coefficient for p_o=10, γ=0, d_o=0.05.....63
Figure 4.6.8: Resonant Frequency vs. Damping Coefficient for p_o=10, γ=0, d_o=0.05.....64
Figure 4.6.9: Transmissibility vs. Frequency for p_o=10, c=1, γ=0, r=1.....64
Figure 4.6.10: Maximum Transmissibility vs. d_o for p_o=10, c=1, γ=0.....65
Figure 4.6.11: Resonant Frequency vs. d_o for p_o=10, c=1, γ=0.....66
Figure 4.6.12: Transmissibility vs. Frequency for c=0.1, γ=0, r=1, d_o=0.05.....67
Figure 4.6.13: Transmissibility vs. Frequency for c=0.1, γ=0, r=1, d_o=0.05.....67
Figure 4.6.14: Transmissibility vs. Frequency for c=0.1, γ=0, r=1, d_o=0.05.....68
Figure 4.6.15: Transmissibility vs. Frequency for c=0.1, γ=0, r=1, d_o=0.05.....70
Figure 4.6.16: Mode Shapes for Various Frequencies for p_o=5.....71

Figure 4.6.17: Mode Shapes for Various Frequencies for p_o=10 72
Figure 5.1.1: Undeformed Strut with Initial Curvature 75
Figure 5.2.1: Initial Shape of Fixed-end Buckled Strut with Initial Curvature 76
Figure 5.3.1: Deflected Shape of Fixed-end Strut with a_o=0.05 77
Figure 5.3.2: Nondimensional Load vs. Mid-span Deflection 78
Figure 5.3.3: Nondimensional Load vs. End Shortening 79
Figure 5.6.1: Transmissibility vs. Frequency for p_o=40, c=1, γ=0, a_o=0.05 81
Figure 5.6.2: Transmissibility vs. Frequency for p_o=40, c=1, γ=0, r=1 82
Figure 5.6.3: Maximum Transmissibility vs. Stiffness Parameter for p_o=40, c=1, γ=0, a_o=0.05 83
Figure 5.6.4: Resonant Frequency vs. Stiffness Parameter for p_o=40, c=1, γ=0, a_o=0.05 83
Figure 5.6.5: Transmissibility vs. Frequency for p_o=40, γ=0, r=1, a_o=0.05 84
Figure 5.6.6: Transmissibility vs. Frequency for p_o=40, c=0.1, γ=0, r=1 85
Figure 5.6.7: Maximum Transmissibility vs. Damping Coefficient for p_o=40, γ=0, a_o=0.05 86
Figure 5.6.8: Resonant Frequency vs. Damping Coefficient for p_o=40, γ=0, a_o=0.05 86
Figure 5.6.9: Transmissibility vs. Frequency for p_o=40, c=1, γ=0, r=1 87
Figure 5.6.10: Maximum Transmissibility vs. a_o for p_o=40, c=1, γ=0 88
Figure 5.6.11: Resonant Frequency vs. a_o for p_o=40, c=1, γ=0 88
Figure 5.6.12: Transmissibility vs. Frequency for c=0.1, γ=0, r=1, a_o=0.05 89
Figure 5.6.13: Transmissibility vs. Frequency for c=0.1, γ=0, r=1, a_o=0.05 90
Figure 5.6.14: Transmissibility vs. Frequency for c=0.1, γ=0, r=1, a_o=0.05 91
Figure 5.6.15: Transmissibility vs. Frequency for c=0.1, γ=0, r=1, a_o=0.05 92
Figure 5.6.16: Mode Shapes for Various Frequencies for p_o=20 93
Figure 5.6.17: Mode Shapes for Various Frequencies for p_o=40 94
Figure 6.2.1: Fixed-end Buckled Strut 97
Figure 6.4.1: Fixed-end Strut under Two-frequency Axial Excitation 98
Figure 6.6.1: Transmissibility vs. Frequency for p_o=40, r=1, c=1, γ=0, r_f=2 102
Figure 6.6.2: Transmissibility vs. Frequency for p_o=40, r=1, c=1, γ=0, r_f=1.5 103
Figure 6.6.3: Transmissibility vs. Frequency for p_o=40, r=1, c=1, γ=0, r_f=2, r_a=0.5 104
Figure 6.6.4: Transmissibility vs. Frequency for p_o=40, c=1, γ=0, r_f=2, r_a=1 105

Figure 6.6.5: Transmissibility vs. Frequency for p_o=40, r=1, c=1, γ=0, r_f=2, r_a=1 106
Figure 6.6.6: Transmissibility vs. Frequency for p_o=40, r=1, γ=0, r_f=2, r_a=1 107
Figure 6.6.7: Transmissibility vs. Frequency for p_o=40, r=1, c=1, γ=0 for Two-frequency Model r_f=2, r_a=1 and Single Frequency Model 107
Figure 6.6.8: Transmissibility vs. Frequency for p_o=40, r=1, c=1, γ=0 for Two-frequency Model r_f=1.5, r_a=1 and Single Frequency Model 109
Figure 6.6.9: Transmissibility vs. Frequency for p_o=40, r=0.1, c=1, γ=0 for Two-frequency Model r_f=2, r_a=1 and Single Frequency Model 110
Figure 6.6.10: Transmissibility vs. Frequency for p_o=40, r=10, c=1, γ=0 for Two-frequency Model r_f=2, r_a=1 and Single Frequency Model 110
Figure A3.1: Transmissibility vs. Frequency for p_o=10, c=1, γ=0 123
Figure A3.2: Transmissibility vs. Frequency for p_o=10, c=10, γ=0 124
Figure A3.3: Transmissibility vs. Frequency for p_o=10, c=0, γ=0.01 124
Figure A3.4: Transmissibility vs. Frequency for p_o=10, c=0, γ=0.1 125
Figure A3.5: Transmissibility vs. Frequency for p_o=10, c=0, r=0.1 125
Figure A3.6: Transmissibility vs. Frequency for p_o=10, c=1, γ=0.001 126
Figure B3.1: Transmissibility vs. Frequency for p_o=40, c=1, γ=0 132
Figure B3.2: Transmissibility vs. Frequency for p_o=40, c=10, γ=0 133
Figure B3.3: Transmissibility vs. Frequency for p_o=40, c=0, γ=0.001 133
Figure B3.4: Transmissibility vs. Frequency for p_o=40, c=0, γ=0.01 134
Figure B3.5: Transmissibility vs. Frequency for p_o=40, c=1, γ=0.1 134
Figure B3.6: Transmissibility vs. Frequency for p_o=40, c=0, r=0.1 135
Figure B3.7: Transmissibility vs. Frequency for p_o=40, c=0, r=0.1 135
Figure B3.8: Transmissibility vs. Frequency for p_o=40, c=0.1, γ=0.01 136
Figure B3.9: Transmissibility vs. Frequency for p_o=40, c=0.1, γ=0.001 136
Figure B3.10: Transmissibility vs. Frequency for p_o=41, c=1, γ=0 137
Figure B3.11: Transmissibility vs. Frequency for p_o=41, c=10, γ=0 137
Figure B3.12: Transmissibility vs. Frequency for p_o=41, γ=0, r=1 138
Figure B3.13: Transmissibility vs. Frequency for p_o=41, c=0, γ=0.001 138
Figure B3.14: Transmissibility vs. Frequency for p_o=41, c=0, γ=0.01 139
Figure B3.15: Transmissibility vs. Frequency for p_o=41, c=0, γ=0.1 139

Figure B3.16: Transmissibility vs. Frequency for p_o=41, c=0, r=1 140
Figure C2.1: Deflected Shape due to Load for d_o=0.01 143
Figure C2.2: Deflected Shape due to Load for d_o=0.01 144
Figure C4.1: Transmissibility vs. Frequency for p_o=10, c=1, γ=0, r=0.1..... 147
Figure C4.2: Transmissibility vs. Frequency for p_o=10, c=1, γ=0, r=10 147
Figure C4.3: Transmissibility vs. Frequency for p_o=10, c=1, γ=0, r=1 148
Figure C4.4: Transmissibility vs. Frequency for p_o=10, c=10, γ=0, r=1 148
Figure C4.5: Transmissibility vs. Frequency for c=1, γ=0, r=1, d_o=0.05..... 149
Figure C4.6: Transmissibility vs. Frequency for c=1, γ=0, r=1, d_o=0.05..... 149
Figure D2.1: Deflected Shape due to Load for a_o=0.01 152
Figure D2.2: Deflected Shape due to Load for a_o=0.1 153
Figure D4.1: Transmissibility vs. Frequency for p_o=10, c=1, γ=0, a_o=0.05..... 157
Figure D4.2: Transmissibility vs. Frequency for p_o=10, c=1, γ=0, a_o=0.05..... 158
Figure D4.3: Transmissibility vs. Frequency for p_o=10, r=1, γ=0, a_o=0.05 158
Figure D4.4: Transmissibility vs. Frequency for p_o=10, c=1, γ=0, r=1 159
Figure D4.5: MaximumTransmissibility vs. γ for p_o=40, c=0, a_o=0.05..... 159
Figure D4.6: Resonant Frequency vs. γ for p_o=40, c=0, a_o=0.05 160
Figure D4.7: Transmissibility vs. Frequency for c=1, r=1, γ=0, a_o=0.05 160

List of Tables

Table 4.3.1: Maximum Mid-span Deflection and End Shortening Values for d_o=0.05.... 54
Table 5.3.1: Maximum Mid-span Deflection and End Shortening for a_o=0.05..... 78
Table C2.1: Maximum Mid-span Deflection and End Shortening Values for d_o=0.01 .. 143
Table C2.2: Maximum Mid-span Deflection and End Shortening Values for d_o=0.1 144
Table D2.1: Maximum Mid-span Deflection and End Shortening Values for a_o=0.1 152
Table D2.2: Maximum Mid-span Deflection and End Shortening Values for a_o=0.01 .. 153

Chapter 1: Introduction and Literature Review

1.1 Introduction

Unwanted vibrations may be very damaging, annoying, and costly to structures. Effective vibration control is necessary to mitigate the harmful effects of these vibrations. Vibration isolators have proven to be effective in controlling both predicted vibrations as well as unanticipated shock vibrations. Vibration isolators aim to minimize the force transmitted to an object from a vibrating source. The excitations may be harmonic, multi-frequency, shock, or impact vibrations, and may be caused by machinery, wind, noise, or earthquakes. When a base excitation is applied, the isolator acts to reduce the dynamic force transmitted to the system by dissipating energy, thus reducing the structural damage to the system. Isolators have proven functional in a wide range of applications, and new improvements to this technology will be extremely beneficial in preventing structural damage in the future.

Vibration isolators are typically found as mechanical or metallic springs, or polymer blocks, and are often referred to as antivibration mounts. This research aims to employ a new type of isolator composed of elastically buckled structures. These buckled columns (struts) will be designed to have a high axial stiffness under static loading to prevent excessive displacement under high axial loads, and a relatively low stiffness during dynamic motion. The post-buckled state of the isolating strut permits the soft spring characteristic necessary to dissipate the energy caused by vibrations.

The results of this research reflect the performance of buckled struts under varying conditions while submitted to base excitations. Several models will be examined with different combinations of parameters and end conditions. The models include single, pinned or fixed columns supporting loads above their buckling load. The varying parameters include external damping, internal damping, stiffness, and initial curvature. Cases of columns with initial curvature subjected to loads below the buckling load also will be investigated. The base of the column is subjected to a small, harmonic, axial

motion, as well as multi-frequency excitations. Analysis will be performed to determine the efficiency of these models.

1.2 Literature Review

1.2.1 Isolators versus Absorbers

Vibrations can be controlled by a number of effective devices. Although many of the fundamental concepts behind these devices are similar, some are more suited to specific applications than others. Many times, vibration control is achieved by employing an isolator or an absorber. Although similar in concept, isolators and absorbers work differently. Since the research being discussed focuses on an effective isolation system, this review will also concentrate on isolators, although absorbers will be discussed and compared briefly.

A vibration isolator can offer damping and stiffness to a system (Sciulli 1997). As shown in Figure 1.2.1, an effective isolator typically employs a spring with a stiffness *k*, and a viscous damper with a damping coefficient *c*. The isolator is supporting a mass, m, and is subjected to a force at the base, F_T. When a system is excited, the spring and damper act to reduce the transmissibility, or relative motion of the equipment being protected. Some examples of this type of isolator include rubber mounts used to isolate vibrating machinery and shock absorbers to improve the quality of ride in an automobile. In both examples, the isolator reduces the motion of the suspended systems. Isolators are most effective when the excitation frequency is much larger than the lowest natural frequency of the system. However, when the excitation frequency is slightly less than the lowest natural frequency of the system, the relative motion is amplified.

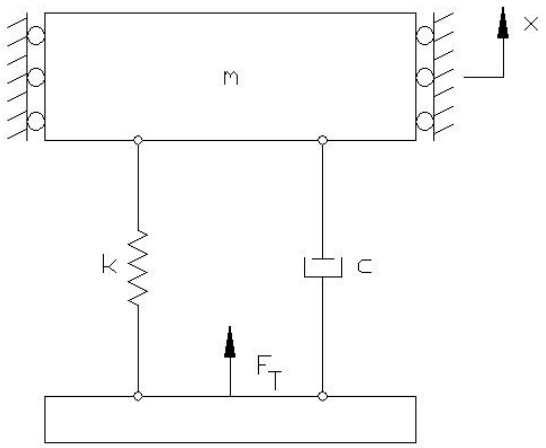

Figure 1.2.1: Single-degree-of-freedom vibration isolator

A vibration absorber adds mass to a system to control vibrations. As shown in Figure 1.2.2, an absorber employs an additional mass, M_a, supported by a spring with a stiffness K_a. The absorber is able to dissipate the energy of a disturbance through the deflection of the additional mass. Therefore, the mass should be placed at the equipment's highest point of acceleration (Sciulli 1997). Absorbers are most effective when they are tuned to a predicted frequency. These devices are called tuned vibration absorbers (TVA), and typically use steel springs to support the additional mass. When a system is excited at the predicted frequency, there is almost no deflection of the system mass. Above or below the tuned frequency, the absorber is less effective. Absorbers can be classified as dynamic absorbers or damped vibration absorbers. Dynamic absorbers provide little damping, while damped vibration absorbers provide some damping to the system.

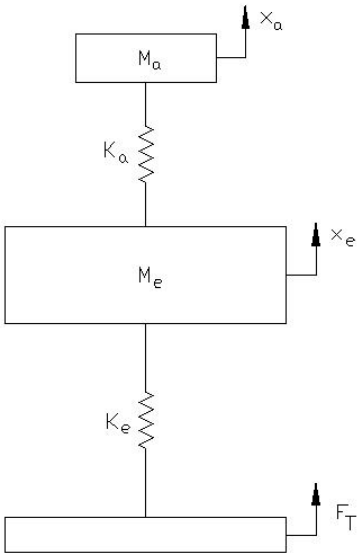

Figure 1.2.2: Vibration absorber

The most obvious difference between an isolator and an absorber is the location of the device. An isolator links the vibrating source to the equipment being protected, whereas an absorber is attached at the highest acceleration point. Due to space constraints, the position of either device may be either beneficial or detrimental, depending on the situation.

Also, an isolator reduces unwanted vibrations through the additional stiffness provided in the device. As stated previously, an absorber works to absorb the unwanted vibration through the deflection of the added mass. Therefore, the absorber spring must be able to withstand both the force and deflection resulting from the motion.

Absorbers are most effective at a predicted frequency, but they may be incapable of resisting unanticipated vibrations, or may become out of tune with the predicted frequency. Isolators, however, are more effective at a vast range of frequencies above a certain limit, and therefore isolators are recommended as an alternative.

1.2.2 Vibration Isolation Models

Vibration control can be classified by methods that affect the source, the path, or the receiver. Vibration isolators are an example of path control because they are connections between the receiver and the path, and the source and the path. Isolators can then be divided into categories of source isolation or receiver isolation. Source isolation mitigates vibrations from a vibrating source to the surrounding structure, and receiver isolation minimizes vibrations between a surrounding structure and a vibration receiver.

An effective isolator is measured by its ability to reduce the transmissibility of the system. Transmissibility (TR) describes the relationship of the force or motion on one end of the isolator to the force or motion on the other end. Force transmissibility is the ratio of the force transmitted to the excitation force. Motion transmissibility is the ratio of the response motion to the excitation motion (Chopra 2001). When an undamped system vibrates at its natural frequency, the transmissibility will be infinite. However, if an isolator is present, the transmissibility will have a finite peak when vibrating at one of the system's natural frequencies, due to the innate damping in any isolator. An effectively designed system will have ample damping to minimize the transmissibility peak at the damped resonant frequency. Since all real systems have inherent damping, the undamped case is merely theoretical, but necessary for complete system analysis.

Vibration isolators can also be divided into a number of categories: passive, semi-active, active, and hybrid. Passive isolators require no power source, and are therefore the most reliable case. Semi-active cases require a limited amount of power which is used to adjust the damping level of the isolator rather than stimulate the isolator. Active absorbers require a large amount of power, and may be deemed useless if an earthquake were to compromise its power supply. Although active absorbers can be the most effective at vibration isolation, the tremendous impact of a loss of power must be considered when utilizing active systems. Hybrid isolators are, perhaps, the most practical type of isolator, since both passive and active components are used. The passive device will control the vibrations if there is a loss of power, and both components can be

used to achieve optimal performance. The post-buckled struts to be analyzed in this research are of the passive case, but can be used in a hybrid system.

Vibration isolators can be modeled in many ways. The simplest analytical model is a single-degree-of-freedom (SDOF) translational spring-mass system. As shown previously in Figure 1.2.1, the SDOF system exhibits motion in only one direction. Although there are few real systems that are actual single-degree-of-freedom systems, the model can be very useful to display the general concepts of vibration isolation. The equipment being supported and the foundation are assumed to be rigid. The stiffness of a spring used in a vibration isolation system is of utmost importance. The spring must be stiff enough to support the load without significant static deflection, but must also be flexible enough to dissipate the dynamic energy from the vibrations (Virgin and Plaut 2002). As one might guess, the necessary stiffness is often hard to predict.

Vertical isolators have presented more problems than horizontal isolators because the vibrational motion in the presence of gravity requires the dynamic storage of significant amounts of energy to absorb this motion (Winterflood et al. 2002). However, typically the amplitude of the vibrations is small compared to the displacement under static load, so only a small amount of dynamic energy is exchanged with the spring. Thus, due to the large amount of static energy caused by the initial deflection, the total energy in the spring is much larger than the dynamic energy storage required during vibration. Because of this large static energy storage, a significant amount of mass is necessary in order to exceed the dynamic energy. On the contrary, large masses are to be avoided because they lead to low resonant frequencies. Motions at low frequencies may be very damaging to a structure, and added mass increases the probability that the system will go into resonance. Therefore, the mass of the system should be decreased. To avoid this spring mass problem, three areas need to be considered, according to Winterflood et al. (2002). First, the entire mass of the spring needs to be stressed to efficiently store its energy. Then, the kinetic energy must be reduced by distributing the mass of the spring in such a way as to reduce its velocity. And lastly, a nonlinear force versus displacement relationship must be produced by reducing the static energy and mass of the spring.

Therefore, the best system would be one in which there is little or no static energy, so that the spring mass must only offset the dynamic energy storage. The Euler buckling spring satisfies this condition.

The Euler buckling spring can support large masses without significant static deflections. A column comprised of elastic material can support this static load until it reaches its critical buckling load. This nonlinear characteristic allows the Euler spring to possess zero static energy, as desired. The critical buckling load for a column with fixed ends is $P_{cr} = 4\pi^2 EI/L^2$ where E represents the modulus of elasticity, I is the moment of inertia, and L is the length of the column. This inextensible, elastically buckled spring is called an elastica. For an elastica to be effective, its static displacement must be less than 1% of its length to minimize its static energy. According to Winterflood et al. (2002), if the working range of these springs is designed to start at the onset of buckling, then all of the energy stored in the spring is the dynamic energy. This dynamic energy is then exchanged in and out of the spring during its working range. This is ideal for proper vertical isolation.

1.2.3 Buckled Columns

This research employs buckled columns to replace the springs typically used in isolation systems; therefore, buckled struts will also be discussed. These struts are statically loaded in slight excess of their buckling load, and subjected to a dynamic vertical excitation. Ideally, the struts serve to minimize the amount of motion of the supported system, if the excitation is applied at the base. If the vibrations emit from the supported system, then the struts act to reduce the transmitted dynamic force to the base.

The static, nonlinear, post-buckling behavior of columns under axial loads is a well-studied problem. Obviously, geometric imperfections will affect the behavior of an axially-loaded column. However, real columns exhibiting signs of imperfections still maintain stable post-buckling load paths. Columns with a small curvature still display a high axial stiffness until the load approaches the buckling load of the ideal column, and

then soften and have a relatively low stiffness (Winterflood et al. 2002). It is the reduction in stiffness that allows the buckled strut to dissipate the dynamic energy in the system. After the strut is in equilibrium under the supported load, it is subjected to dynamic axial excitation at its base. Thus, the equations of motion contain both parametric and forcing excitations.

1.3 Objective of Research

1.3.1 Overview

Reducing unwanted vibrations may be achieved by using a new type of passive vibration isolator comprised of elastically buckled columns as shown in Figure 1.3.1. These columns sustain high axial loads, but, after initial buckling, they exhibit a soft spring characteristic that is useful to dissipate the dynamic energy caused by vibration. These isolators aim to reduce the dynamic force transmitted from a vibrating source to sensitive equipment or supported structures. These vibrations may emanate from operating machinery or may take the form of applied accelerations at the base of the isolator. If the use of buckled struts proves to be effective in mitigating the effects of unwanted vibrations, the applications could be numerous. Not only could they be employed as isolators for vibrating machinery or equipment, but they could also be used in conjunction with active isolation systems for more complex purposes, such as earthquake engineering applications. This research aims to show the efficacy and simplicity of an isolator comprised of buckled columns.

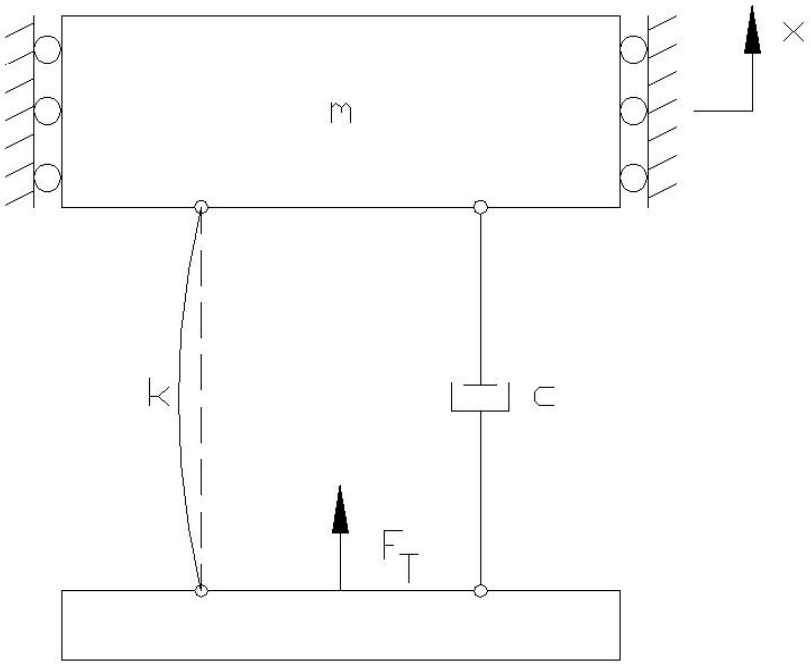

Figure 1.3.1: Vibration Isolator with Pinned Buckled Strut

1.3.2 Description of models

Isolators comprised of buckled struts will be analyzed. The isolator will be designed so that the supported load is slightly above the buckling load of the strut. Both ideal and imperfect columns will be examined. Ideal column analysis is useful since the equilibrium path is close to that of the imperfect case. Imperfect columns are more practical since all real columns have imperfections such as small curvatures. The initial curvature of the models will be varied and the behavior will be analyzed. Imperfect columns will also be examined at loads below the buckling load of the strut.

Different boundary conditions will be investigated for the isolators. Struts with pinned and fixed ends will be examined and compared. However, the case with fixed ends will be more practical for higher axial loads.

Several parameters will be incorporated in the various models. Damping is important to any system to reduce the motion, and will be included in the models. The effectiveness

of any isolator depends on damping because it is influential on the dynamic motion of all systems. Both viscous damping and internal material damping properties will be included in the models, both separately and in combination. Also, the isolators will be analyzed with a varying degree of stiffness. The dynamic equation of motion of the system is also dependent on the stiffness of the model; therefore, it is necessary to examine the effects of changing the stiffness.

The strut will be modeled as an elastica, and the shooting method will be utilized to determine the equilibrium configuration. This method will allow both small and large deflections and rotations of the isolator. The equations of motion will be written about the static equilibrium state. The information gained from the static equilibrium will be used in the dynamic analysis of each model.

The struts will be subjected to different dynamic excitations. First, simple harmonic motion will be applied to the base of the struts, and dynamic equilibrium will be applied. The steady-state response of the system can be obtained using the shooting method and the static equilibrium information. Then, a two-frequency excitation will be applied to the fixed-end strut. This will be useful since systems are not always subjected to harmonic motion. The dynamic response of each system will be analyzed and presented.

Chapter 2 will focus on the analysis of a pinned-end strut under harmonic axial base excitation. The same analysis will be performed on a fixed-end buckled strut in Chapter 3. The results of these different cases will be compared.

In Chapter 4, the pinned-end column will be analyzed with an initial curvature. The struts will be subjected to loads above and below their buckling load. Harmonic excitation will be applied at the base of the imperfect strut. The same analysis will then be performed on a fixed-end column with initial curvature, and in Chapter 5, the results will be presented.

Chapter 6 will include the analysis of a pinned-end strut under a multi-frequency excitation. The strut will be supporting a load above its buckling load, and then the strut will be subjected to a two-frequency excitation applied at the base of the strut. This analysis will be useful since not all forcing frequencies are harmonic.

The many cases examined in this thesis will help to explain the behavior of buckled and pre-bent columns used as vibration isolators. This research may identify buckled struts as new and effective devices in vibration isolation systems. Chapter 7 will offer a brief summary of the findings of this research and will offer ideas and recommendations for future research.

Chapter 2: Pinned-end Buckled Column under Forced Harmonic Axial Excitation

2.1 Introduction

The most basic model to be analyzed is a pinned-end strut. This is the simplest model that can represent a post-buckled system. The strut is a pinned column that is supporting a load above its buckling load. The column, in its undeformed shape, can be seen in Figure 2.1.1 in a horizontal configuration. The basic assumptions and equation derivations presented in this chapter also apply to the fixed-end model, which is the subject of chapter 3. However, there are some differences between the two analyses, and they will be addressed later. The results of the many situations examined for the pinned-end strut are presented in this chapter. The numerical results come from a Mathematica (Wolfram 1996) program that iterates to solve the necessary equations to a specified accuracy level using a set of initial guesses for several variables. Graphical results are then created in Excel to show the trends of the data.

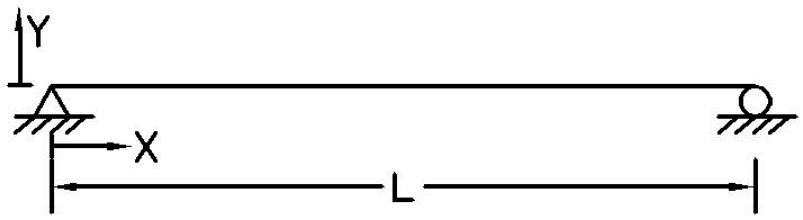

Figure 2.1.1: Undeformed Pinned-end Strut

2.2 Basic Assumptions and Formulations

The basic assumptions and equation formulations are the same for the pinned-end and the fixed-end buckled strut. However, the boundary conditions will obviously be different. The formulation will be presented in this chapter, but the applicable changes for the fixed-end strut will be addressed in Chapter 3.

First, a post-buckled condition is created by applying a load above the column's buckling load. The deformed strut can be seen in Figure 2.2.1. The strut is assumed to be an elastica, which means the length of the strut does not change as the load is increased. The strut is permitted to have large deflections along its length; therefore, the change in the angle at the end of the strut can be used to measure the curvature of the strut. The deflection of the buckled strut can be seen in Figure 2.2.1.

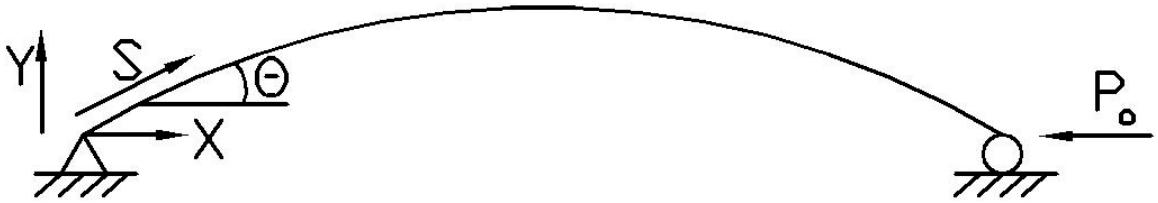

Figure 2.2.1: Pinned-end Buckled Strut

The following variables apply to the pinned-end strut in Figures 2.2.1 and 2.2.2:

L is the length of the strut;

S is the arc length of the strut;

P_o is the applied static force being supported by the strut;

P is the horizontal component of the force in the strut;

Q is the vertical component of the force in the strut;

M is the induced moment in the strut from the applied force and inertia;

θ is the angle between the X-axis and the deflected strut;

E is the modulus of elasticity of the strut;

I is the moment of inertia of the strut.

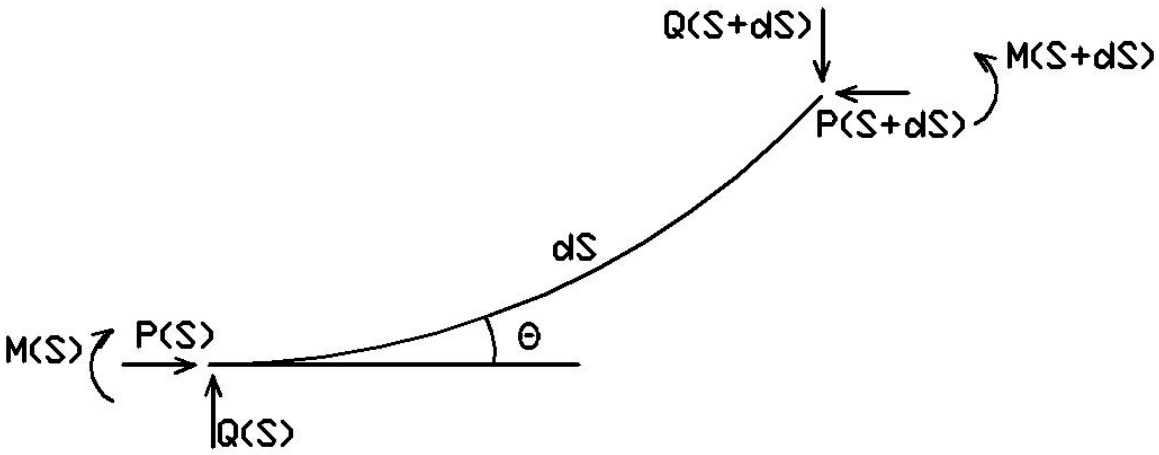

Figure 2.2.2: Free-Body Diagram of Element of Pinned-end Buckled Strut

The behavior of the strut under the static load is determined by analyzing the free-body diagram of an infinitesimal element of the strut. Figure 2.2.2 shows the forces acting on the element in static equilibrium. The X and Y components of the element length are shown in Figure 2.2.3.

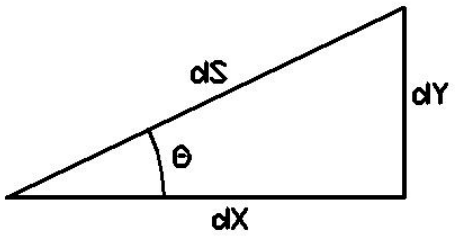

Figure 2.2.3: Pinned-end Element Components

The following relationships can be determined from geometric and equilibrium constraints:

$$\frac{dX}{dS} = \cos\theta \tag{2.1}$$

$$\frac{dY}{dS} = \sin\theta \tag{2.2}$$

$$\frac{d\theta}{dS} = Curvature \tag{2.3}$$

$$M = EI\frac{d\theta}{dS} \tag{2.4}$$

$$\frac{dM}{dS} = -P\sin\theta + Q\cos\theta \tag{2.5}$$

The analysis of the models is easier when units are eliminated. Therefore, the variables in all models are nondimensionalized. The nondimensional variables are as follows:

$$x = \frac{X}{L} \qquad y = \frac{Y}{L} \qquad s = \frac{S}{L} \tag{2.6, 2.7, 2.8}$$

$$q = \frac{QL^2}{EI} \qquad p = \frac{PL^2}{EI} \tag{2.9, 2.10}$$

$$m = \frac{ML}{EI} \tag{2.11}$$

Using the above nondimensional relationships, the following differential equations can be established for $0 < s < 1$:

$$\frac{dx}{ds} = \cos\theta \tag{2.12}$$

$$\frac{dy}{ds} = \sin\theta \tag{2.13}$$

$$\frac{d\theta}{ds} = m \tag{2.14}$$

$$\frac{dm}{ds} = -p\sin\theta + q\cos\theta \tag{2.15}$$

As stated previously, the strut is in a post-buckled condition. For a pinned-end strut, the Euler buckling load is $P = \pi^2 EI/L^2$. In this analysis, the nondimensional buckling load will be $p_o = PL^2/EI$, thus $p_o = \pi^2 \approx 9.87$ for a pinned-end strut. The strut will be examined at p_o values of 10 and 11.

2.3 Numerical Solution of a Pinned-end Buckled Strut in Static Equilibrium

As shown in Figure 2.2.1, the strut is pinned at the left end, and is attached to a roller at the right end. The pin does not allow for movement in the horizontal or vertical direction. The roller, however, allows the strut to move in the horizontal direction. Neither boundary condition may support an end moment. Therefore, the boundary conditions of the pinned-end strut are as follows:

At s=0: x=0, y=0, m=0

At s=1: y=0, m=0.

The numerical solution of the strut can be found by using the shooting method in a Mathematica program. The known value of the applied force p_o is used as input, and an initial guess is made for the value of the shear force, q. After applying the known boundary conditions stated above, the program solves the system of differential equations

in a trial and error method. Iterations must be performed if the initial guesses do not allow convergence of the solution to the prescribed accuracy. The equilibrium program used for this static analysis can be found in Appendix A.1.

2.4 Forced Vibration of Pinned-end Buckled Strut due to Harmonic Base Motion

Using the resulting moment from the static analysis, the strut is subjected to a forced vibration and analyzed to determine the transmissibility of the system. The excitations are axial, single-frequency harmonic motions applied at the base of the strut. The vibrations due to this excitation are assumed to be small, and the steady-state motion is examined. Resonant frequencies are found by applying an initial guess and iterating until the transmissibility reaches infinity for a model without damping. The transmissibility can be found for any model by applying a range of different frequencies. It is independent of the amplitude of the base excitation. The forced axial motion is shown in Figure 2.4.1.

Figure 2.4.1: Pinned Strut Under Forced Vibration

The variables used in this analysis are as follows:

W is the weight supported by the column;

T is the time;

Ω is the applied frequency on the strut;

$U_o\sin(\Omega T)$ is the axial displacement of the base of the strut;

g is the gravitational acceleration;

W/g is the mass of the supported weight;

μ is the mass per unit length of the strut;

p_w is the ratio of the weight supported by the strut to the weight of the strut;

r is the stiffness parameter;

c is the external damping coefficient;

γ is the internal damping coefficient.

Using d'Alembert's Principle, dynamic equilibrium is applied to the model. The infinitesimal element used for analysis without damping is shown in Figure 2.4.2. The dynamic forces resulting from the forced vibration are shown on the figure. The case including external and internal damping will be addressed later.

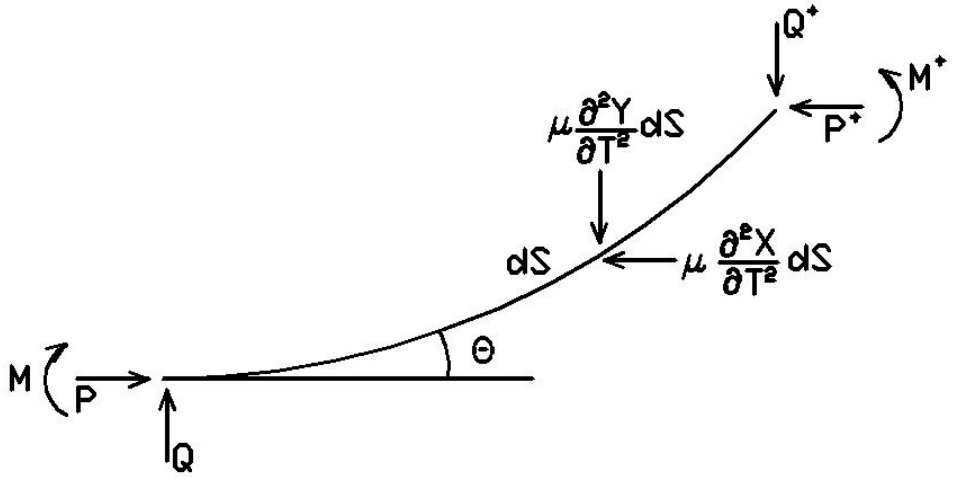

Figure 2.4.2: Free-Body Diagram of Element of Pinned-end Buckled Strut Under Forced Vibrations

Using the element under dynamic equilibrium, the following equations can be established:

$$\frac{\partial X}{\partial S} = cos\,\theta \tag{2.16}$$

$$\frac{\partial Y}{\partial S} = \sin\theta \tag{2.17}$$

$$\frac{\partial \theta}{\partial S} = \frac{M}{EI} \tag{2.18}$$

$$\frac{\partial M}{\partial S} = -P\sin\theta + Q\cos\theta \tag{2.19}$$

$$\frac{\partial P}{\partial S} = -\mu\frac{\partial^2 X}{\partial T^2} \tag{2.20}$$

$$\frac{\partial Q}{\partial S} = -\mu\frac{\partial^2 Y}{\partial T^2} \tag{2.21}$$

In addition to the above variables, the following nondimensional relationships are used in the analysis:

Time: $t = T\sqrt{\frac{EI}{\mu L^4}}$ (2.22)

Applied Frequency: $\omega = \Omega\sqrt{\frac{\mu L^4}{EI}}$ (2.23)

End Displacement Amplitude: $u_o = \frac{U_o}{L}$ (2.24)

Forces: $p_w = \frac{W}{\mu g L}$, $p_o = \frac{WL^2}{EI}$ (2.25, 2.26)

Stiffness Parameter: $r = \frac{p_w}{p_o} = \frac{EI}{\mu g L^3}$ (2.27)

Using the static and dynamic equations of equilibrium, the following differential equations are established for 0 < s < 1:

$$\frac{\partial x}{\partial s} = \cos\theta \tag{2.28}$$

$$\frac{\partial y}{\partial s} = \sin\theta \tag{2.29}$$

$$\frac{\partial \theta}{\partial s} = m \tag{2.30}$$

$$\frac{\partial m}{\partial s} = -p\sin\theta + q\cos\theta \tag{2.31}$$

$$\frac{\partial p}{\partial s} = -\frac{\partial^2 x}{\partial t^2} \tag{2.32}$$

$$\frac{\partial q}{\partial s} = -\frac{\partial^2 y}{\partial t^2} \tag{2.33}$$

The boundary conditions for the dynamic model are:

At s=0: $X = U_o sin(\Omega T),\ Y=0,\ M=0$

At s=L $Y=0,\ M=0,\ P = \frac{W}{g}\frac{\partial^2 X}{\partial T^2} + W$

The boundary conditions must also be nondimensional. Therefore:

At s=0: $x = u_o\ sin(\omega t)$, $y=0,\ m=0$

At s=1: $y=0,\ m=0,\ p = p_o(1 + r\frac{\partial^2 x}{\partial t^2})$

As stated previously, the axial base motion applied to the strut is assumed to be harmonic with nondimensional frequency ω. The following equations describe the response of the strut under the steady-state vibrations, where e represents equilibrium and d stands for dynamic:

$$x(s,t) = x_e(s) + x_d(s)\sin(\omega t) \tag{2.34}$$

$$y(s,t) = y_e(s) + y_d(s)\sin(\omega t) \tag{2.35}$$

$$\theta(s,t) = \theta_e(s) + \theta_d(s)\sin(\omega t) \tag{2.36}$$

$$m(s,t) = m_e(s) + m_d(s)\sin(\omega t) \tag{2.37}$$

$$p(s,t) = p_o + p_d(s)\sin(\omega t) \tag{2.38}$$

$$q(s,t) = q_e + q_d(s)\sin(\omega t) \tag{2.39}$$

Equations 2.12 through 2.15 represent the equilibrium relationships for x_e, y_e, θ_e, and m_e. Since the assumption is that the dynamic vibrations will be small, small-angle theory is applied to the analysis. The following dynamic relationships result:

$$\frac{dx_d}{ds} = -\theta_d \sin\theta_e \tag{2.40}$$

$$\frac{dy_d}{ds} = \theta_d \cos\theta_e \tag{2.41}$$

$$\frac{d\theta_d}{ds} = m_d \tag{2.42}$$

$$\frac{dm_d}{ds} = (q_d - p_o\theta_d)\cos\theta_e - (p_d + q_e\theta_d)\sin\theta_e \tag{2.43}$$

$$\frac{dp_d}{ds} = \omega^2 x_d \tag{2.44}$$

$$\frac{dq_d}{ds} = \omega^2 y_d \tag{2.45}$$

Because all real systems have inherent damping, many cases including external and internal damping were considered. For cases with external damping, viscous damping is assumed. The internal, or viscoelastic damping is based on the Kelvin-Voigt model. Internal damping is not proportional to the velocity of the system, as is external damping. Instead, internal damping influences the system as the bending stress increases or decreases. Therefore, the internal damping coefficient is seen in its effect on the rate of change in moment (or curvature) of the element. The addition of damping does not affect the static equilibrium, but damping does influence the dynamic equilibrium. Therefore, a

new element must be examined. As shown in Figure 2.5.1, the new element includes the additional forces due to external damping. The nondimensional external damping coefficient, c, and internal damping coefficient, γ, are defined in terms of the dimensional coefficients C and Γ as:

$$c = \frac{CL^2}{\sqrt{\mu EI}} \tag{2.46}$$

$$\gamma = \frac{\Gamma\sqrt{I}}{\sqrt{\mu EL^4}} \tag{2.47}$$

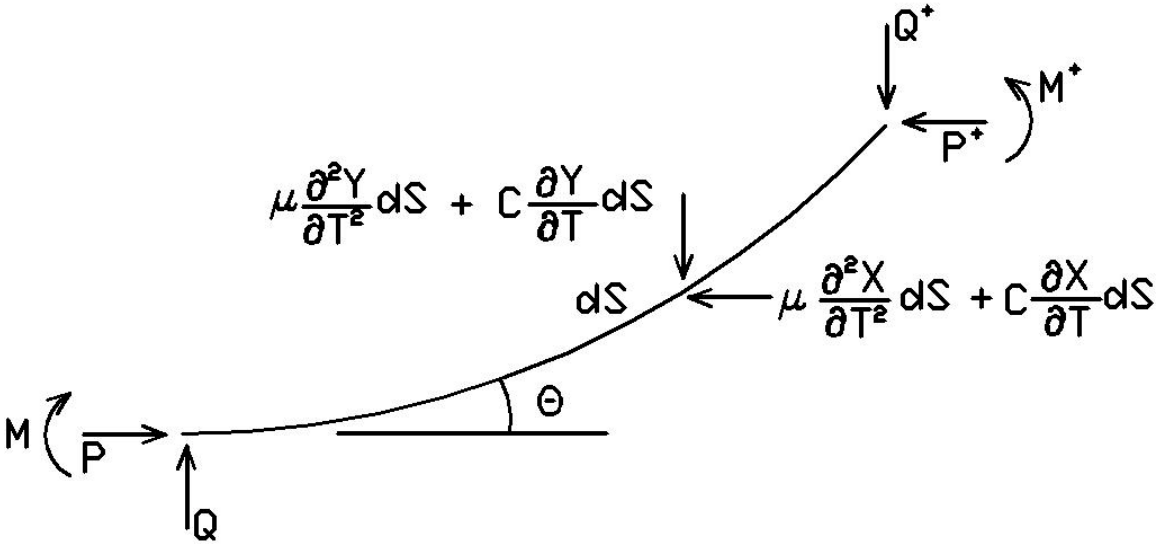

Figure 2.5.1: Free-Body Diagram of Element of Pinned-end Buckled Strut Under Forced Vibrations with Damping

The following nondimensional equations replace equations 2.31-2.33 for cases with damping:

$$m = \frac{\partial\theta}{\partial s} + \gamma\frac{\partial^2\theta}{\partial t\partial s} \tag{2.48}$$

$$\frac{\partial p}{\partial s} = -\frac{\partial^2 x}{\partial t^2} - c\frac{dx}{dt} \tag{2.49}$$

$$\frac{\partial q}{\partial s} = -\frac{\partial^2 y}{\partial t^2} - c\frac{dy}{dt} \tag{2.50}$$

The function sin(ωt) is replaced by $e^{i\omega t}$, and a new set of complex dynamic equations is established for cases with damping:

$$\frac{dx_d}{ds} = -\theta_d \sin\theta_e \tag{2.51}$$

$$\frac{dy_d}{ds} = \theta_d \cos\theta_e \tag{2.52}$$

$$\frac{d\theta_d}{ds} = \frac{m_d}{(1+i\omega\gamma)} \tag{2.53}$$

$$\frac{dm_d}{ds} = (q_d - p_o\theta_d)\cos\theta_e - (p_d + q_e\theta_d)\sin\theta_e \tag{2.54}$$

$$\frac{dp_d}{ds} = (\omega^2 - i\omega c)x_d \tag{2.55}$$

$$\frac{dq_d}{ds} = (\omega^2 - i\omega c)y_d \tag{2.56}$$

For cases without damping, the values of c and γ are set to zero; therefore, one Mathematica program can be used for both undamped and damped cases.

2.5 Numerical Solution of a Pinned-end Buckled Strut Under Forced Vibrations

Another Mathematica program is employed to gain the desired numerical solution. Again, the shooting method is used. The known values of p_o, u_o, r, c, γ, and ω are used as input, and initial guesses are made for $p_d(0)$, $q_d(0)$, and $m_d(0)$. The values of $\theta_e(0)$ and q_e are known from the static equilibrium solution. Iteration is necessary to ensure convergence of the boundary conditions at the end of the strut. The Mathematica program used for the dynamic analysis can be found in Appendix A.2.

Using the resulting dynamic displacement, the transmissibility of the strut is determined. The transmissibility for the undamped case is defined as:

$$TR = \left| \frac{x_d(1)}{u_o} \right| \tag{2.57}$$

With the addition of damping, the end displacement in the Mathematica program is complex; consequently, the resulting transmissibility is as follows:

$$TR = \frac{\sqrt{\{Re[x_d(1)]\}^2 + \{I_m[x_d(1)]\}^2}}{|u_o|} \tag{2.58}$$

The program is repeated for a wide range of excitation frequencies in order to gain an accurate representation of the response of the strut. The transmissibility (TR) is plotted as a function of the applied nondimensional frequency ω. The resonant frequency, ω_n, can be found for the undamped case when the transmissibility is infinite. Iteration is necessary to find the resonant frequency for each case. For cases with damping, the damped resonant frequency is found when the transmissibility is at its maximum. For all cases the resulting transmissibility is desired to be less than one because this means that the motion of the supported load is smaller than the applied motion at the base.

2.6 Results for Forced Vibrations of the Pinned-end Buckled Strut

Using Excel, plots were created to show the efficacy of a pinned-end buckled strut used as a vibration isolator. Many factors affect the performance of the buckled strut; therefore, many cases were examined with varying parameters. To create a buckled condition, the columns support nondimensional loads of 10 or 11. Different combinations of external and internal damping are considered, and the stiffness parameter is varied for most plots. All variables shown on the plots are nondimensional.

Additional plots for the pinned-end buckled strut under simple harmonic forced vibrations can be found in Appendix A.3.

The first group of plots shows the transmissibility curve for a range of frequencies. This first peak for the system occurs at the fundamental resonant frequency for the undamped cases. For cases with damping, this frequency will be referred to as the damped resonant frequency or peak frequency. The forced motion of the strut about equilibrium is assumed to be small and harmonic.

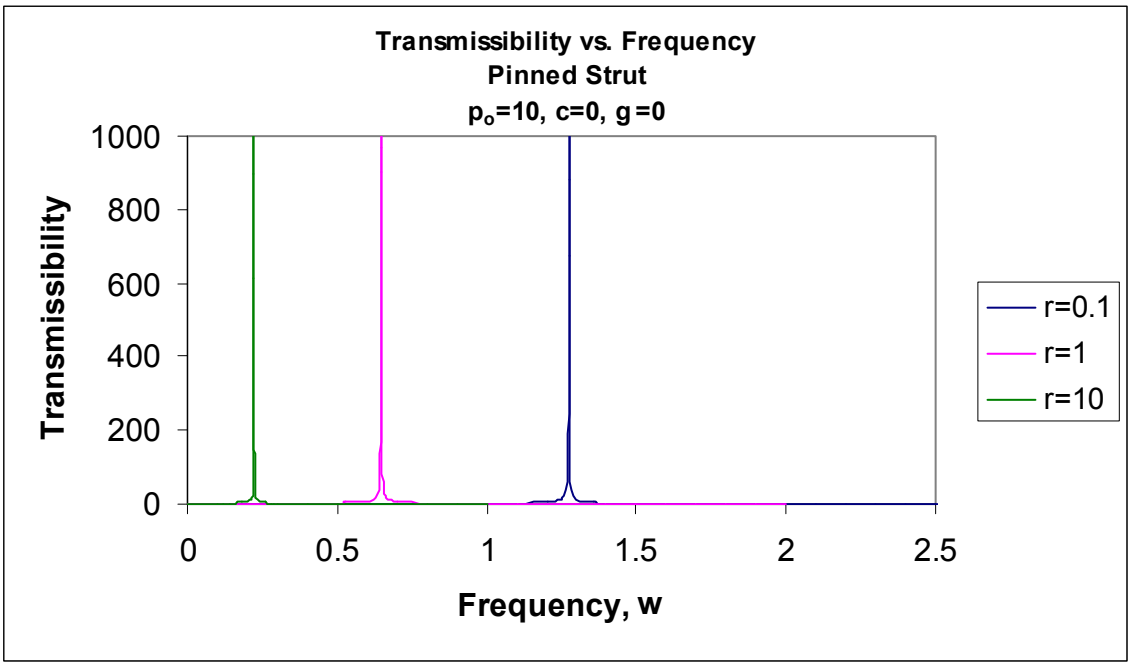

Figure 2.6.1: Transmissibility vs. Frequency for p_o=10, c=0, γ=0

In Figure 2.6.1, the transmissibility is plotted against a varying applied frequency for a pinned-end strut under a load of p_o=10. As indicated on the plot, the system was analyzed with stiffness parameters of r = 0.1, 1, and 10. Damping is not included in this system. Although the plot only shows the transmissibility up to a value of 1000, the value of the transmissibility at the peaks is infinite because no damping is present. From this plot, it is evident that the stiffness parameter has a large effect on the resonant frequency. As the stiffness parameter increases, the nondimensional resonant frequency decreases. Typically, the isolator will be designed to operate at a frequency higher than

its fundamental natural frequency. Therefore, by reducing the natural frequency, the isolator becomes effective at a larger range of excitations. It is noted that both the stiffness parameter r and the nondimensional frequency ω depend on the strut's bending stiffness EI, as seen in equations 2.23 and 2.27, and an increase in EI tends to increase the dimensional resonant frequency Ω even though the nondimensional resonant frequency decreases.

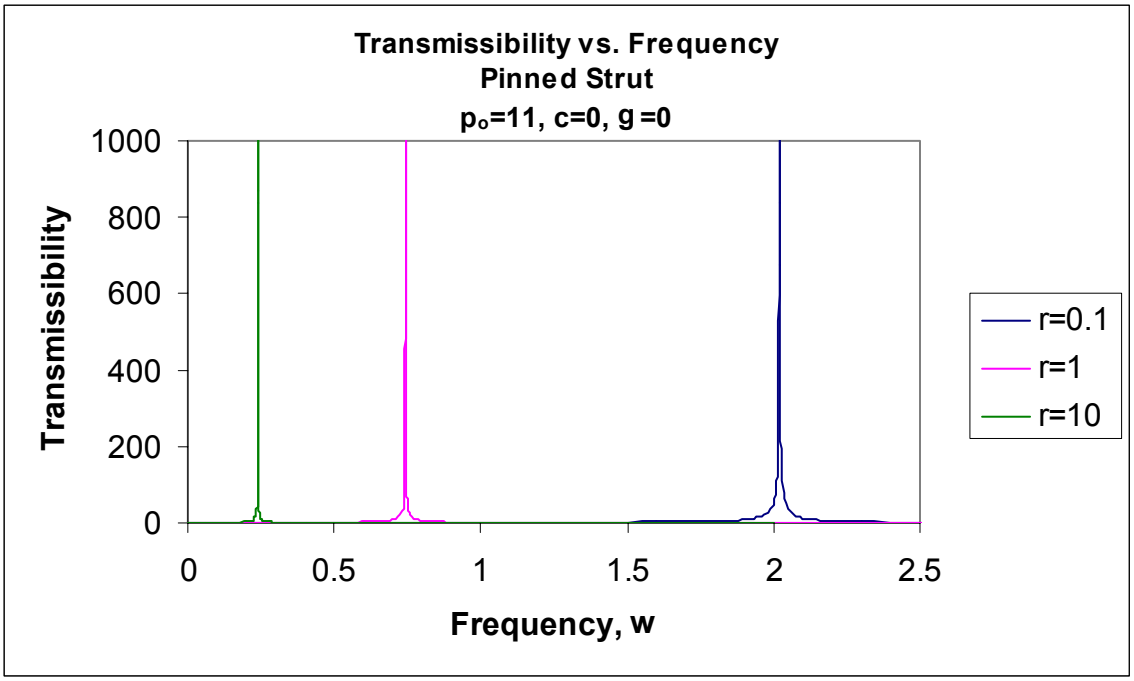

Figure 2.6.2: Transmissibility vs. Frequency for p_o=11, c=0, γ=0

A similar shift in natural frequencies results from the increasing stiffness parameter in Figure 2.6.2, as well. This plot, however, shows the response of the same strut under a different load of 11. Because this system is also undamped, the three peaks extend to infinity again.

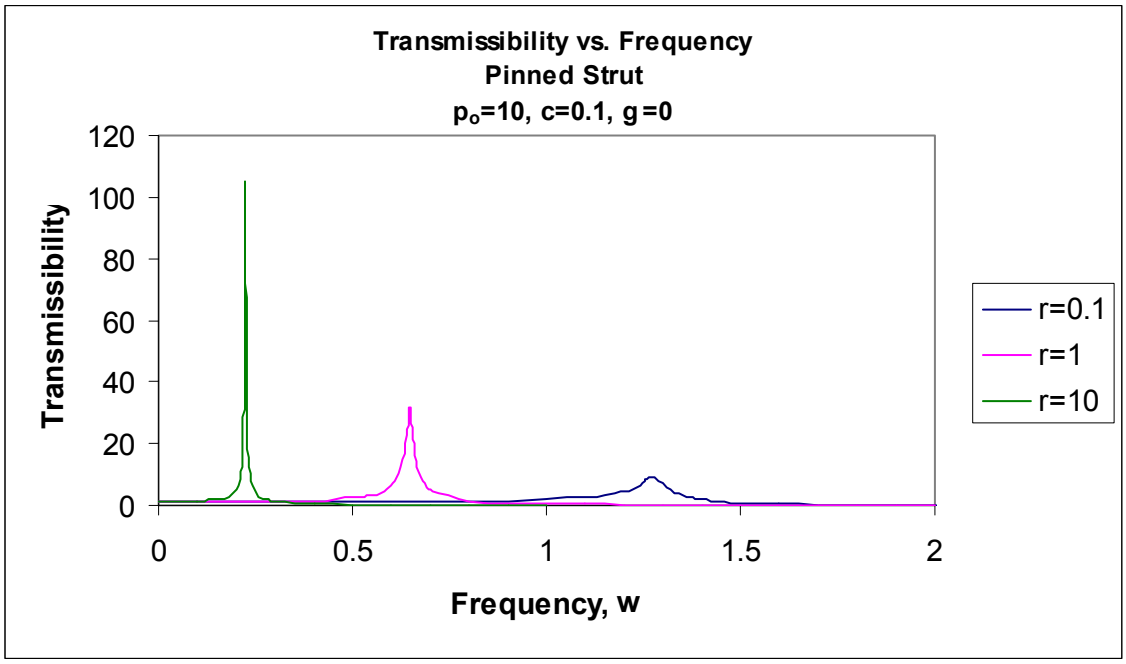

Figure 2.6.3: Transmissibility vs. Frequency for p_o=10, c=0.1, γ=0

Figure 2.6.3 shows the effect of damping on the system. No internal damping is included, but even with a small external damping coefficient of c=0.1, the peaks are reduced from their undamped values of infinity. The damped resonant peaks provide a large amount of information on the behavior of the system. The damped resonant peaks occur at the same frequency as the undamped resonant peaks. However, the reduction in the transmissibility is largely influenced by the stiffness parameter. As the stiffness parameter increases, the maximum value of the transmissibility increases. Also, as the stiffness parameter increases, the range of large transmissibilities becomes smaller. So even though the transmissibility may be larger at its peak for a stiffness parameter of r=0.1, the transmissibility decreases at a faster rate than it would for a stiffness parameter of r=1. Because the goal of the isolator is to keep the transmissibility less than 1, it is desirable to increase the rate of change of the transmissibility so that the motion is reduced for a larger range of frequencies.

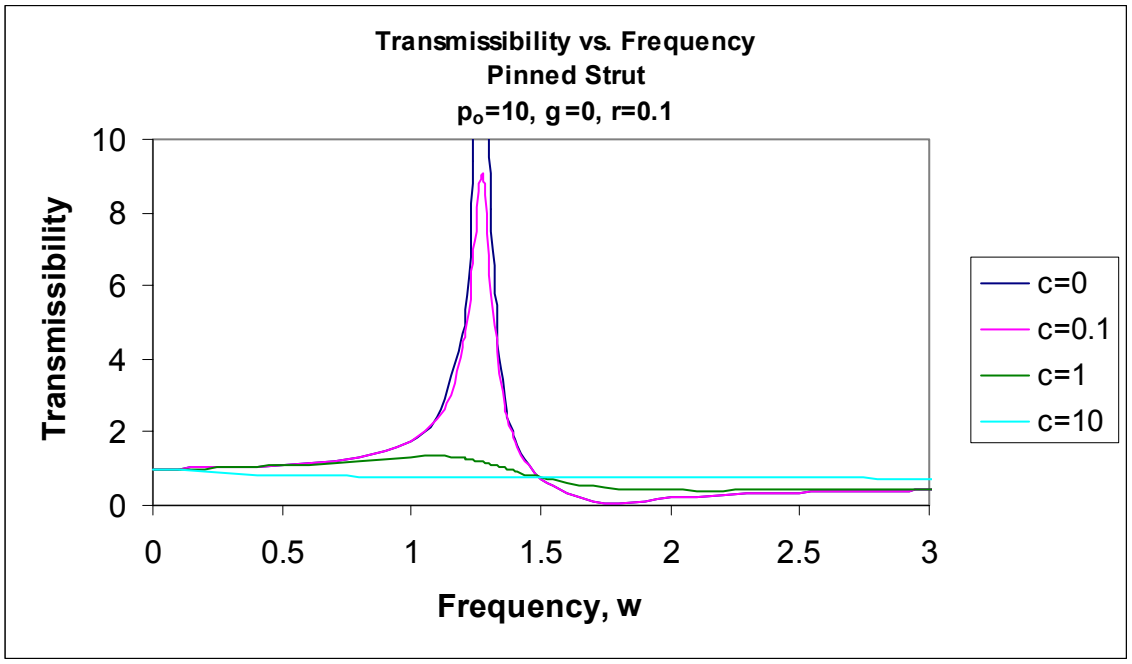

Figure 2.6.4: Transmissibility vs. Frequency for p_o=10, r=0.1, γ=0

The effect of increasing the amount of external damping is shown in Figure 2.6.4. The strut shown in this plot supports a load of p_o=10 and has a stiffness parameter of r=0.1. The external damping coefficient varies from 0 to 10. When c=0, the maximum transmissibility is infinite. When damping is added, the maximum transmissibility is reduced over 80% from c=0.1 to c=1. As the damping coefficient increases further, the decrease in the maximum transmissibility is not as significant. As the damping is increased, the system eventually becomes overdamped, and the motion of the supported mass is always less than the base motion. This would, of course, be advantageous; however, it is often impractical to achieve such a high level of damping.

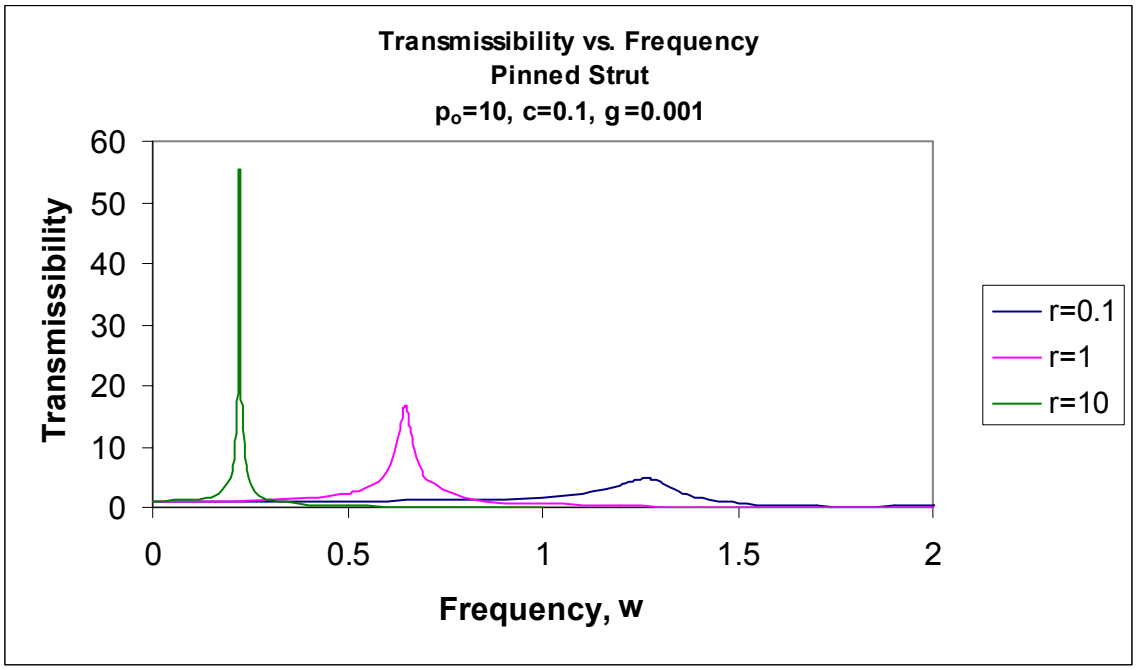

Figure 2.6.5: Transmissibility vs. Frequency for p_o=10, c=0.1, γ=0.001

Figure 2.6.5 shows the effect of internal damping on the system. For the same amount of external damping as in Figure 2.6.3, the maximum transmissibility is reduced about 50% by the addition of a very small amount of internal damping (γ=0.001). Figure 2.6.5 is representative of a typical system since all real struts inherently have both internal (viscoelastic) and external (viscous) damping.

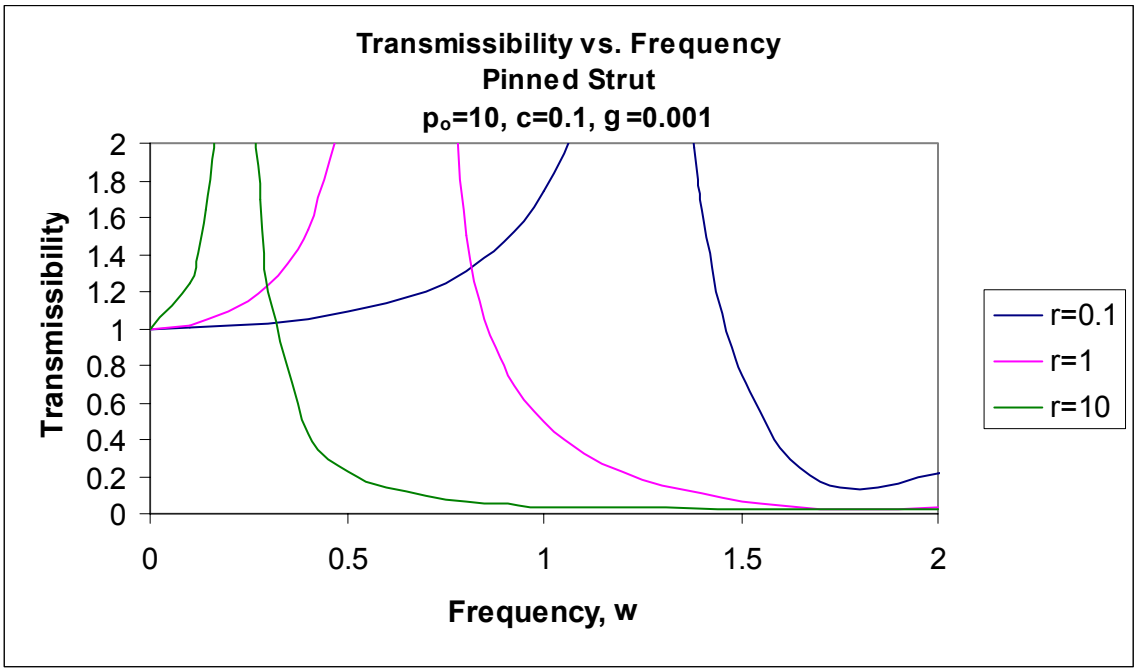

Figure 2.6.6: Transmissibility vs. Frequency for p_o=10, c=0.1, γ=0.001

Figure 2.6.6 is the same system shown in Figure 2.6.5, but the range of the transmissibility has been modified. This view is useful to examine the behavior of the system when the motion of the supported mass is close to that of the base motion. As is evident from Figure 2.6.6, the most efficient system of the three shown would be the strut with a stiffness parameter of r=10. When surveying Figure 2.6.5, the strut with r=0.1 might seem to be the most attractive option because of its lower peak transmissibility. But taking a closer look would reveal that the same strut does not decrease the motion of the supported mass for as many frequencies as the strut with r=10. Also, the lower resonant frequency of the strut with r=10 increases the working range of the isolator, as stated previously.

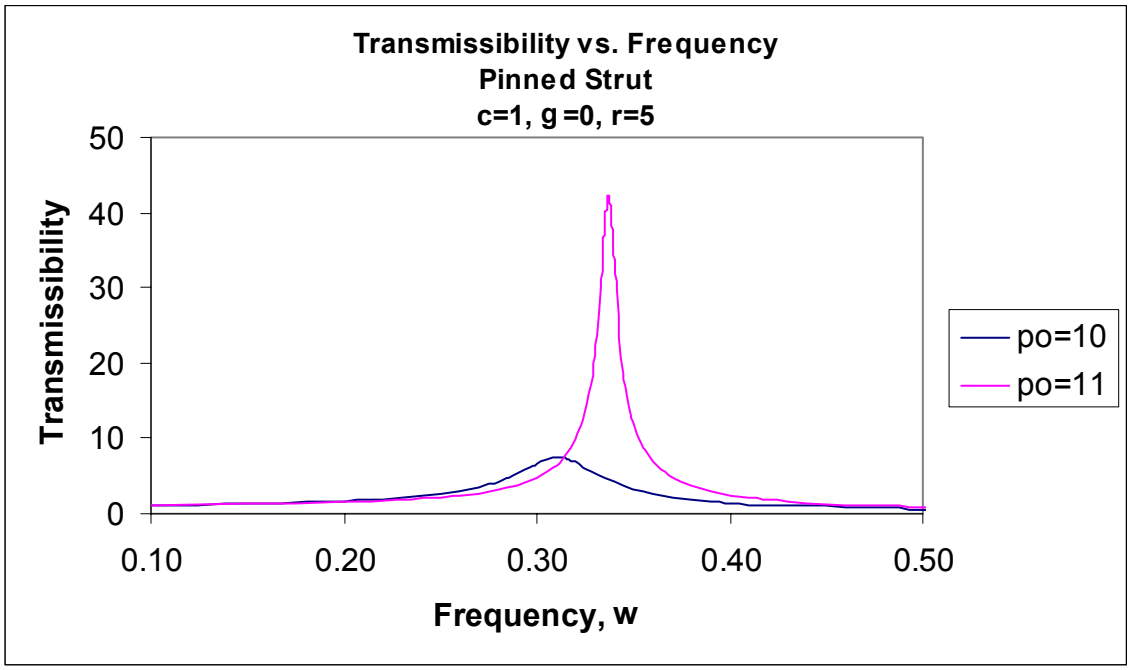

Figure 2.6.7: Transmissibility vs. Frequency for c=1, γ=0, r=5

The effect of the supported load on the system can be seen in Figure 2.6.7. First, the maximum transmissibility is greatly reduced when the supported load is closer to the buckling load. Also, the damped resonant frequency is decreased when the load is closer to the buckling load of the strut. Therefore, the closer the load is to the buckling load, the more effective the isolator would be, as long as the load does not descend below the buckling load.

Figure 2.6.8 shows that the resonant frequency is somewhat affected by the supported load on the strut. For a stiffness parameter of r=0.1, the resonant frequency gradually increases as the load increases. Initially, the rate of change of the resonant frequency is large, but as the load increases, the rate of change decreases. As the stiffness parameter increases, the resonant frequency tends to remain more constant as the load increases. As shown in previous plots, it is obvious that the resonant frequency decreases as the stiffness parameter increases for any given load.

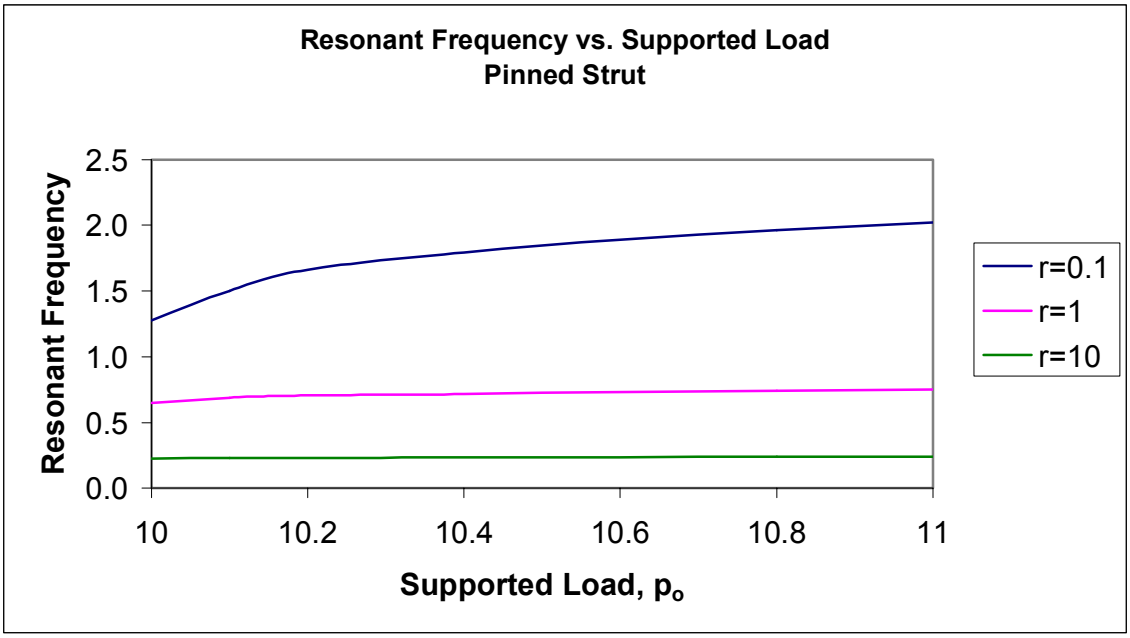

Figure 2.6.8: Resonant Frequency vs. Supported Load for c=0, γ=0

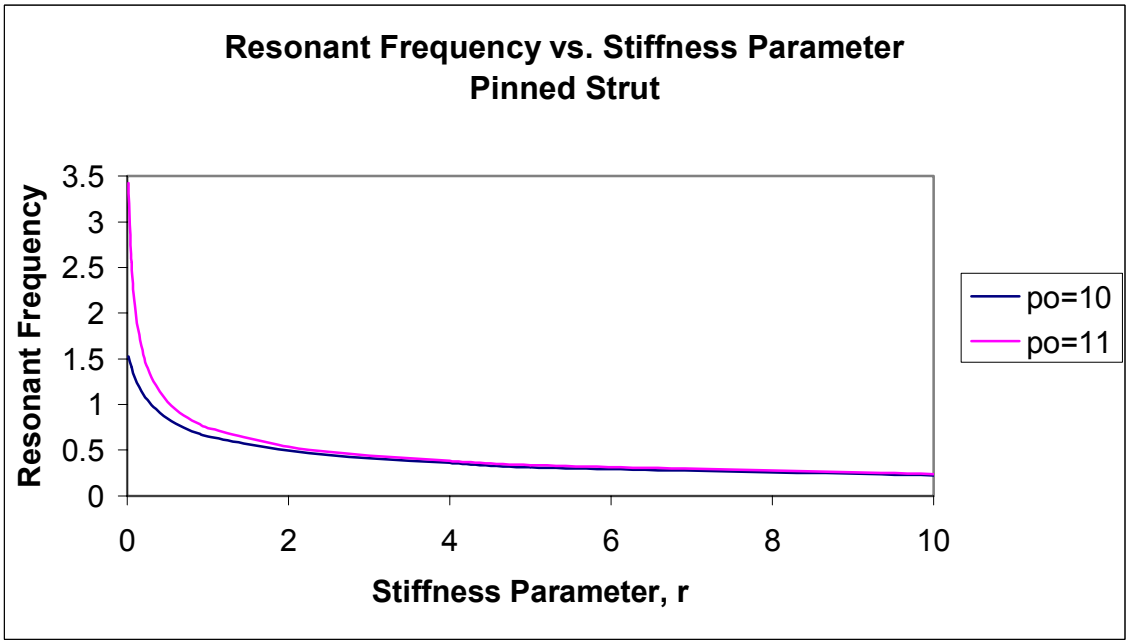

Figure 2.6.9: Resonant Frequency vs. Stiffness Parameter for c=0, γ=0

Figure 2.6.9 shows the dramatic decrease in the nondimensional resonant frequency as the stiffness parameter increases. Initially, the rate of change of the resonant frequency is highly dramatic and negative, but as the stiffness parameter increases, the rate of change

decreases. The differently loaded systems are similar in nature. However, the strut supporting a load of p_o=11 has a higher resonant frequency at first, but then the two systems converge to similar responses at higher degrees of stiffness. This graph does not mean that the dimensional resonant frequency is decreasing as the stiffness parameter increases. The stiffness parameter is directly proportional to the bending stiffness, EI, but the nondimensional term ω is inversely proportional to the square root of the bending stiffness, EI. So as the bending stiffness increases, the stiffness parameter increases and the nondimensional frequency decreases. The dimensional frequency, Ω, satisfies $\Omega^2=r\omega^2 g/L$, and from the data, Ω increases as r increases. Figure 2.6.10 better explains this relationship. Since g/L is constant for a given system, Ω depends on $\omega\sqrt{r}$, as plotted in Figure 2.6.10. From Figure 2.6.9, it is known that the nondimensional resonant frequency ω decreases as the stiffness parameter increases. Now, from Figure 2.6.10, when the stiffness parameter increases and the nondimensional resonant frequency decreases, the dimensional resonant frequency increases. Therefore, as the stiffness parameter increases, the dimensional resonant frequency also increases.

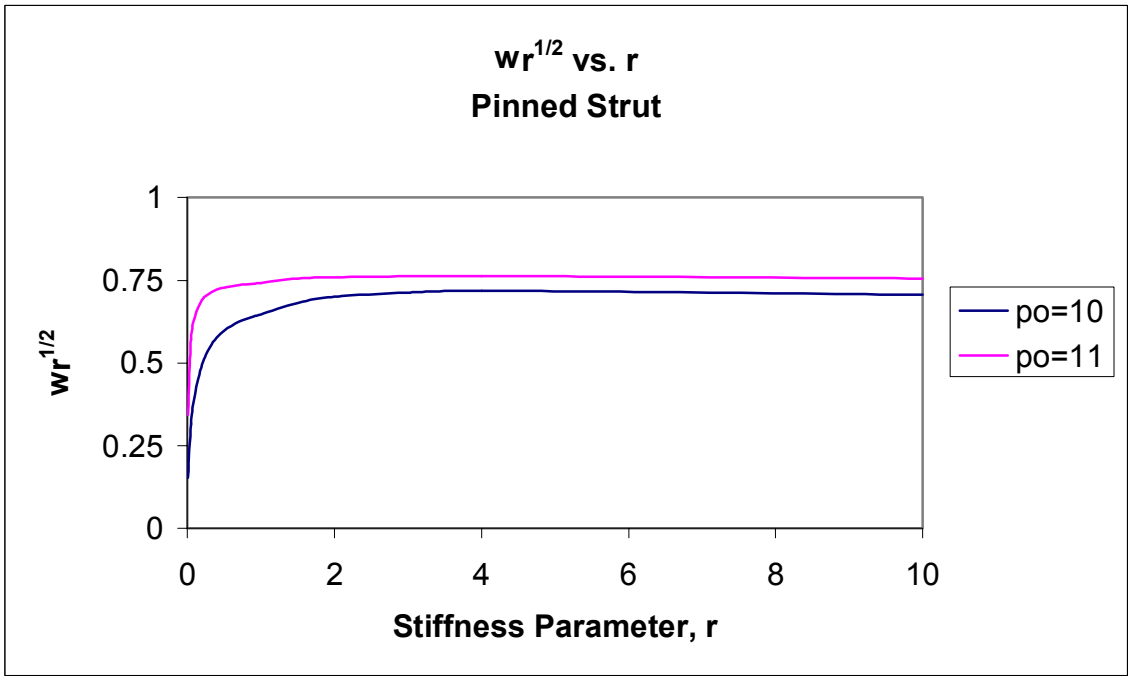

Figure 2.6.10: $\omega\sqrt{r}$ vs. r for Pinned Strut

The relationship between the stiffness parameter and the dimensional frequency can also be seen in Figure 2.6.11. It is obvious that the dimensional resonant frequency, as well as the maximum transmissibility increases as the stiffness parameter increases. Therefore, a low stiffness parameter would be required for the isolator to be effective.

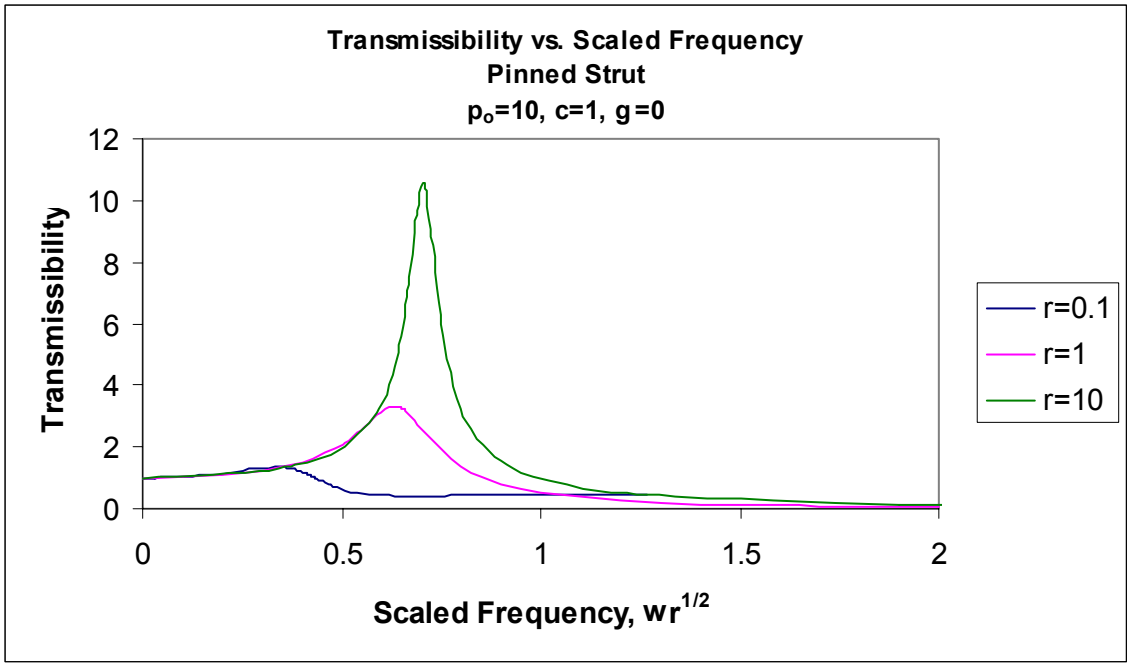

Figure 2.6.11: Transmissibility vs. Scaled Frequency for p_o=10, c=1, γ=0

2.7 Conclusions

After examining the case of the pinned-end buckled strut under forced harmonic vibrations, several conclusions can be made. First, it is obvious that the success of the isolator depends on more than one factor. At first glance, the results may seem to indicate that the stiffness parameter should be increased to reduce the resonant frequency of the system. However, because the dimensional resonant frequency Ω depends on $\sqrt{r}$ and ω, increasing r causes ω_{peak} to decrease, but it may not cause Ω_{peak} to decrease because one variable is increasing and one is decreasing. Also, the damping coefficient should be increased so that the maximum transmissibility is decreased. However, practical designs will limit the amount of damping that can be used in a system. Models that include external damping have similar results to those with internal damping. Since

all real systems naturally possess external and internal damping, the most practical models would include both of these properties. By utilizing a high damping coefficient, the pinned-end isolator will be effective at reducing the motion of the supported load. The strut should be designed so that the supported load is only slightly larger than the buckling load. As the load escalates from the buckling load, the efficacy of the system declines because the resonant frequency increases. It is necessary to consider all of the above factors when designing a vibration control system composed of pinned-end buckled struts.

Chapter 3: Fixed-end Buckled Column under Forced Harmonic Axial Excitation

3.1 Introduction

The next model to be analyzed is a fixed-end strut. This system is only slightly more complex than the pinned-end strut. The fixed strut might be more practical for some systems because it can support higher loads. The strut is a fixed column that is supporting a load above its buckling load. The column, in its undeformed shape, can be seen in Figure 3.1.1 in a horizontal configuration to save space. The basic assumptions and equation derivations used to analyze this model are discussed previously in Chapter 2. However, the small differences in the models will be discussed in this chapter. The results of the many situations examined for the fixed-end strut are presented in this chapter, also. As stated previously, all numerical solutions are performed in Mathematica, and all graphical results are plotted using Excel.

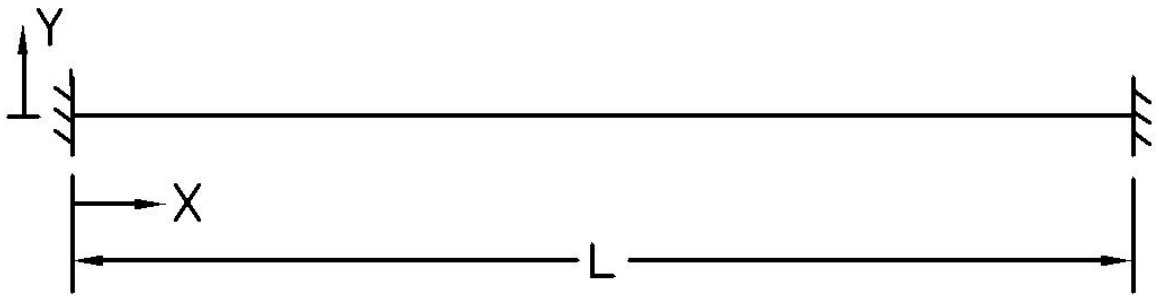

Figure 3.1.1: Undeformed Fixed-end Strut

3.2 Basic Assumptions and Formulations

The basic assumptions and equation formulation are presented in Chapter 2. The main difference between the pinned-end model and the fixed-end model is the set of boundary

conditions of the strut. The same equilibrium equations can be used for both models because equilibrium does not depend on the boundary conditions of the strut. The formulation will not be repeated, but the equations used by the Mathematica programs for this model will be presented.

The fixed-end strut is analyzed in the same manner as the pinned-end strut. First, a post-buckled condition is created by applying a load above the buckling load on the column. The shape of the fixed-end buckled strut can be seen in Figure 3.2.1. For a pinned-end strut, the Euler buckling load is $P = \pi^2 EI/L^2$. Again, the nondimensional buckling load will be $p_o = PL^2/EI$, thus $p_o = \pi^2 \approx 9.87$ for a pinned-end strut. However, the Euler buckling load for a fixed-end strut is $P=4\pi^2 EI/L^2$. Therefore, the nondimensional buckling load used for the fixed-end model will be $p_o = 4\pi^2 \approx 39.48$. To create our post-buckled model, nondimensional loads of 40 and 41 will be used.

Figure 3.2.1: Fixed-end Buckled Strut

3.3 Numerical Solution of a Fixed-end Buckled Strut in Static Equilibrium

As shown in Figure 3.2.1, the strut is fixed at both ends. The fixed boundary conditions are such that no rotation is permitted at either end of the strut. To prevent rotation at the ends of the strut, a moment must be present to counter the internal moment in the strut. Therefore, the boundary conditions of the fixed-end strut are as follows:

At s=0: x=0, y=0, θ=0

At s=1: y=0, θ =0.

The numerical solution of the strut can be found by using the shooting method in a Mathematica program. The following equations of equilibrium are used in this program and were previously derived in Chapter 2:

$$\frac{dx}{ds} = \cos\theta \tag{3.1}$$

$$\frac{dy}{ds} = \sin\theta \tag{3.2}$$

$$\frac{d\theta}{ds} = m \tag{3.3}$$

$$\frac{dm}{ds} = -p_o \sin\theta + q\cos\theta \tag{3.4}$$

The known value of the applied force p_o is used as input, and initial guesses are made for the values of the moment m at s=0 and the shear force q. After applying the known boundary conditions stated above, the program solves the system of differential equations for the moment at s=0 and the shear force in a trial and error method. Iterations must be performed if the initial guesses do not allow convergence of the solution to the prescribed accuracy. The equilibrium program used for this static analysis can be found in Appendix B.1.

3.4 Forced Vibration of Fixed-end Buckled Strut due to Harmonic Base Motion

Using the resulting moment at s=0 and shear force from the static analysis, the strut is subjected to a forced vibration and analyzed to determine the transmissibility of the system. The excitations are axial, single-frequency harmonic motions applied at the base of the strut. The vibrations due to this excitation are again assumed to be small, and the steady-state motion is examined. Resonant frequencies are found by applying an initial

guess and iterating until the transmissibility reaches infinity for a model without damping. The transmissibility can be found for any model by applying a range of different frequencies. The forced axial motion on the fixed-end strut is shown in Figure 3.4.1.

Figure 3.4.1: Fixed-end Strut under Forced Vibration

The equations used to describe the response of the fixed-end strut under the steady-state vibrations, where e represents equilibrium and d stands for dynamic, are as follows:

$$x(s,t) = x_e(s) + x_d(s)e^{i\omega t} \tag{3.5}$$

$$y(s,t) = y_e(s) + y_d(s)e^{i\omega t} \tag{3.6}$$

$$\theta(s,t) = \theta_e(s) + \theta_d(s)e^{i\omega t} \tag{3.7}$$

$$m(s,t) = m_e(s) + m_d(s)e^{i\omega t} \tag{3.8}$$

$$p(s,t) = p_o + p_d(s)e^{i\omega t} \tag{3.9}$$

$$q(s,t) = q_e + q_d(s)e^{i\omega t} \tag{3.10}$$

Also, the previously derived equations from the static and dynamic equilibrium of the strut are:

$$\frac{dx_d}{ds} = -\theta_d \sin\theta_e \tag{3.11}$$

$$\frac{dy_d}{ds} = \theta_d \cos\theta_e \tag{3.12}$$

$$\frac{d\theta_d}{ds} = \frac{m_d}{(1+i\omega\gamma)} \tag{3.13}$$

$$\frac{dm_d}{ds} = (q_d - p_o\theta_d)\cos\theta_e - (p_d + q_e\theta_d)\sin\theta_e \tag{3.14}$$

$$\frac{dp_d}{ds} = (\omega^2 - i\omega c)x_d \tag{3.15}$$

$$\frac{dq_d}{ds} = (\omega^2 - i\omega c)y_d \tag{3.16}$$

The boundary conditions for the dynamic model are:

At s=0: $X = U_o e^{i\Omega t}$, $Y=0$, $\theta=0$

At s=L $Y=0$, $\theta=0$

The boundary conditions must also be nondimensional. Therefore:

At s=0: $x = u_o e^{i\omega t}$, $y=0$, $\theta=0$

At s=1: $y=0$, $\theta=0$

3.5 Numerical Solution of a Fixed-end Buckled Strut Under Forced Vibrations

Another Mathematica program is employed to gain the desired numerical solution. Again, the shooting method is used. The known values of p_o, u_o, r, c, γ, and ω are used as input, and initial guesses are made for $p_d(0)$, $q_d(0)$, and $m_d(0)$. The values of $m_e(0)$ and q_e are known from the static equilibrium solution. Iteration is necessary to ensure convergence of the boundary conditions at the end of the strut. The Mathematica program used for the dynamic analysis can be found in Appendix B.2.

The equation used to solve for the transmissibility is:

$$TR = \frac{\sqrt{\{Re[x_d(1)]\}^2 + \{I_m[x_d(1)]\}^2}}{|u_o|} \tag{3.17}$$

The program is repeated for a wide range of excitation frequencies in order to gain an accurate representation of the response of the fixed-end strut. The transmissibility (TR) is plotted as a function of the applied nondimensional frequency ω. The resonant frequency, ω_n, can be found for the undamped case when the transmissibility is infinite. For cases with damping, the damped resonant frequency is found when the transmissibility is at its maximum. Iteration is necessary to find the resonant frequency for each case. Again, the resulting transmissibility is desired to be less than one because this means that the motion of the supported load is smaller than the applied motion at the base.

3.6 Results for Forced Vibrations of the Fixed-end Buckled Strut

Using Excel, plots were created to show the results of a fixed-end buckled strut used as a vibration isolator. Many factors affect the performance of the buckled strut; therefore, many cases were examined with varying parameters. In order to create a buckled condition, the columns support nondimensional loads of 40 or 41. Different combinations of external and internal damping are considered, and the stiffness parameter is varied for most plots. All variables shown on the plots are nondimensional. Additional plots for the pinned-end buckled strut under simple harmonic forced vibrations can be found in Appendix B.3.

The first group of plots shows the transmissibility curve for a range of frequencies. This first peak for the system occurs at the fundamental resonant frequency for the undamped cases. For cases with damping, this frequency will be referred to as the damped resonant frequency or peak frequency.

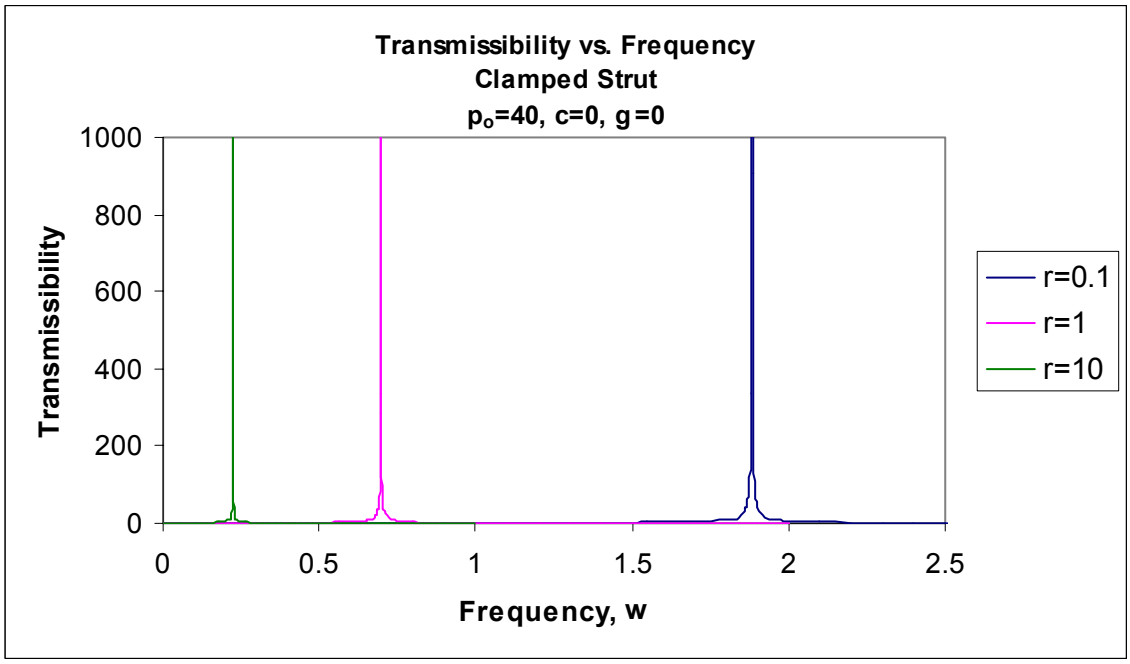

Figure 3.6.1: Transmissibility vs. Frequency for p_o=40, c=0, γ=0

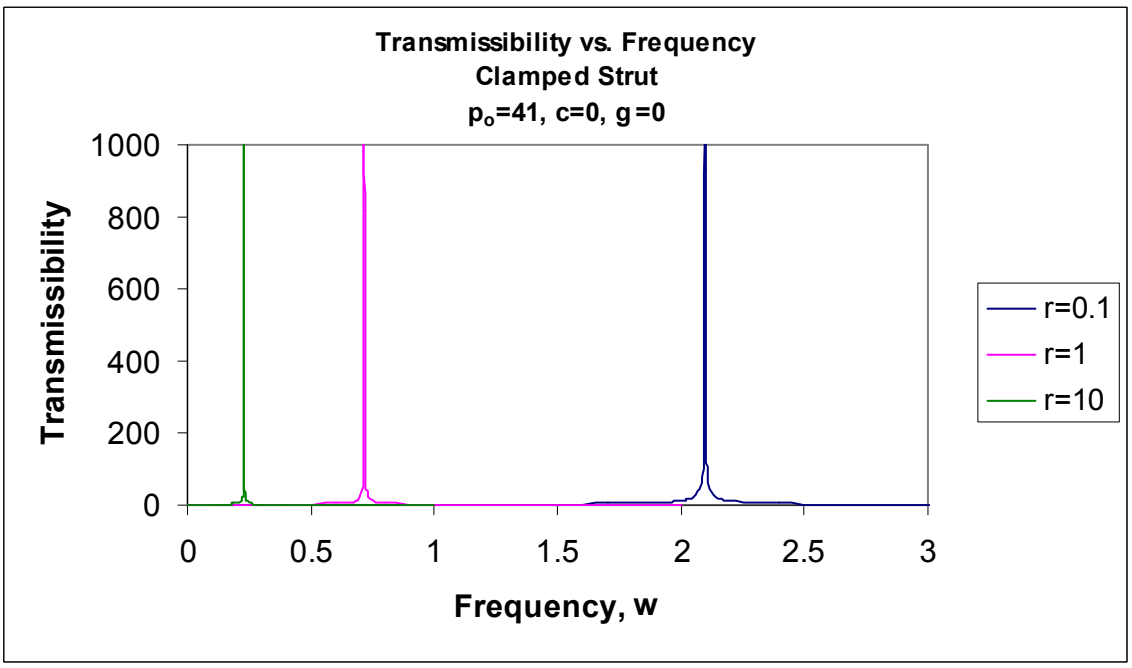

Figure 3.6.2: Transmissibility vs. Frequency for p_o=41, c=0, γ=0

In Figures 3.6.1 and 3.6.2, the undamped case is shown for two different loads. No damping is present in this system, and results for stiffness parameters of 0.1, 1, and 10 are shown. As expected, the transmissibilities are infinite at their resonant frequencies

because of the lack of damping. The results for these cases are similar to those of the undamped pinned-end model in Figures 2.6.1 and 2.6.2. Again, a shift in the resonant frequencies is apparent when the supported load increases. This shift is not as obvious as it was with the pinned-end strut, but it is still apparent. The stiffness parameter still plays an important role in the value of the resonant frequency.

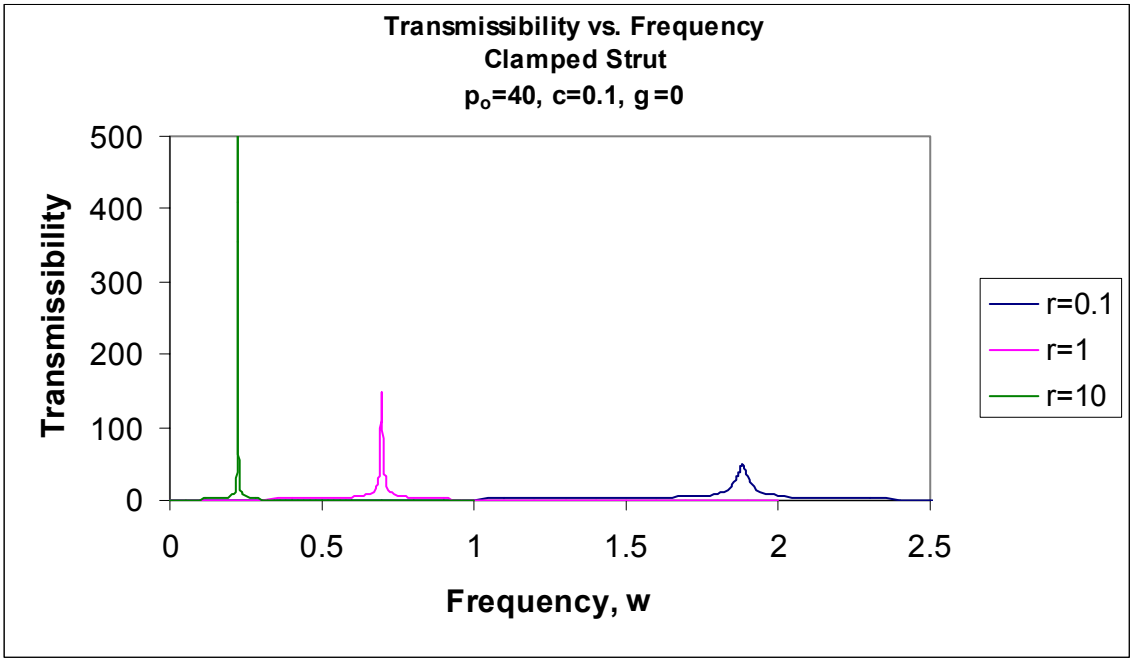

Figure 3.6.3: Transmissibility vs. Frequency for p_o=41, c=0.1, γ=0

Figure 3.6.3 shows the results for the fixed-end model with an external damping coefficient of c=0.1. Even this small amount of damping has a huge effect on reducing the maximum transmissibility of the strut. It is clear that damping is necessary to reduce the motion of any system comprised of these buckled struts. Also, the effect of the stiffness parameter is shown in this plot, as well. As the stiffness decreases, so does the maximum transmissibility of the strut. However, as the stiffness parameter increases, the range of frequencies that produce high transmissibilities is lower. This can be seen in more detail in Figure 3.6.4.

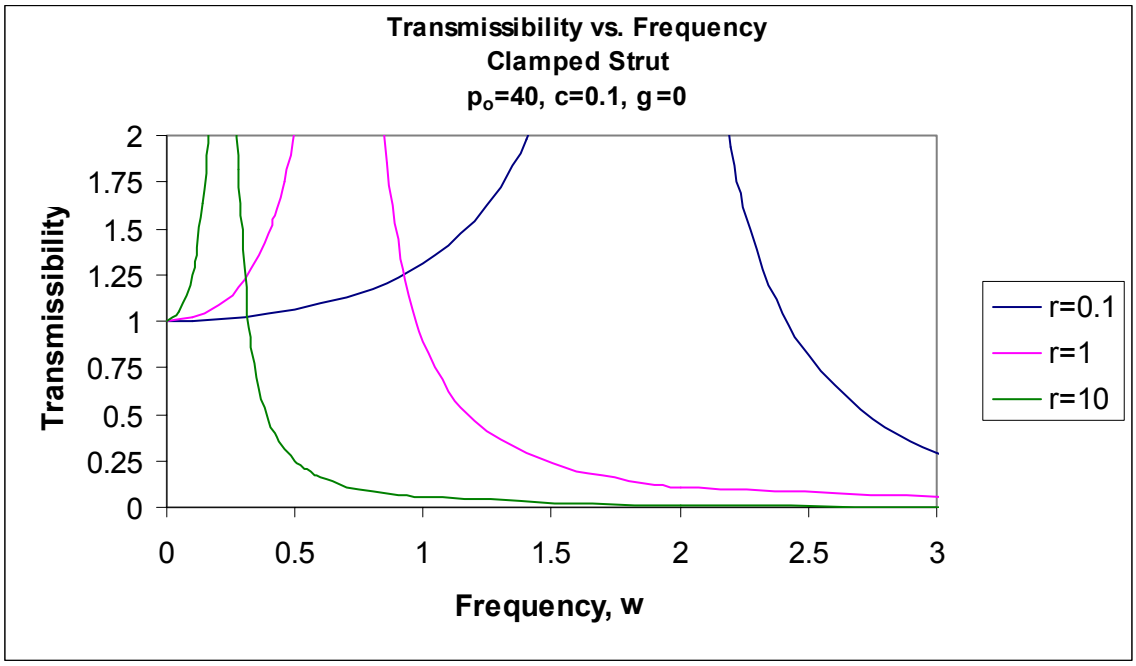

Figure 3.6.4: Transmissibility vs. Frequency for p_o=40, c=0.1, γ=0

Figure 3.6.4 shows the same results as Figure 3.6.3, but the Y-axis shows the results at low transmissibilities. Obviously, the strut with a stiffness parameter of r=10 would be more effective because it reduces the transmissibility quicker than the struts with lower stiffness parameters. Therefore, the strut with the high stiffness parameter would be effective at a larger range of frequencies. This is important since it is usually hard to predict the frequency of an unexpected vibration.

Figure 3.6.5 shows the results of the same system shown in Figure 3.6.4, but this strut supports a load of 41 instead of 40. This increase in load causes each peak to increase in its range of high transmissibilities. For example, the transmissibility for the strut with a stiffness parameter of 0.1 in Figure 3.6.4 drops below one at a frequency of about 2.4. However, in Figure 3.6.5, the same strut supporting a higher load does not reduce the motion until it reaches a frequency of about 3. Thus, the design should aim to keep the supported load of the strut to just slightly above its buckling load. This will allow the strut to be more effective at reducing the transmissibility at lower frequencies.

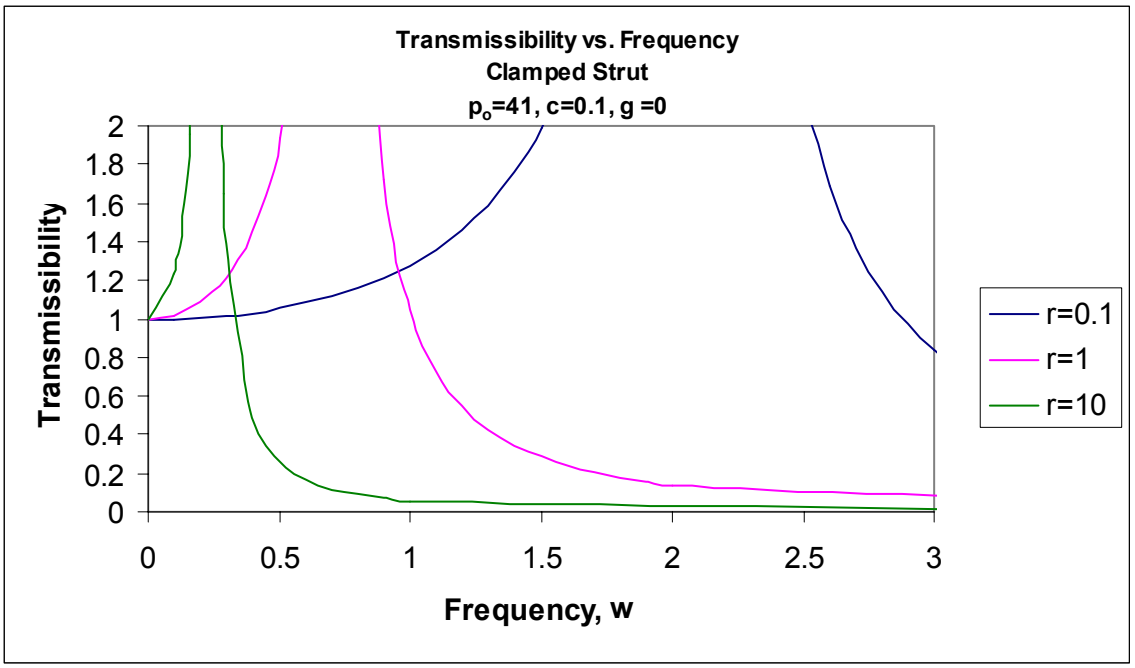

Figure 3.6.5: Transmissibility vs. Frequency for p_o=41, c=0.1, γ=0

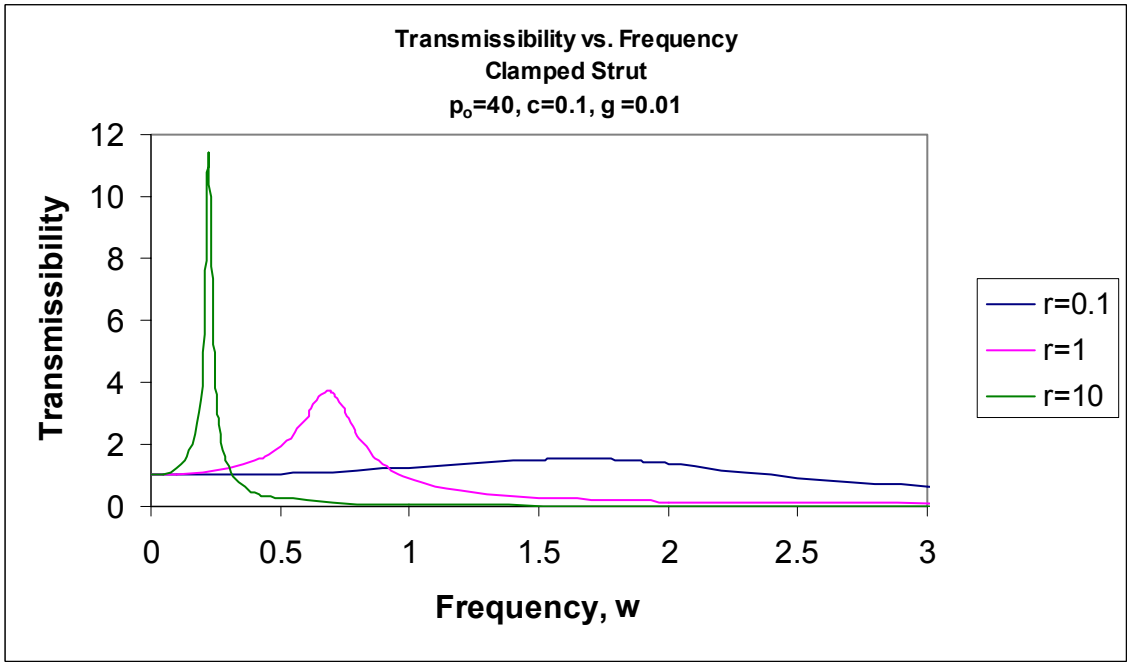

Figure 3.6.6: Transmissibility vs. Frequency for p_o=40, c=0.1, γ=0.01

Figure 3.6.6 shows the effects of adding internal damping to a system. This system is the same system as in Figure 3.6.3 except the internal damping coefficient is increased to 0.01. This small amount of viscoelastic damping greatly reduces the maximum

transmissibility of each strut. For example, the maximum transmissibility for the strut with a stiffness parameter of 1 has been reduced from about 150 to about 4.

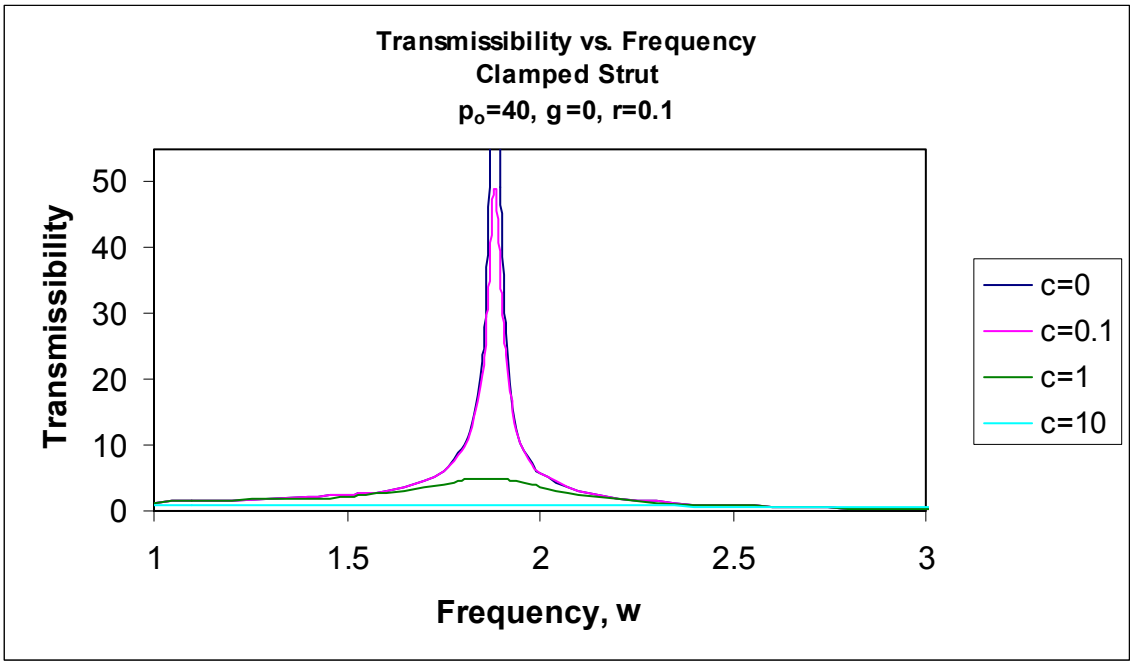

Figure 3.6.7: Transmissibility vs. Frequency for p_o=40, γ=0, r=0.1

The effect of increasing the amount of external damping is shown in Figure 3.6.7. For example, when c=0, the maximum transmissibility is infinite, but when damping is added, the maximum transmissibility is reduced over 80% from c=0.1 to c=1. As the damping coefficient increases further, the decrease in the maximum transmissibility is not as considerable Again, the system eventually becomes overdamped as the amount of damping increases, and the motion of the supported mass is always less than the base motion.

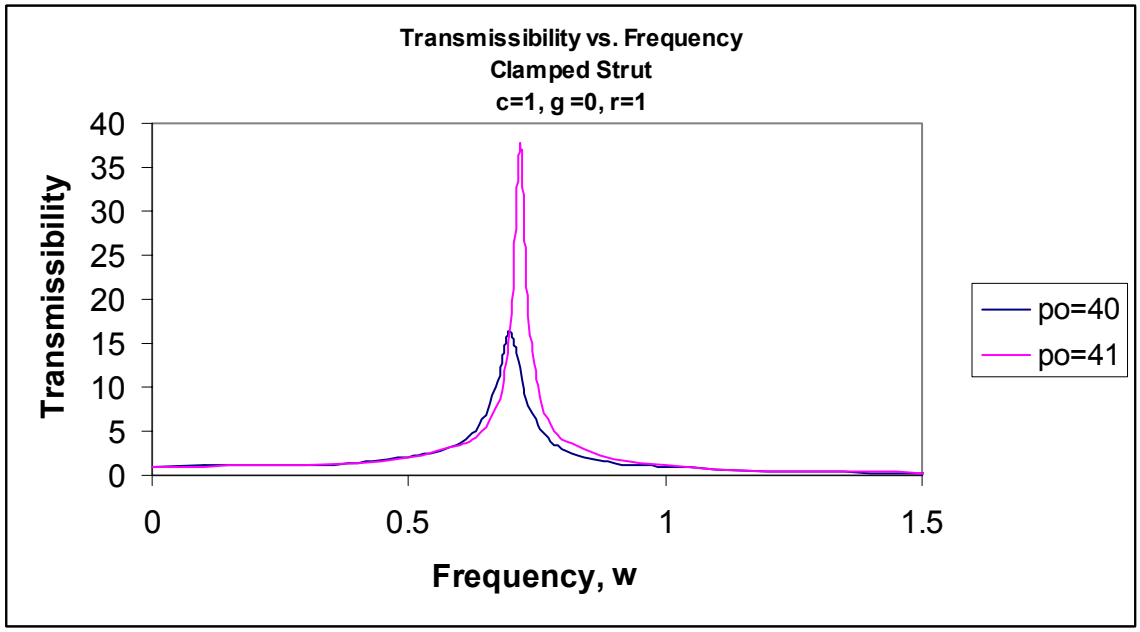

Figure 3.6.8: Transmissibility vs. Frequency for c=1, γ=0, r=1

The effect of the supported load on the system can be seen again in Figure 3.6.8. First, the maximum transmissibility is greatly reduced when the supported load is closer to the buckling load. Also, the damped resonant frequency is decreased when the load is closer to the buckling load of the strut. Yet again this shows that the closer the load is to the buckling load, the more effective the isolator would be, as long as the load does not descend below the buckling load.

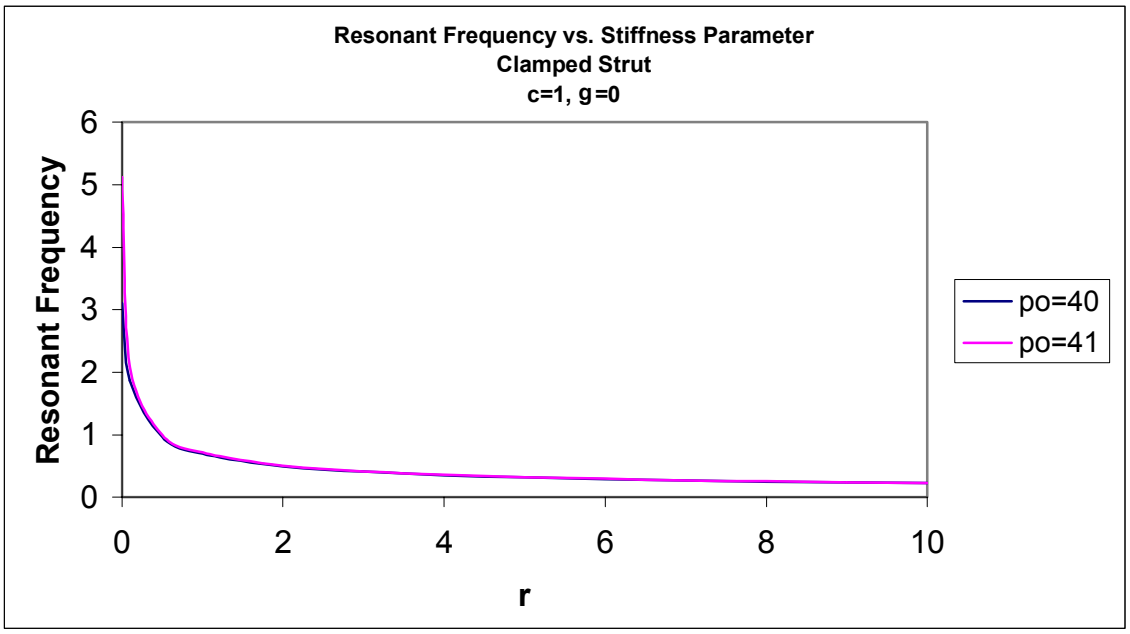

Figure 3.6.9: Peak Frequency vs. Stiffness Parameter for c=1, γ=0

In Figure 3.6.9, the nondimensional resonant frequency is plotted versus the stiffness parameter for two different loads. At low stiffness values, the higher load has a higher peak frequency than the smaller load, but the two plots converge quickly, and are almost identical as the stiffness parameter value rises. As discussed previously, since the dimensional resonant frequency depends on $\omega\sqrt{r}$, and $\omega\sqrt{r}$ increases as the stiffness increases, then the dimensional resonant frequency also increases as the stiffness parameter increases.

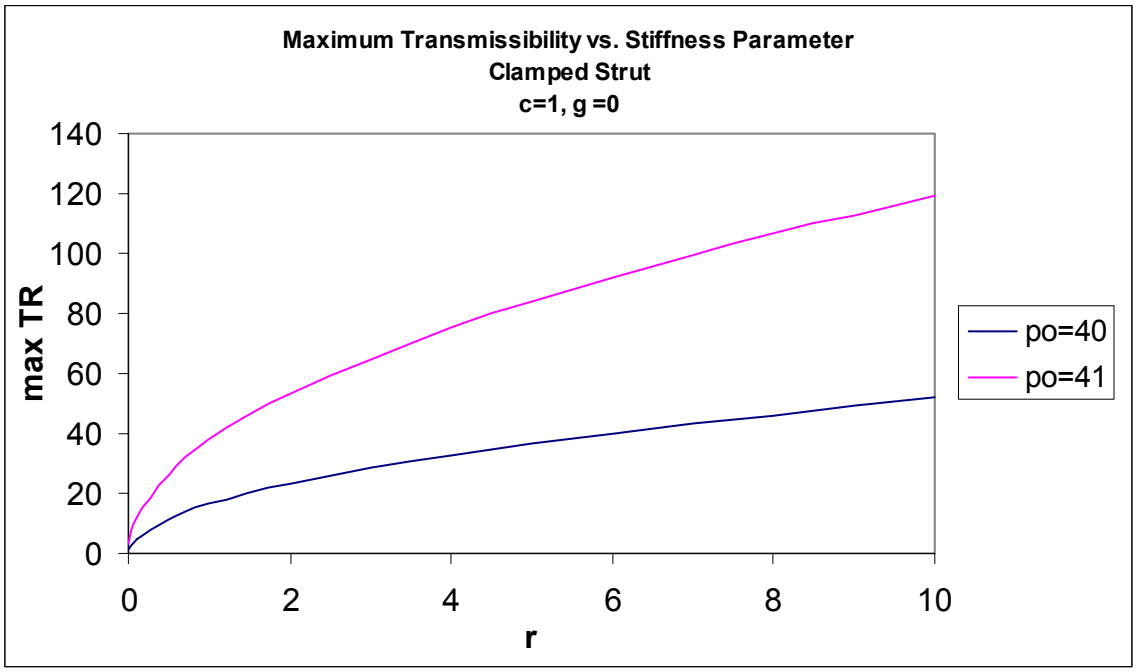

Figure 3.6.10: Maximum Transmissibility vs. Stiffness Parameter for c=1, γ=0

As shown in Figure 3.6.10, the maximum transmissibility (TR) of a system increases as the stiffness parameter increases. At low stiffness values, the maximum transmissibility increases at a faster rate. Also, as the buckling load increases, the maximum transmissibility is higher for any given stiffness value. Therefore, an effective system would require more damping at a higher buckling load than at a lower buckling load for a given stiffness parameter value.

3.7 Conclusions

After examining the case of the fixed-end buckled strut under forced harmonic vibrations, it is apparent that the fixed-end strut's behavior is similar to that of the pinned-end strut. Again, the stiffness parameter will affect the resulting transmissibility of a fixed-end strut in the same manner as the pinned-end strut. Also, the damping coefficient should be increased so that the maximum transmissibility is decreased. However, practical designs will limit the amount of damping that can be used in a system. Models that include external damping have similar results to those with internal damping for the clamped strut. Again, the strut should be designed so that the supported load is only slightly larger

than the buckling load. As the load escalates from the buckling load, the efficacy of the system declines because the resonant frequency increases. As concluded in Chapter 2, all of these factors must be considered when employing a fixed-end buckled strut as a vibration isolator.

Chapter 4: Pinned-end Column with Initial Curvature under Forced Harmonic Axial Excitation

4.1 Introduction

The model to be reviewed in this chapter is a pinned-end strut with an initial curvature. Since no real column is ideal, this model helps to predict the response of a real column. Imperfect columns exist because fabrication of a perfectly straight and upright column is impossible. The small imperfections in these columns may have an impact on the results of this study. The pinned strut to be used in this chapter is the same one identified in Chapter 2, but it will have an initial curvature in its undeformed shape as shown in Figure 4.1.1. The strut will be analyzed at loads above and below the buckling load since the initial curvature may affect the response of the strut prior to buckling. The results of each case will be presented and some will be compared to the corresponding ideal case.

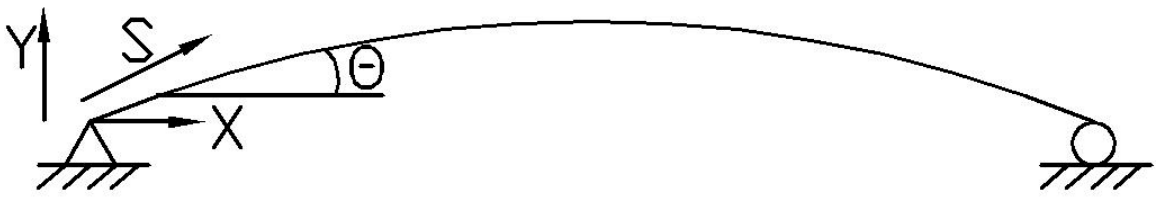

Figure 4.1.1: Undeformed Strut with Initial Curvature

4.2 Basic Assumptions and Formulations

The pinned-end strut will be given a constant initial curvature by applying an equation to describe the shape of the strut before loading. The strut is assumed to be unstrained in its initial shape. Also, internal, or viscoelastic, damping will not be included in this model.

The initial shape will be assigned an amplitude, d_o. For the pinned-end strut, the equations that describe the assumed initial shape of the strut are as follows:

$$\theta_o(s) = d_o(\tfrac{1}{2} - s) \qquad y \approx \tfrac{1}{2} d_o s(1-s) \qquad \max y \approx \frac{d_o}{8} \tag{4.1}$$

Amplitudes of 0.01, 0.5, and 0.1 were applied to vary the severity of the initial curvature. The initial shapes of the strut can be seen in Figure 4.2.1.

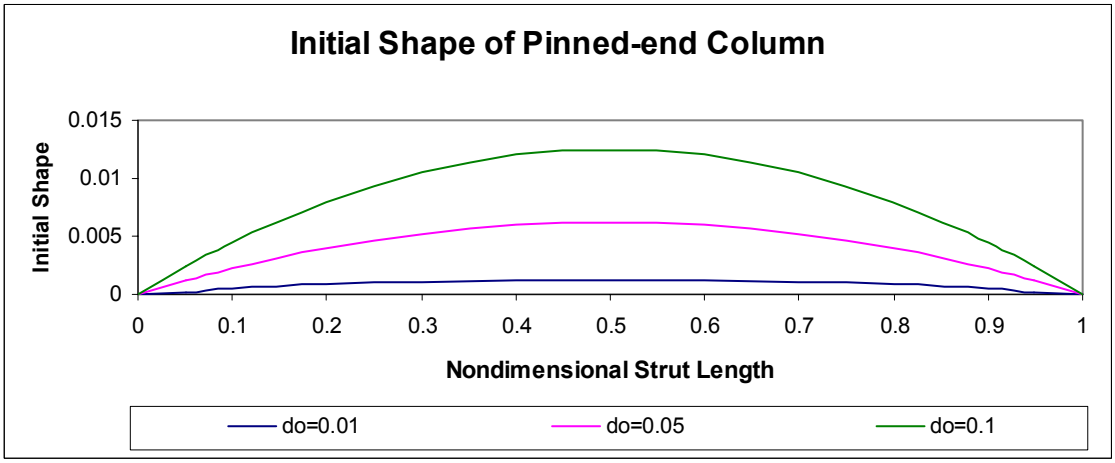

Figure 4.2.1: Initial Shape of Pinned-end Buckled Strut with Initial Curvature

The buckling load of the ideal pinned-end column is $p_o=\pi^2=9.87$. The strut will be examined under nondimensional loads of 2.5, 5, 7.5, and 10 to determine the response of the pre-bent strut at smaller loads in addition to a load above buckling.

4.3 Numerical Solution of a Pinned-end Column with Initial Curvature in Static Equilibrium

Due to the initial curvature of the strut, the static equilibrium equations are not the same as for the ideal column. The equation for curvature is affected by the initial curvature in the strut. The following equations can be established from the static equilibrium of the curved strut:

$$\frac{dx}{ds} = \cos\theta \tag{4.2}$$

$$\frac{dy}{ds} = \sin\theta \tag{4.3}$$

$$\frac{d\theta}{ds} = m + \frac{d\theta_o}{ds} = m - d_o \tag{4.4}$$

$$\frac{dm}{ds} = -p_o \sin\theta + q\cos\theta \tag{4.5}$$

As shown in Figure 4.1.1, the pinned-end strut has the same boundary conditions that were established in Chapter 2. They are:

At s=0: x=0, y=0, m=0

At s=1: y=0, m=0.

There are no end moments for the pinned-end strut. The load and amplitude of the initial curvature are used as input for the Mathematica program, and an initial guess is made for the shear force, q. The program uses the shooting method to obtain the internal variables of the strut due to the input load. Iterations may be necessary if the program fails to converge to the ordered accuracy. The Mathematica code for this program can be found in Appendix C.1.

Because these models are examined at loads above and below the buckling load, the shape of the strut before the application of dynamic motion will depend on the initial curvature and the supported load. Some examples can be seen in Figure 4.3.1 for the nondimensional loads of 2.5, 5, 7.5, and 10 and an initial curvature amplitude of d_o=0.05. As the initial amplitude of the strut increases, the deflected shape of the strut is more dramatic. Additional plots of the deflected shapes of struts with other initial curvatures can be found in Appendix C.2.

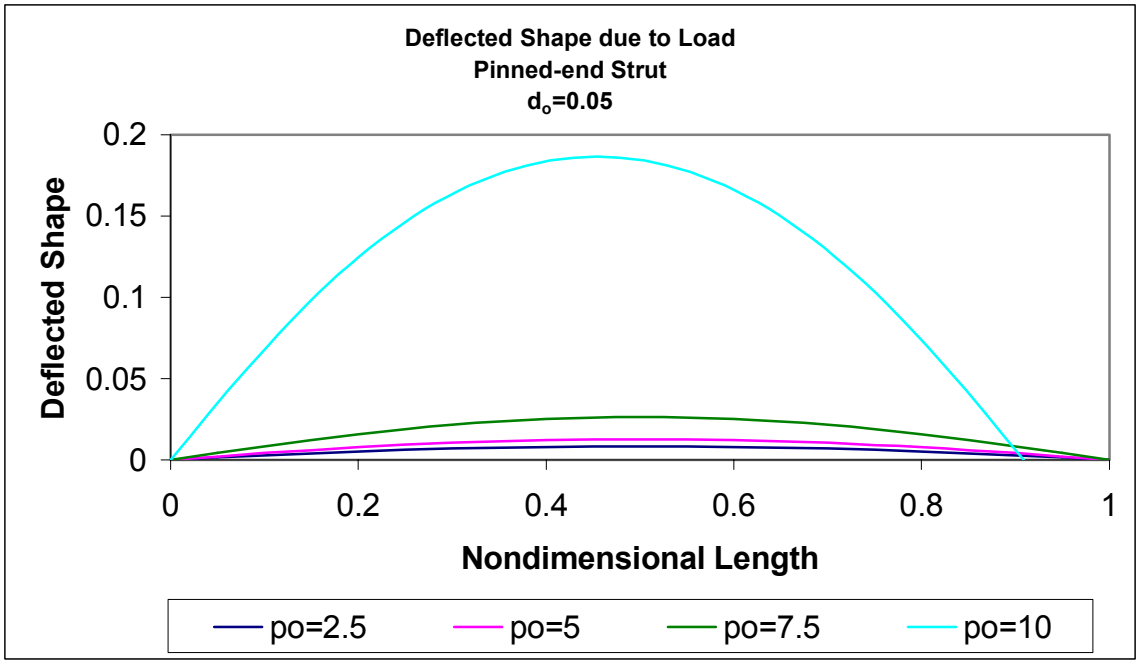

Figure 4.3.1: Deflected Shape of Pinned-end Strut with do=0.05

The values for the maximum mid-span deflection and end shortening for the strut with an amplitude of initial curvature d_o=0.05 can be seen in Table 4.1, where max y is defined as y(0.5) and end shortening is defined by 1-x(1). It is obvious from these values that as the load increases, the mid-span and vertical deflections increase, with the most deformation occurring after the buckling load is reached. Tables showing the mid-span and vertical deflections for other struts can be found in Appendix C.2.

Table 4.3.1: Maximum Mid-span Deflection and End Shortening Values for d_o=0.05

p_o	max y	End shortening
0	0.00625	0.000104
2.5	0.008431	0.000186
5	0.012807	0.000421
7.5	0.02656	0.001773
10	0.186421	0.091126

In Figure 4.3.2, the maximum deflection of the strut is plotted as the supported load is increased. The maximum deflection occurs at mid-span, as indicated on the plot. As

shown in the figure, when the load is zero, the mid-span deflection is only that due to the initial curvature. For the strut whose amplitude of initial curvature is d_o=0.05, the midspan deflection under zero load is about 0.006. This deflection represents about 0.6% of the length of the strut. When the amplitude of the initial curvature is low, the strut has very little deflection as the load is increased, until the load approaches the nondimensional buckling load of 9.87. As the load approaches the buckling load, the deflection increases dramatically. As the amplitude of the initial curvature increases, the strut tends to have higher deflections at lower loads. This is expected since the smaller the initial curvature, the closer the column is to ideal. Thus, it will support more load without significant deflection until buckling is achieved.

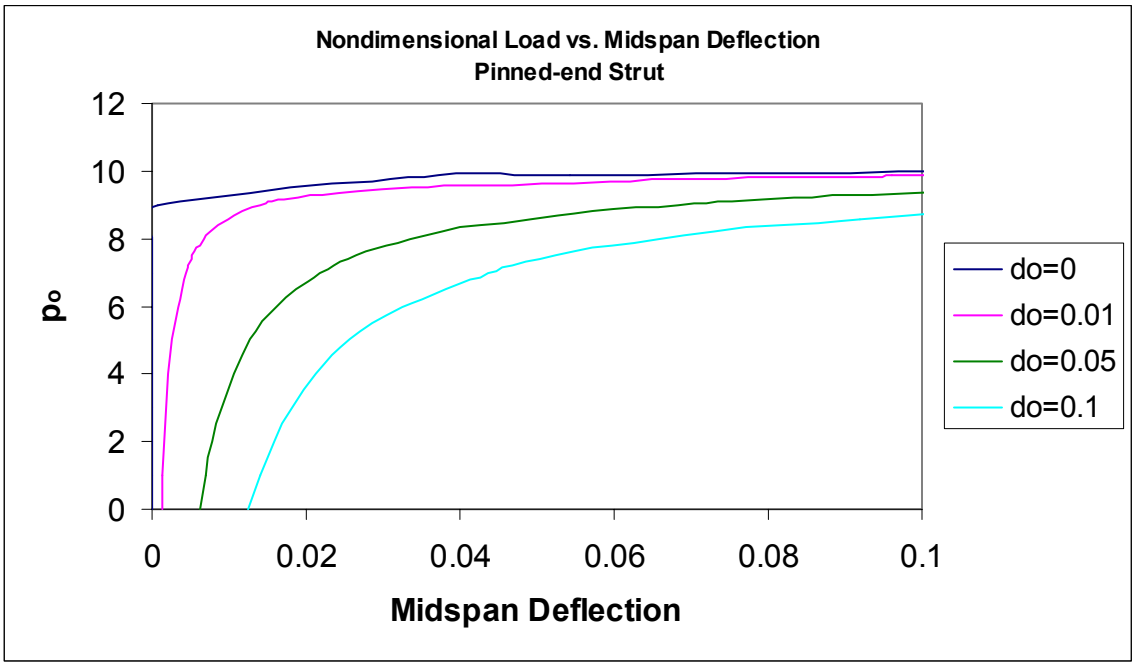

Figure 4.3.2: Nondimensional Load vs. Midspan Deflection

It is interesting to see how much the struts deflect vertically due to the initial curvature, as well. This vertical deflection, known as end shortening, can be seen in Figure 4.3.3. Similar to the results of the midspan deflection, Figure 4.3.3 shows how increasing the initial curvature of a strut will increase the vertical deflection of the strut under loading. At a given load below the critical load, when the amplitude of the initial curvature is 0.1,

the vertical deflection is much greater than for the strut with an amplitude of initial curvature of 0.01.

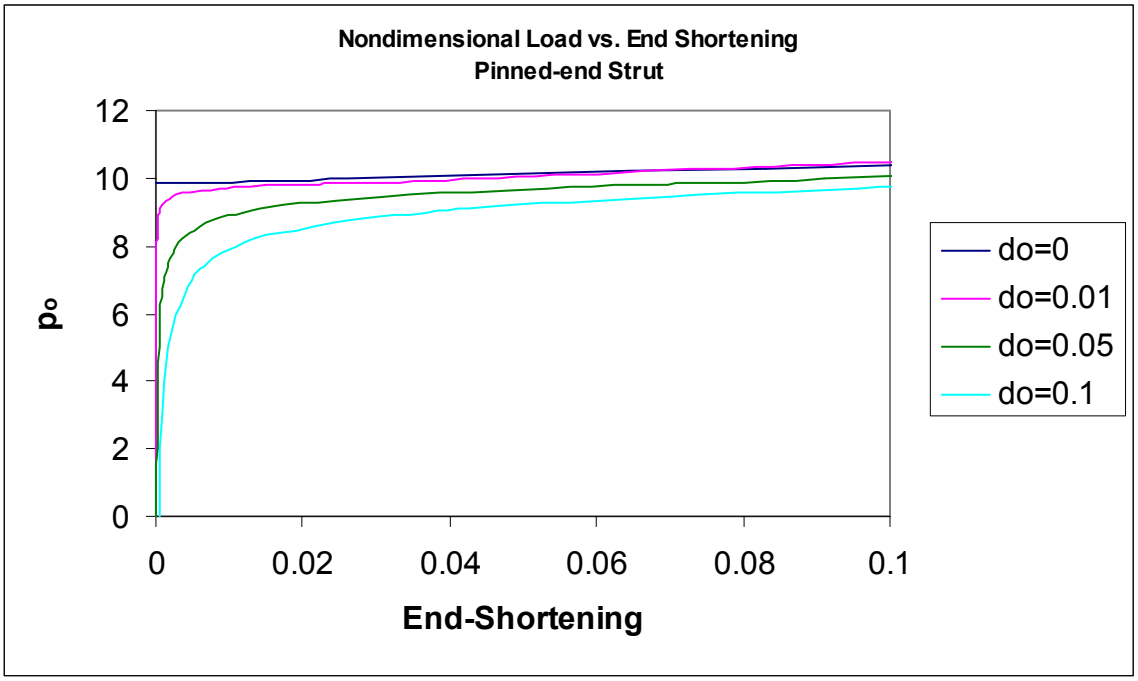

Figure 4.3.3: Nondimensional Load vs. End Shortening

Depending on the applied load and amplitude of the initial curvature, the resulting slope at s=0, determined from the numerical solution, is used in the dynamic analysis.

4.4 Forced Vibration of a Pinned-end Strut with Initial Curvature due to Harmonic Base Motion

The dynamic excitations applied to the curved strut are axial, harmonic vibrations. The vibrations are assumed to be small, and the steady-state response is examined. The response of the strut is determined from the equations of static equilibrium (4.2-4.5) and the following equations for dynamic equilibrium (with q_e=0):

$$\frac{dx_d}{ds} = -\theta_d \sin\theta_e \tag{4.6}$$

$$\frac{dy_d}{ds} = \theta_d \cos\theta_e \tag{4.7}$$

$$\frac{d\theta_d}{ds} = \frac{m_d}{(1+i\omega\gamma)} \tag{4.8}$$

$$\frac{dm_d}{ds} = (q_d - p_o\theta_d)\cos\theta_e - (p_d + q_e\theta_d)\sin\theta_e \tag{4.9}$$

$$\frac{dp_d}{ds} = (\omega^2 - i\omega c)x_d \tag{4.10}$$

$$\frac{dq_d}{ds} = (\omega^2 - i\omega c)y_d \tag{4.11}$$

The dynamic equations that describe the model are not affected by the initial curvature; only the equation for curvature from the static analysis is altered.

4.5 Numerical Solution of a Pinned-end Buckled Strut with Initial Curvature Under Forced Vibrations

The numerical solution of the pre-bent strut is solved using Mathematica. The static and dynamic equations are used, and the program shoots for a set of specified conditions. The boundary conditions for the pinned-end model are:

At s=0: $x_d = u_o$, y_d=0, m_d=0

At s=1: y_d=0, m_d=0, $p_d = -rp_o\omega^2 x_d$

The known values of p_o, u_o, r, c, ω, and $\theta_e(0)$ are used as input, and initial guesses are made for $p_d(0)$, $q_d(0)$, and $\theta_d(0)$. All cases examined for this model do not include internal damping, thus γ=0. Iterations are completed when sufficient convergence has been obtained for the boundary conditions at the end s=1 of the strut. The Mathematica program can be found in Appendix C.3.

The transmissibility for the strut is defined as:

$$TR = \frac{\sqrt{\{Re[x_d(1)]\}^2 + \{I_m[x_d(1)]\}^2}}{|u_o|} \tag{4.12}$$

The resonant frequency, ω_n, can be found for the undamped case when the transmissibility is infinite. The transmissibility is found over a wide range of frequencies to accurately represent the response of the strut. Results are plotted using Excel.

4.6 Results for Forced Vibrations of the Pinned-end Strut with Initial Curvature

The first set of plots show the Transmissibility versus Frequency for selected cases of the pre-bent strut. The stiffness parameter, damping coefficient, curvature, and loading are varied. Also, several cases will be compared to the ideal column results to show the effect of the initial curvature on the response. Additional plots can be found in Appendix C.4.

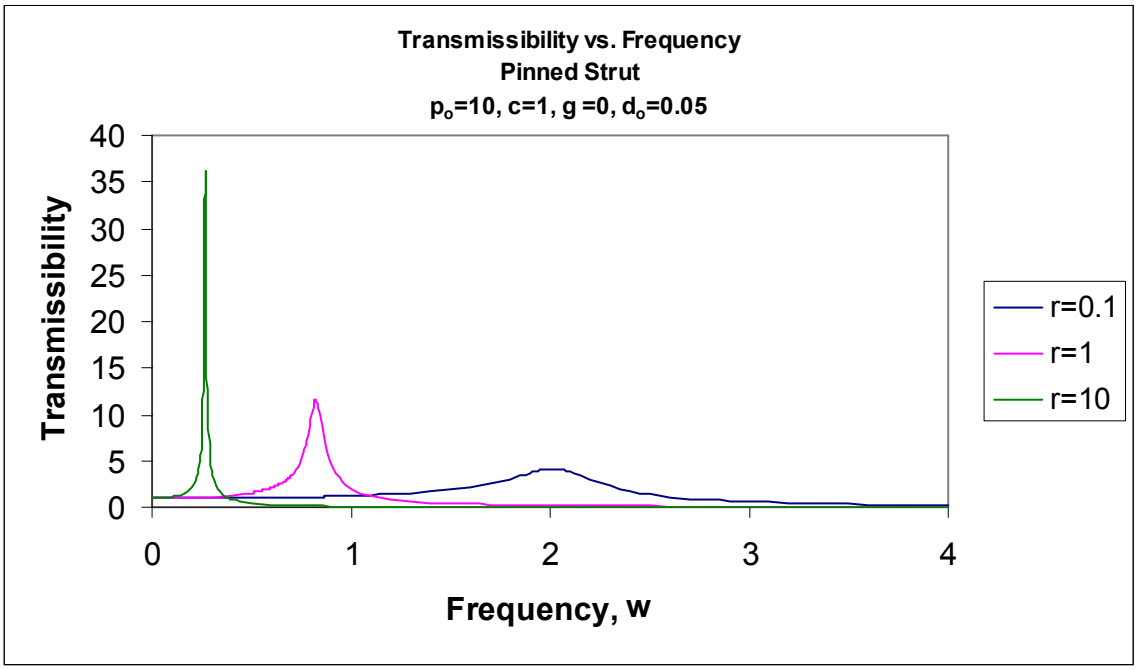

Figure 4.6.1: Transmissibility vs. Frequency for p_o=10, c=1, γ=0, d_o=0.05

Figure 4.6.1 shows the results of a strut with an amplitude of initial curvature of 0.05. The strut supports a load of 10, and the damping coefficient is 1. The results demonstrate the same trends as the ideal case. For instance, the maximum transmissibility increases as the stiffness parameter increases. Also, the range of frequencies that produce a high transmissibility decreases as the stiffness parameter increases, and the nondimensional

resonant frequency is lower when the stiffness is greater (although the dimensional frequency will be higher). The plot mimics the results for the ideal case. However, it is clear in Figure 4.6.2 that the results for the two cases are not the same. The results for the strut with a stiffness parameter of r=1 are shown for the pre-bent strut and the ideal column. It is evident that the initial curvature has a large effect on the maximum transmissibility. The maximum transmissibility for the pre-bent strut is over three times as high as for the ideal case. Also, the damped resonant peak occurs at a slightly lower frequency for the ideal case. The negative effects of the initial curvature can already be seen in the comparison of these two struts.

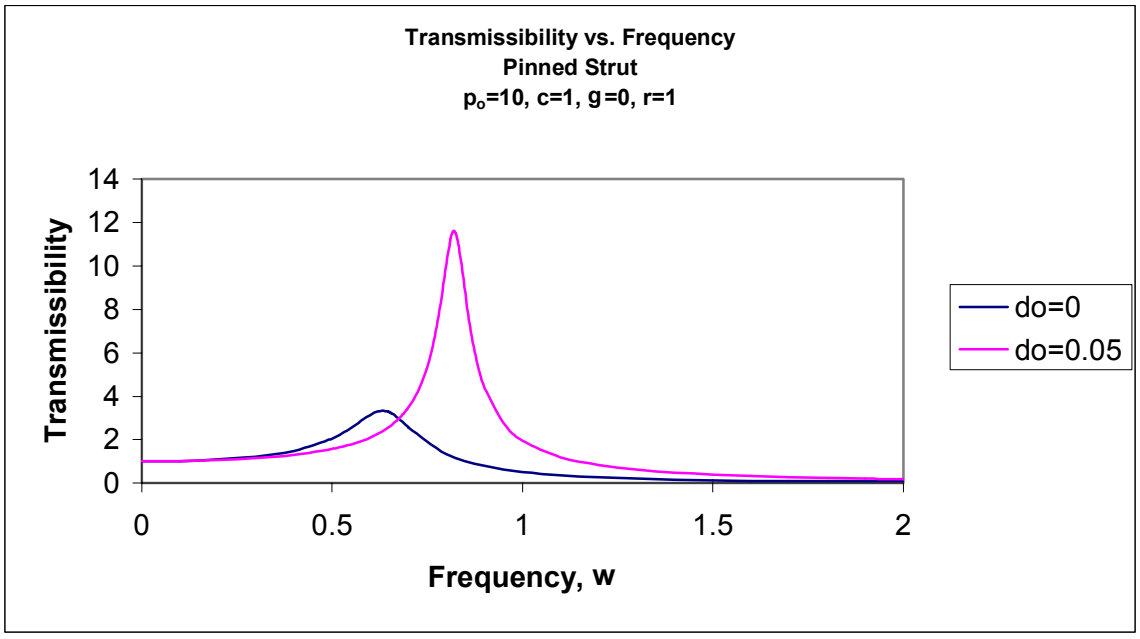

Figure 4.6.2: Transmissibility vs. Frequency for po=10, c=1, γ=0, r=1

Figure 4.6.3 graphs the effect of the stiffness parameter on the maximum transmissibility for the system with p_o=10, c=1, γ=0, and d_o=0.05. As the stiffness parameter increases, the maximum transmissibility grows, with a decreasing rate. This increase in maximum transmissibility due to increased stiffness has been apparent in previous graphs as well.

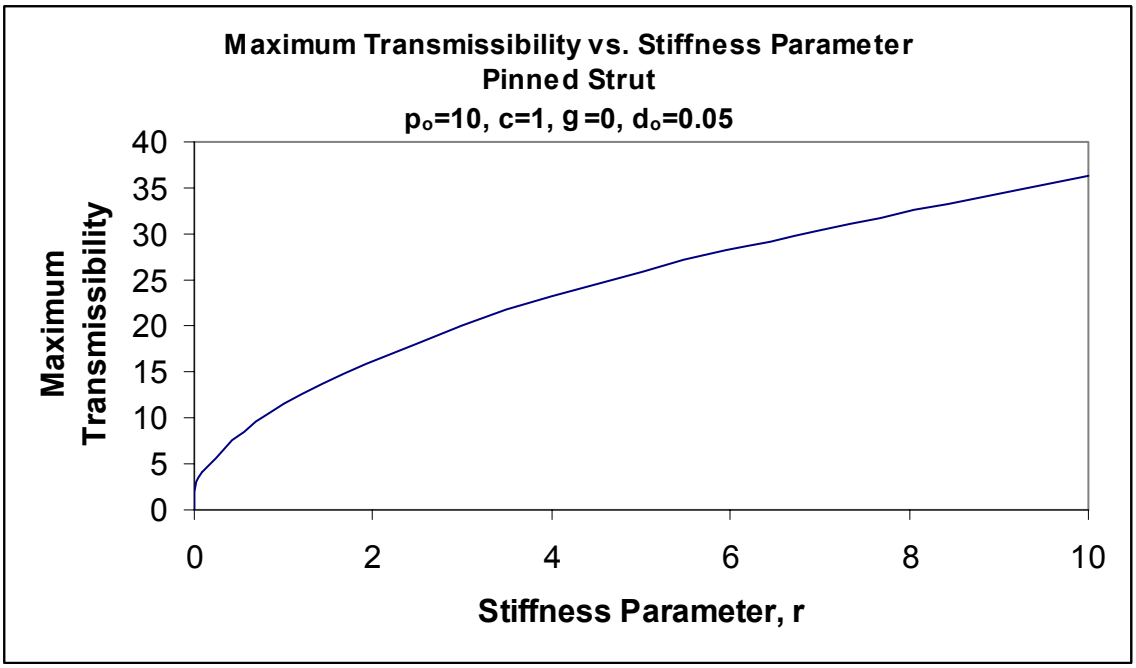

Figure 4.6.3: Maximum Transmissibility vs. Stiffness Parameter for p_o=10, c=1, γ=0, d_o=0.05

Also, the relationship between the resonant frequency and the stiffness parameter can be seen in Figure 4.6.4. The location of the resonant frequency is found by applying a range of frequencies until the damped resonant peak is found. The frequencies shown in Figure 4.6.4 are found over a range of stiffness parameter values. As the stiffness parameter increases, the resonant frequency decreases. Initially the rate of change of the resonant frequency is large, but once the stiffness parameter is approximately 2, the rate of change of the resonant frequency is not as drastic.

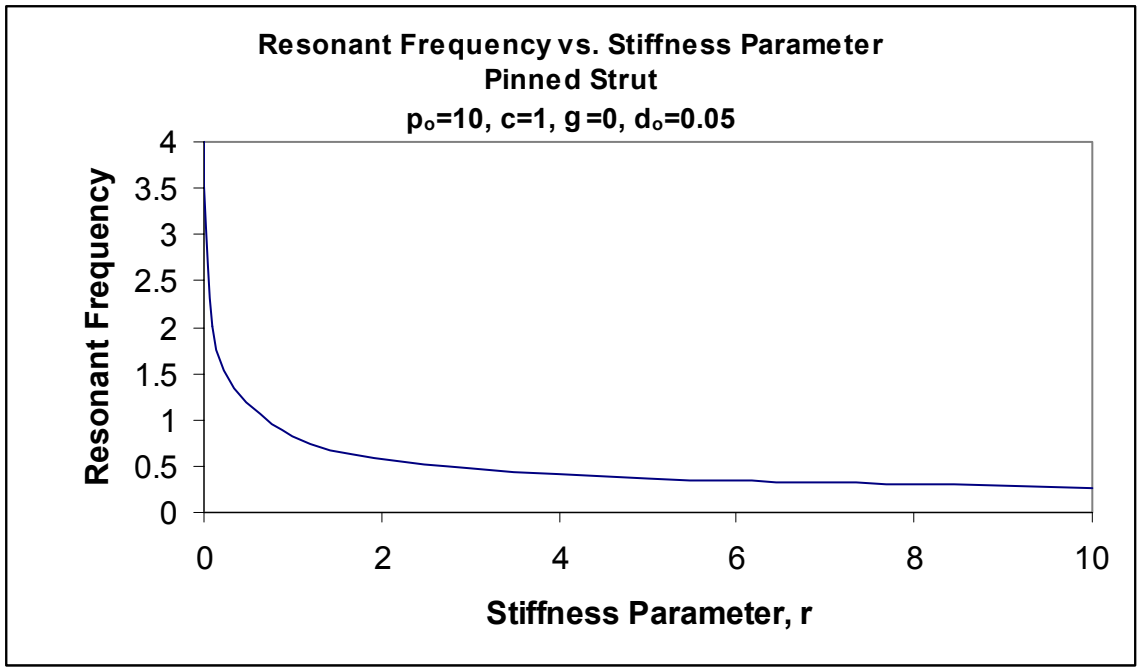

Figure 4.6.4: Resonant Frequency vs. Stiffness Parameter for p_o=10, c=1, γ=0, d_o=0.05

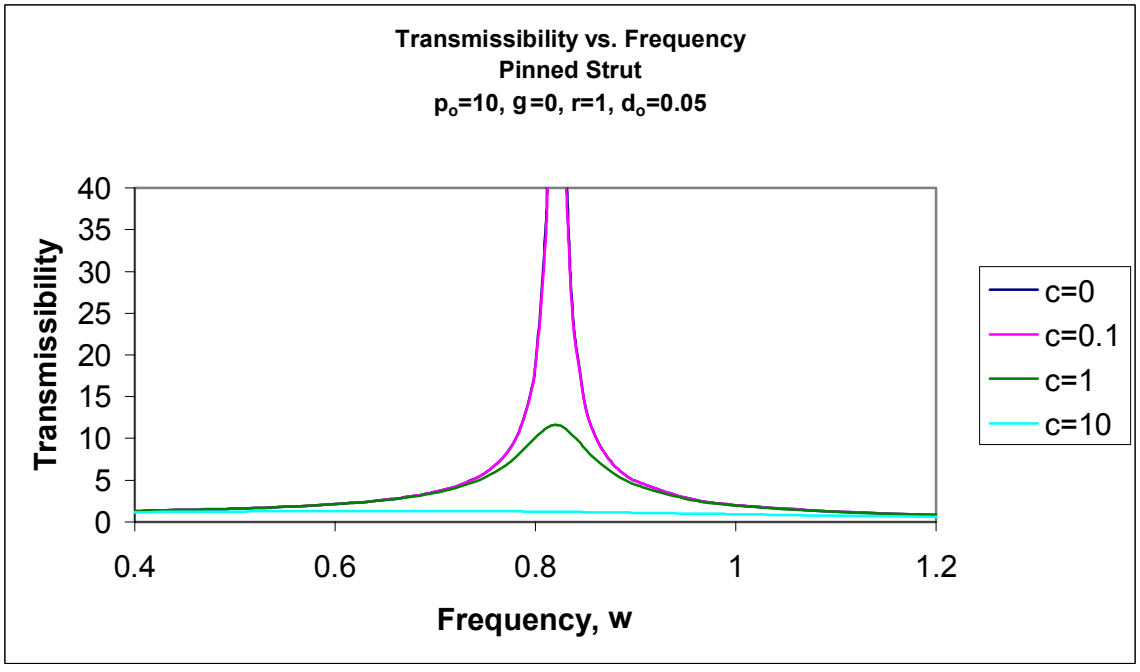

Figure 4.6.5: Transmissibility vs. Frequency for p_o=10, γ=0, r=1, d_o=0.05

Figure 4.6.5 shows the results of a strut with varying degrees of damping. As usual, as the damping coefficient increases, the maximum transmissibility of the strut decreases. It

is interesting to compare these results with the ideal case, also. Figure 4.6.6 compares the pre-bent column to its ideal counterpart for a strut with a damping coefficient of c=0.1. Again, the maximum transmissibility is much higher for the pre-bent case. Also, the damped resonant peak occurs at a lower nondimensional frequency for the ideal case. Additional damping would need to be added if the maximum transmissibility were to be reduced to that of the ideal case.

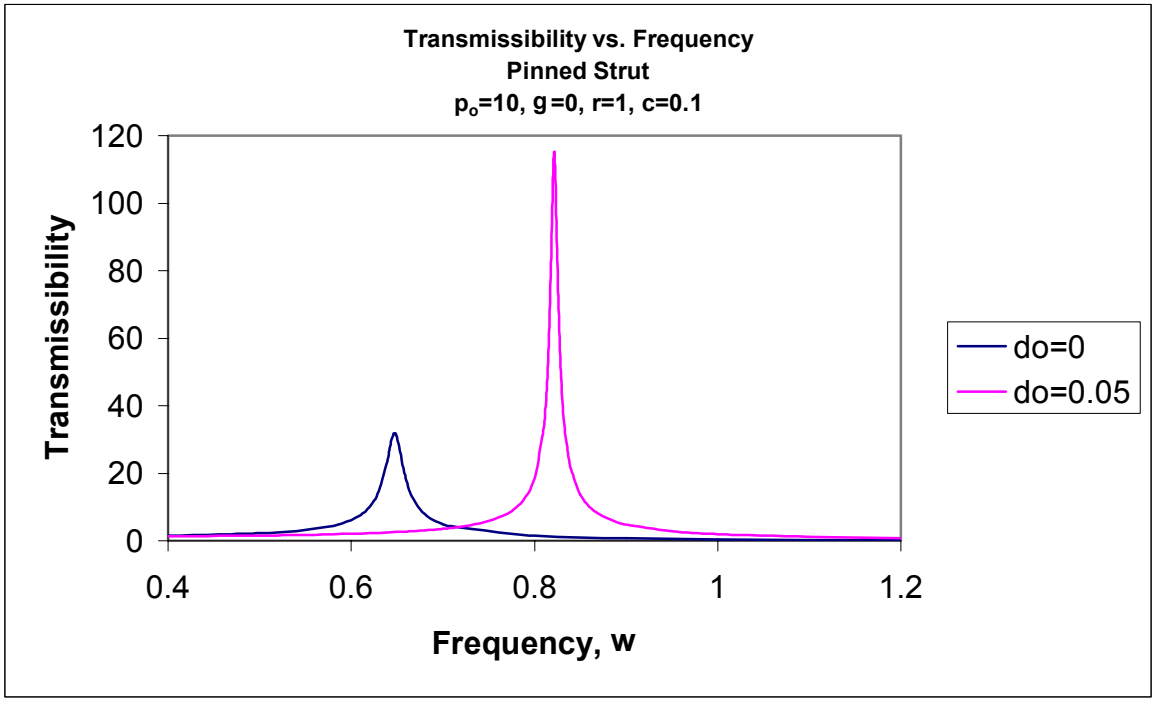

Figure 4.6.6: Transmissibility vs. Frequency for p_o=10, γ=0, r=1, c=0.1

The relationship between the damping coefficient and the maximum transmissibility can be seen directly from Figure 4.6.7. The system is analyzed with p_o=10, γ=0, and d_o=0.05. As the damping coefficient increases, the maximum transmissibility is reduced. Since the transmissibility of an undamped system, when c=0, is infinite, it is apparent that even with a small amount of damping, the maximum transmissibility is greatly reduced. Also, the relative effects of several stiffness parameter values can be seen. When r=0.1, the maximum transmissibility is reduced to a greater extent with less damping than for the case when r=10. The greatest difference between the three stiffness parameter values is at lower damping values. However, as the damping increases, the maximum

transmissibilities of the three systems become more constant despite the increasing damping coefficient.

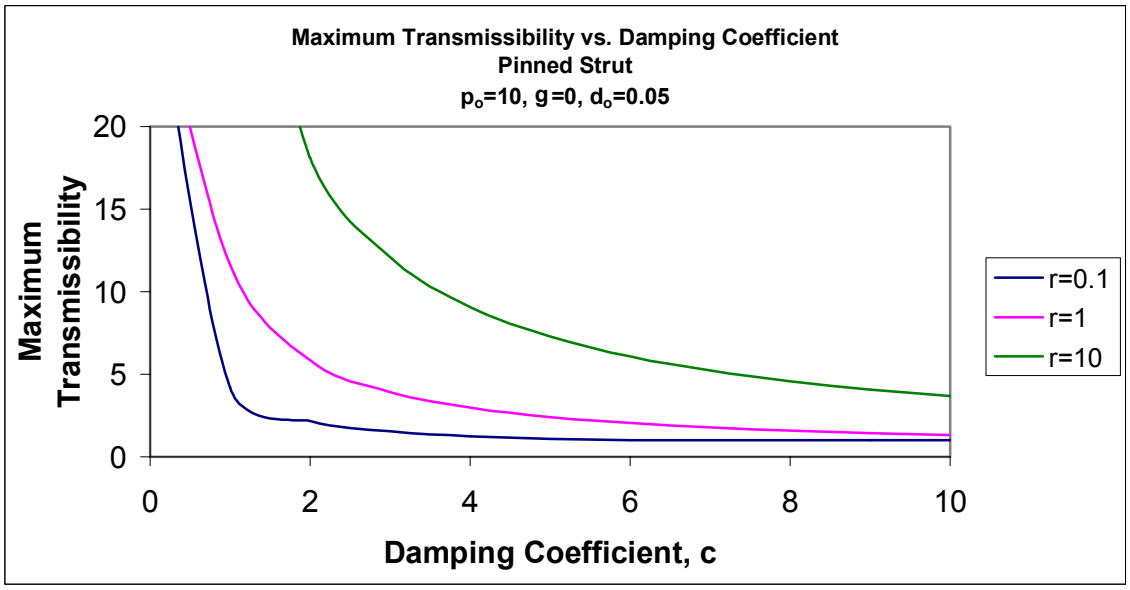

Figure 4.6.7: Maximum Transmissibility vs. Damping Coefficient for p_o=10, γ=0, d_o=0.05

Figure 4.6.8 shows the effect of the damping coefficient on the resonant frequency for several stiffness parameter values. It is obvious that when the stiffness parameter is lower, the resonant frequency is higher if the damping coefficient is small. The curves describing the results for stiffness parameters of r=1 and r=10 show that the resonant frequency may decrease slightly as the damping is increased, but not significantly, in the range shown. The case for r=0.1 is interesting because it displays the result for a system which has become overdamped. The resonant frequency is zero when the damping coefficient is about 7. This means that no matter what frequency of motion is applied to the strut, the motion will always be reduced when the damping coefficient is 7 or greater. This would be an ideal situation, but an overdamped system is typically impractical.

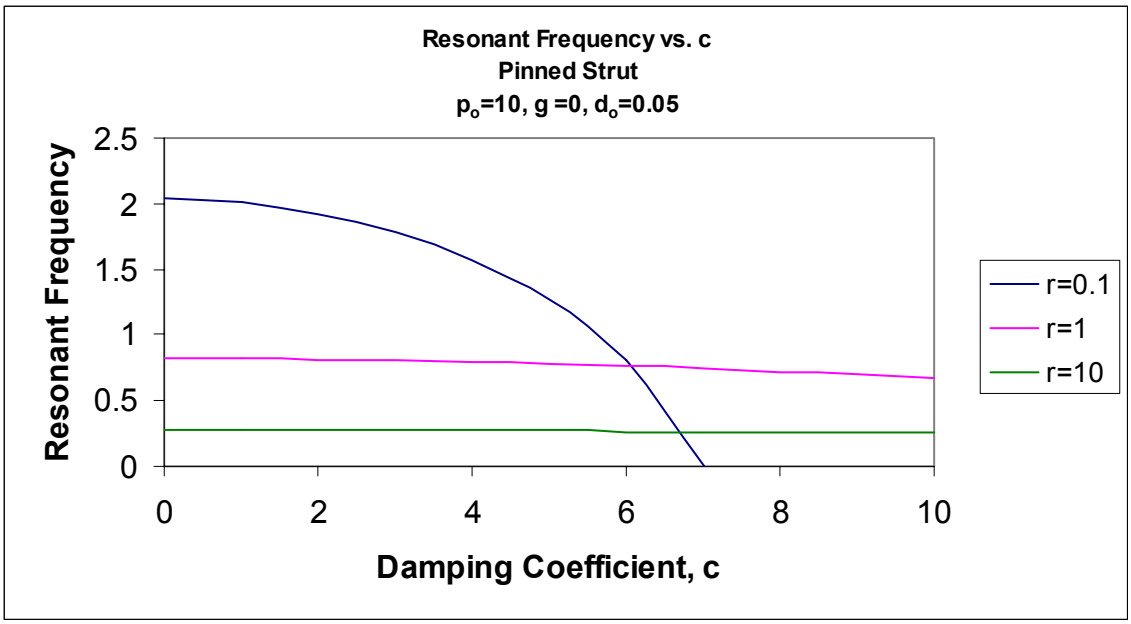

Figure 4.6.8: Resonant Frequency vs. Damping Coefficient for p_o=10, γ=0, d_o=0.05

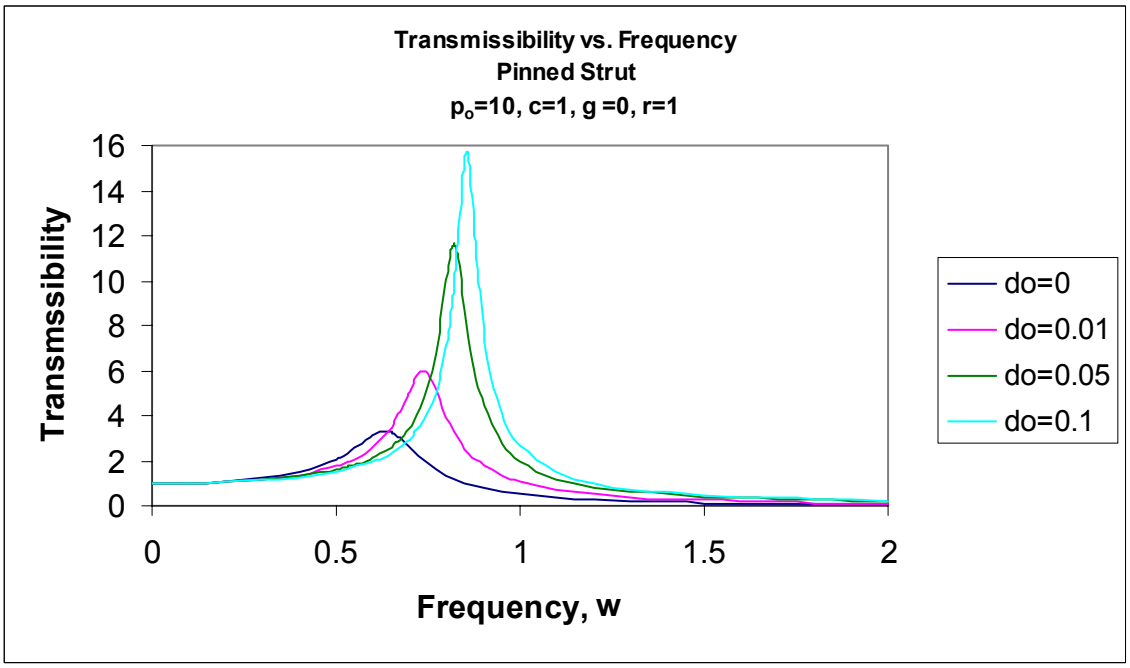

Figure 4.6.9: Transmissibility vs. Frequency for p_o=10, c=1, γ=0, r=1

Previously, the effect of the amplitude of the initial curvature on the static response of the strut was discussed. The amplitude of the initial curvature is also instrumental in the dynamic response of the strut. In Figure 4.6.9, the transmissibility of the strut is shown for different initial curvatures. When the strut has no initial curvature, the peak

transmissibility is minimized, and the damped resonant peak occurs at a low frequency. However, as the amplitude of the curvature is increased, the resonant frequency gradually increases, and the peak transmissibility of the supported load increases. This supports the results of the previous plots, as well. It is obvious that as the initial curvature of the strut increases, the strut becomes less effective in mitigating the vibrations. Thus, it is desirable that the struts be well fabricated and have minimum camber.

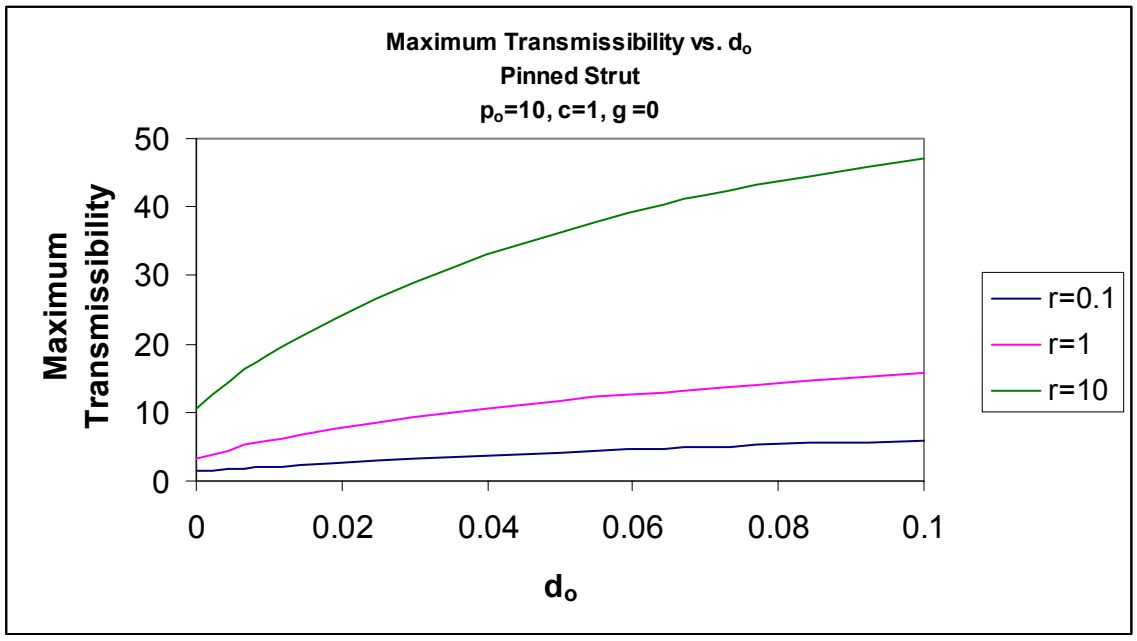

Figure 4.6.10: Maximum Transmissibility vs. d_o for p_o=10, c=1, γ=0

The effect of the amplitude of initial curvature on the maximum transmissibility can be seen directly in Figure 4.6.10. The maximum transmissibility for the system increases as the amplitude of initial curvature increases. The increase is more profound as the stiffness parameter increases, and it is not so obvious when the stiffness parameter is low.

Figure 4.6.11 shows the resulting resonant frequency for an increasing amplitude of initial curvature. When the stiffness parameter is low, the nondimensional resonant frequency increases at a decreasing rate. When the stiffness parameter is high, the resonant frequency increases slightly, but tends to remain rather constant.

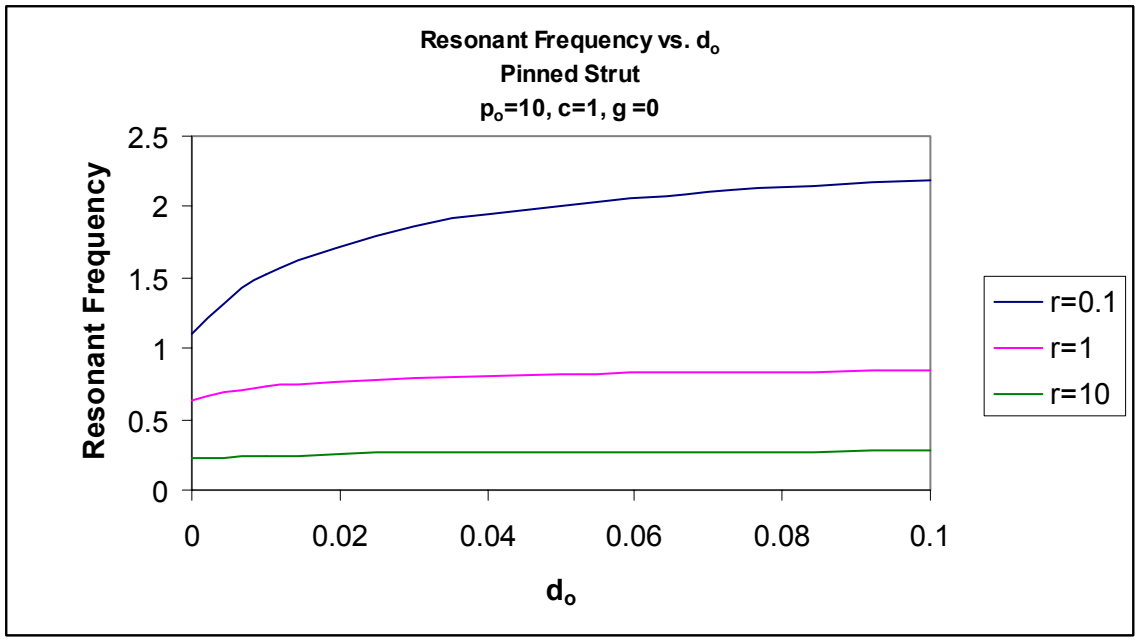

Figure 4.6.11: Resonant Frequency vs. d_o for p_o=10, c=1, γ=0

The next four plots display the results for a system with c=0.1, γ=0, r=1, d_o=0.05, and the load is varied. The nondimensional loads are 2.5, 5, 7.5, and 10. The axes are arranged differently on each plot so that certain features are easily viewed.

Figure 4.6.12 shows the fundamental resonant frequency for the system under the four different loads. It is obvious that the strut with the lowest fundamental frequency is the strut supporting the load of p_o=10. As the load decreases, the fundamental resonant frequency increases. The strut supporting a load above the buckling load is most effective since the goal is to reduce the resonant frequency in order to increase the working range of the strut. The maximum transmissibility is reduced when the load is lower. However, the transmissibility could be reduced with additional damping for the strut supporting the highest of these loads.

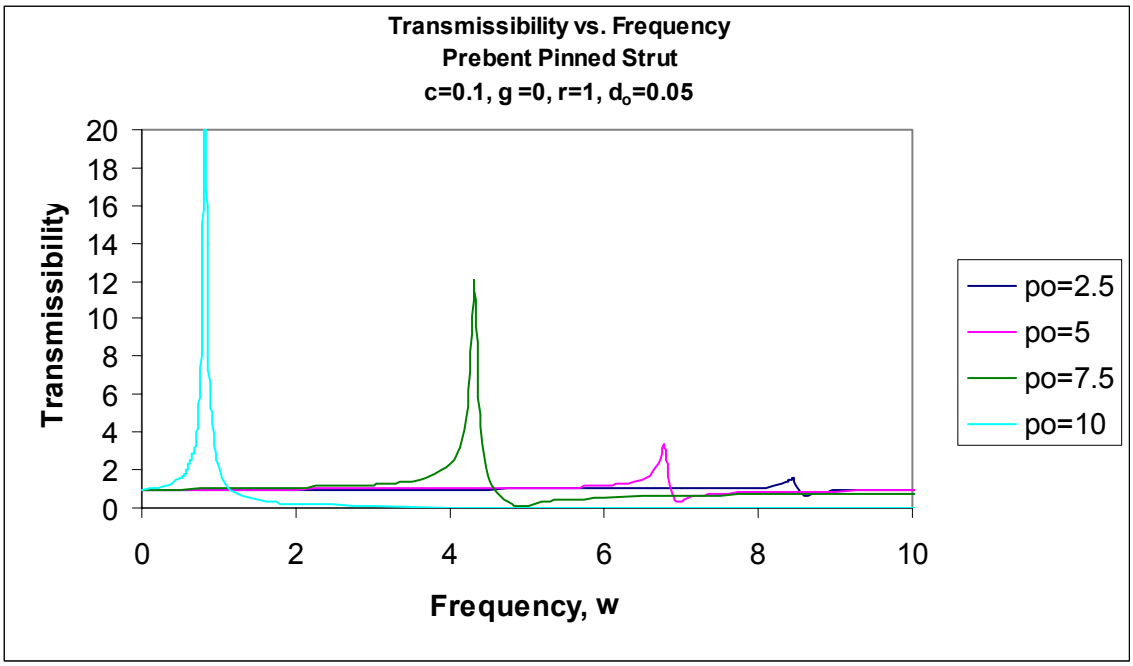

Figure 4.6.12: Transmissibility vs. Frequency for c=0.1, γ=0, r=1, d_o=0.05

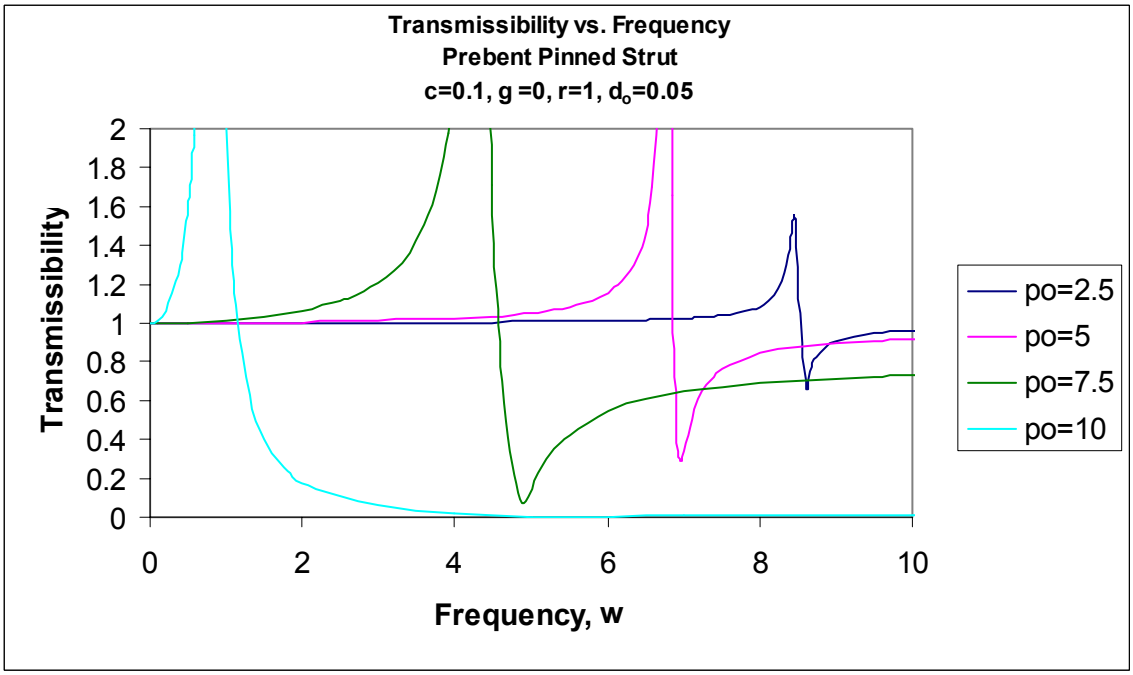

Figure 4.6.13: Transmissibility vs. Frequency for c=0.1, γ=0, r=1, d_o=0.05

Figure 4.6.13 shows the same system with the Y-axis displaying only low transmissibilities. This view is of interest since it is easier to see exactly when the strut motion is reduced, or the transmissibility falls below 1. It is clear that the buckled strut reduces the motion at the lowest frequency. It is also interesting to see the response of the strut once the motion has been reduced. Initially, all of the struts reduce the transmissibility after the resonant peak, but the three struts supporting loads of 2.5, 5, and 7.5 are not able to sustain the reduced motion. For instance, the strut supporting the load of 7.5 is able to reduce the motion to a transmissibility of about 0.1, but gradually the motion increases and is sustained at a transmissibility of about 0.8. The buckled strut, however, reduces the motion almost entirely and without the gradual increase that is apparent with the other struts.

Several peaks can be seen in Figure 4.6.14 because the X-axis has been modified to show the results at higher frequencies. Clearly, the overall motion of the supported load is reduced the most by the buckled strut. The farther the load deviates below the buckling load, the less effective it is at reducing the motion.

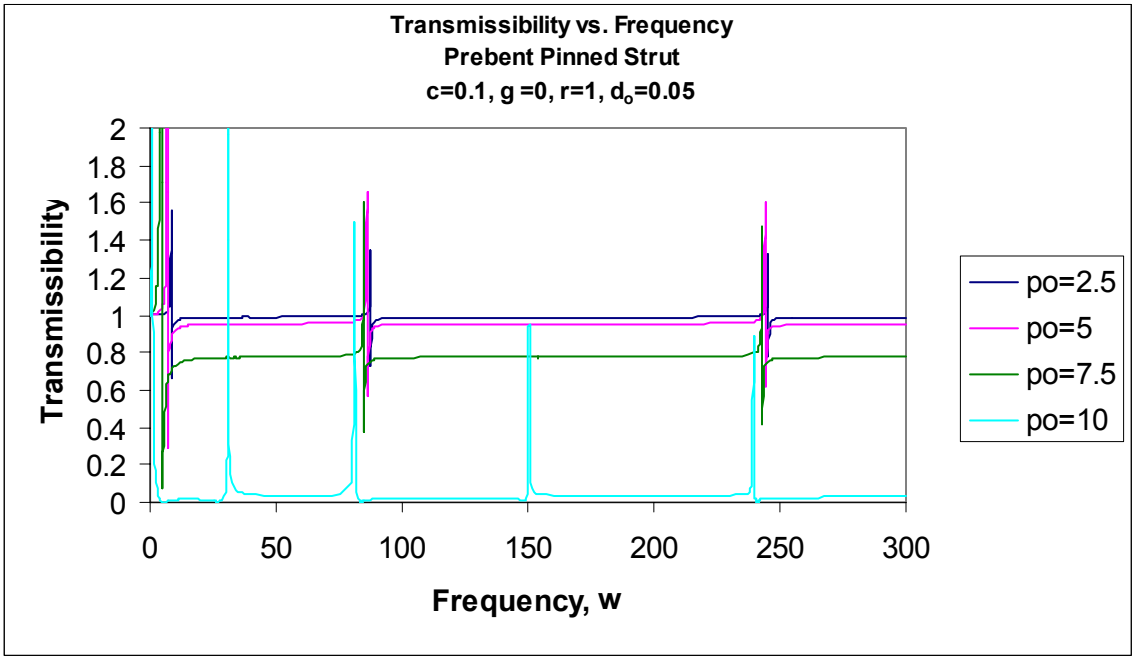

Figure 4.6.14: Transmissibility vs. Frequency for c=0.1, γ=0, r=1, d_o=0.05

It is clear that many peaks occur over this range of frequencies. Five peaks are evident for the case with p_o=10. There are also five peaks for the other cases, but two of the resonant peaks are so small in magnitude that they cannot be seen on this scale. The resonant peaks for these struts correspond to mode shape changes as the frequency is varied. Figure 4.6.15 shows the response for the struts with nondimensional loads of 5 and 10, and the mode shapes at various frequencies for these struts can be seen in Figures 4.6.16 and 4.6.17, respectively. Each resonant frequency corresponds to the change from one mode to the next. The gradual progression of the struts' mode shapes can be followed in Figures 4.6.16 and 4.6.17, and the corresponding transmissibility for the forcing frequency producing the mode shapes can be seen in Figure 4.6.15. The results for the two struts are similar, but there is one main difference: the absence of a large resonant peak for two of the mode changes in the strut supporting a load of p_o=5. When p_o=5, and the frequency is about 6.96, the strut depicts its first mode shape. As the frequency increases, the strut begins to transform into its second mode shape (ω=35). The second mode shape is achieved at the next resonant peak when ω=36.97. The second mode shape is an anti-symmetric mode, and does not produce a large response for the case when p_o=5. There is still a small peak due to this mode change, however. For the strut supporting a load of p_o=10, there is a large response at this mode change. When ω=31, there is an obvious peak. As the frequency increases, both struts continue changing mode shapes, with resonant peaks to mark the transformation. However, the strut supporting a load of p_o=5 does not yield a high transmissibility again when it changes from the third to the fourth mode shape. The fourth mode shape is also an anti-symmetric mode shape. The strut supporting a load of p_o=10 does produce a large resonant peak at this mode change. However, it is evident from the data that these small resonant peaks for the anti-symmetric mode shapes for the struts supporting the loads below the buckling loads tend to grow as the load approaches buckling. It is obvious from the figures that there is a large resonant peak when the load is above buckling. Despite the large resonant peaks present for the buckled strut, the transmissibility is still much lower between the peaks.

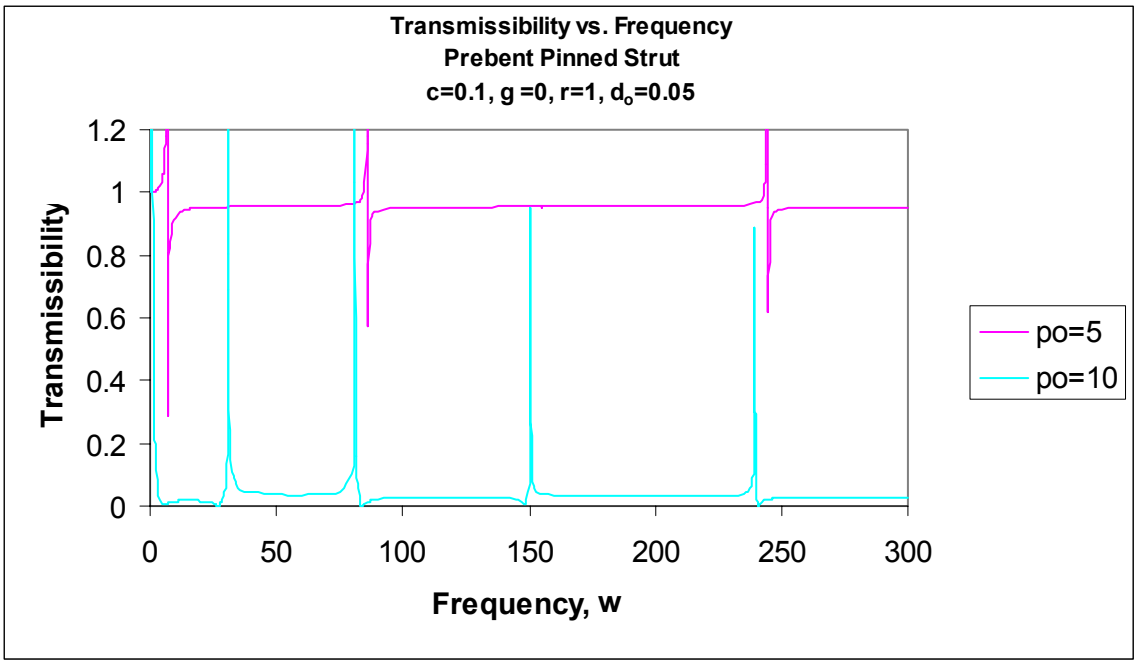

Figure 4.6.15: Transmissibility vs. Frequency for c=0.1, γ=0, r=1, d_o=0.05

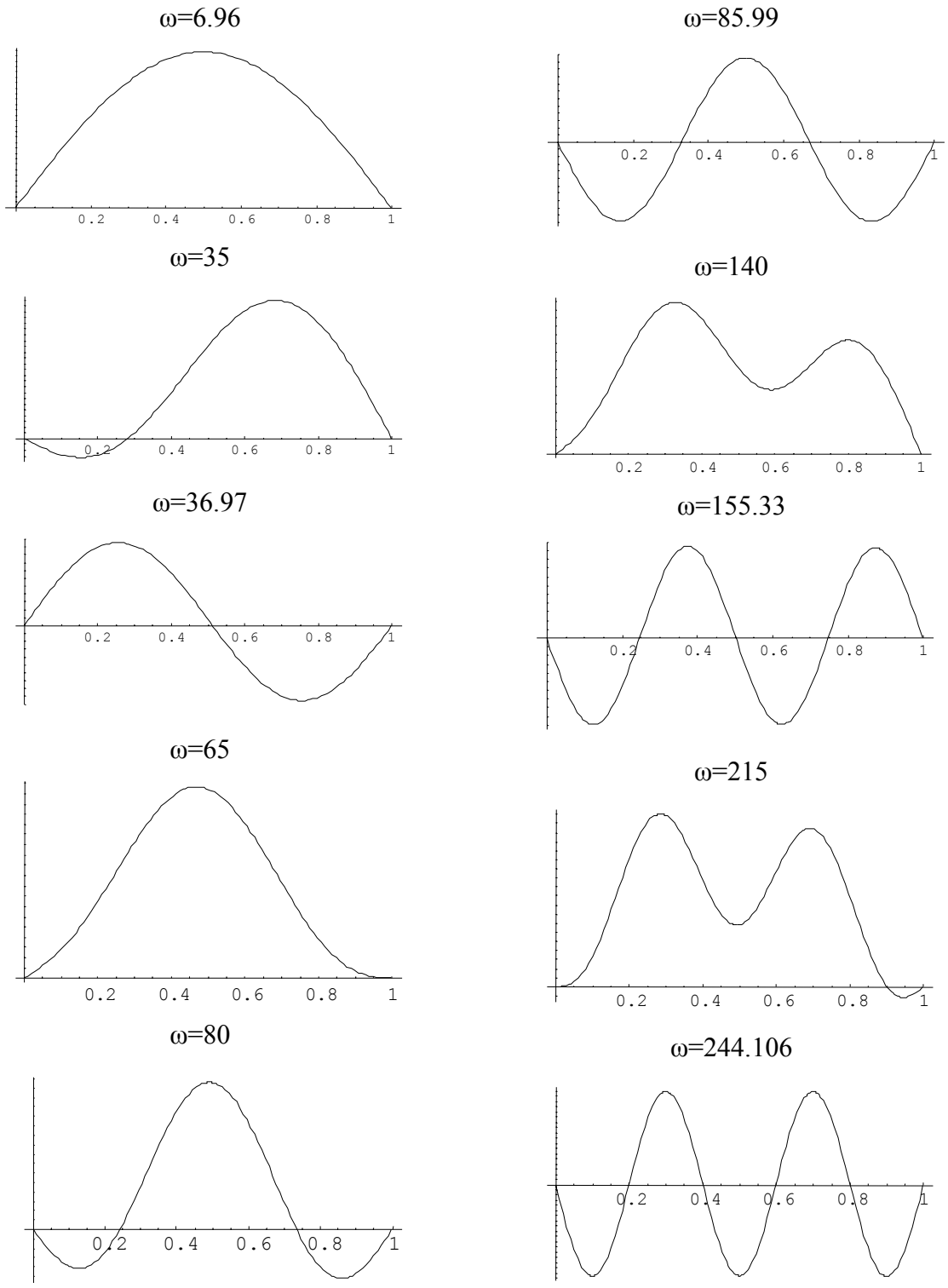

Figure 4.6.16: Mode Shapes for Various Frequencies for p_o=5

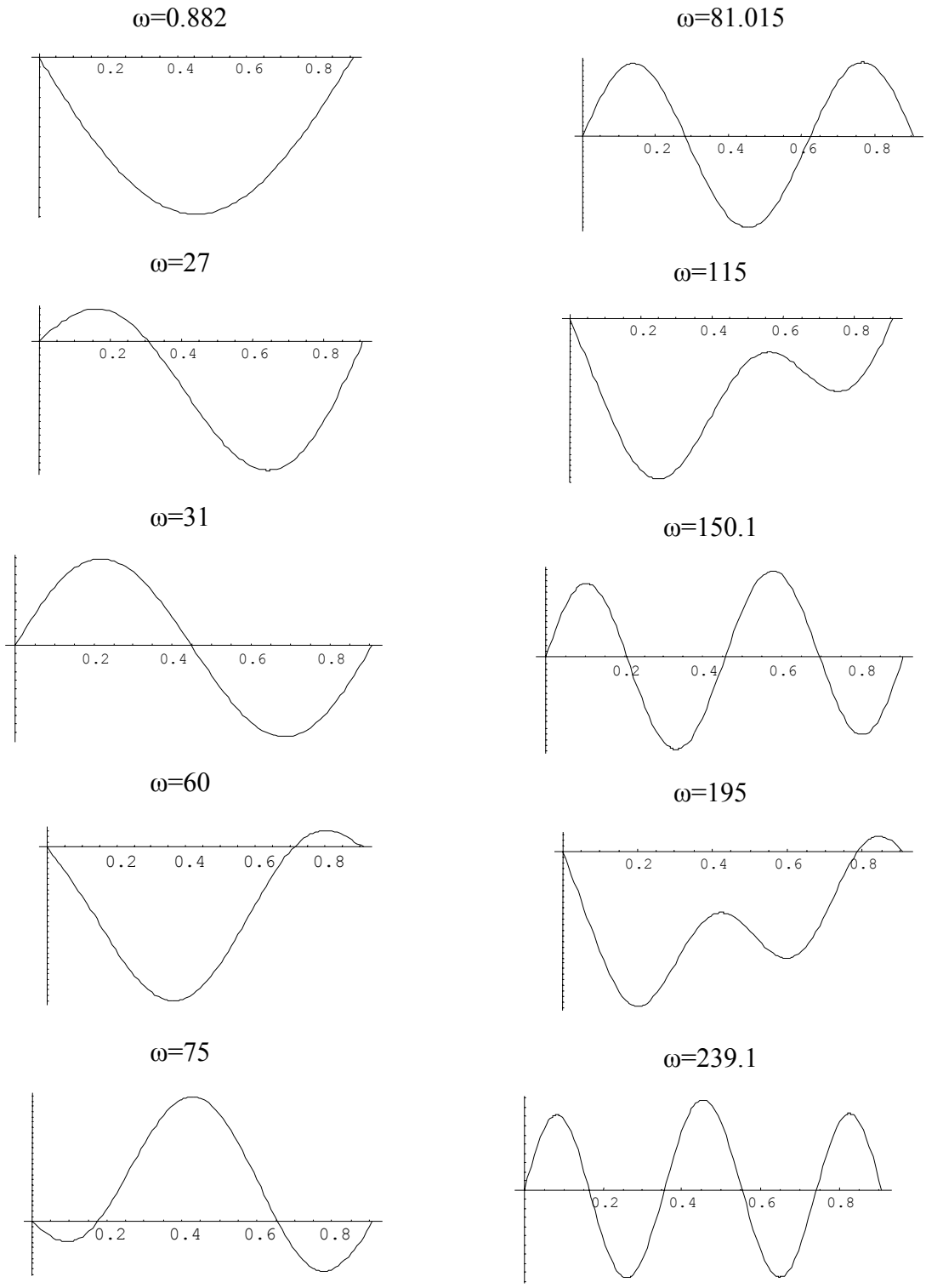

Figure 4.6.17: Mode Shapes for Various Frequencies for p_o=10

4.7 Conclusions

The results in this chapter delineate the efficacy of a pinned-end buckled strut with an initial curvature. Since no real column is ideal, this model helps to predict the response of a real column. The model was first analyzed to determine the effect of the initial curvature on the static equilibrium of the strut supporting various loads. Obviously, the larger the initial curvature, the larger the static displacement of the strut under a given load. The strut was examined for multiple initial curvatures and under multiple loads. Using the results from the static analysis, many cases were subjected to an axial, harmonic base motion, and the response was observed.

The damping coefficient and stiffness parameter influenced the strut in the same manner as in previous chapters. However, the exact response of the struts was compared to the ideal case, and several observations were made. First, it is apparent that the maximum transmissibility for the pre-bent strut tends to be much higher than for the ideal case. Also, the damped resonant peak occurs at a slightly lower frequency for the ideal case. As the damping coefficient increases, the maximum transmissibility is reduced, and the resonant frequency may decrease slightly, but not significantly.

Then, the effect of the initial curvature on the maximum transmissibility and resonant frequency was examined. Initially, the resonant frequency increases slightly, but as the curvature continues to increase, the resonant frequency tends to become constant. The maximum transmissibility for the system increases as the amplitude of initial curvature increases, and the increase is more profound when the stiffness parameter is high.

Since the strut has an initial curvature, loads above and below the buckling load are used. As the load decreases, the fundamental resonant frequency increases. The strut supporting a load above the buckling load is most effective, since the goal is to reduce the resonant frequency in order to increase the working range of the strut. The maximum transmissibility is reduced when the load is lower. However, a lower fundamental

frequency can be achieved with a buckled strut, and then the transmissibility can be reduced with additional damping.

Overall, the initial curvature of imperfect columns seems to have minimal effects on their ability to reduce vibrations if the column supports a load close to buckling. Therefore, it is important to ensure that the strut supports a load close to its buckling load in order to maximize its functionality as an isolator. Also, the initial curvature should be minimized, so that the column more closely parallels the ideal case.

Chapter 5: Fixed-end Column with Initial Curvature under Forced Harmonic Axial Excitation

5.1 Introduction

A fixed-end strut with an initial curvature subjected to axial, harmonic motion is to be discussed in this chapter. Again, the imperfect column is a more practical model since all real columns have imperfections due to fabrication. The fixed-end model will also be subjected to loads above and below its buckling load. The initial shape of the strut before loading can be seen in Figure 5.1.1. The results of the static analysis are presented first, followed by the dynamic response of the fixed-end strut due to harmonic base motion.

Figure 5.1.1: Undeformed Strut with Initial Curvature

5.2 Basic Assumptions and Formulations

The fixed-end strut will be given an imperfection by applying an equation to describe the shape of the strut before loading. The strut is assumed to be unstrained in its initial shape. The strut will be assigned an amplitude, a_o. For the fixed-end strut, the equations that describe the rotation and deflection of the strut are assumed as follows:

$$\theta_o(s) = a_o \sin 2\pi s \qquad y \approx \frac{a_o}{2\pi}(1-\cos 2\pi s) \quad \max y \approx \frac{a_o}{\pi} \tag{5.1}$$

Amplitudes of 0.01, 0.05, and 0.1 were applied to vary the severity of the initial curvature. The initial shapes of the strut with an amplitude of a_o=0.05 can be seen in Figure 5.2.1.

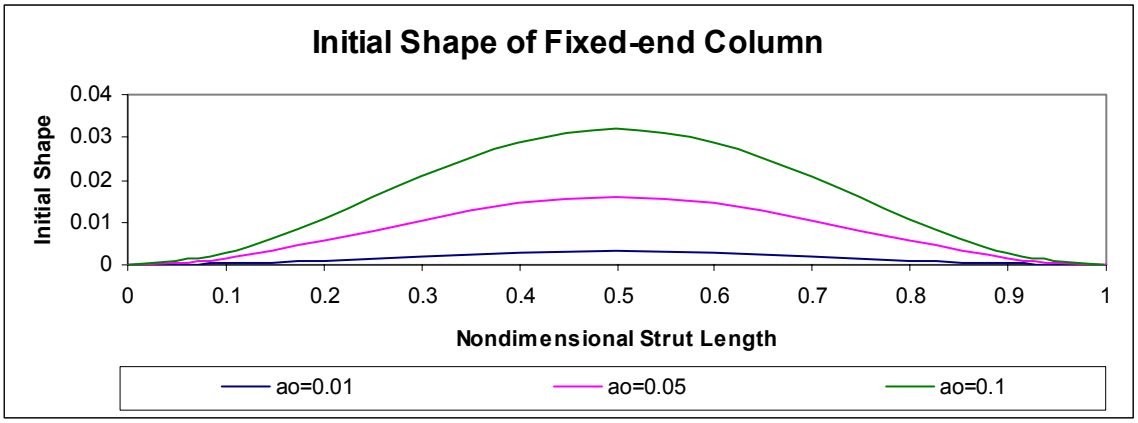

Figure 5.2.1: Initial Shape of Fixed-end Buckled Strut with Initial Curvature

The buckling load of the ideal fixed-end column is po=$4\pi^2$=39.48. The strut will be examined under nondimensional loads of 10, 20, 30, and 40 to determine the response of the pre-bent strut at smaller loads in addition to a load above buckling.

5.3 Numerical Solution of a Fixed-end Column with Initial Curvature in Static Equilibrium

The equation for curvature is affected by the initial curvature in the strut; therefore the following equations are established for the static equilibrium of the imperfect column:

$$\frac{dx}{ds} = \cos\theta \tag{5.2}$$

$$\frac{dy}{ds} = \sin\theta \tag{5.3}$$

$$\frac{d\theta}{ds} = m + \frac{d\theta_o}{ds} = m + 2\pi a_o \cos 2\pi s \tag{5.4}$$

$$\frac{dm}{ds} = -p_o \sin\theta + q\cos\theta \tag{5.5}$$

The fixed-end strut has the same boundary conditions that were established in Chapter 3. They are:

At s=0: x=0, y=0, θ=0

At s=1: y=0, θ=0.

The load and the amplitude of the initial curvature are used as input for the Mathematica program, and an initial guess is made for the shear force, q. The program uses the shooting method to obtain the internal variables of the strut due to the input load. Iterations may be necessary if the program fails to converge to the ordered accuracy. The Mathematica code for this program can be found in Appendix D.1.

The shape of the strut before the application of dynamic motion will again depend on the supported load. One example can be seen in Figure 5.3.1 for the nondimensional loads of 10, 20, 30, and 40 and an initial curvature amplitude of a_o=0.05. Additional plots of the deflected shapes of struts with other initial curvatures can be found in Appendix D.2.

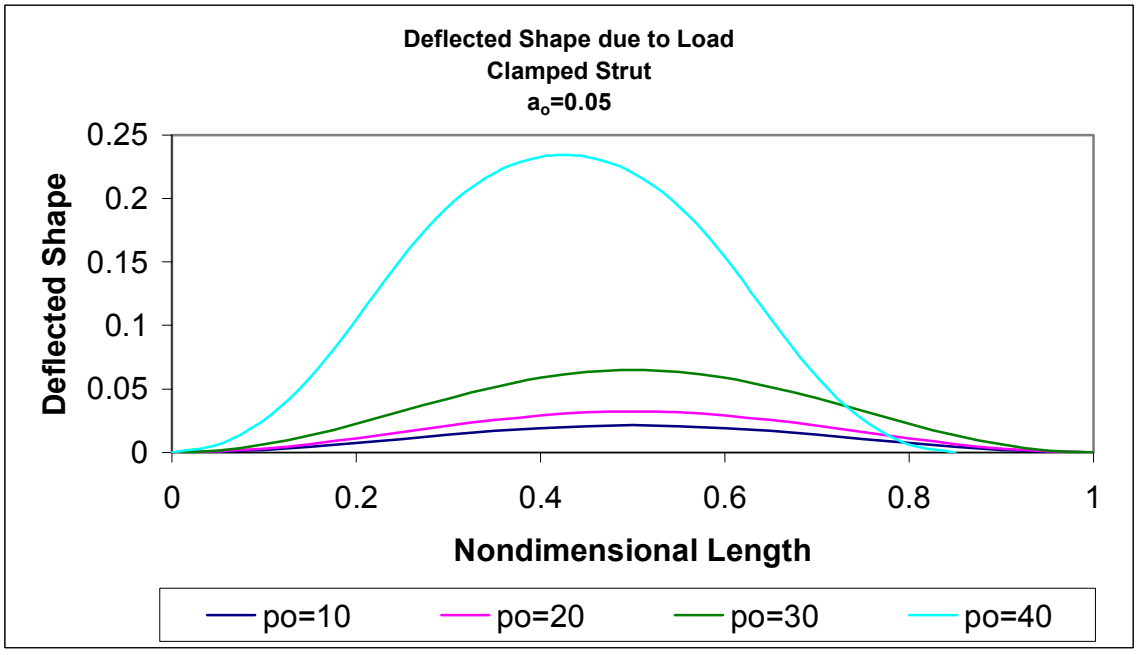

Figure 5.3.1: Deflected Shape of Fixed-end Strut with a_o=0.05

The values for the maximum mid-span deflection and end shortening are shown in Table 5.3.1, where max y is y(0.5) and end shortening is defined as 1-x(1). The values of the mid-span deflection and end shortening for the other curved struts can be found in Appendix D.2.

Table 5.3.1: Maximum Mid-span Deflection and End Shortening for a_o=0.05

po	max y	End Shortening
0	0.015911	0.000625
10	0.0213	0.00112
20	0.032177	0.002559
30	0.064916	0.010466
40	0.234501	0.149713

In Figure 5.3.2, the maximum or mid-span deflection of the strut is plotted as the supported load is increased.

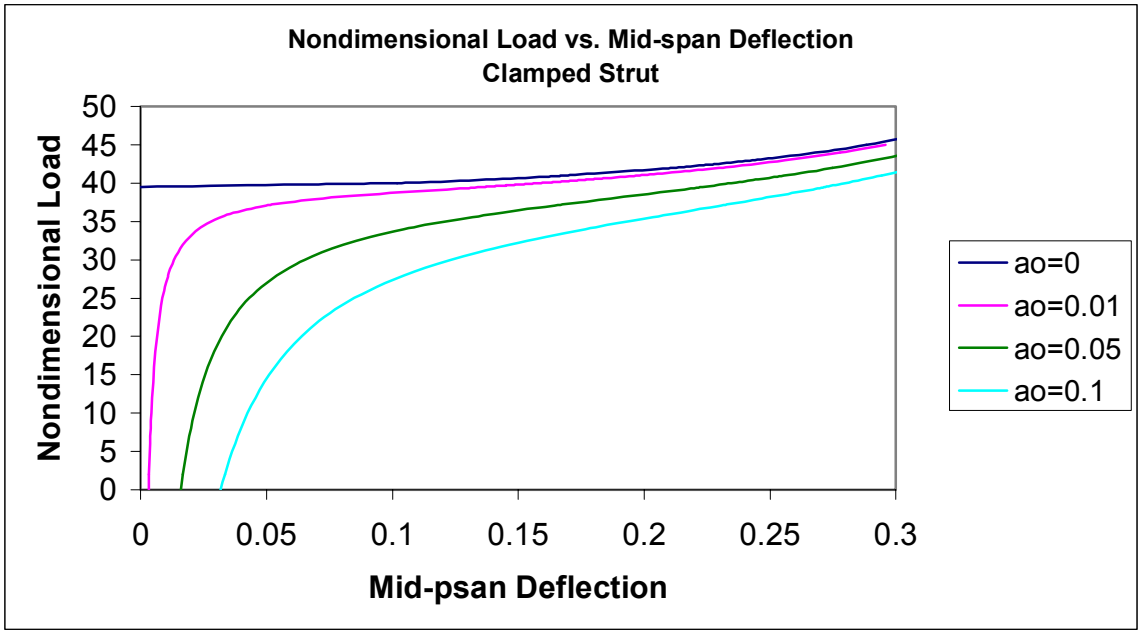

Figure 5.3.2: Nondimensional Load vs. Mid-span Deflection

The vertical deflection or end shortening of the strut can be seen in Figure 5.3.3. The figure shows how increasing the initial curvature of a strut will increase the vertical deflection of the strut under loading.

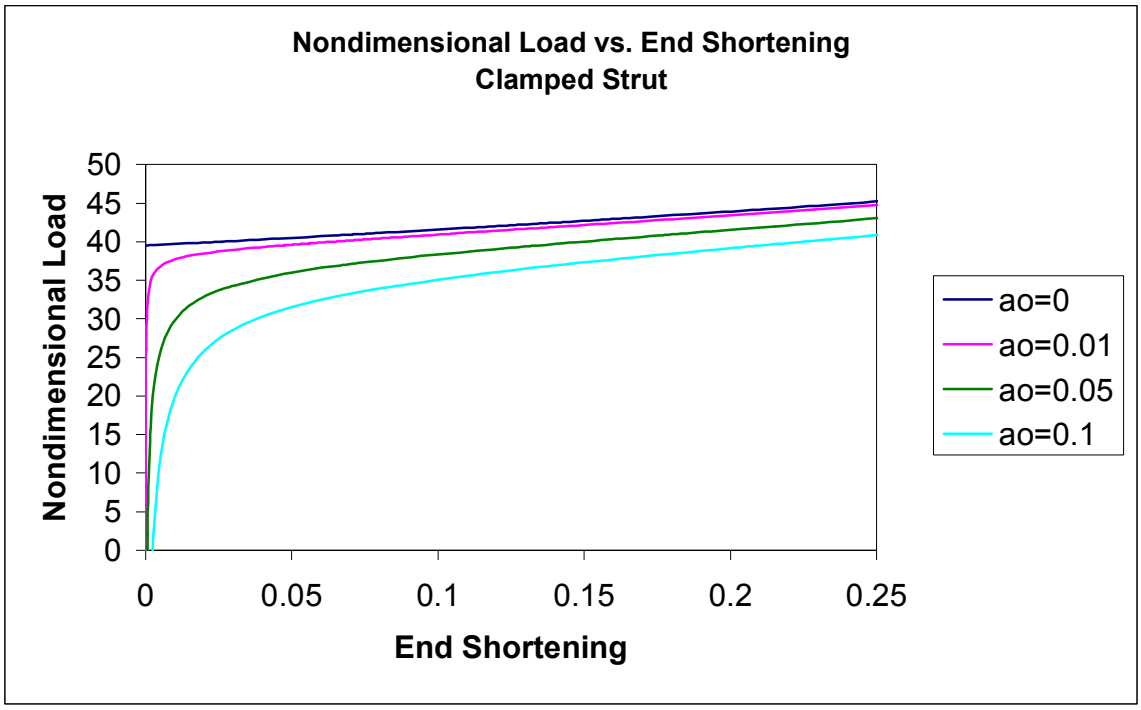

Figure 5.3.3: Nondimensional Load vs. End Shortening

Depending on the applied load and amplitude of the initial curvature, the resulting moment at s=0 determined from the numerical solution is used in the dynamic analysis.

5.4 Forced Vibration of a Fixed-end Strut with Initial Curvature due to Harmonic Base Motion

The dynamic excitations applied to the curved strut are axial, harmonic vibrations. The vibrations are assumed to be small, and the steady-state response is examined. The response of the strut is determined from the equations of static equilibrium (5.2-5.5), and the following equations for dynamic equilibrium (with q_e=0):

$$\frac{dx_d}{ds} = -\theta_d \sin\theta_e \tag{5.6}$$

$$\frac{dy_d}{ds} = \theta_d \cos\theta_e \tag{5.7}$$

$$\frac{d\theta_d}{ds} = \frac{m_d}{(1+i\omega\gamma)} \tag{5.8}$$

$$\frac{dm_d}{ds} = (q_d - p_o\theta_d)\cos\theta_e - (p_d + q_e\theta_d)\sin\theta_e \tag{5.9}$$

$$\frac{dp_d}{ds} = (\omega^2 - i\omega c)x_d \tag{5.10}$$

$$\frac{dq_d}{ds} = (\omega^2 - i\omega c)y_d \tag{5.11}$$

The dynamic equations that describe the model are not affected by the initial curvature; only the equation for curvature from the static analysis is altered.

5.5 Numerical Solution of a Fixed-end Buckled Strut with Initial Curvature Under Forced Vibrations

The numerical solution of the pre-bent strut is solved using Mathematica. The static and dynamic equations are used, and the program shoots for a set of specified conditions. The boundary conditions for the pinned-end model are:

At s=0: $x_d = u_o$, y_d=0, θ_d=0

At s=1: y_d=0, θ_d=0, $p_d = -rp_o\omega^2 x_d$

The known values of p_o, u_o, r, c, ω, and $m_e(0)$ are used as input, and initial guesses are made for $p_d(0)$, $q_d(0)$, and $m_d(0)$. All cases examined for this model do not include internal damping, thus γ=0. Convergence is mandatory for the boundary conditions at the end of the strut, and iterations are completed when necessary. The Mathematica program can be found in Appendix D.3.

The transmissibility for the strut is defined as:

$$TR = \frac{\sqrt{\{Re[x_d(1)]\}^2 + \{I_m[x_d(1)]\}^2}}{|u_o|} \tag{5.12}$$

The transmissibility is found over a wide range of frequencies, and the results are plotted using Excel.

5.6 Results for Forced Vibrations of the Fixed-end Strut with Initial Curvature

First, the transmissibility versus the applied nondimensional frequency is shown for several cases as the different parameters are varied. The effects of the stiffness parameter, damping coefficient, and initial curvature on the transmissibility and nondimensional frequency are shown. Additional plots can be seen in Appendix D.4

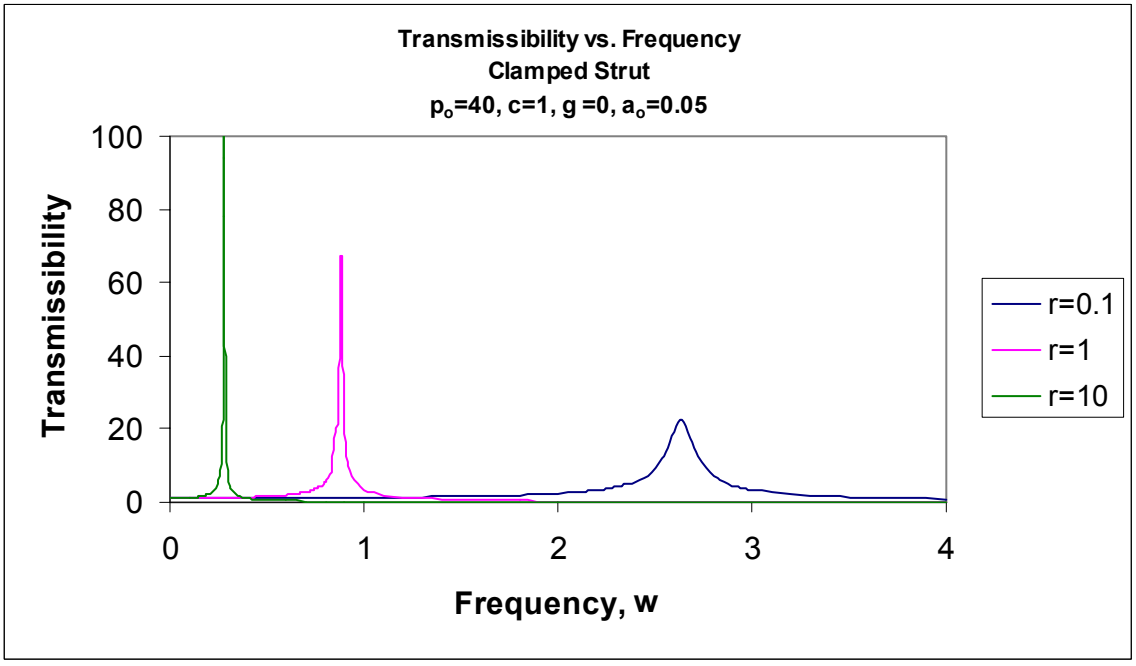

Figure 5.6.1: Transmissibility vs. Frequency for p_o=40, c=1, γ=0, a_o=0.05

Figure 5.6.1 shows the result for a strut supporting a load above its buckling load. The stiffness parameter is varied to show its effect on the response. Again, as the stiffness parameter increases, the nondimensional resonant frequency decreases, but the maximum

transmissibility increases. The dimensional resonant frequency, Ω, increases as the stiffness parameter increases. It is obvious that the maximum transmissibility is directly influenced by the increasing stiffness parameter.

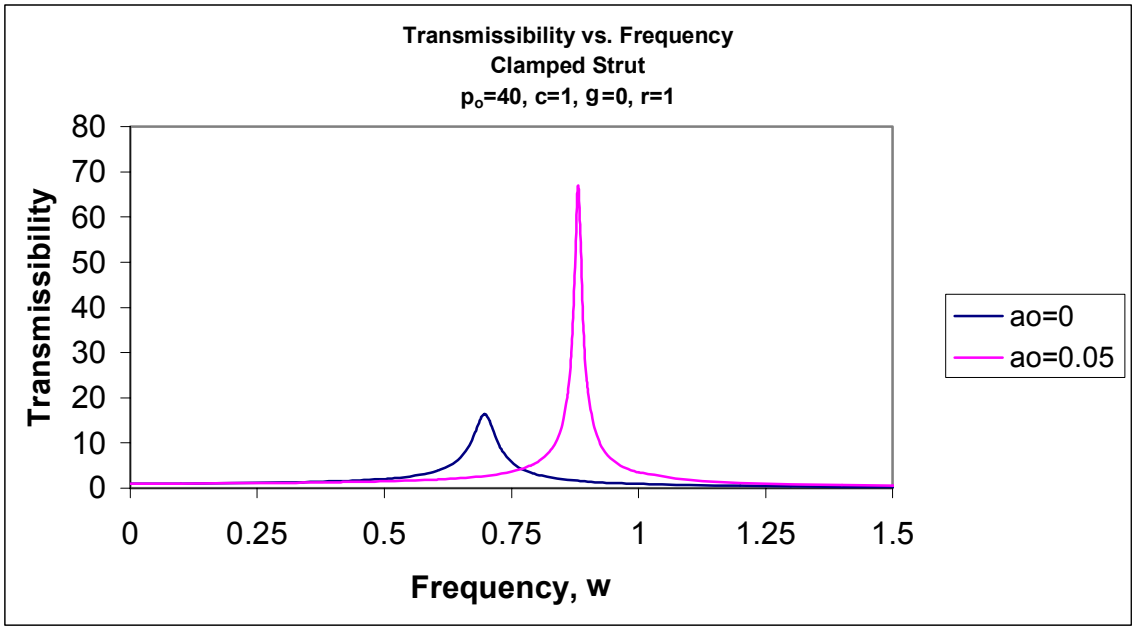

Figure 5.6.2: Transmissibility vs. Frequency for p_o=40, c=1, γ=0, r=1

In Figure 5.6.2, the result of the ideal case is plotted along with that for a strut with an amplitude of initial curvature of 0.05. It is apparent that the maximum transmissibility is much greater for the case with the initial curvature. Also, the nondimensional resonant frequency increases for the strut with an initial curvature. Obviously, an ideal column is more effective as a vibration isolator, but it is unrealistic.

The maximum transmissibility is plotted against the stiffness parameter for a strut with a load of p_o=40, a damping coefficient of c=1, and an initial curvature of a_o=0.05 in Figure 5.6.3. The figure shows how the maximum transmissibility increases with the stiffness parameter. If the stiffness of the strut is low, the strut is able to dissipate the energy more effectively and reduce the motion of the supported load.

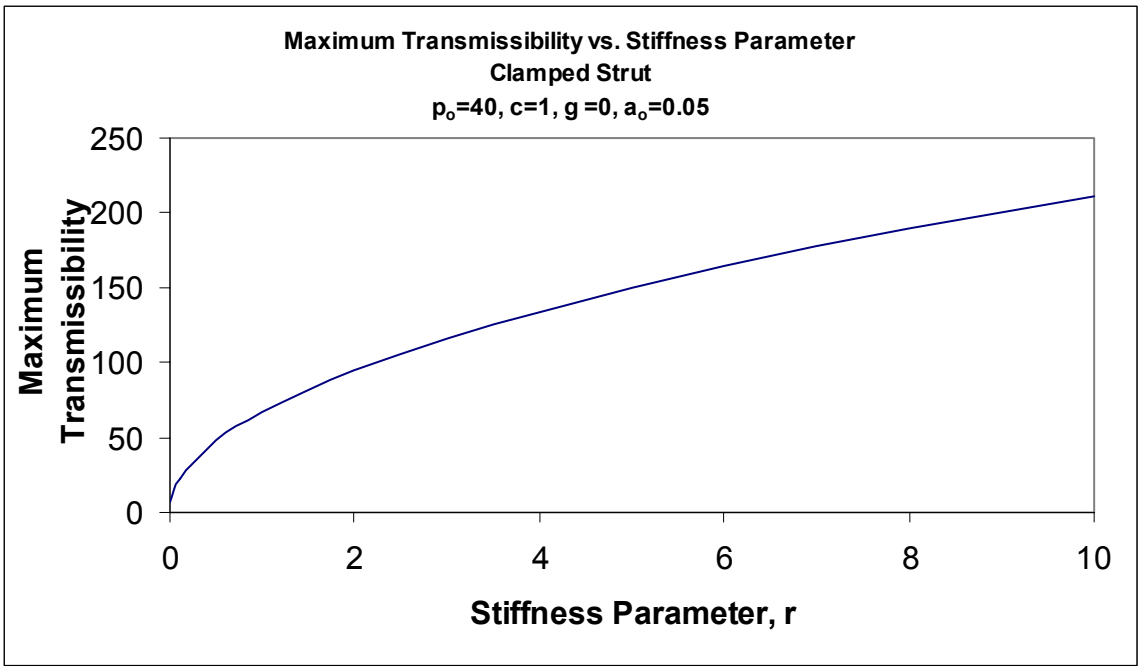

Figure 5.6.3: Maximum Transmissibility vs. Stiffness Parameter for p_o=40, c=1, γ=0, a_o=0.05

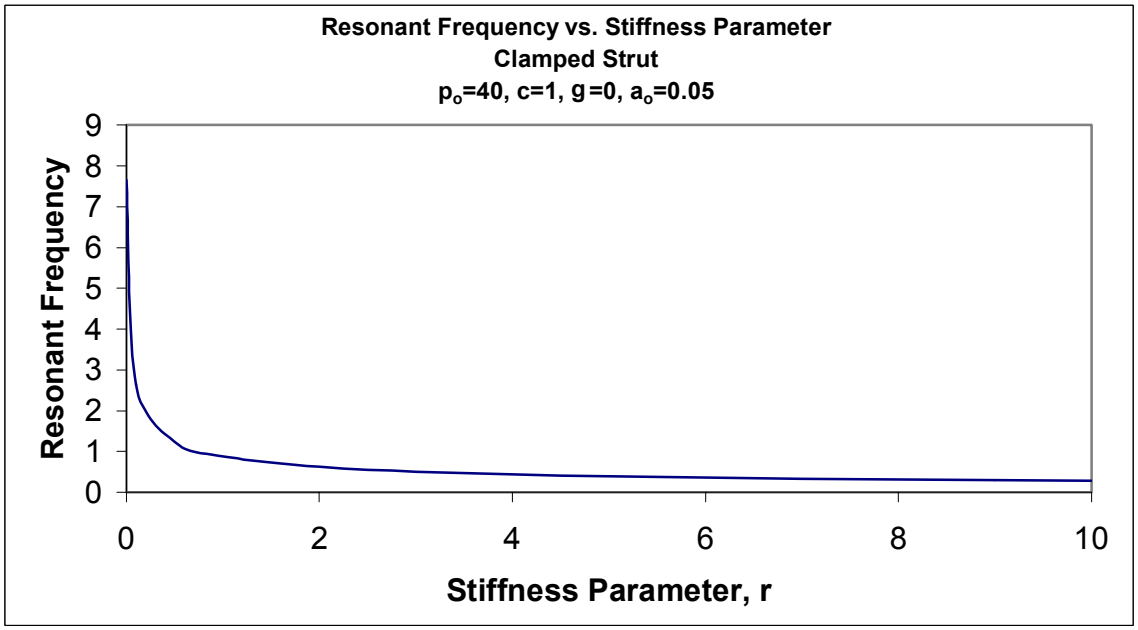

Figure 5.6.4: Resonant Frequency vs. Stiffness Parameter for p_o=40, c=1, γ=0, a_o=0.05

Figure 5.6.4 shows the nondimensional resonant frequency decreasing as the stiffness parameter increases for the same strut shown in Figure 5.6.3. Again, this graph does not mean that the actual resonant frequency is decreasing as the stiffness parameter increases. The stiffness parameter is directly proportional to the bending stiffness, EI, but the nondimensional term ω is inversely proportional to the square root of the bending stiffness, EI. So as the bending stiffness increases, the stiffness parameter increases and the nondimensional frequency decreases. The dimensional frequency, Ω, satisfies $\Omega^2=r\omega^2 g/L$, and from the data, Ω increases as r increases.

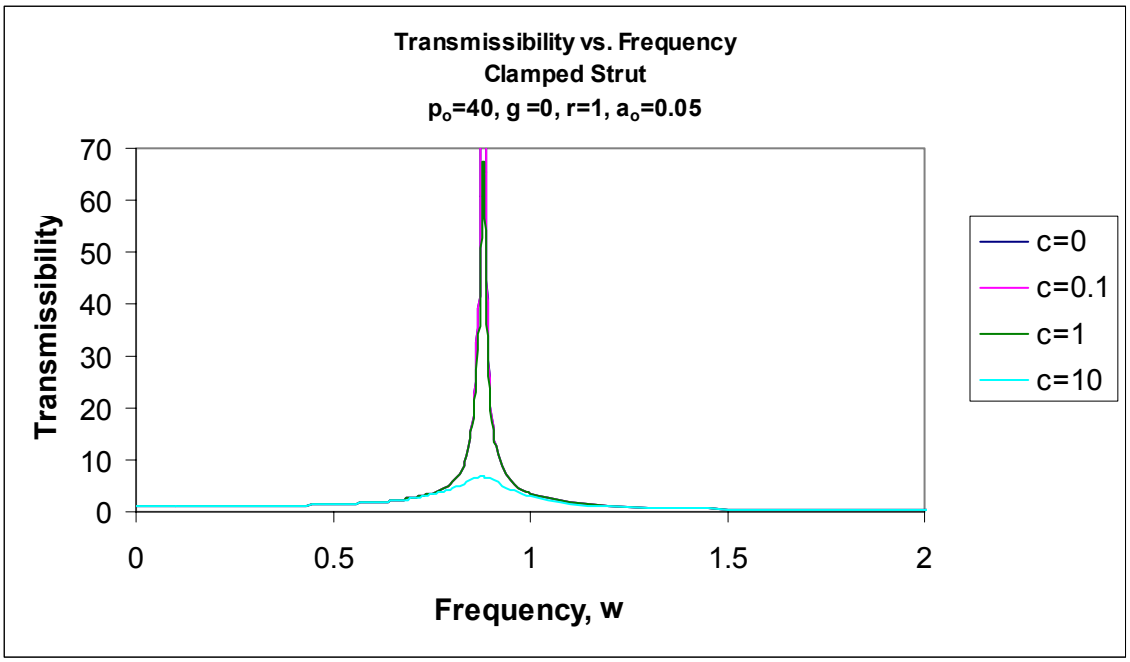

Figure 5.6.5: Transmissibility vs. Frequency for p_o=40, γ=0, r=1, a_o=0.05

Figure 5.6.5 shows the transmissibility versus the frequency for different damping coefficients. As anticipated, the maximum transmissibility decreases as the damping coefficient increases. Therefore, the resonant motion of any system can be reduced with additional damping.

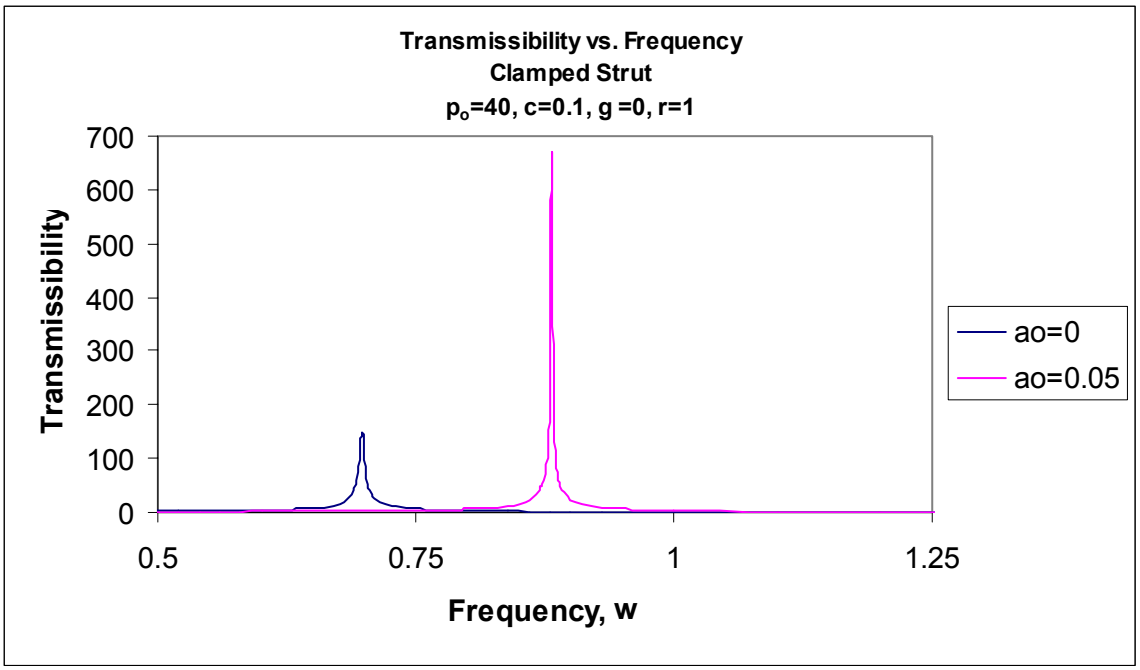

Figure 5.6.6: Transmissibility vs. Frequency for p_o=40, c=0.1, γ=0, r=1

Figure 5.6.6 shows the results for the ideal case and for a strut with an amplitude of initial curvature of 0.05. Again, the curved strut has a higher maximum transmissibility and a higher nondimensional resonant frequency.

In the next figure, the maximum transmissibility is plotted as the damping coefficient increases. It is evident in Figure 5.6.7 that for any stiffness parameter value, the maximum transmissibility is reduced as the damping coefficient increases. The decline in the maxiumum transmissibility is more dramatic for a lower stiffness value, but eventually the maximum transmissibility is reduced despite the value of the stiffness parameter.

In Figure 5.6.8, the nondimensional resonant frequency seems to be about constant as the damping coefficient increases. A slight decrease can be seen in the resonant frequency as the damping coefficient increases for the stiffness parameter equal to 0.1, but a significant change is not obvious.

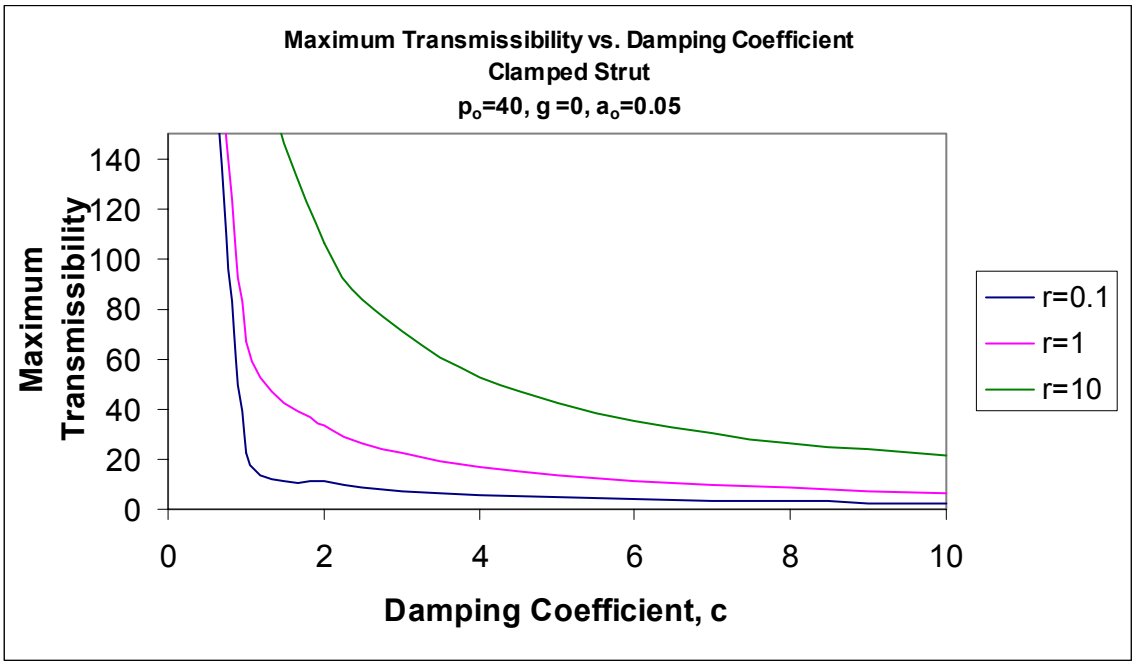

Figure 5.6.7: Maximum Transmissibility vs. Damping Coefficient for p_o=40, γ=0, a_o=0.05

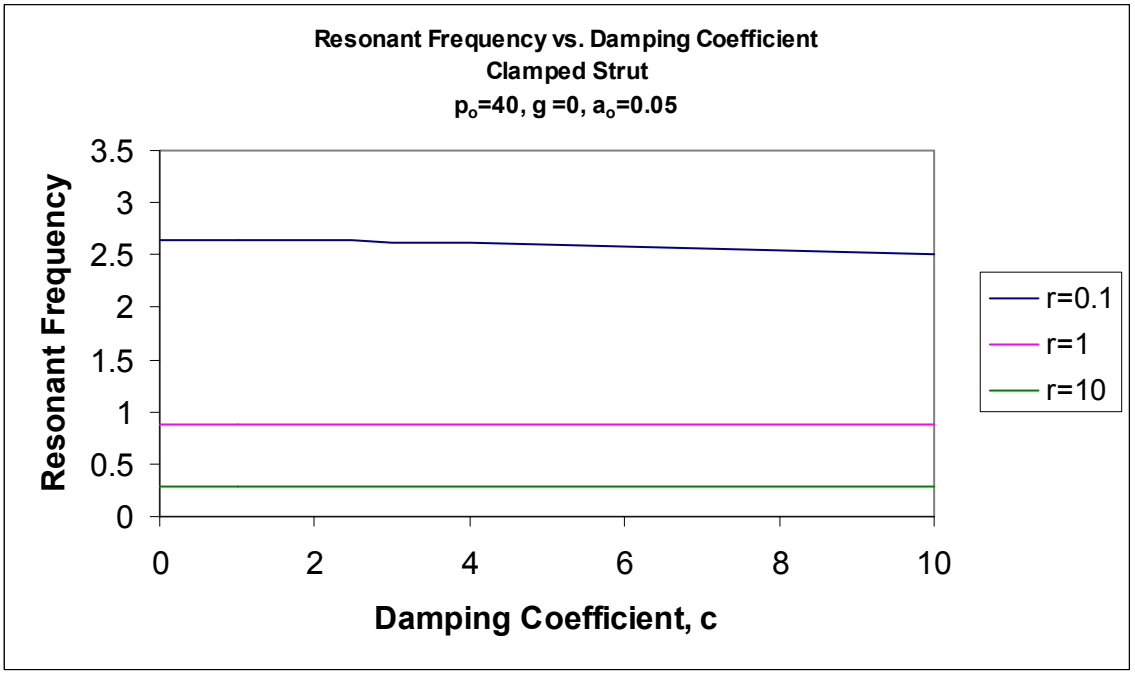

Figure 5.6.8: Resonant Frequency vs. Damping Coefficient for p_o=40, γ=0, a_o=0.05

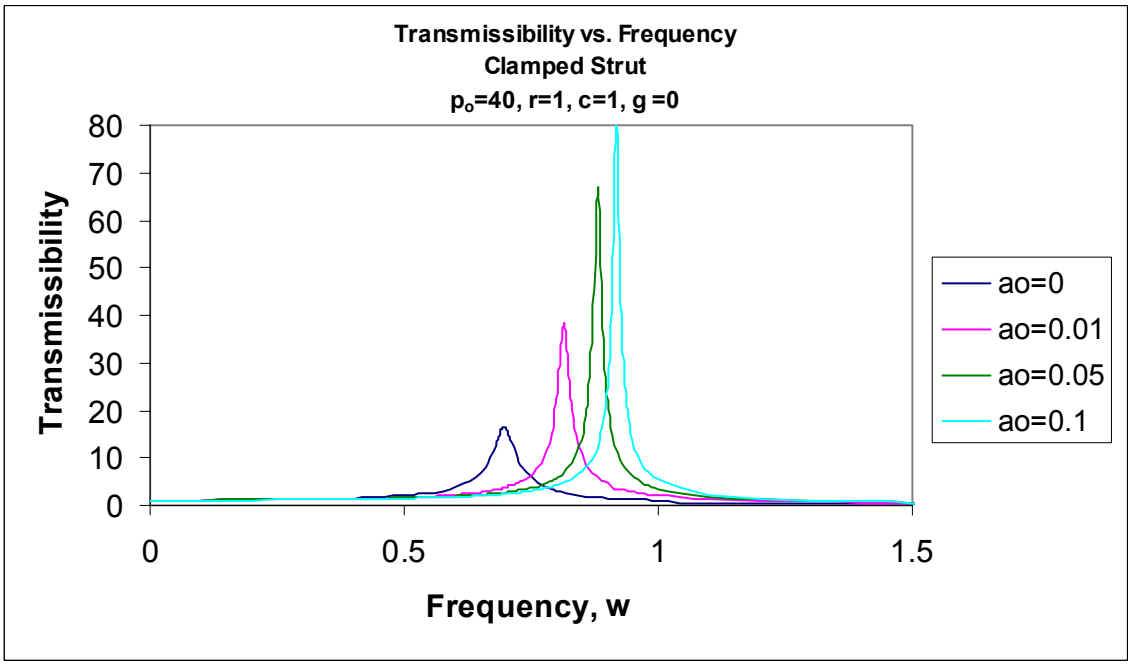

Figure 5.6.9: Transmissibility vs. Frequency for p_o=40, c=1, γ=0, r=1

The effect of the initial curvature on the response of the strut can be seen in Figure 5.6.9. The maximum transmissibility and the nondimensional resonant frequency increase as the initial curvature increases. Again the ideal strut performs the best in reducing the motion of the supported mass.

The direct effect of the initial curvature on the maximum transmissibility can be seen in Figure 5.6.10. For all stiffness parameter values, the maximum transmissibility increases as the initial curvature increases. However, the maximum transmissibility increases at a greater rate when the stiffness parameter is high. As before, the maximum transmissibility is lowest when a_o=0.

The nondimensional resonant frequency is plotted against the increasing initial amplitude of curvature in Figure 5.6.11. The resonant frequency again tends to stay rather constant when the stiffness parameter is high. For a lower value of the stiffness parameter, the nondimensional resonant frequency has a slight increase.

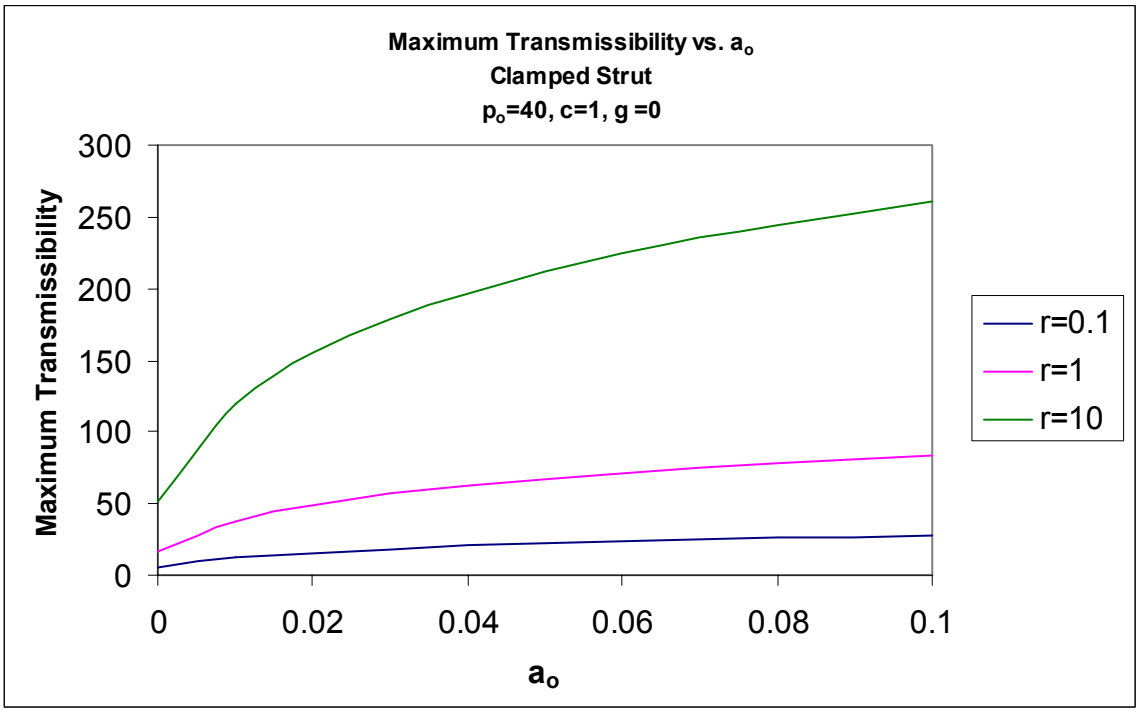

Figure 5.6.10: Maximum Transmissibility vs. a_o for p_o=40, c=1, γ=0

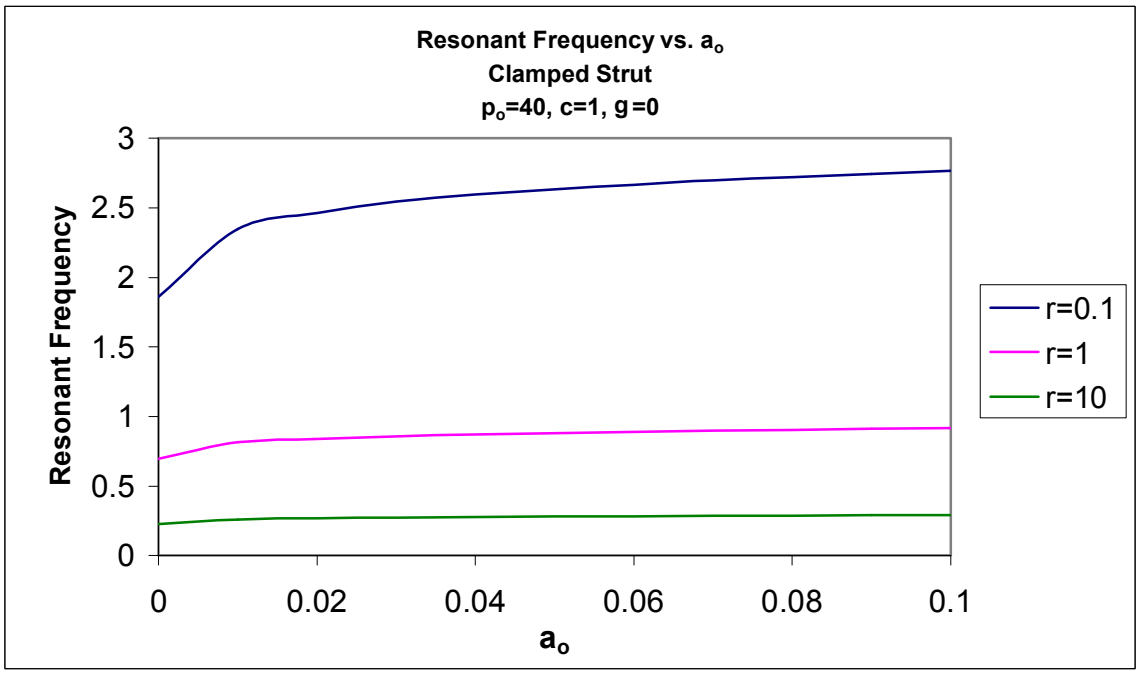

Figure 5.6.11: Resonant Frequency vs. a_o for p_o=40, c=1, γ=0

The next four figures show the same system with different X and Y axes. The system shown is analyzed under nondimensional loads of 10, 20, 30, and 40. The strut has a damping coefficient of c=0.1, a stiffness parameter of r=1, and an initial curvature of a_o=0.05.

The fundamental resonant frequency of the system for the various loads is shown in Figure 5.6.12. Obviously, the maximum transmissibility increases as the supported load increases. Also, the nondimensional resonant frequency decreases as the load increases. Since the stiffness parameter is constant for the four cases, when the nondimensional frequency decreases, it can be concluded that the dimensional resonant frequency also decreases. Therefore, the strut supporting the load above the buckling load has a larger working range of frequencies since the resonant frequency is lowest and the motion is only reduced when the forcing frequency is above the resonant frequency, for an underdamped system.

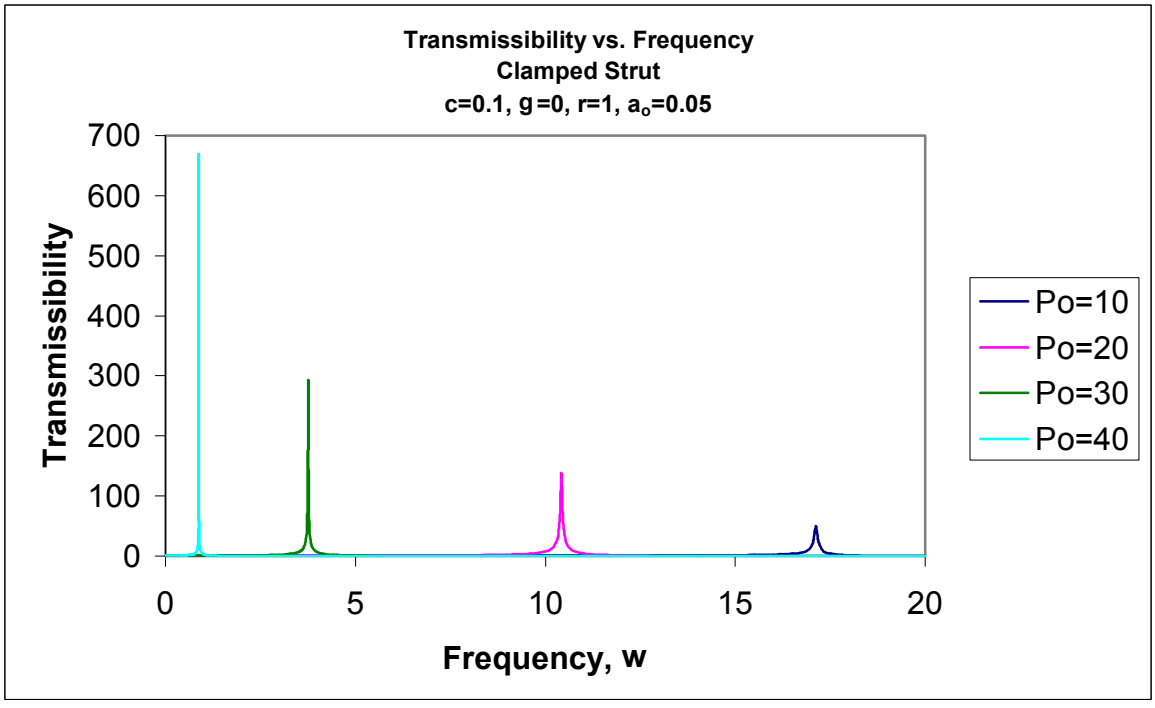

Figure 5.6.12: Transmissibility vs. Frequency for c=0.1, γ=0, r=1, a_o=0.05

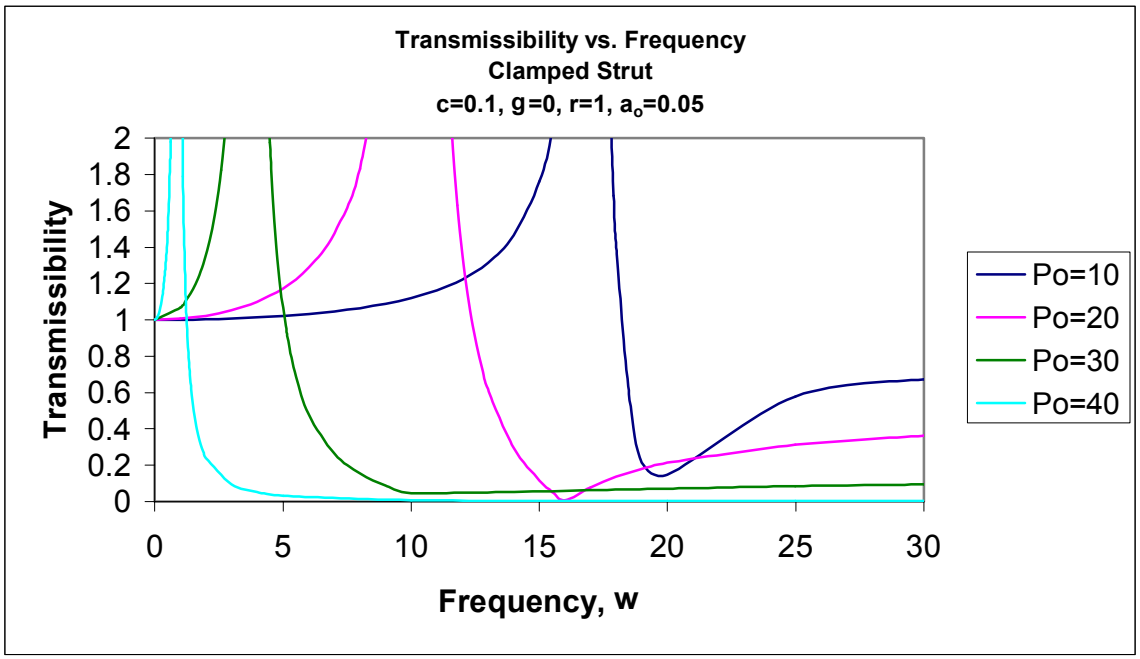

Figure 5.6.13: Transmissibility vs. Frequency for c=0.1, γ=0, r=1, a_o=0.05

Figure 5.6.13 shows the system with the Y-axis only revealing the lower transmissibilities. Since the transmissibility is defined as the motion at the top of the strut divided by the input motion at the bottom of the strut, the top motion is reduced when the transmissibility is less than one. As in Figure 4.6.13, the strut supporting a load above the buckling load has the best response in terms of reducing the motion of the supported load. The motion of the strut supporting this load is almost negligible. The other struts, however, do not sustain the reduced motion after the nondimensional resonant frequency, as is evident by the increasing transmissibility.

Figure 5.6.14 shows the continued response as the nondimensional frequency increases. Similar to the results of the pinned-end case, the struts supporting loads below the buckling load do not have large resonant peaks when the mode shape is symmetric, although the small resonant peaks can be seen more clearly for the fixed-end case. Also, the motion between the resonant peaks is much smaller for the buckled strut than for the other cases.

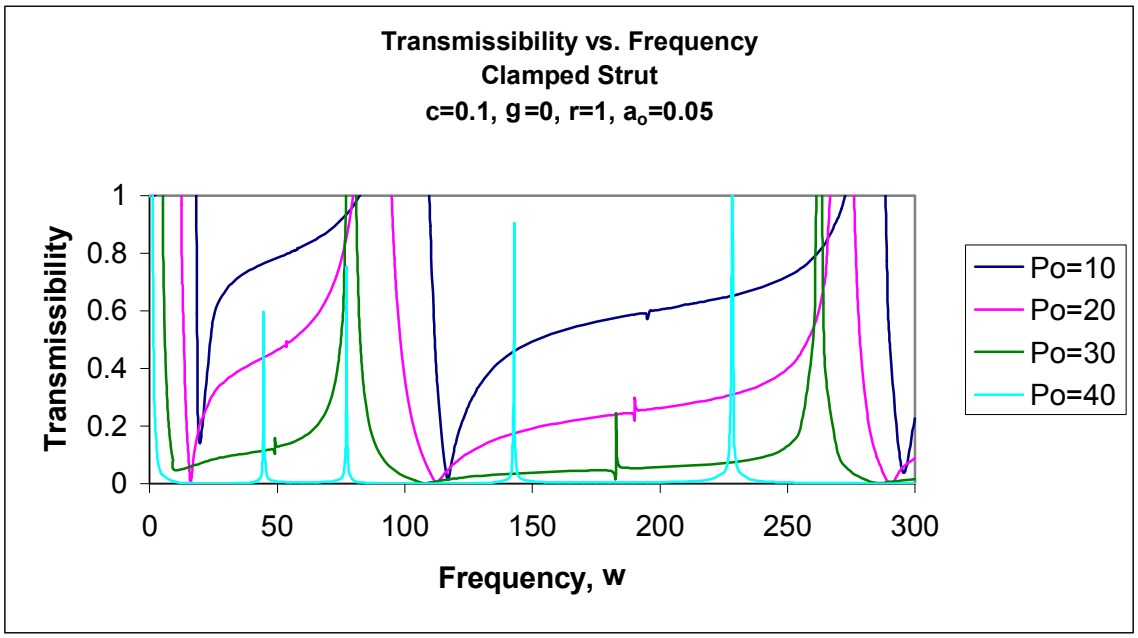

Figure 5.6.14: Transmissibility vs. Frequency for c=0.1, γ=0, r=1, a_o=0.05

Figure 5.6.15 shows the results for nondimensional loads of 20 and 40. The mode shapes at various frequencies for these two cases can been in Figures 5.6.16 and 5.6.17. It is clear that each resonant peak corresponds to a mode change. For example, for the buckled strut, when ω=0.881, the strut is in resonance in its first mode shape. After the resonant peak, the motion is significantly reduced, and the changing mode shape can be seen when ω=30. The second mode shape can be seen at the second resonant peak, when ω=44.8. This progressive change of shapes continues as the frequency increases and more resonant peaks are achieved. Like the pinned-end case, the strut supporting a load below the buckling load does not exhibit the large resonance for the symmetric mode shapes. However, the resonant peaks and mode changes are still present, as shown in the figures.

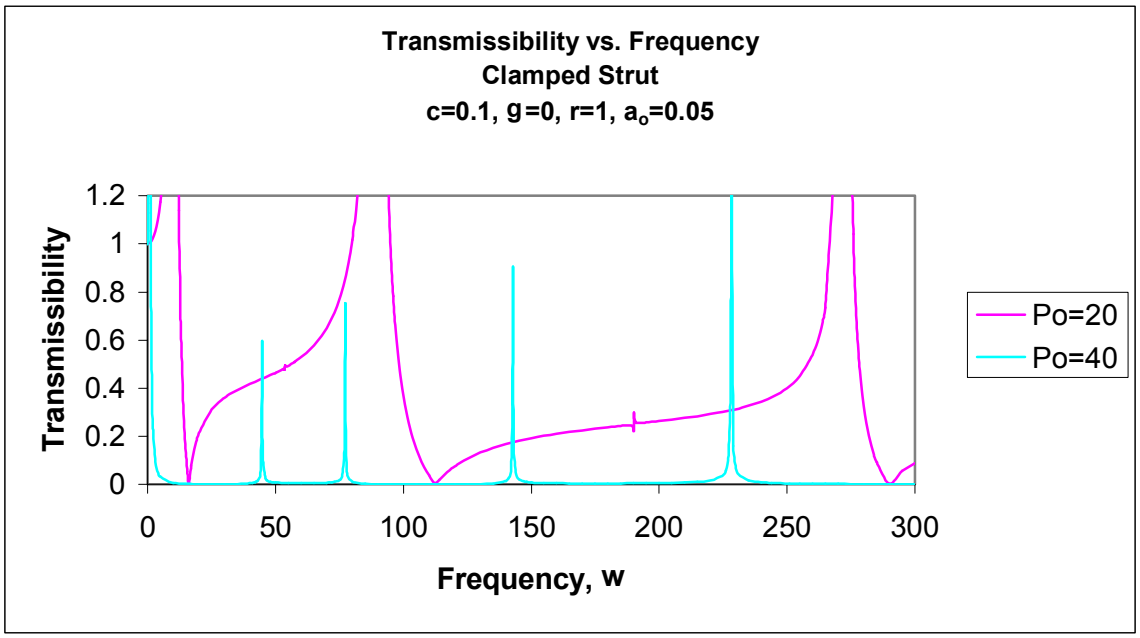

Figure 5.6.15: Transmissibility vs. Frequency for c=0.1, γ=0, r=1, a_o=0.05

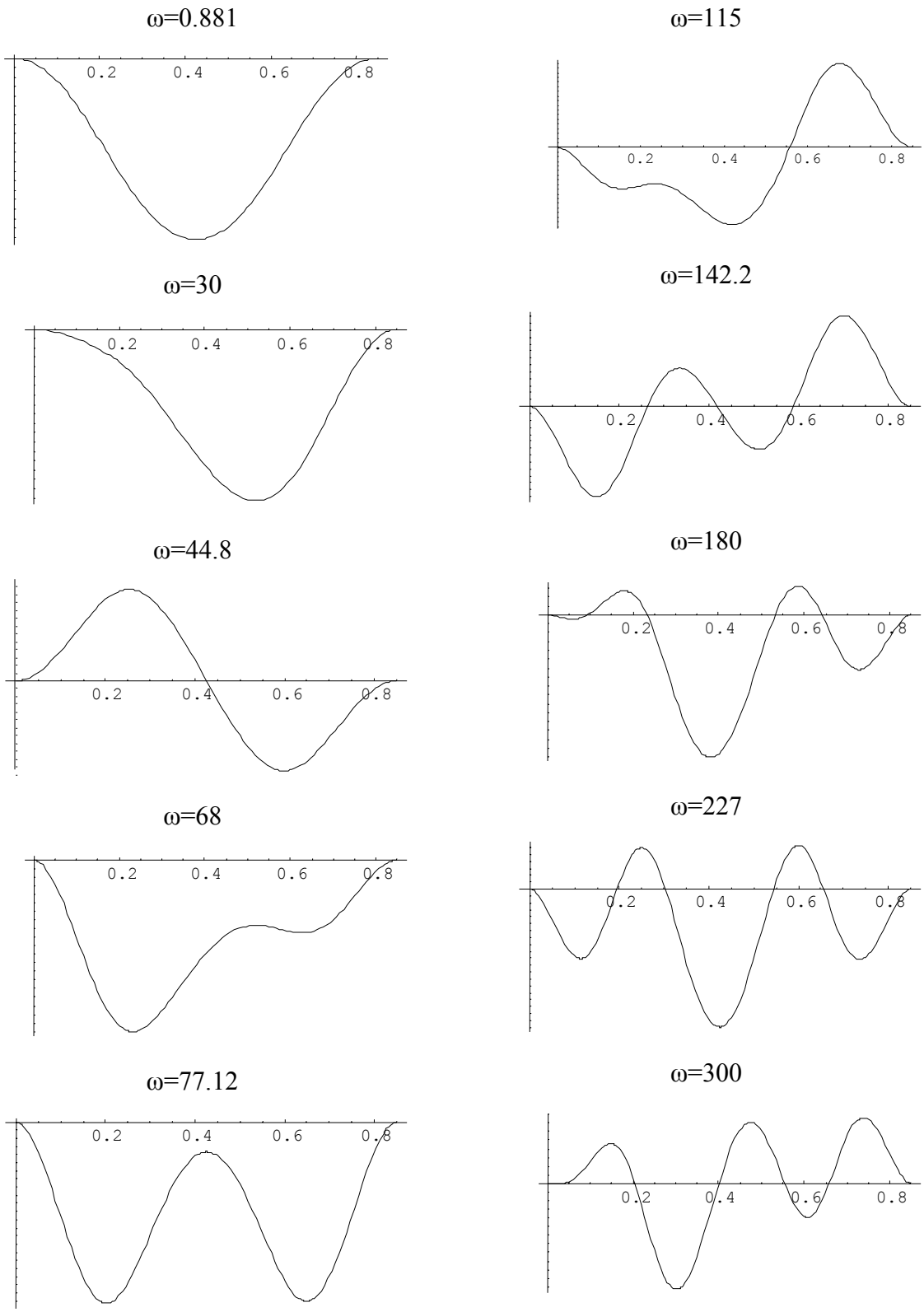

Figure 5.6.16: Mode Shapes for Various Frequencies for p_o=20

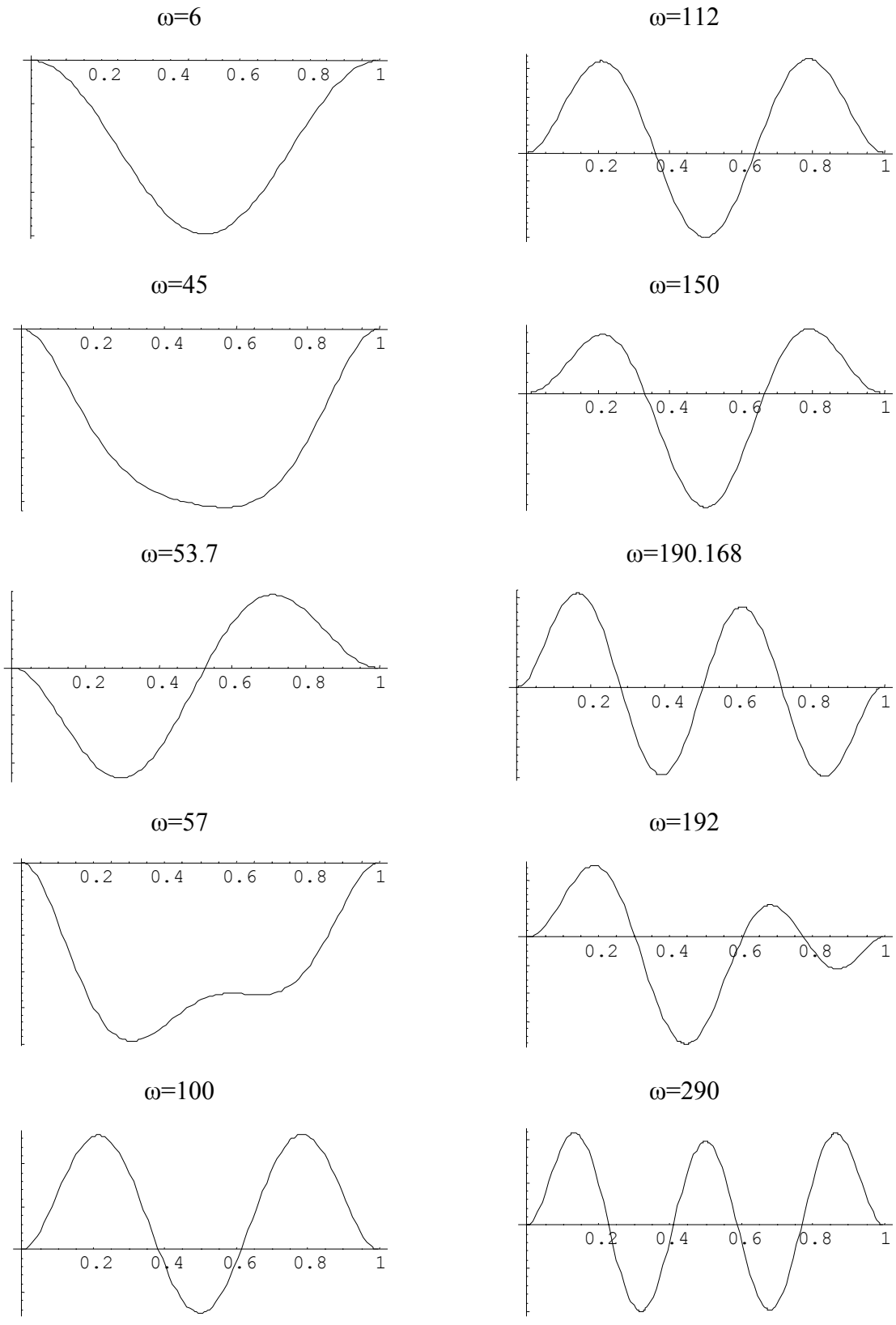

Figure 5.6.17: Mode Shapes for Various Frequencies for p_o=40

5.7 Conclusions

The fixed-end strut with an initial curvature produces similar results to the pinned-end case. First, the model was analyzed to determine the effect of the initial curvature on the static equilibrium of the strut supporting various loads. Obviously, the larger the initial curvature, the larger the static displacement of the strut under a given load. Then, the model was subjected to a harmonic axial excitation and the effect of the initial curvature was noted. As the initial curvature increased, the nondimensional resonant frequency increased slightly, but then became almost constant. The maximum transmissibility for the system increases as the amplitude of initial curvature increases, and the increase is more profound when the stiffness parameter is high.

The strut was examined at loads above and below the buckling load. As the load increases, the fundamental resonant frequency decreases. Thus, the buckled strut has the largest working range since it has the lowest resonant frequency. The maximum transmissibility is reduced when the load is lower. However, the amplified motion can be controlled by additional damping.

Overall, the same conclusions made in chapter 4 apply to the fixed-end strut. The presence of an initial curvature has a minimal negative effect on the response of the strut, but if the load is above the buckling load, the buckled strut will still effectively reduce the motion of the supported load.

Chapter 6: Fixed-end Buckled Column Under Forced Two-frequency Axial Excitation

6.1 Introduction

The overall goal of this research aims to identify buckled columns to be useful in vibration control. Up until now, all models have been forced to vibrate at a harmonic excitation and analyzed. However, not all vibrations are harmonic. To further examine the capabilities of the buckled struts used as vibration isolators, multi-frequency vibrations need to be applied to the models. In this chapter, the same fixed-end strut that has been used in previous chapters will be subjected to a two-frequency axial excitation. The previous assumptions made for the fixed-end strut will apply here, as well, but several governing equations will be different due to the altered input. The Excel plots presented in this chapter reflect the results of the new model, as well as a comparison to its forced harmonic counterpart.

6.2 Basic Assumptions and Formulation

The fixed-end strut model will be used again for this analysis. The strut is assumed to be an elastica, and the nondimensional buckling load is $p_o = 4\pi^2 \approx 39.48$. The strut is clamped on both ends, preventing any rotation. A load above the buckling load is applied, and the strut is first analyzed under static equilibrium. The static analysis does not change in this chapter since the only difference is the dynamic motion being applied to the model. The deformed strut can be seen again in Figure 6.2.1.

Figure 6.2.1: Fixed-end Buckled Strut

6.3 Numerical Solution of a Fixed-end Buckled Strut in Static Equilibrium

The fixed-end boundary conditions used in the Mathematica program are as follows:

At s=0: x=0, y=0, θ=0

At s=1: y=0, θ =0.

The same equilibrium program will be used to establish the end moment and shear force of the strut due to the applied load, and it can be found in Appendix E.1. The applicable equations are as follows:

$$\frac{dx}{ds} = \cos\theta \tag{6.1}$$

$$\frac{dy}{ds} = \sin\theta \tag{6.2}$$

$$\frac{d\theta}{ds} = m \tag{6.3}$$

$$\frac{dm}{ds} = -p_o \sin\theta + q\cos\theta \tag{6.4}$$

These equations will be used in the dynamic analysis, and may be referred to with a subscript ‘e’ for static equilibrium.

6.4 Forced Vibration of Fixed-end Buckled Strut due to a Two-frequency Excitation

Using the resulting moment at s=0 and shear force from the static analysis, the strut is subjected to a two-frequency excitation and analyzed to determine the transmissibility of the system. The excitations are axial and applied at the base of the strut. The vibrations due to this excitation are again assumed to be small. The forced axial motion on the fixed-end strut is shown in Figure 6.4.1.

Figure 6.4.1: Fixed-end Strut under Two-frequency Axial Excitation

The equation that describes the base motion is as follows:

$$u(t) = u_o e^{i\omega t} + r_a u_o e^{i r_f \omega t} \tag{6.5}$$

where r_a and r_f are constants ('a' for amplitude and 'f' for frequency). Since the dynamic equations are linear, the result can be obtained by superimposing the response to $u_o e^{i\omega t}$ and $r_a u_o e^{i r_f \omega t}$. To simplify the equation, the following relationships will be used:

$$u_1 = u_o \qquad u_2 = r_a u_o \qquad \omega_1 = \omega \qquad \omega_2 = r_f \omega$$

Therefore, the new equation describing the base motion applied to the strut is:

$$u(t) = u_1 e^{i\omega_1 t} + u_2 e^{i\omega_2 t} \tag{6.6}$$

The static and dynamic relationships derived for this model are:

$$\frac{dx_e}{ds} = \cos\theta_e \tag{6.7}$$

$$\frac{dy_e}{ds} = \sin\theta_e \tag{6.8}$$

$$\frac{d\theta_e}{ds} = m_e \tag{6.9}$$

$$\frac{dm_e}{ds} = -p_o \sin\theta_e + q_e \cos\theta_e \tag{6.10}$$

$$\frac{dx_1}{ds} = -\theta_1 \sin\theta_e \tag{6.11}$$

$$\frac{dy_1}{ds} = \theta_1 \cos\theta_e \tag{6.12}$$

$$\frac{d\theta_1}{ds} = \frac{m_1}{(1 + i\omega_1\gamma)} \tag{6.13}$$

$$\frac{dm_1}{ds} = (q_1 - p_o\theta_1)\cos\theta_e - (p_1 + q_e\theta_1)\sin\theta_e \tag{6.14}$$

$$\frac{dp_1}{ds} = (\omega_1^{\,2} - i\omega_1 c)x_1 \tag{6.15}$$

$$\frac{dq_1}{ds} = (\omega_1^{\,2} - i\omega_1 c)y_1 \tag{6.16}$$

$$\frac{dx_2}{ds} = -\theta_2 \sin\theta_e \tag{6.17}$$

$$\frac{dy_2}{ds} = \theta_2 \cos\theta_e \tag{6.18}$$

$$\frac{d\theta_2}{ds} = \frac{m_2}{(1 + i\omega_2\gamma)} \tag{6.19}$$

$$\frac{dm_2}{ds} = (q_2 - p_o\theta_2)\cos\theta_e - (p_2 + q_e\theta_2)\sin\theta_e \tag{6.20}$$

$$\frac{dp_2}{ds} = (\omega_2{}^2 - i\omega_2 c)x_2 \tag{6.21}$$

$$\frac{dq_2}{ds} = (\omega_2{}^2 - i\omega_2 c)y_2 \tag{6.22}$$

Then, the response of the strut is described by the following equations, where $p_e = p_o$ and $q_e = 0$:

$$x(s,t) = x_e(s) + x_1(s)e^{i\omega_1 t} + x_2(s)e^{i\omega_2 t} \tag{6.23}$$

$$y(s,t) = y_e(s) + y_1(s)e^{i\omega_1 t} + y_2(s)e^{i\omega_2 t} \tag{6.24}$$

$$\theta(s,t) = \theta_e(s) + \theta_1(s)e^{i\omega_1 t} + \theta_2(s)e^{i\omega_2 t} \tag{6.25}$$

$$m(s,t) = m_e(s) + m_1(s)e^{i\omega_1 t} + m_2(s)e^{i\omega_2 t} \tag{6.26}$$

$$p(s,t) = p_e + p_1(s)e^{i\omega_1 t} + p_2(s)e^{i\omega_2 t} \tag{6.27}$$

$$q(s,t) = q_e + q_1(s)e^{i\omega_1 t} + q_2(s)e^{i\omega_2 t} \tag{6.28}$$

Again, because the dynamic equations are linear, the contributions of each component can be superimposed to get the final response, as evident from the above equations.

6.5 Numerical Solution of a Fixed-end Buckled Strut Under Forced Two-frequency Axial Excitation

The numerical solution for this model is obtained with another Mathematica program. From the static equilibrium solution, $m_e(0)$ and q_e are known. The frequency ω is used for ω_1, and the value of ω_2 is set to equal $r_f\,\omega$. Also, the values of p_o, r, c, g, r_f, and r_a are set at selected values. The Mathematica code can be found in Appendix E.2.

The input conditions at s=0 are:

$x_e = 0 \qquad y_e = 0 \qquad \theta_e = 0 \qquad m_e = m$

$$x_1 = u_o \qquad y_1 = 0 \qquad \theta_1 = 0$$

$$x_2 = r_a u_o \qquad y_2 = 0 \qquad \theta_2 = 0$$

The unknowns at s=0 are m_1, p_1, q_1, m_2, p_2, and q_2.

The shooting conditions at s=1 are:

$$y_1 = 0 \qquad \theta_1 = 0 \qquad p_1 = -rp_o\omega_1^{\,2}x_1$$

$$y_2 = 0 \qquad \theta_2 = 0 \qquad p_2 = -rp_o\omega_2^{\,2}x_2$$

First, the magnitude of the input is found and is defined as:

$$U_m = \left| \; u_o \cos\omega_1 t + r_a u_o \cos\omega_2 t \; \right| \tag{6.29}$$

Since the response of the strut is complex, the following equation for the magnitude of the response contains both real (Re) and imaginary (Im) parts:

$$R = \left| \; \mathrm{Re}[x_1(1)]\cos\omega_1 t + \mathrm{Re}[x_2(1)]\sin\omega_2 t - \mathrm{Im}[x_1(1)]\sin\omega_1 t - \mathrm{Im}[x_2(1)]\sin\omega_2 t \; \right| \tag{6.30}$$

The two magnitudes are computed for many values of t, and the root mean square values of the resulting amplitudes are used to define a measure of the input and the response. Thus, the transmissibility of the strut is:

$$TR = \frac{RootMeanSquare[R]}{RootMeanSquare[U_m]} \tag{6.31}$$

The transmissibility is computed over a wide range of frequencies to establish the resulting response curves for various cases. Again, the goal is to reduce the transmissibility to below one for as many frequencies as possible so that the isolator works effectively.

6.6 Results for a Fixed-end Buckled Strut Under Forced Two-frequency Axial Excitation

All of the following response curves were created in Excel. The stiffness parameter, damping coefficients, amplitude factor, and frequency factor are varied for different cases. The transmissibility is plotted versus the frequency and, in some cases, compared to the fixed-end forced harmonic model counterpart.

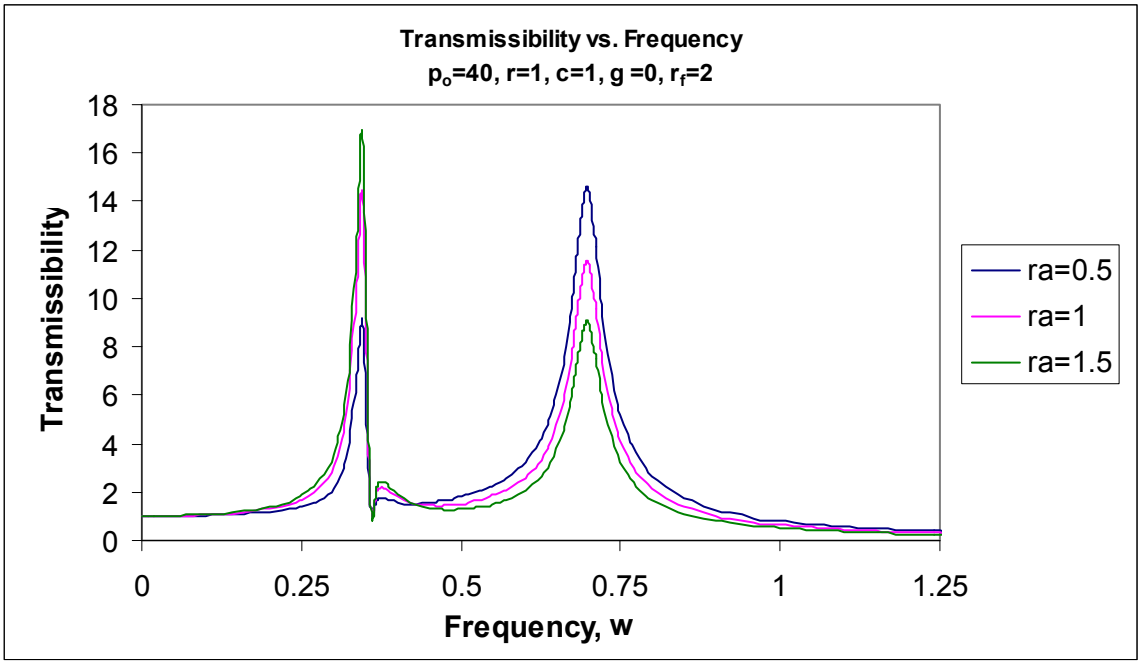

Figure 6.6.1: Transmissibility vs. Frequency for p_o=40, r=1, c=1, γ=0, r_f=2

Figure 6.6.1 shows the first set of peaks for three different cases. The struts in Figure 6.6.1 support a load of p_o=40, the stiffness parameter is r=1, the external damping coefficient is c=1, and the frequency factor for the second input frequency is r_f=2. The response is shown for r_a values of 0.5, 1, and 1.5. Varying the amplitude factors for the second input frequency has an obvious effect on the response of the strut. For example, for r_a=0.5, the first peak is much smaller than the second peak, but for r_a=1.5, the first peak is much larger than the second peak. Also, the frequency factor has an interesting effect on the response of the strut. As seen in the figure, the second peak occurs at

ω=0.697 and the first peak occurs at ω=0.345, which is about half of the second frequency.

In Figure 6.6.2, several similarities are evident. The strut in this figure supports the same load and has the same stiffness parameter and damping coefficient as in Figure 6.6.1. However, the frequency factor applied to the second input frequency is 1.5 instead of 2. The change in frequency factors again affects the location of the peak frequencies. The first peak occurs at about ω=0.460, and the second peak occurs at about ω=0.697 which is about 1.5 times the first peak. This is expected since the frequency factor applied to the second input frequency is 1.5. Therefore, it is concluded that the location of the first peak frequency is a result of the second input frequency and occurs at the value of the second peak frequency divided by the frequency factor, r_f. Also, r_a has the same effect as in Figure 6.6.1. Again, for r_a=0.5, the first peak is smaller than the second peak, but for r_a=1.5, the first peak is larger than the second peak. It is interesting that as r_a increases, the first peak increases, but the second peak decreases.

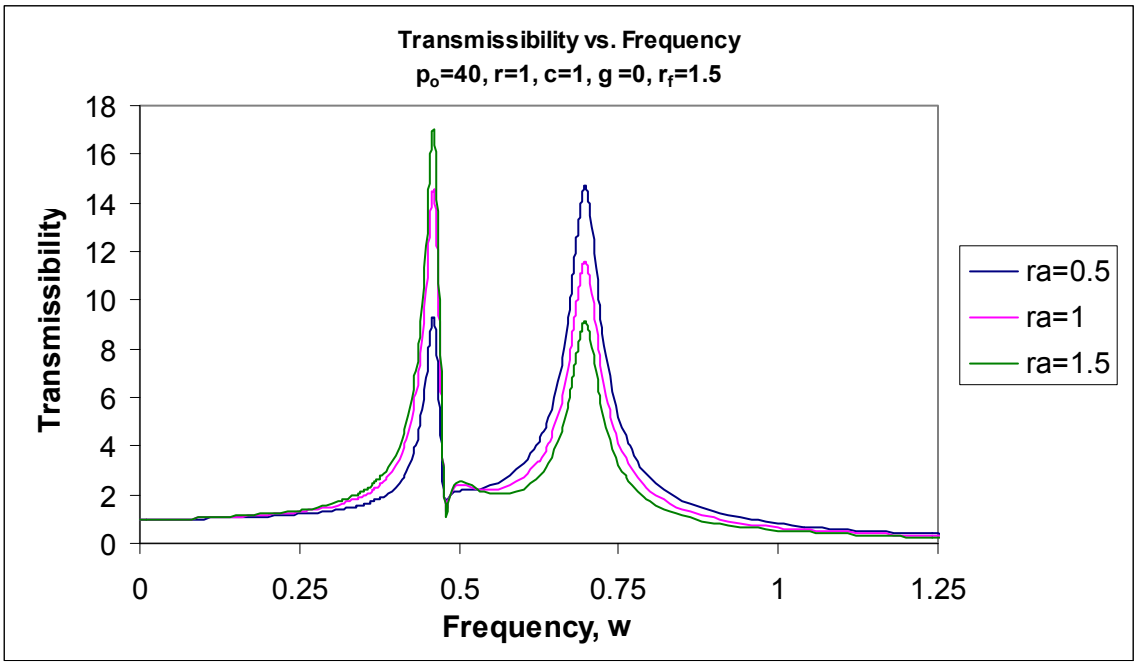

Figure 6.6.2: Transmissibility vs. Frequency for p_o=40, r=1, c=1, γ=0, r_f=1.5

Figure 6.6.3 shows the response of the same strut as in Figure 6.6.1 for r_a=0.5, but the range of frequencies plotted captures the response of the second set of transmissibility peaks. For this set of peaks, the first peak is maximum at ω=37.5 and the second peak is maximum at about ω=75.3 which is about twice the first peak frequency. However, for this set of peaks, the maximum transmissibilities for both peaks fall below one. Therefore, the motion of the system should be reduced at any applied frequency once the transmissibility following the fundamental set of peaks falls below one. As shown in Figure 6.6.1, the motion of the system is reduced after ω=0.95. This strut will work effectively to reduce the motion at frequencies ω above 0.95.

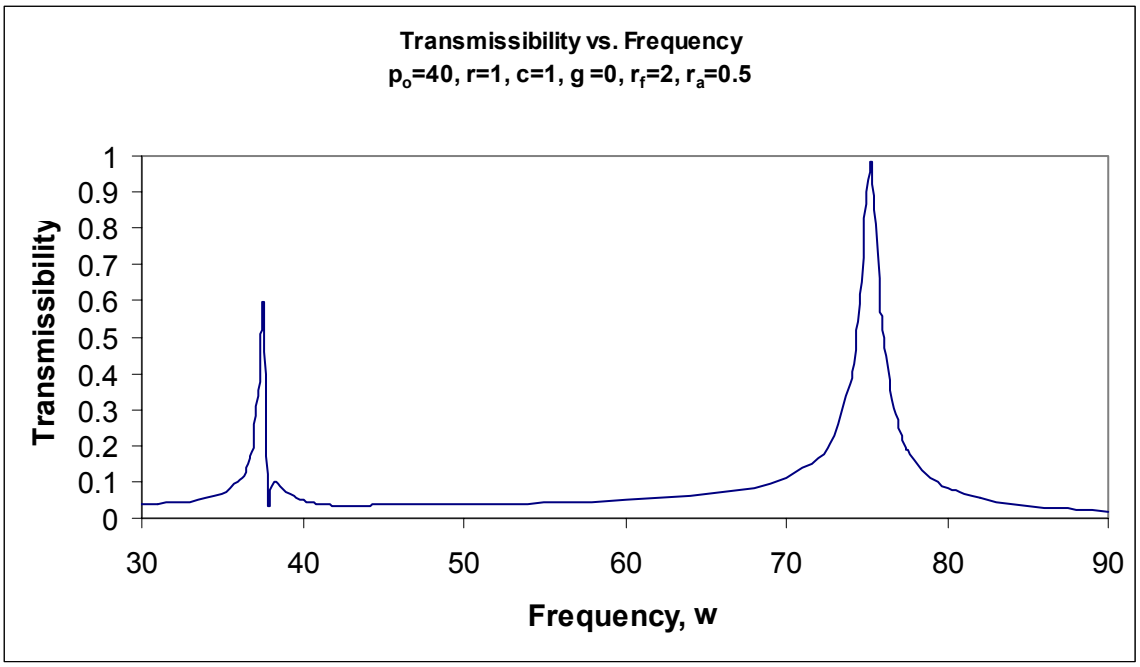

Figure 6.6.3: Transmissibility vs. Frequency for p_o=40, r=1, c=1, γ=0, r_f=2, r_a=0.5

Figures 6.6.4 and 6.6.5 show the results of the same model as in Figure 6.6.1 for r_a=1 and three r values, with different scales on the Y-axis. The full view can be seen in Figure 6.6.4, while Figure 6.6.5 focuses on the frequencies with lower transmissibilities when the motion is reduced. As shown in Figure 6.6.4, the varying stiffness parameter has a similar effect as it did on the strut under harmonic motion. First, as the stiffness parameter increases, the damped resonant frequency decreases. Also, the magnitude of the maximum transmissibility increases as the stiffness parameter increases.

In Figure 6.6.5, it is apparent that the range of high transmissibilities decreases as the stiffness parameter increases. For example, when r=10 the transmissibility drops below one when ω is about equal to 0.3, but when r=0.1, the motion is not reduced until ω is about 1.03. This is comparable to the response of the strut under harmonic motion, as well.

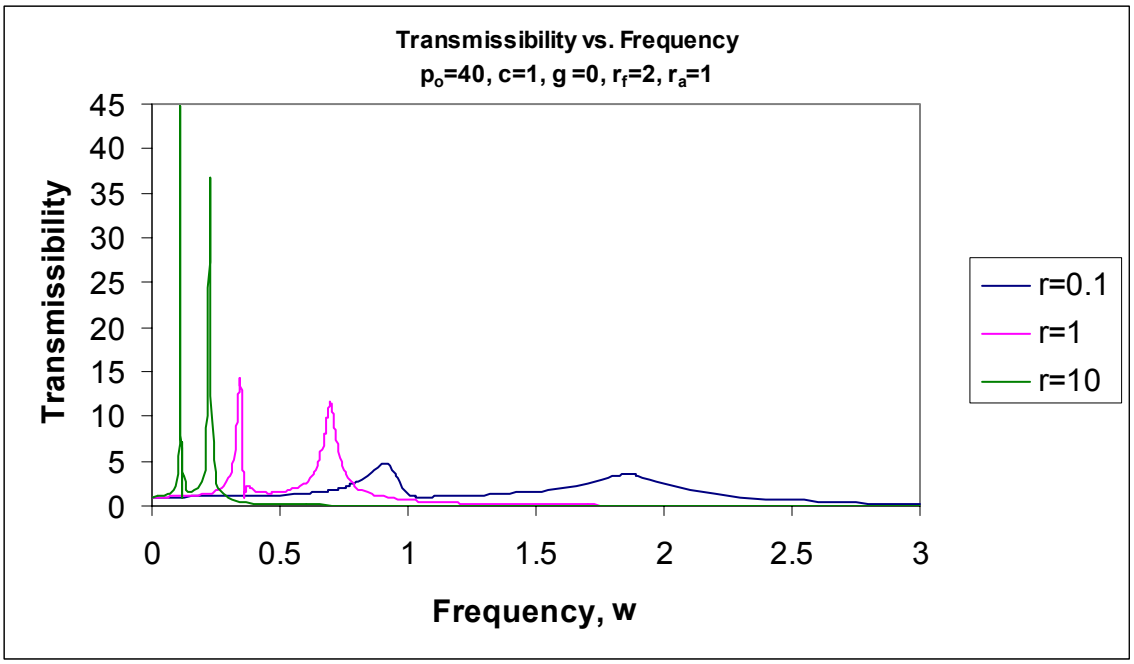

Figure 6.6.4: Transmissibility vs. Frequency for p_o=40, c=1, γ=0, r_f=2, r_a=1

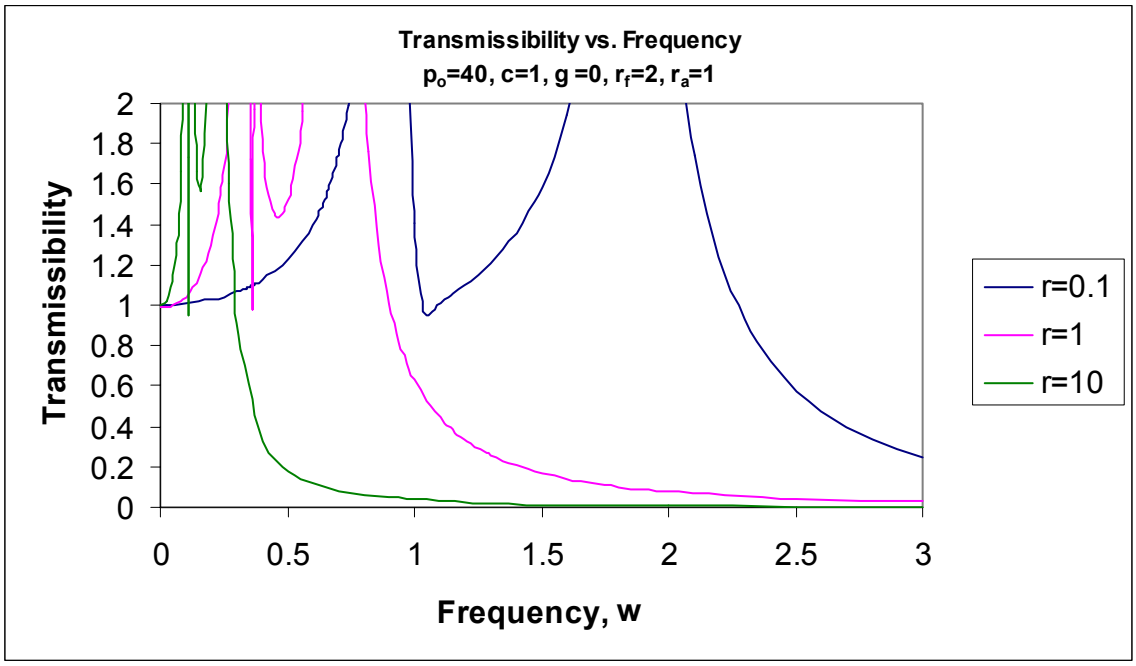

Figure 6.6.5: Transmissibility vs. Frequency for p_o=40, r=1, c=1, γ=0, r_f=2, r_a=1

Figure 6.6.6 shows the effect of increasing the external damping coefficient on the system. The strut shown in this figure supports a load of p_o=40, the stiffness parameter is r=1, the frequency factor for the second input frequency is r_f=2, and the amplitude factor for the second input frequency is r_a=1. The external damping coefficient is varied from c=0.1 to 10. Clearly the maximum transmissibility is reduced as the damping coefficient increases. When c=10 the damped resonant peaks are small and come close to an overdamped case. In any case, the addition of damping reduces the maximum transmissibility for both peaks of this model.

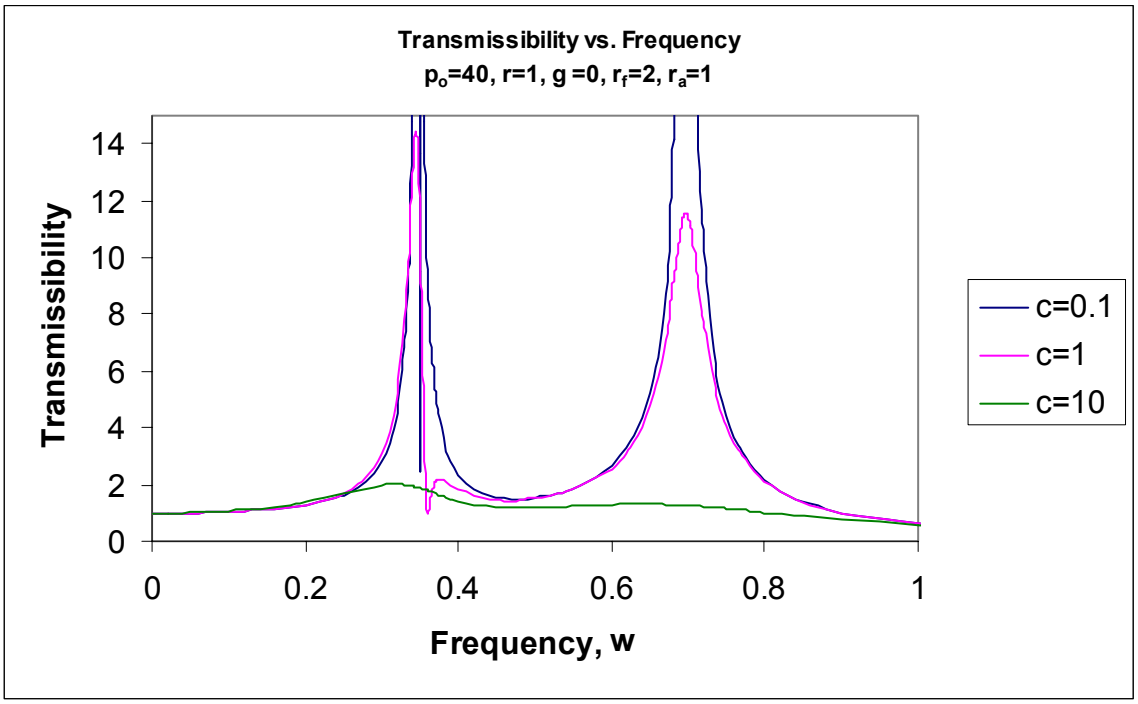

Figure 6.6.6: Transmissibility vs. Frequency for p_o=40, r=1, γ=0, r_f=2, r_a=1

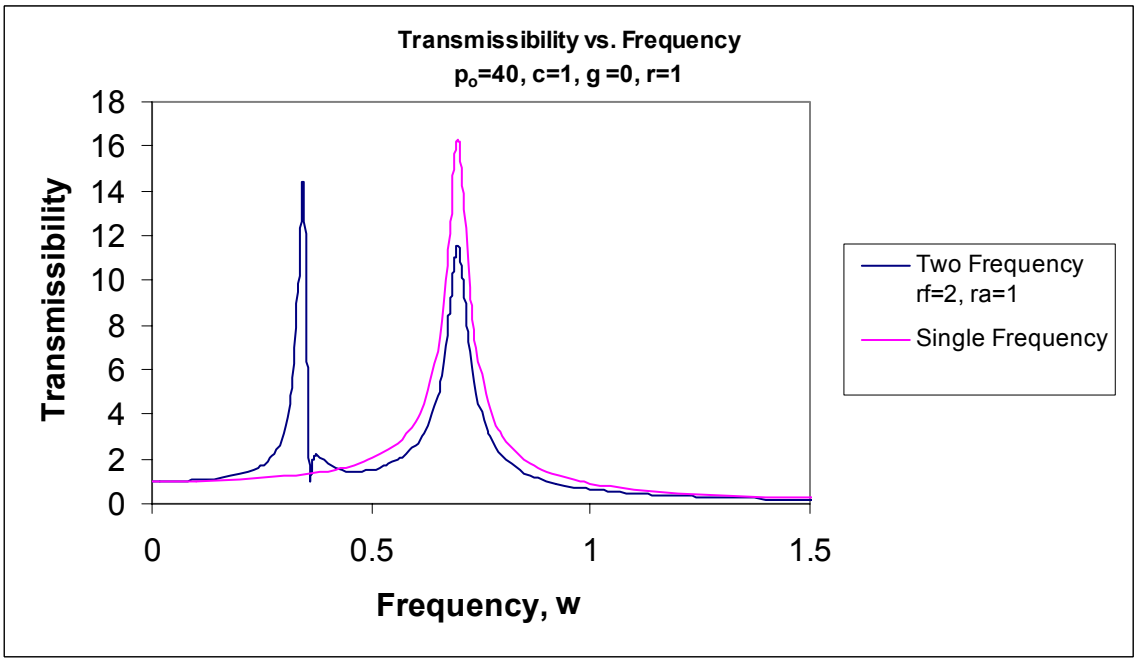

Figure 6.6.7: Transmissibility vs. Frequency for p_o=40, r=1, c=1, γ=0 for Two-frequency Model r_f=2, r_a=1 and Single Frequency Model

Figure 6.6.7 shows the results of the two-frequency input with r_f=2 and r_a =1 plotted with the single-frequency, harmonic case. The strut supports a load of p_o=40, has a stiffness parameter of r=1, and has a damping coefficient of c=1. As mentioned previously, the first peak of the two-frequency case occurs at half of the frequency of the second peak since r_f=2 for this case. In Figure 6.6.8, the two-frequency model with r_f=1.5 and r_a =1, and the single-frequency model are compared. Again, the first peak of the two-frequency case depends on the r_f value of 1.5

The most interesting feature of Figures 6.6.7 and 6.6.8 is the location of the second peak of the two-frequency model. It is obvious that the second peak coincides with the same frequency as the peak for the harmonic case. The presence of the two peaks results from the input of $u(t) = u_1 e^{i\omega_1 t} + u_2 e^{i\omega_2 t}$. If the single-frequency system has a natural frequency of ω_n, then for the two-frequency system, $e^{i\omega t}$ will have a larger response at ω near ω_n and $e^{ir_f \omega t}$ will have a larger response for $r_f\omega$ near ω_n. Therefore, if $r_f > 1$, then the peak will be at an ω lower than ω_n, as seen in these figures.

Although the transmissibility of the two-frequency input has two peaks, the motion is still reduced at about the same frequency. Since the working range of the strut under harmonic motion would be set at the point where motion is reduced, the addition of a second frequency would not affect the strut's performance over its working range. However, below this lower limit of the working range, the motion of the supported load will be amplified over a larger range of frequencies.

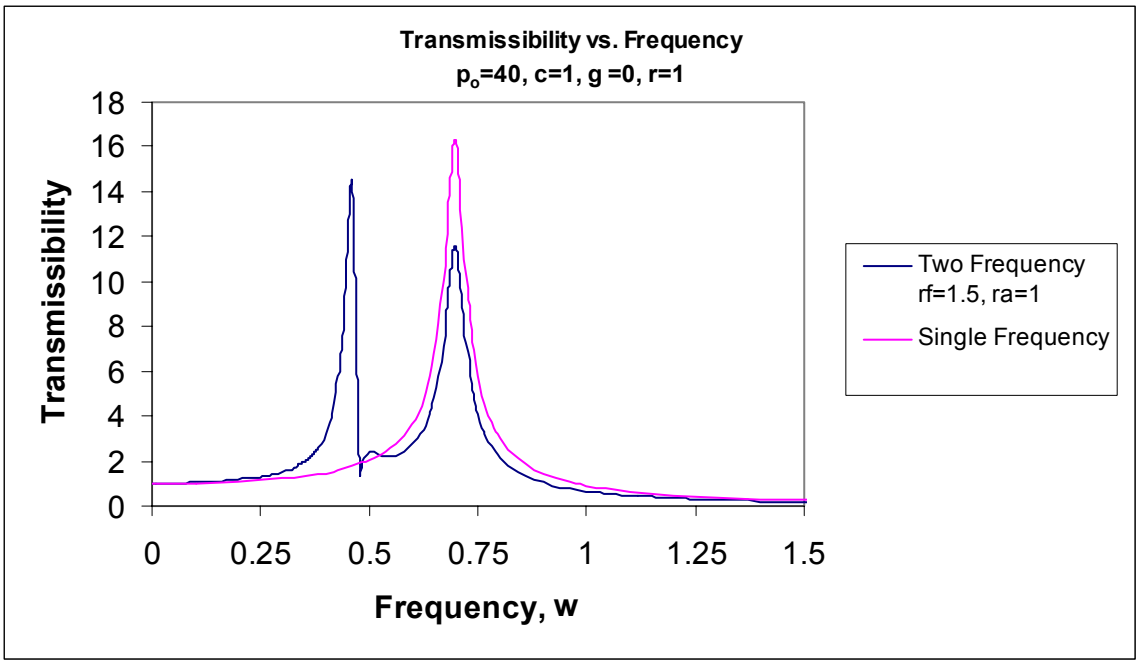

Figure 6.6.8: Transmissibility vs. Frequency for p_o=40, r=1, c=1, γ=0 for Two-frequency Model r_f=1.5, r_a=1 and Single Frequency Model

In Figures 6.6.9 and 6.6.10, the effect of the stiffness parameter can be seen for both the two-frequency model and the harmonic model. Comparing the two figures, it is obvious that the increased stiffness parameter in Figure 6.6.10 reduces the range of frequencies over which the motion of the supported load is reduced for both the two-frequency model and the harmonic model. In Figure 6.6.9, the motion is reduced at ω=2.25 and ω=2.4 for the two-frequency and harmonic cases, respectively. In Figure 6.6.10, the motion is reduced at ω=0.29 and ω=0.31 for the two-frequency and harmonic cases, respectively. This is a significant difference for both models, despite the type of axial motion applied.

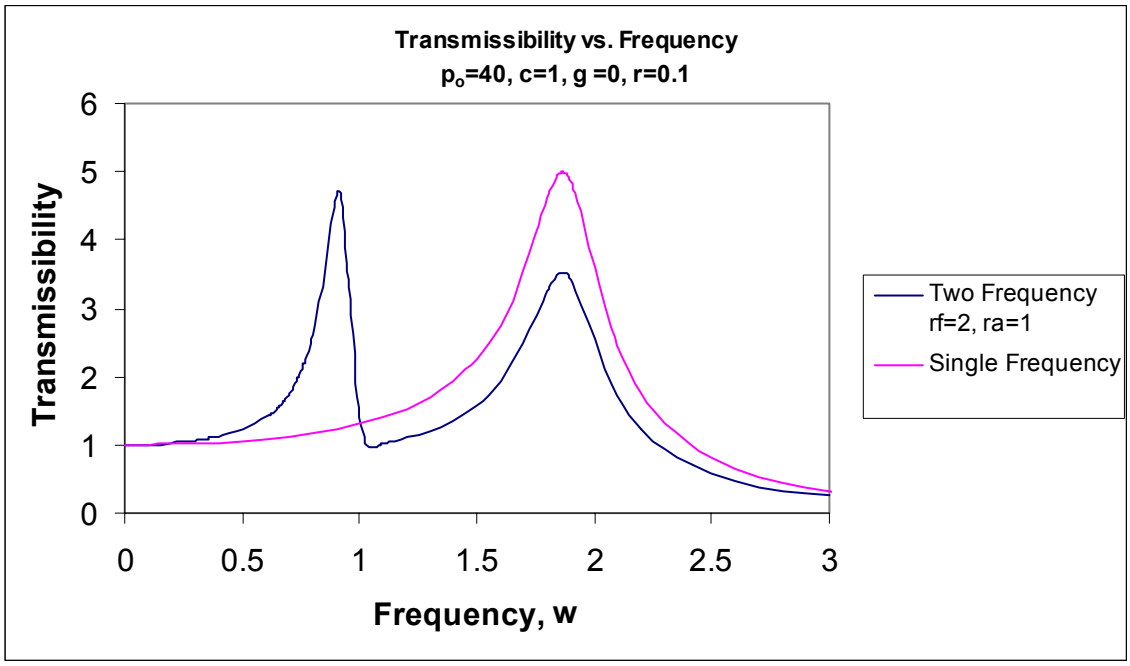

Figure 6.6.9: Transmissibility vs. Frequency for p_o=40, r=0.1, c=1, γ=0 for Two-frequency Model r_f=2, r_a=1 and Single Frequency Model

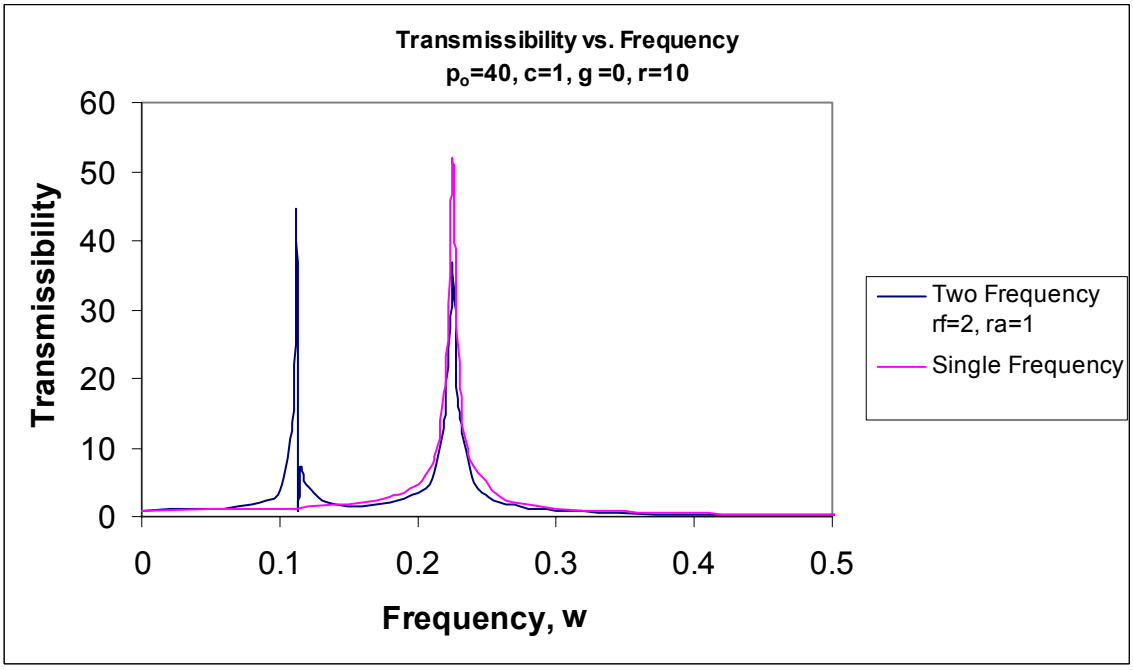

Figure 6.6.10: Transmissibility vs. Frequency for p_o=40, r=10, c=1, γ=0 for Two-frequency Model r_f=2, r_a=1 and Single Frequency Model

6.7 Conclusions

The results of the two-frequency excitation model show some similarities to the results of the models with applied harmonic motion. First, increasing the damping coefficient reduces the maximum transmissibility for both peaks of the two-frequency model in the same manner as it did with the single-frequency system. Also, it is possible to have a system become overdamped when the damping coefficient surpasses its critical damping value. In addition, the stiffness parameter significantly affects the results of the model. As the stiffness parameter is increased, the nondimensional resonant frequency is decreased, and the range of frequencies that produces high transmissibilities is reduced.

The main difference evident in this model is the additional peak that results from the addition of the second frequency. The second peak occurs at a frequency equal to the value of the frequency of the second peak divided by the frequency factor applied to the input frequency. Also, for a given case, the second peak occurs at the same frequency as the resonant peak for its harmonic counterpart. This coincidence allows the strut to be as effective when a multi-frequency vibration is applied as it is when a harmonic frequency is applied. The working range of the strut is actually slightly larger than for the harmonic counterpart. In any case, adding a second harmonic excitation with a higher frequency does not diminish the ability of these buckled struts to reduce vibrations in a range above the resonant frequency for harmonic excitation.

Chapter 7: Summary and Conclusions

7.1 Summary of Models

Overall, five models are examined in this thesis. All of the models are assumed to be inextensible along their lengths. First, two ideal, buckled columns with different boundary conditions are subjected to harmonic, axial excitations. One, presented in chapter 2, is a pinned-end column with rotation but no moment at its ends. The topic of chapter 3 is a fixed-end column which supports end moments to prevent any rotation at its ends. Both of these models support loads above their buckling load.

Columns with initial curvature subjected to axial harmonic motion are analyzed next. The pinned-end column of chapter 4 mimics imperfections in columns resulting from fabrication. The strut is analyzed with several amounts of curvature under loads above and below the buckling load. A similar analysis is presented in chapter 5 for a fixed-end column.

Chapter 6 is dedicated to a fixed-end ideal column subjected to two-frequency axial excitations. The results are presented and compared to the cases with motion from a single-frequency input.

Results from each model make significant contributions to the complete understanding of the way these buckled struts may be useful as vibration isolators.

7.2 Summary of Analysis Procedure

Small variations exist between the analysis procedure and the equations used for different models, but the general procedure can be outlined. Each Mathematica program uses the known parameters and known boundary conditions at the base of the column. The boundary value problem is treated as an initial value problem. The unknown parameters and unknown boundary conditions at the base are varied until the solution satisfies the

known boundary conditions at the top of the column with sufficient accuracy. This is called a shooting method. All programs can be found in the appendices.

All of the models are first examined under static equilibrium. Meeting all geometric and equilibrium constraints for each model, the static equations of equilibrium are established and used in a Mathematica program. The numerical solution for the static equilibrium solves for the necessary variables to be used as input for the dynamic analysis.

Then, the dynamic analysis is performed repeatedly over hundreds of frequencies for each case. The transmissibility is determined using a Mathematica program, and the results are plotted over the many frequency values. Many cases are evaluated, presented, and compared to other similar cases, and conclusions can be made from these results.

7.3 Conclusions

The results for certain features of the models are similar in nature, and they can be presented together. First, the stiffness parameter seems to affect all of the models in a similar way. Most of the Excel plots are presented for the same strut with three different stiffness parameter values. For every result, as the stiffness parameter increases, the nondimensional frequency, ω, which produces the lowest resonance is reduced. The dimensional frequency was found to increase as the stiffness parameter increases. Also, as the stiffness parameter increases, the maximum transmissibility increases, but the range of frequencies with high transmissibilities decreases. So, increasing the stiffness parameter can be an advantage and a disadvantage. A good balance must be found to make the isolator effective.

Next, the damping coefficients are varied for each model, and their effects are significant. Both external damping and internal damping are included in certain models. However, the effects from each are similar, and they will be addressed together. From the results of any model, it is completely apparent that increasing the damping coefficient is desirable to reduce the maximum transmissibility. Many plots are presented with the undamped

case included for comparison, and even the smallest damping coefficient effectively reduces the infinite peak of the undamped case. Also, several overdamped cases are presented, showing the effect of very high amounts of damping on a system. For the overdamped case, the motion of the system is always reduced. However, overdamped systems are typically impractical. In any case, the damping coefficient significantly reduces the motion of the supported load and a significant amount of damping should be included in this vibration isolation system.

The models with initial curvature are considered with supported loads above and below their buckling loads. The results for the struts supporting various loads introduced some new data trends for the transmissibility plotted over a very wide range of frequencies. When the load is below the buckling load and the initial deflection is symmetric, only the symmetric mode shapes produce a large resonant peak, but when the load is above buckling, all of the mode shapes produce large resonant peaks. Resonant peaks are still present for the struts supporting loads below the buckling load, but the transmissibility is not large. When the load is above the buckling load, the motion between the peaks is reduced much more than for the lower loads. Basically, the system is more effective when the load is above buckling as long as the applied excitations occur between the resonant peaks.

The last model presented is a fixed-end strut with a two-frequency axial excitation applied at the base of the model. The results for this model are somewhat different from the previous models since the input excitation is quite different. The main distinction evident in the results is the additional peak (for each resonance) that results from the addition of the second frequency. It is obvious that the second peak corresponds to the same natural frequency as the peak for the harmonic case. The presence of the two peaks results from the input of $u(t) = u_1 e^{i\omega_1 t} + u_2 e^{i\omega_2 t}$. If the system has a natural frequency of ω_n, then for the two-frequency input, $e^{i\omega t}$ will cause a large response at ω near ω_n and $e^{ir_f \omega t}$ will cause a large response for $r_f\omega$ near ω_n. Therefore, if $r_f > 1$, the additional peak will be at a frequency lower than ω_n. In any case, adding a second harmonic excitation

with a higher frequency does not diminish the ability of these buckled struts to reduce vibrations in a range above the resonant frequency for harmonic excitation.

Overall, buckled struts seem to be rather effective at reducing the motion of a system when the applied excitation is above the fundamental resonant frequency. Damping can be used to reduce the motion of the supported load, while the stiffness parameter can be designed to effectively absorb the energy of the applied motion in the strut. Imperfect columns show their efficacy as long as the load is close to the buckling load. Also, models with multi-frequency excitations tend to be effective if the applied frequency is above the natural frequency. All of the models examined in this thesis effectively reduce the motion of the system over a certain range of frequencies.

However, despite the ability of the struts to perform over a specific range of frequencies, unanticipated or shock excitations are unpredictable in regard to the frequency of excitation. If the applied frequency from some unexpected source were to be around the resonant frequency of any of these models, the system is susceptible to failure. The motion of the system is amplified around the resonant frequency, and despite the reduction of motion above this frequency, the presence of this dangerous frequency range should not be ignored.

7.4 Recommendations for Future Research

Vibration suppression is necessary for so many structures and machinery that continued research can easily be justified. Perhaps other structures may be suitable to help mitigate damaging vibrations, such as buckled plates. Buckled plates may be useful when torsional components are induced as a response to the excitation. Also, with the torsional resistance available in buckled plates, other types of excitations can be applied to the models. In addition to the vertical motion applied to the struts in this thesis, rotational motion may be applied, as well.

Also, different types of excitation could be explored rather than simple harmonic motion and multi-frequency vibrations. For instance, shock and impact loadings could be explored to improve the performance of the isolators. These types of excitation may disturb the buckled static equilibrium of the models used in this thesis, and might lead to some new ideas of how to avoid damage due to such unexpected motion.

In general, many new models can be identified which would be helpful in securing buckled structures as effective vibration isolators. These new models could be the next step in finding a solution to the recurring structural damage due to earthquakes, vibrating machinery, or unanticipated impacts.

References

Alloway, L.A. (2003). Analysis of Buckled Columns and Rigid-Link Mechanisms Used as Vibration Isolators. M.E. Report, Virginia Tech, Blacksburg, VA

Chen, S., Liu, K., and Liu, Z. (1998). "Spectrum and Stability for Elastic Systems with Global or Local Kelvin-Voigt Damping," SIAM Journal on Applied Mathematics, Vol. 59, No. 2, pp. 651-668.

Chopra, A.K. (2001). Dynamics of Structures, 2nd ed. Prentice Hall, Inc., Upper Saddle River, NJ.

Clough, R.W., and Penzien, J. (1975). Dynamics of Structures. McGraw-Hill, New York, NY.

Davis, R.B., and Virgin, L.N. (2003). "Vibration Isolation Using Buckled Struts," Journal of Sound and Vibration, Vol. 260, pp. 965-973.

Karnopp, D. (1995). "Active and Semi-Active Vibration Isolation," Journal of Vibration and Acoustics, Vol. 117, pp. 177-185.

Nelson, F.C. (1994). "Vibration Isolation: A Review, I. Sinusoidal and Random Excitations," Shock and Vibration, Vol. 1, pp. 485-493.

Nelson, F.C. (1996). "Vibration Isolation Review: II. Shock Excitation," Shock and Vibration, Vol. 3, pp. 451-459.

Rivin, E.I. (2003). Passive Vibration Isolation. American Society of Mechanical Engineers Press, New York, NY.

Sciulli, D. (1997). Dynamics and Control for Vibration Isolation Design. Ph.D. Dissertation, Virginia Tech, Blacksburg, VA.

Virgin, L.N., and Plaut, R.H. (2002). "A Novel Type of Vibration Isolator Utilizing Buckled Structures," Proposal to National Science Foundation, Project Summary and Description.

Winterflood, J., Barber, T., and Blair, D.G. (2002a). "Using Euler Buckling Springs for Vibration Isolation," Classical and Quantum Gravity, Vol. 19, pp.1639-1645.

Winterflood, J., Blair, D.G., and Slagmolen, B. (2002b). "High Performance Vibration Isolation Using Springs in Euler Column Buckling Mode," Physics Letters A, Vol. 300, pp. 122-130.

Winterflood, J., Barber, T.A., and Blair, D.G. (2002c). "Mathematical Analysis of an Euler Spring Vibration Isolator," Physics Letters A, Vol. 300, pp.131-139.

Appendix A

A.1 Pinned-end Strut, Static Equilibrium

Mathematica code

Input and Initial Guesses

```
(*Equilibrium,pinned buckled strut,y1=x,y2=y,y3=theta,y4=moment,
  doesn't include shear force q which is zero; m in leftBC is theta at s=0,
  p=po (larger than 9.87)*)
Clear[pi,gm,m,c]
pi = N[\[Pi]];
pe=10;
gm = 0.53 ;
```

Equations from equilibrium

```
de[y3_,y4_]:={y1'[t]\[Equal]Cos[y3[t]],y2'[t]\[Equal]Sin[y3[t]],
   y3'[t]\[Equal]y4[t],y4'[t]\[Equal]-pe*Sin[y3[t]]}
```

Boundary conditions at s=0

```
leftBC[m_]:={y1[0]\[Equal]0,y2[0]\[Equal]0,y3[0]\[Equal]m,y4[0]\[Equal]0}
```

Numerical Solution

```
soln:=NDSolve[Flatten[Append[de[y3,y4],leftBC[m]]],{y1,y2,y3,y4},{t,0,1},
   MaxSteps\[Rule]2000]
endpt[m_]:={y1[t],y2[t],y3[t],y4[t]}/.First[
        NDSolve[Flatten[Append[de[y3,y4],leftBC[m]]],{y1[t],y2[t],y3[t],
           y4[t]},{t,0,1},MaxSteps\[Rule]2000]]/.t\[Rule]1;
endpt[gm]
{0.931553,0.00565365,-0.529684,-0.0565365}
Clear[m]
```

```
rts:=FindRoot[{endpt[m][[2]]\[Equal]0},{m,{gm,0.99gm}},AccuracyGoal\[Rule]6,
   MaxIterations\[Rule]1000]
endpt[m/.rts]
({0.9739486243181599`,
   5.85563414090887`*^-7, \(-0.3236878896230692`\), \
\(-5.855634140839004`*^-6\)}

Solving for the moment
m=m/.rts
0.323689

 Plotting strut
{yy1[t_],yy2[t_],yy3[t_],yy4[t_]}={y1[t],y2[t],y3[t],y4[t]}/.First[soln];
ParametricPlot[Evaluate[{yy1[t],yy2[t]}/.soln/.rts],{t,0,1},
  PlotRange\[Rule]All,AspectRatio\[Rule]Automatic,PlotPoints\[Rule]100]
```

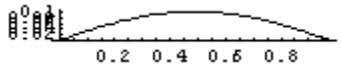

A.2 Pinned-end Strut Dynamic Analysis

Mathematica code

Input and Initial Guesses

```
(*Forced small vibrations about buckled equilibrium; pinned strut; y1=xe,
  y2=ye,y3=theta_e,y4=me, y5=xd,y6=yd,y7=theta_d,y8=md,y9=pd,y10=qd;
  given po and uo and frequency,
  and theta_e(0) which is value m from StrutEquil3*)

Clear[pi,uo,po,\[Omega],gpd,gqd,gy3a,gy7a,pd,qd,y3a,y7a]
  pi = N[\[Pi]];
  uo=0.011;
  po=10;
  m=0.32368906976279493`;

  \[Omega]=1;
  r=10;
  c=0;
  i=(-1)^0.5;
  g=.1
  gpd=-1;
  gqd=-0.02;
  gy7a=0.25;

Equations from equilibrium
de[y3_,y4_,y5_,y6_,y7_,y8_,y9_,y10_]:= {y1'[t]\[Equal]Cos[y3[t]],
    y2'[t]\[Equal]Sin[y3[t]],y3'[t]\[Equal]y4[t],y4'[t]\[Equal]-po*Sin[y3[t]],
    y5'[t]\[Equal]-y7[t]*Sin[y3[t]],y6'[t]\[Equal]y7[t]*Cos[y3[t]],
    y7'[t]\[Equal]y8[t]/(1+i*\[Omega]*g),
    y8'[t]\[Equal](y10[t]-po*y7[t])*Cos[y3[t]]-y9[t]*Sin[y3[t]],
    y9'[t]\[Equal](\[Omega]^2-i*\[Omega]*c)*y5[t],
    y10'[t]==(\[Omega]^2-i*\[Omega]*c)*y6[t]}

Boundary Conditions at s=0
leftBC[pd_,qd_,y7a_] := {y1[0]\[Equal]0,y2[0]\[Equal]0,y3[0]\[Equal]m,
    y4[0]\[Equal]0,y5[0]\[Equal]uo,y6[0]\[Equal]0,y7[0]\[Equal]y7a,
    y8[0]\[Equal]0,y9[0]\[Equal]pd,y10[0]\[Equal]qd}

Numerical Solution
soln:=NDSolve[
    Flatten[Append[de[y3,y4,y5,y6,y7,y8,y9,y10],leftBC[pd,qd,y7a]]],{y1,y2,y3,
      y4,y5,y6,y7,y8,y9,y10},{t,0,1}, MaxSteps\[Rule]2000]
```

```
endpt[pd_,qd_,
     y7a_]:={y1[t],y2[t],y3[t],y4[t],y5[t],y6[t],y7[t],y8[t],y9[t],
        y10[t]}/.First[
        NDSolve[Flatten[
           Append[de[y3,y4,y5,y6,y7,y8,y9,y10],leftBC[pd,qd,y7a]]],{y1[t],
           y2[t],y3[t],y4[t],y5[t],y6[t],y7[t],y8[t],y9[t],y10[t]},{t,0,1},
          MaxSteps\[Rule]1000]]/.t\[Rule]1;
endpt[gpd,gqd,gy7a];

Shooting for boundary conditions at s=1
Clear[pd,qd,y7a]
rts:=FindRoot[{endpt[pd,qd,y7a][[9]]\[Equal]-r*
        po*(\[Omega]^2)*(endpt[pd,qd,y7a][[5]]),
     endpt[pd,qd,y7a][[6]]\[Equal]0,
     endpt[pd,qd,y7a][[8]]\[Equal]0},{pd, {gpd,0.99*gpd}},{qd, {gqd,
       0.99*gqd}},{y7a, {gy7a,0.99*gy7a}},AccuracyGoal\[Rule]6,
   MaxIterations\[Rule]2000]

Solving for endpoint solution
endpt[pd/.rts,qd/.rts,y7a/.rts]
\!\({0.9739485908661369`,
   6.030546019939143`*^-7, \(-0.32368784078946994`\), \
\(-6.030546019676754`*^-6\), \(\(0.000042508638833742O4`\)\(\[InvisibleSpace]\
\)\) - 0.0021814502230348646`\ \[ImaginaryI], \(-1.1047101225100172`*^-12\) +
     8.346888987189179`*^-13\ \[ImaginaryI], \(-0.06845741295987326`\) -
     0.013630354925343417`\ \[ImaginaryI],
   1.0752748173441937`*^-11 -
     7.510758504575928`*^-12\ \[ImaginaryI], \(-0.004250863781237399`\) +
     0.21814502209471312`\ \[ImaginaryI], \(\(0.006297605182867748`\)\(\
\[InvisibleSpace]\)\) + 0.0013993769617233337`\ \[ImaginaryI]}\)

pd=pd/.rts
qd=qd/.rts
y7a=y7a/.rts

-0.0097726+0.219236 \[ImaginaryI]
-0.00703105-0.00125431 \[ImaginaryI]
0.0684305\[InvisibleSpace]+0.0136396 \[ImaginaryI]

Solving for the Transmissibility
{yy1[t_],yy2[t_],yy3[t_],yy4[t_],yy5[t_],yy6[t_],yy7[t_],yy8[t_],yy9[t_],
     yy10[t_]}={y1[t],y2[t],y3[t],y4[t],y5[t],y6[t],y7[t],y8[t],y9[t],
       y10[t]}/.First[soln];
TR=((((Re[N[yy5[1]]])^2+(Im[N[yy5[1]]])^2))^0.5)/uo

0.198351
```

A.3 Additional Results for Forced Vibrations of the Pinned-end Buckled Strut

The following plots are additional cases that were analyzed. In order to prevent repetition, these plots were not included in the text of the thesis. All plots corroborate the findings presented in Chapter 2.

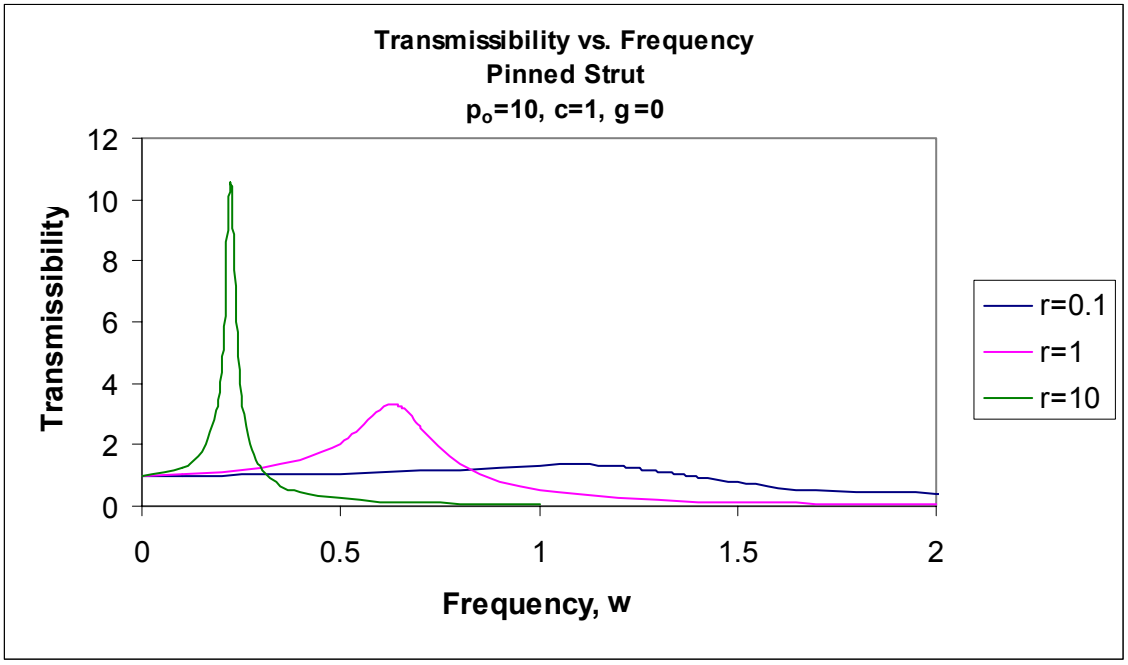

Figure A3.1: Transmissibility vs. Frequency for p_o=10, c=1, γ=0

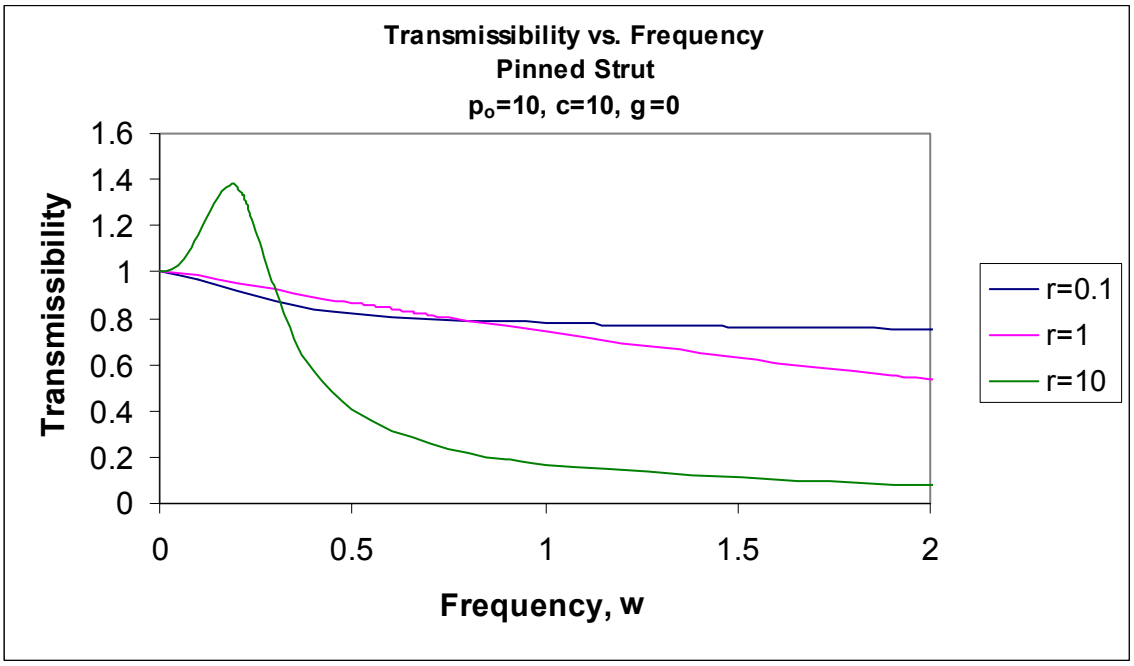

Figure A3.2: Transmissibility vs. Frequency for p_o=10, c=10, γ=0

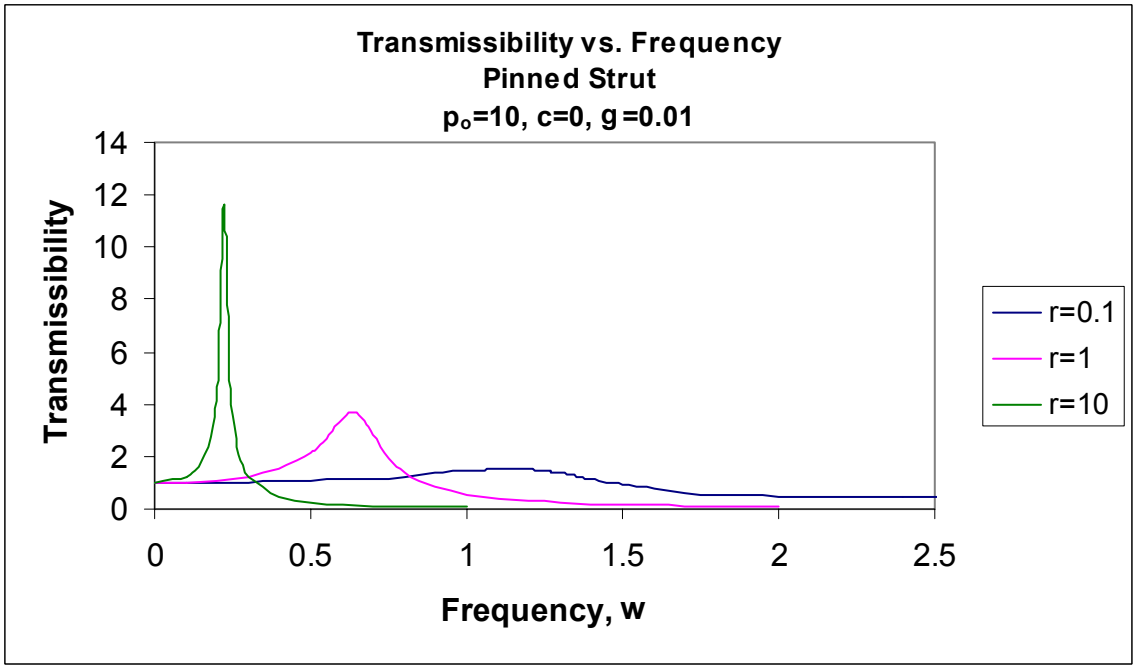

Figure A3.3: Transmissibility vs. Frequency for p_o=10, c=0, γ=0.01

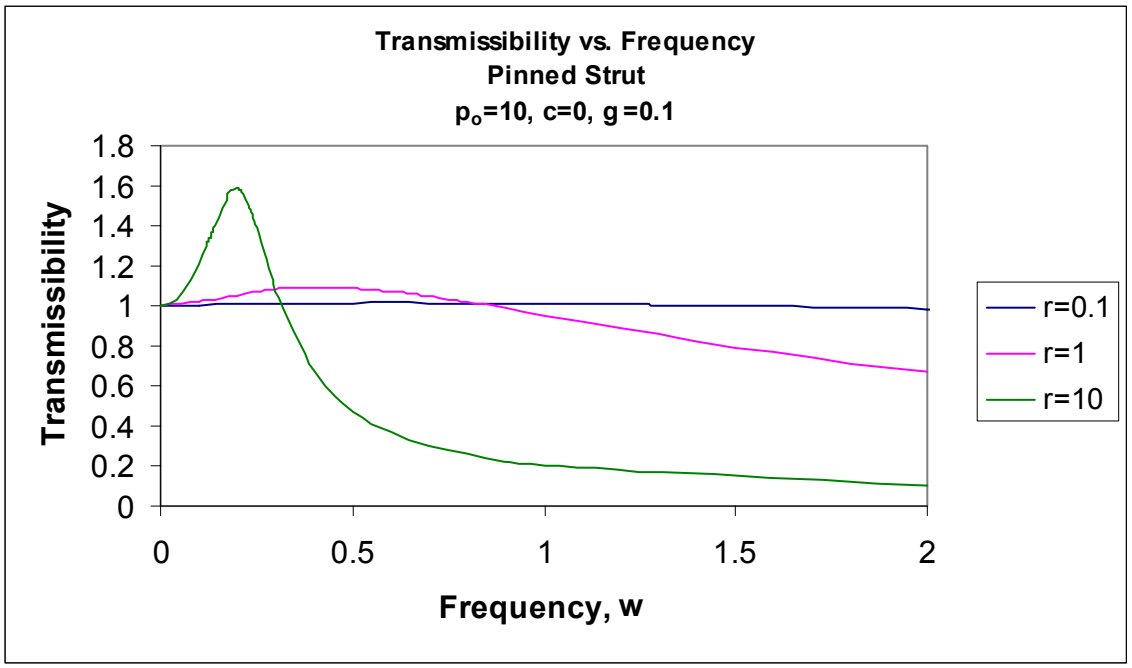

Figure A3.4: Transmissibility vs. Frequency for p_o=10, c=0, γ=0.1

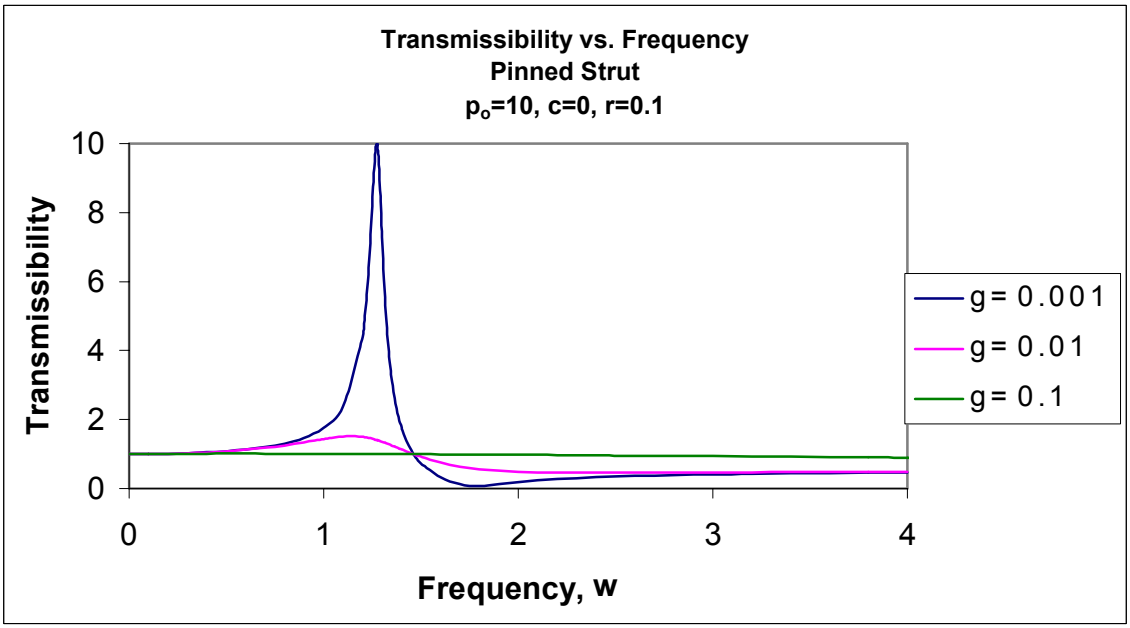

Figure A3.5: Transmissibility vs. Frequency for p_o=10, c=0, r=0.1

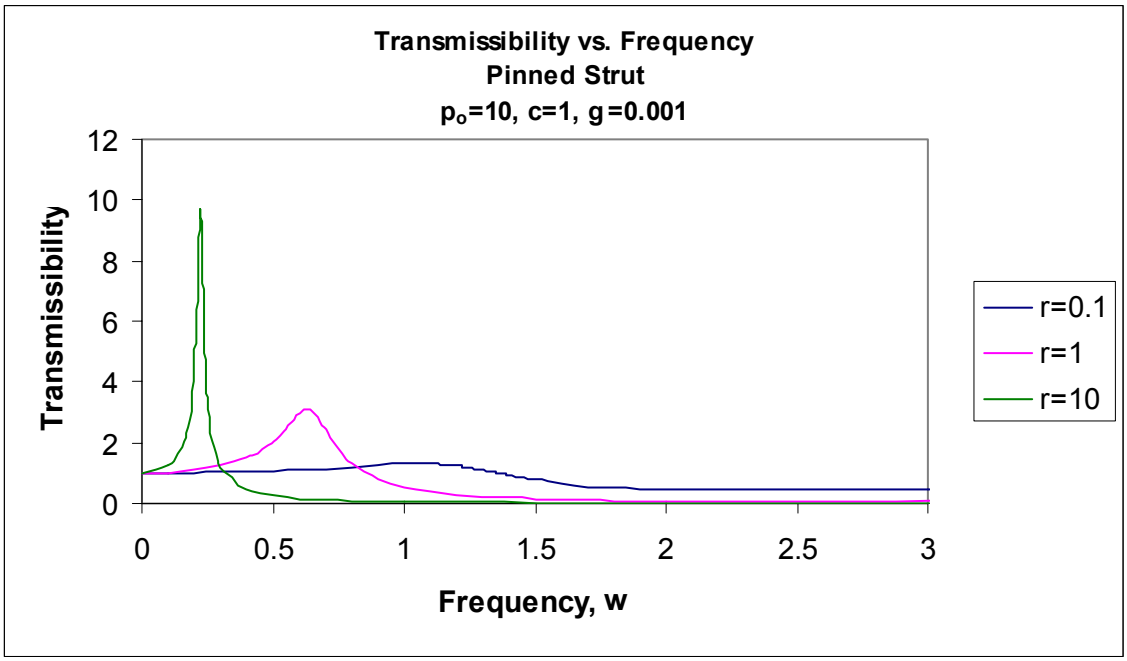

Figure A3.6: Transmissibility vs. Frequency for p_o=10, c=1, γ=0.001

Appendix B

B.1 Fixed-end Strut, Static Equilibrium

Mathematica Code

Input and Initial Guesses

```
(*Equilibrium, clamped buckled strut,y1=x,y2=y,y3=theta,y4=moment,
  includes shear force q which is not zero; m in leftBC is theta at s=0,
  p=po (larger than 39.48 = 4*pi^2)*)

Clear[pi,gm,gq,m,q,po]
pi = N[\[Pi]];

po = 40;
gm = 2.04;
gq = -0.00002;

Equations from equilibrium
de[y3_,y4_,q_]:={y1'[t]\[Equal]Cos[y3[t]],y2'[t]\[Equal]Sin[y3[t]],
   y3'[t]\[Equal]y4[t],y4'[t]\[Equal]-po*Sin[y3[t]]+q*Cos[y3[t]]}

Boundary conditions at s=0
leftBC[m_]:={y1[0]\[Equal]0,y2[0]\[Equal]0,y3[0]\[Equal]0,y4[0]\[Equal]m}

Numerical Solution
soln:=NDSolve[Flatten[Append[de[y3,y4,q],leftBC[m]]],{y1,y2,y3,y4},{t,0,1},
   MaxSteps\[Rule]2000]
endpt[m_,q_]:={y1[t],y2[t],y3[t],y4[t]}/.First[
        NDSolve[Flatten[Append[de[y3,y4,q],leftBC[m]]],{y1[t],y2[t],y3[t],
           y4[t]},{t,0,1},MaxSteps\[Rule]2000]]/.t\[Rule]1;
endpt[gm,gq]
\!\({0.9739042924518324`, \(-5.4737131136458815`*^-8\), \
\(-0.000029197552945157166`\), 2.039982711399395`}\)
Clear[m,q]

Solving for the moment and shear force
rts:=FindRoot[{endpt[m,q][[2]]\[Equal]0,
     endpt[m,q][[3]]\[Equal]0},{m,{gm,0.98*gm}},{q,{gq,0.98*gq}},
   AccuracyGoal\[Rule]8,MaxIterations\[Rule]1000]
endpt[m/.rts,q/.rts]
\!\({0.9739609773283532`, \(-1.5247386679445382`*^-14\),
   3.5765328536778025`*^-12, 2.0377877750502646`}\)
```

m=m/.rts
q=q/.rts
2.03781
-0.0000177529

Plotting strut

```
{yy1[t_],yy2[t_],yy3[t_],yy4[t_]}={y1[t],y2[t],y3[t],y4[t]}/.First[soln];
ParametricPlot[Evaluate[{yy1[t],yy2[t]}/.soln/.rts],{t,0,1},
  PlotRange\[Rule]All,AspectRatio\[Rule]Automatic,PlotPoints\[Rule]100]
```

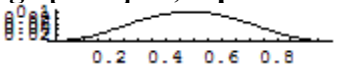

B.2 Fixed-end Strut, Dynamic Analysis

Mathematica Code

Input and Initial Guesses

```
(*Forced small vibrations about buckled equilibrium; clamped strut; y1=xe,
  y2=ye,y3=theta_e,y4=me, y5=xd,y6=yd,y7=theta_d,y8=md,y9=pd,y10=qd;
  given po and uo and frequency, and moment m from StrutEquilClamped,
  and q which is from StrutEquilClamped*)

Clear[pi,uo,po,m,c,\[Omega],q,gpd,gqd,gy8a]
  pi = N[\[Pi]];
  i=(-1)^0.5;
  uo=0.011;
  po=40;
  m=2.037804969875939`;
  q=0`;
  \[Omega]=.76;
  c=0;
  gpd=-0.393;
  gqd=-0.01;
  gy8a=0.82;
  r=1;
  g=0;
```

Equations from equilibrium

```
de[y3_,y4_,y5_,y6_,y7_,y8_,y9_,y10_] := {y1'[t]\[Equal]Cos[y3[t]],
    y2'[t]\[Equal]Sin[y3[t]],y3'[t]\[Equal]y4[t],
    y4'[t]\[Equal]-po*Sin[y3[t]]+q*Cos[y3[t]],y5'[t]\[Equal]-y7[t]*Sin[y3[t]],
    y6'[t]\[Equal]y7[t]*Cos[y3[t]],y7'[t]\[Equal]y8[t]/(1+i*\[Omega]*g),
    y8'[t]\[Equal](y10[t]-po*y7[t])*Cos[y3[t]]-(y9[t]+q*y7[t])*Sin[y3[t]],
    y9'[t]\[Equal](\[Omega]^2-i*\[Omega]*c)*y5[t],
    y10'[t]==(\[Omega]^2-i*\[Omega]*c)*y6[t]}
```

Boundary Conditions at s=0

```
leftBC[pd_,qd_,y8a_] := {y1[0]\[Equal]0,y2[0]\[Equal]0,y3[0]\[Equal]0,
    y4[0]\[Equal]m,y5[0]\[Equal]uo,y6[0]\[Equal]0,y7[0]\[Equal]0,
    y8[0]\[Equal]y8a,y9[0]\[Equal]pd,y10[0]\[Equal]qd}
```

Numerical Solution

```
soln:=NDSolve[
    Flatten[Append[de[y3,y4,y5,y6,y7,y8,y9,y10],leftBC[pd,qd,y8a]]],{y1,y2,y3,
      y4,y5,y6,y7,y8,y9,y10},{t,0,1}, MaxSteps\[Rule]2000]
endpt[pd_,qd_,
```

```
    y8a_]:={y1[t],y2[t],y3[t],y4[t],y5[t],y6[t],y7[t],y8[t],y9[t],
       y10[t]}/.First[
       NDSolve[Flatten[
          Append[de[y3,y4,y5,y6,y7,y8,y9,y10],leftBC[pd,qd,y8a]]],{y1[t],
          y2[t],y3[t],y4[t],y5[t],y6[t],y7[t],y8[t],y9[t],y10[t]},{t,0,1},
        MaxSteps\[Rule]1000]]/.t\[Rule]1;
endpt[gpd,gqd,gy8a];

Shooting for boundary conditions at s=1
Clear[pd,qd,y8a]
rts:=FindRoot[{endpt[pd,qd,y8a][[9]]\[Equal]-po*
       r*(\[Omega]^2)*(endpt[pd,qd,y8a][[5]]),
    endpt[pd,qd,y8a][[6]]\[Equal]0,
    endpt[pd,qd,y8a][[7]]\[Equal]0},{pd, {gpd,0.98*gpd}},{qd, {gqd,
     0.98*gqd}},{y8a, {gy8a,0.98*gy8a}},AccuracyGoal\[Rule]4,
  MaxIterations\[Rule]2000]

Solving for endpoint solution
endpt[pd/.rts,qd/.rts,y8a/.rts]
\!\({0.9739608828183183`,
  2.0462549077483016`*^-7, \(-7.385619451795505`*^-7\),
  2.0377967848563077`, \(-0.057191595670651185`\), \
\(-1.7954589856121407`*^-6\), \(-8.33207063759653`*^-7\),
  2.6961002274901946`, 1.3213134783161524`, 0.019385747776465817`}\)

pd=pd/.rts
qd=qd/.rts
y8a=y8a/.rts
1.33465
-0.0185095
2.69628

Solving for the Transmissibility and Plotting the Strut
{yy1[t_],yy2[t_],yy3[t_],yy4[t_],yy5[t_],yy6[t_],yy7[t_],yy8[t_],yy9[t_],
    yy10[t_]}={y1[t],y2[t],y3[t],y4[t],y5[t],y6[t],y7[t],y8[t],y9[t],
     y10[t]}/.First[soln];

TR=((((Re[N[yy5[1]]])^2+(Im[N[yy5[1]]])^2))^0.5)/uo

F=ParametricPlot[Evaluate[{yy1[t],yy2[t]}/.soln/.rts],{t,0,1},
    PlotRange\[Rule]All,AspectRatio\[Rule]Automatic,PlotPoints\[Rule]100];

G=ParametricPlot[Evaluate[{Re[yy1[t]],Re[yy2[t]+yy6[t]]}/.soln/.rts],{t,0,1},
    PlotRange\[Rule]All,AspectRatio\[Rule]Automatic,PlotPoints\[Rule]100];

H=ParametricPlot[Evaluate[{Re[yy1[t]],Re[yy2[t]-yy6[t]]}/.soln/.rts],{t,0,1},
```

PlotRange\[Rule]All,AspectRatio\[Rule]Automatic,PlotPoints\[Rule]100];

Show[F,G,H];

5.19924

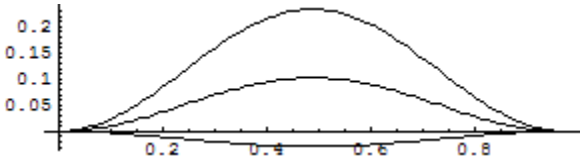

B.3 Additional Results for Forced Vibrations of the Fixed-end Buckled Strut

The following plots are additional cases that were analyzed. In order to prevent repetition, these plots were not included in the text of the thesis. All plots corroborate the findings presented in Chapter 3.

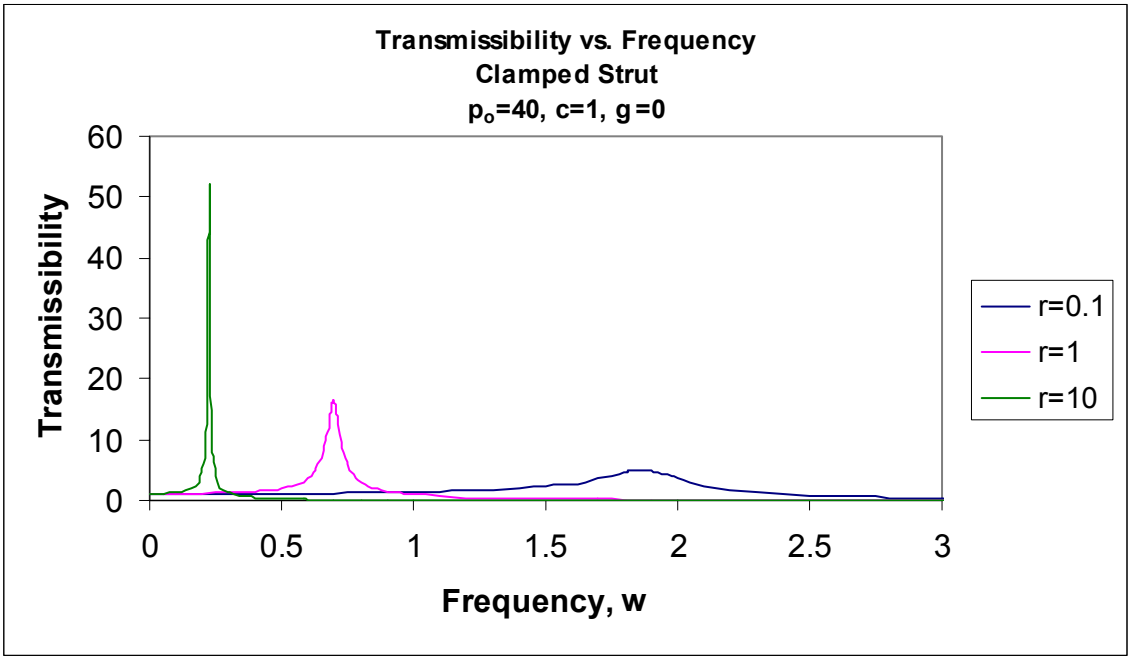

Figure B3.1: Transmissibility vs. Frequency for p_o=40, c=1, γ=0

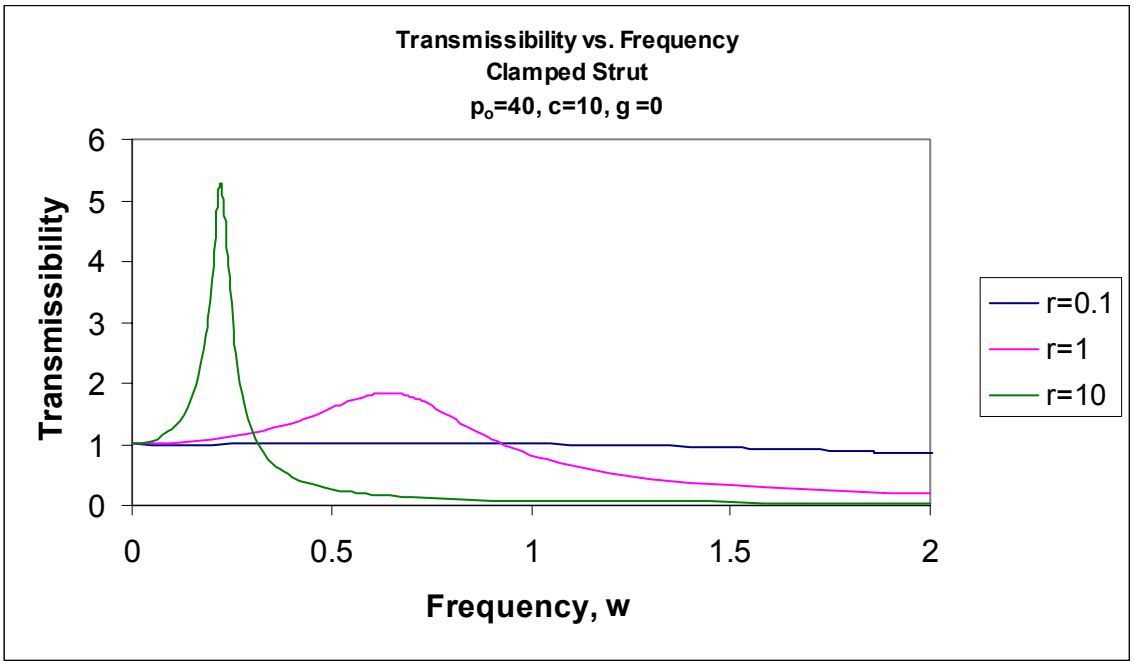

Figure B3.2: Transmissibility vs. Frequency for p_o=40, c=10, γ=0

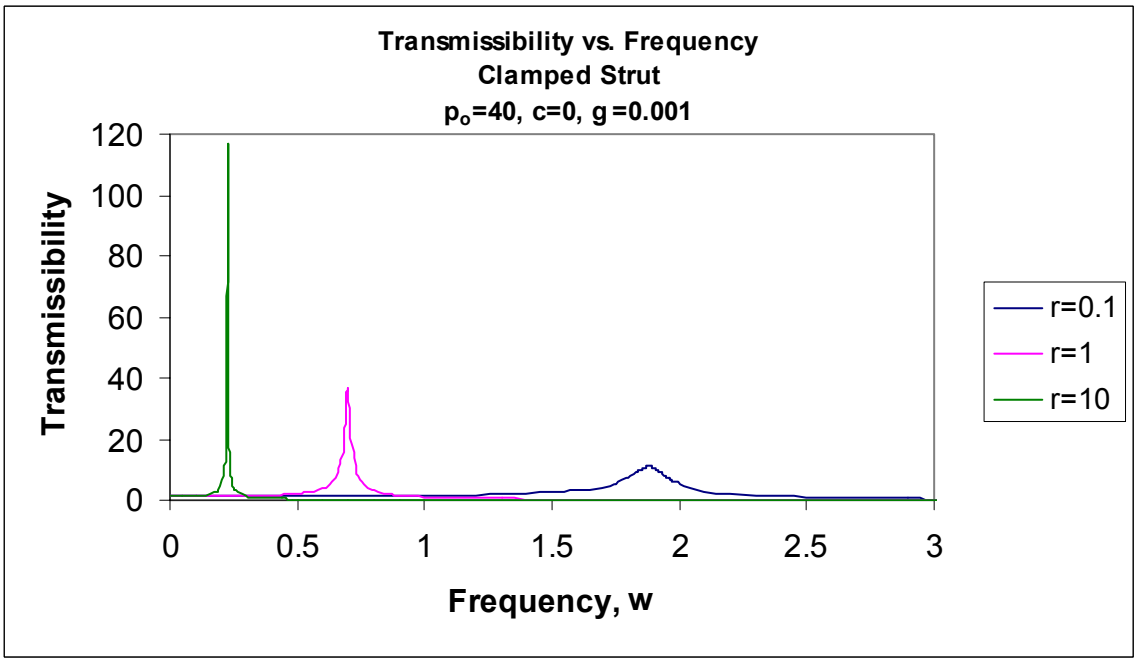

Figure B3.3: Transmissibility vs. Frequency for p_o=40, c=0, γ=0.001

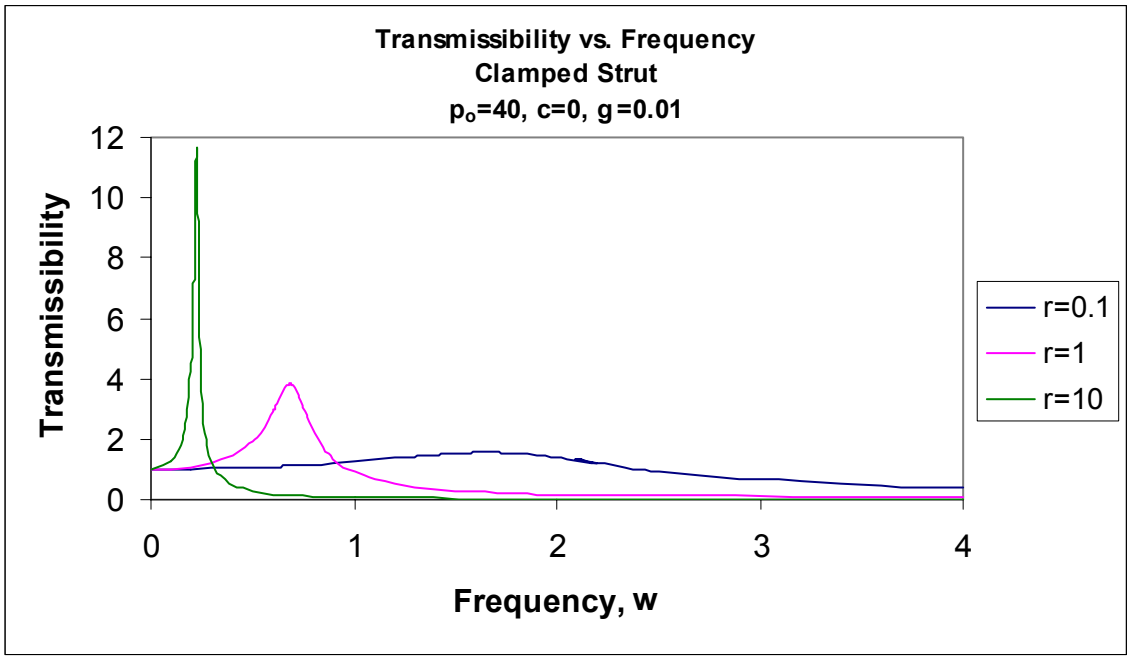

Figure B3.4: Transmissibility vs. Frequency for p_o=40, c=0, γ=0.01

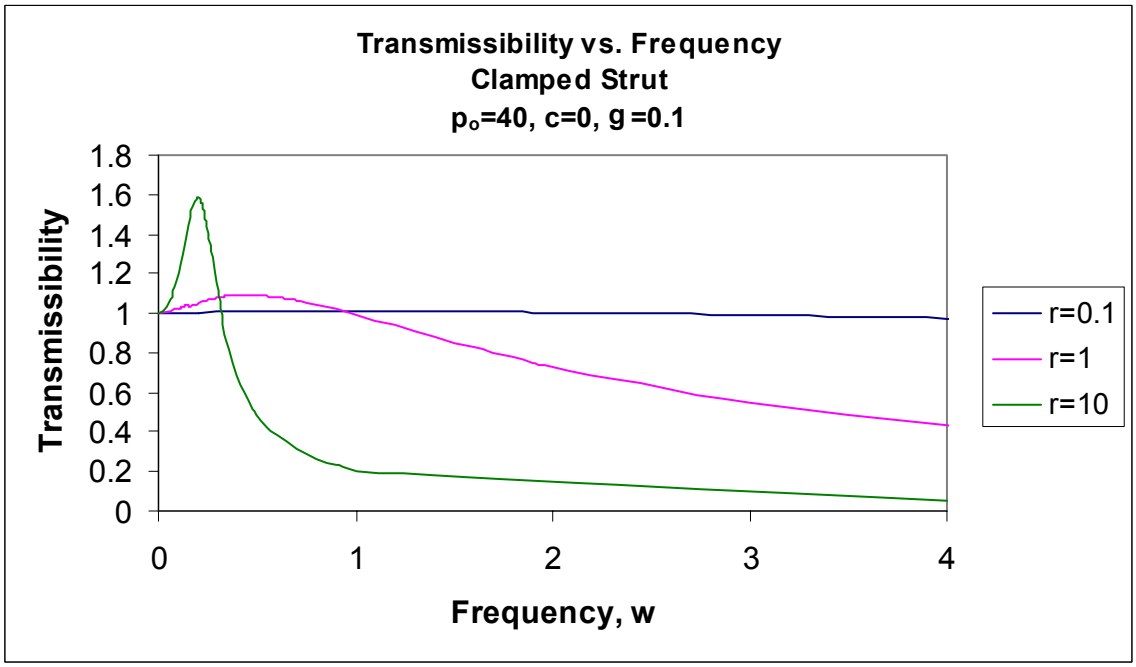

Figure B3.5: Transmissibility vs. Frequency for p_o=40, c=1, γ=0.1

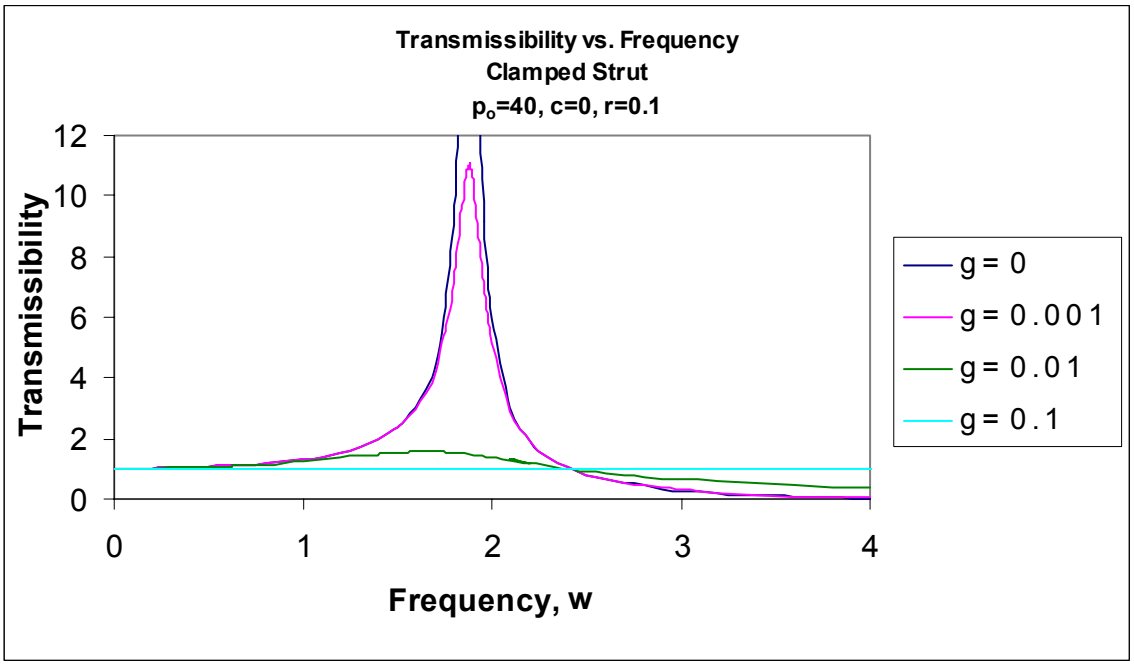

Figure B3.6: Transmissibility vs. Frequency for p_o=40, c=0, r=0.1

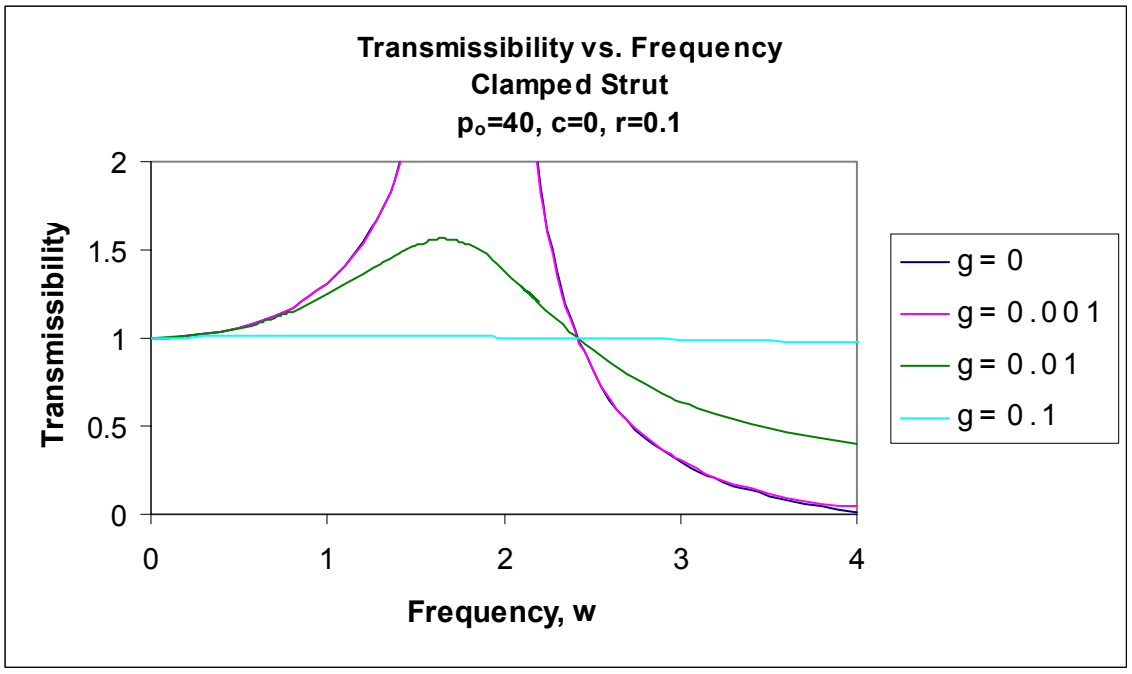

Figure B3.7: Transmissibility vs. Frequency for p_o=40, c=0, r=0.1

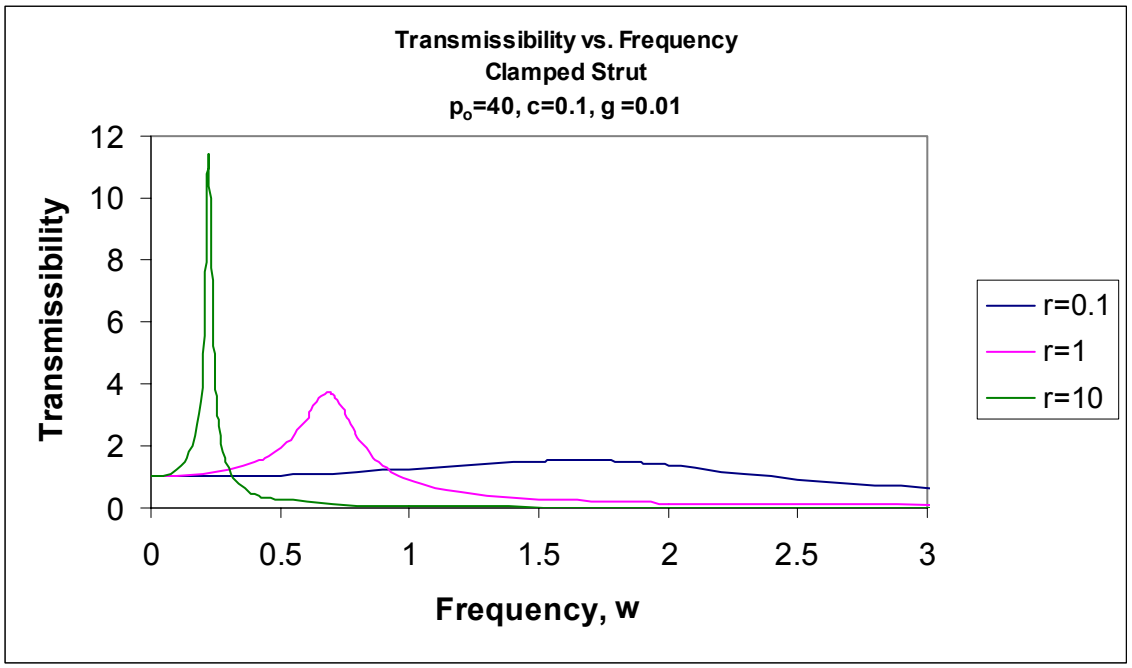

Figure B3.8: Transmissibility vs. Frequency for p_o=40, c=0.1, γ=0.01

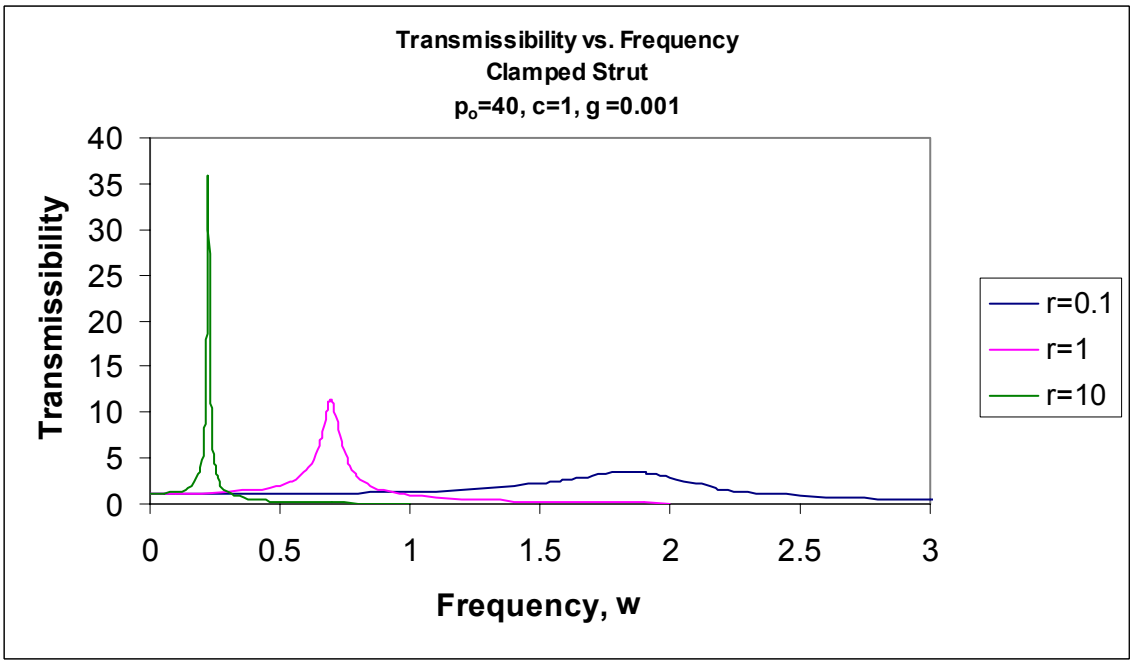

Figure B3.9: Transmissibility vs. Frequency for p_o=40, c=0.1, γ=0.001

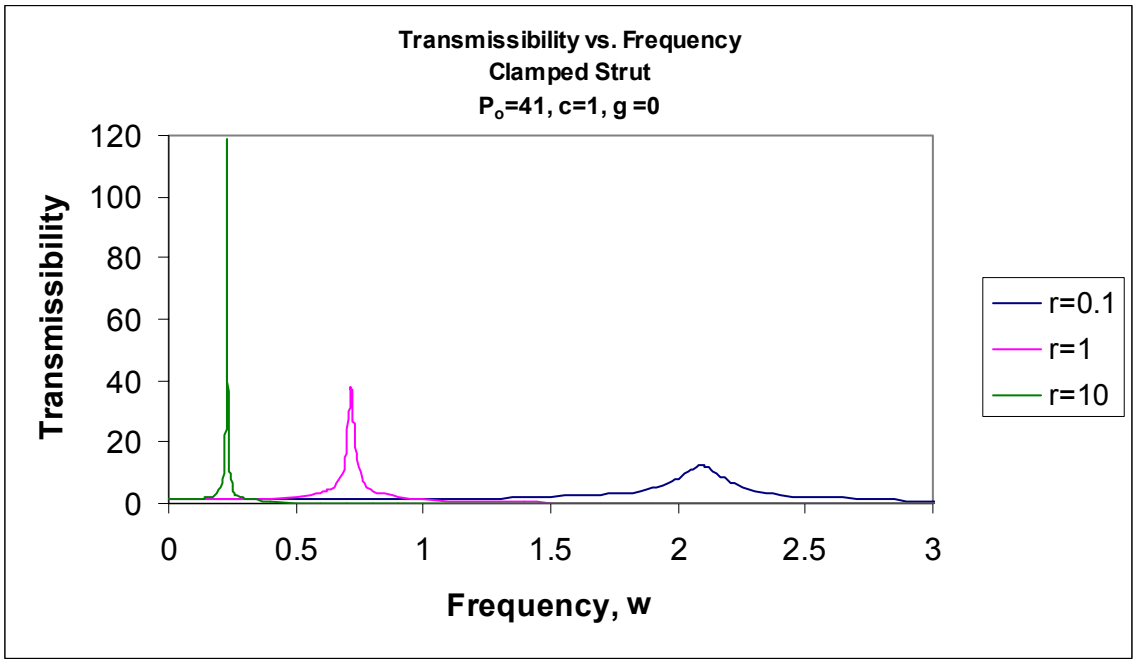

Figure B3.10: Transmissibility vs. Frequency for p_o=41, c=1, γ=0

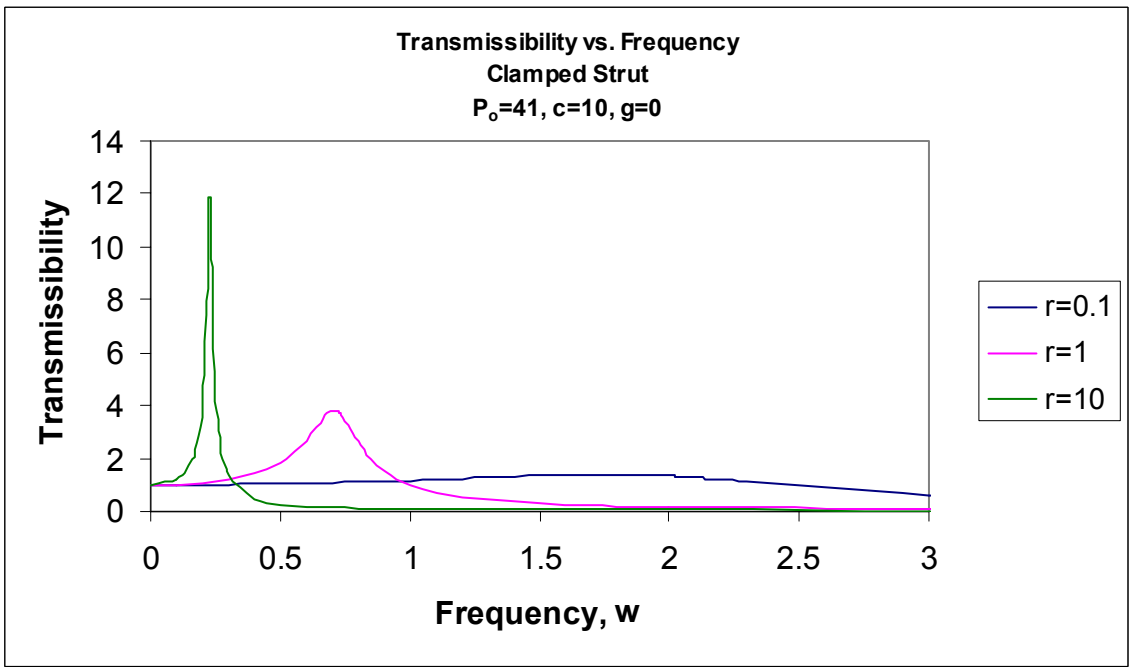

Figure B3.11: Transmissibility vs. Frequency for p_o=41, c=10, γ=0

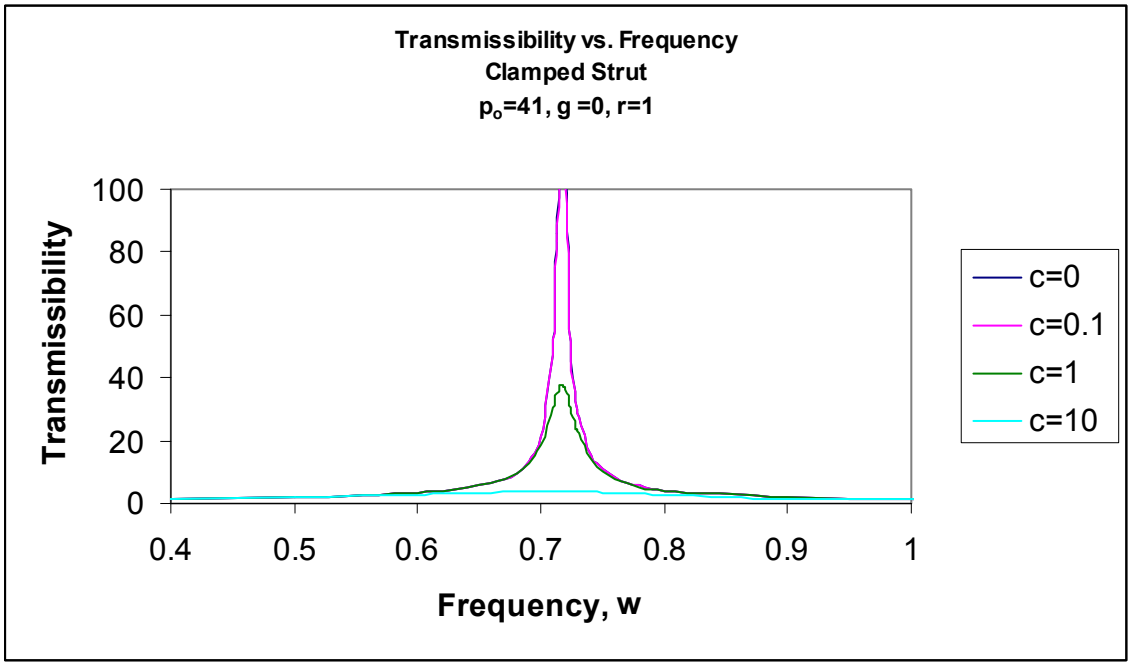

Figure B3.12: Transmissibility vs. Frequency for p_o=41, γ=0, r=1

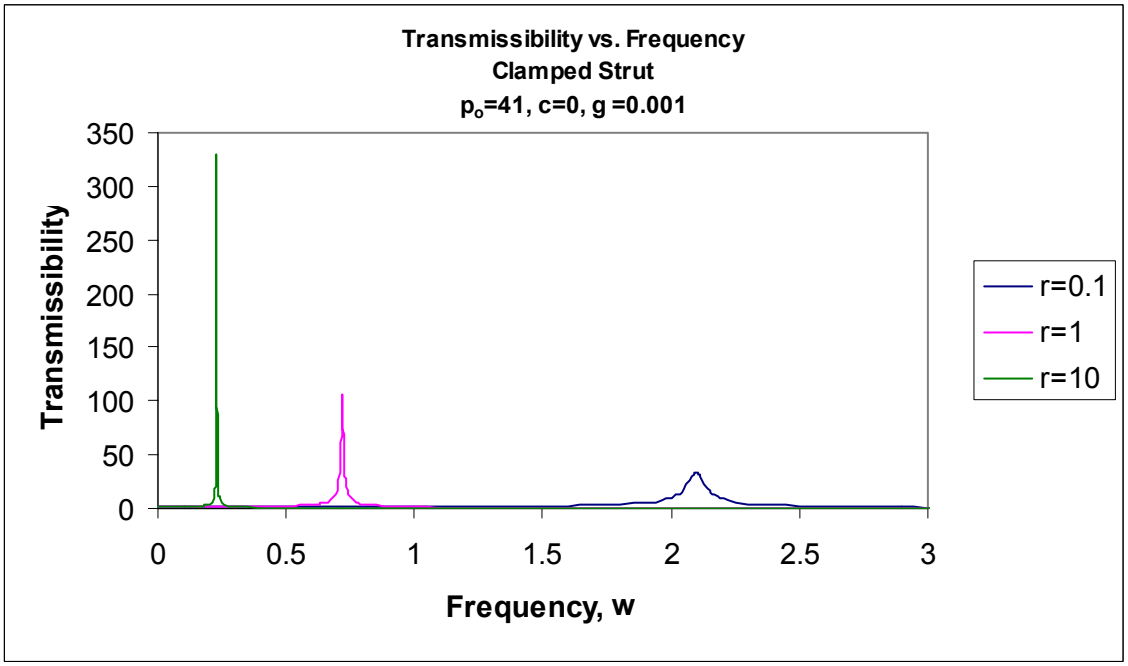

Figure B3.13: Transmissibility vs. Frequency for p_o=41, c=0, γ=0.001

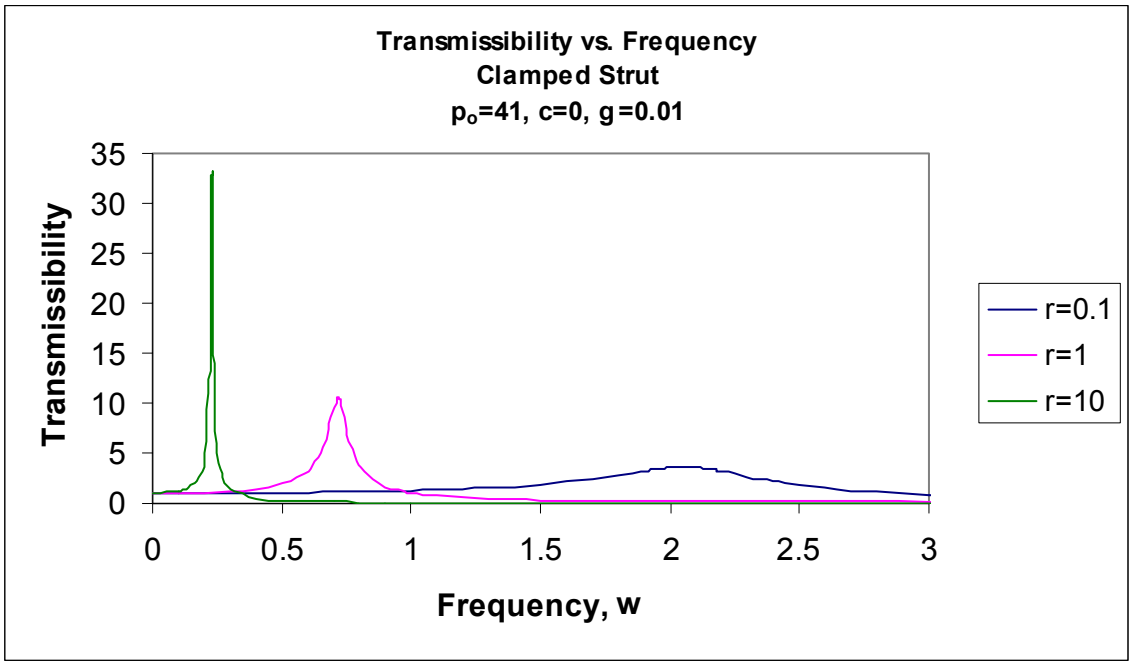

Figure B3.14: Transmissibility vs. Frequency for p_o=41, c=0, γ=0.01

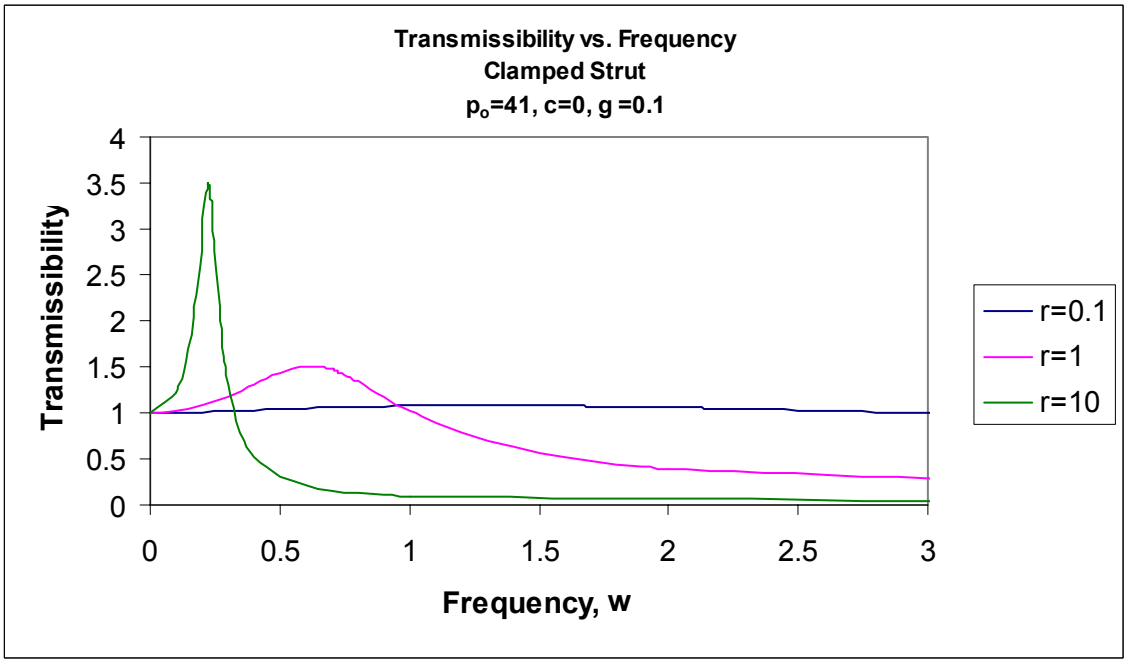

Figure B3.15: Transmissibility vs. Frequency for p_o=41, c=0, γ=0.1

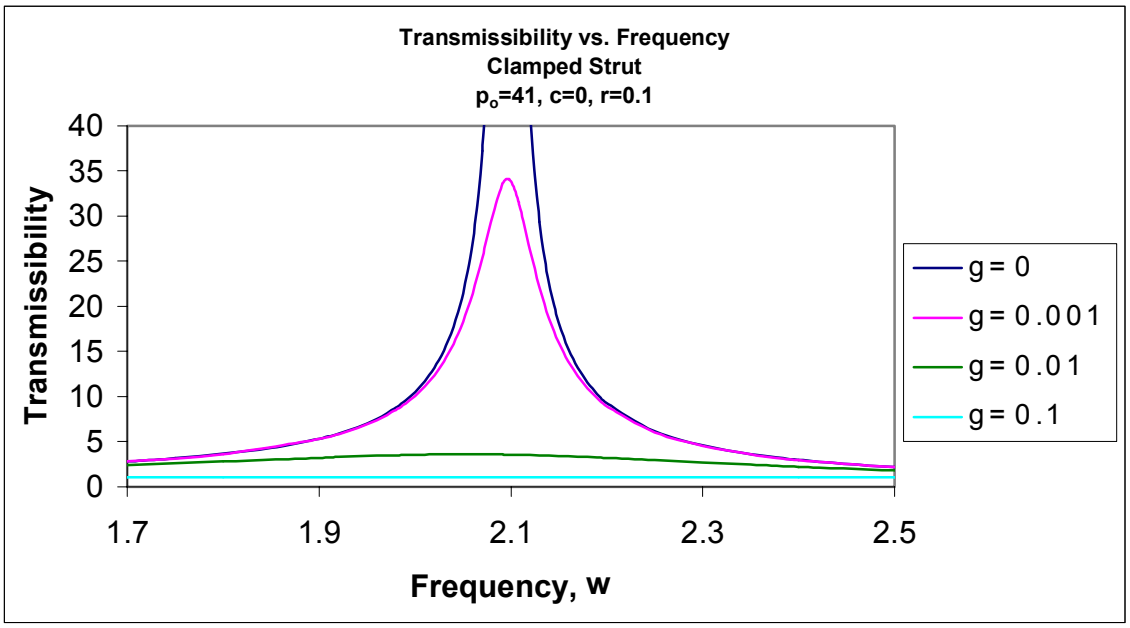

Figure B3.16: Transmissibility vs. Frequency for p_o=41, c=0, r=1

Appendix C

C.1 Pinned-end Strut with Initial Curvature; Static Equilibrium

Mathematica code

```
Input and Initial Guesses
(*Equilibrium,pinned buckled strut,y1=x,y2=y,y3=theta,y4=moment,
  doesn't include shear force q which is zero; m in leftBC is theta at s=0,
  p=po (larger than 9.87)*)

Clear[pi,gm,m,c]
pi = N[\[Pi]];

pe=9.6;
do=0.05;

gm = 0.53 ;

Equations from equilibrium
de[y3_,y4_]:={y1'[t]\[Equal]Cos[y3[t]],y2'[t]\[Equal]Sin[y3[t]],
   y3'[t]\[Equal]y4[t]+do,y4'[t]\[Equal]-pe*Sin[y3[t]]}

Boundary conditions at s=0
leftBC[m_]:={y1[0]\[Equal]0,y2[0]\[Equal]0,y3[0]\[Equal]m,y4[0]\[Equal]0}

Numerical Solution
soln:=NDSolve[Flatten[Append[de[y3,y4],leftBC[m]]],{y1,y2,y3,y4},{t,0,1},
   MaxSteps\[Rule]2000]
endpt[m_]:={y1[t],y2[t],y3[t],y4[t]}/.First[
        NDSolve[Flatten[Append[de[y3,y4],leftBC[m]]],{y1[t],y2[t],y3[t],
           y4[t]},{t,0,1},MaxSteps\[Rule]2000]]/.t\[Rule]1;
endpt[gm]
{0.932878,0.0265762,-0.525908,-0.255131}
Clear[m]

Solving for the moment
rts:=FindRoot[{endpt[m][[2]]\[Equal]0},{m,{gm,0.99gm}},AccuracyGoal\[Rule]4,
   MaxIterations\[Rule]2000]
endpt[m/.rts]
{0.957077,0.000056952,0.421271,-0.00054674}
m=m/.rts
-0.421266
```

Plotting the Strut

```
{yy1[t_],yy2[t_],yy3[t_],yy4[t_]}={y1[t],y2[t],y3[t],y4[t]}/.First[soln];
ParametricPlot[Evaluate[{yy1[t],yy2[t]}/.soln/.rts],{t,0,1},
  PlotRange\[Rule]All,AspectRatio\[Rule]Automatic,PlotPoints\[Rule]100]
```

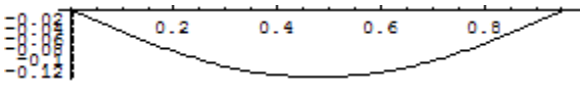

C.2 Deflected Shapes due to Load

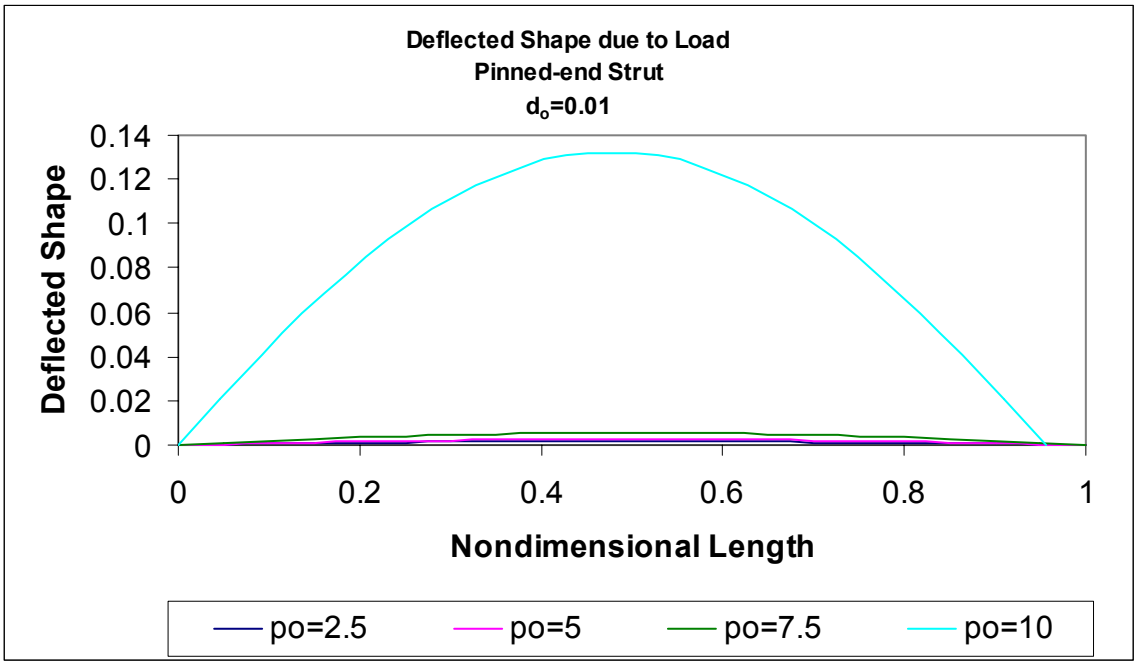

Figure C2.1: Deflected Shape due to Load for d_o=0.01

Table C2.1: Maximum Mid-span Deflection and End Shortening Values for d_o=0.01

p_o	max y	End shortening
0	0.00625	0
2.5	0.008431	0
5	0.012807	0.0000170
7.5	0.02656	0.0000710
10	0.186421	0.044389

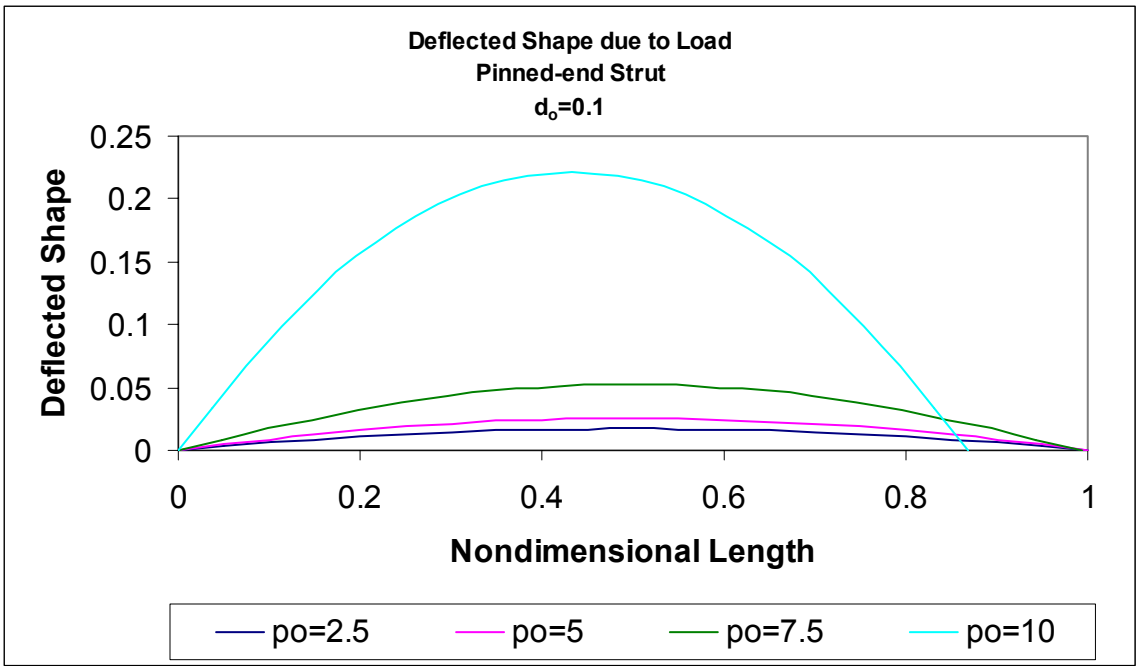

Figure C2.2: Deflected Shape due to Load for d_o=0.01

Table C2.2: Maximum Mid-span Deflection and End Shortening Values for d_o=0.1

p_o	max y	End shortening
0	0.00625	0.000417
2.5	0.008431	0.000742
5	0.012807	0.001686
7.5	0.02656	0.006964
10	0.186421	0.132159

C.3 Pinned-end Strut with Initial Curvature; Dynamic Analysis

Mathematica code

```
Input and Initial Guesses
(*Forced small vibrations about buckled equilibrium; pinned strut; y1=xe,
  y2=ye,y3=theta_e,y4=me, y5=xd,y6=yd,y7=theta_d,y8=md,y9=pd,y10=qd;
  given po and uo and frequency,
  and theta_e(0) which is value m from StrutEquil3*)

Clear[pi,uo,po,\[Omega],gpd,gqd,gy3a,gy7a,pd,qd,y3a,y7a]
  pi = N[\[Pi]];
  uo=0.011;
  po=5;
  m=-0.04583672116835365`;

  \[Omega]=85.99;
  r=1;
  c=.1;
  i=(-1)^0.5;
  g=0;
  gpd=-2927.3763166457716`+0.28947740137039285` \[ImaginaryI];
  gqd=120.32764358365513`\[InvisibleSpace]+0.005917219640769121` \
\[ImaginaryI];
  gy7a=-0.00109534503374853`-0.00009073013080150389` \[ImaginaryI];
  do=0.05;

Equations from equilibrium
de[y3_,y4_,y5_,y6_,y7_,y8_,y9_,y10_]:= {y1'[t]\[Equal]Cos[y3[t]],
    y2'[t]\[Equal]Sin[y3[t]],y3'[t]\[Equal]y4[t]+do,
    y4'[t]\[Equal]-po*Sin[y3[t]],y5'[t]\[Equal]-y7[t]*Sin[y3[t]],
    y6'[t]\[Equal]y7[t]*Cos[y3[t]],y7'[t]\[Equal]y8[t]/(1+i*\[Omega]*g),
    y8'[t]\[Equal](y10[t]-po*y7[t])*Cos[y3[t]]-y9[t]*Sin[y3[t]],
    y9'[t]\[Equal](\[Omega]^2-i*\[Omega]*c)*y5[t],
    y10'[t]==(\[Omega]^2-i*\[Omega]*c)*y6[t]}

Boundary Conditions at s=0
leftBC[pd_,qd_,y7a_] := {y1[0]\[Equal]0,y2[0]\[Equal]0,y3[0]\[Equal]m,
    y4[0]\[Equal]0,y5[0]\[Equal]uo,y6[0]\[Equal]0,y7[0]\[Equal]y7a,
    y8[0]\[Equal]0,y9[0]\[Equal]pd,y10[0]\[Equal]qd}

Numerical Solution
soln:=NDSolve[
    Flatten[Append[de[y3,y4,y5,y6,y7,y8,y9,y10],leftBC[pd,qd,y7a]]],{y1,y2,y3,
      y4,y5,y6,y7,y8,y9,y10},{t,0,1}, MaxSteps\[Rule]2000]
```

```
endpt[pd_,qd_,
     y7a_]:={y1[t],y2[t],y3[t],y4[t],y5[t],y6[t],y7[t],y8[t],y9[t],
        y10[t]}/.First[
        NDSolve[Flatten[
           Append[de[y3,y4,y5,y6,y7,y8,y9,y10],leftBC[pd,qd,y7a]]],{y1[t],
           y2[t],y3[t],y4[t],y5[t],y6[t],y7[t],y8[t],y9[t],y10[t]},{t,0,1},
         MaxSteps\[Rule]1000]]/.t\[Rule]1;

Shooting for boundary conditions at s=1
endpt[gpd,gqd,gy7a];
Clear[pd,qd,y7a]
rts:=FindRoot[{endpt[pd,qd,y7a][[9]]\[Equal]-r*
        po*(\[Omega]^2)*(endpt[pd,qd,y7a][[5]]),
     endpt[pd,qd,y7a][[6]]\[Equal]0,
     endpt[pd,qd,y7a][[8]]\[Equal]0},{pd, {gpd,0.99*gpd}},{qd, {gqd,
       0.99*gqd}},{y7a, {gy7a,0.99*gy7a}},AccuracyGoal\[Rule]3,
   MaxIterations\[Rule]2000]

Solving for endpoint solution
endpt[pd/.rts,qd/.rts,y7a/.rts]
\!\({0.999578633606342`, 0.00004189039065959168`,
   0.04588231189802479`, \(-0.0002094519532979789`\), \
\(\(0.012917975449990187`\)\(\[InvisibleSpace]\)\) -
     0.0004953542358753946`\ \[ImaginaryI],
   3.773794503246497`*^-7 -
     8.820036144783791`*^-8\ \[ImaginaryI], \(-2.0718527773133224`\) +
     0.4306863061247838`\ \[ImaginaryI], \(\(0.00003082198384869573`\)\(\
\[InvisibleSpace]\)\) -
     7.247025277575135`*^-6\ \[ImaginaryI], \(-477.59616795296955`\) +
     18.314061152312835`\ \[ImaginaryI], \(\(154.61804208232493`\)\(\
\[InvisibleSpace]\)\) - 35.389101358590224`\ \[ImaginaryI]}\)

pd=pd/.rts
qd=qd/.rts
y7a=y7a/.rts
-565.841+20.2463 \[ImaginaryI]
-151.221+35.3159 \[ImaginaryI]
2.06444\[InvisibleSpace]-0.430543 \[ImaginaryI]
{yy1[t_],yy2[t_],yy3[t_],yy4[t_],yy5[t_],yy6[t_],yy7[t_],yy8[t_],yy9[t_],
     yy10[t_]}={y1[t],y2[t],y3[t],y4[t],y5[t],y6[t],y7[t],y8[t],y9[t],
       y10[t]}/.First[soln];
Solving for the Transmissibility
TR=((((Re[N[yy5[1]]])^2+(Im[N[yy5[1]]])^2))^0.5)/uo
1.17522
```

C.4 Additional Results for Forced Vibrations of the Pinned-end Strut with Initial Curvature

The following plots support the conclusions made in Chapter 4. All of the plots were completed in Excel using data generated by Mathematica.

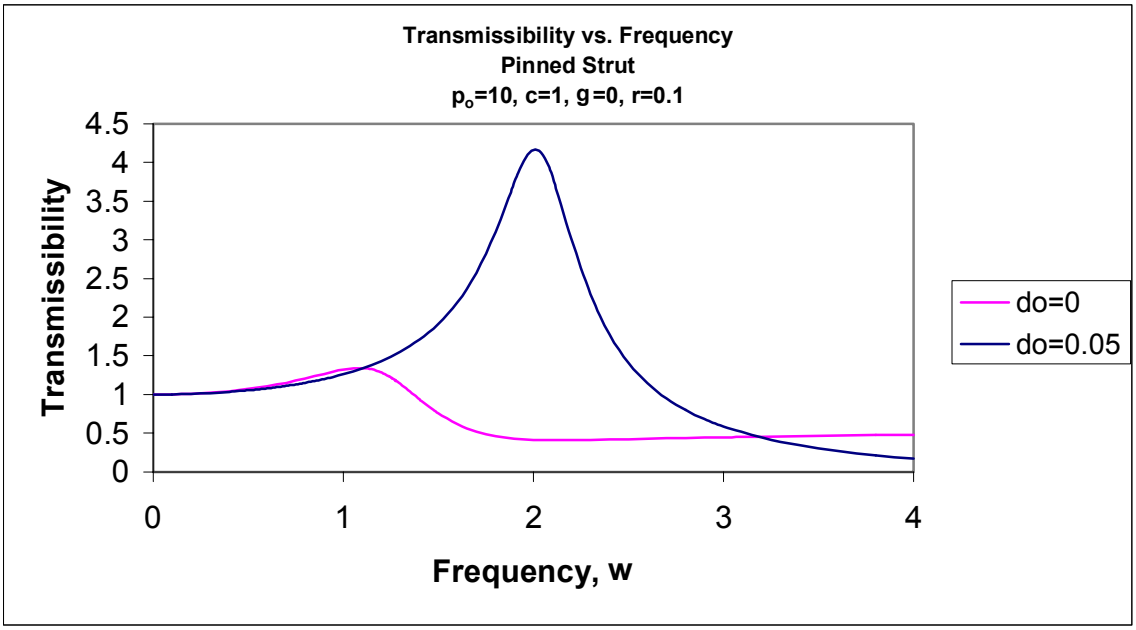

Figure C4.1: Transmissibility vs. Frequency for p_o=10, c=1, γ=0, r=0.1

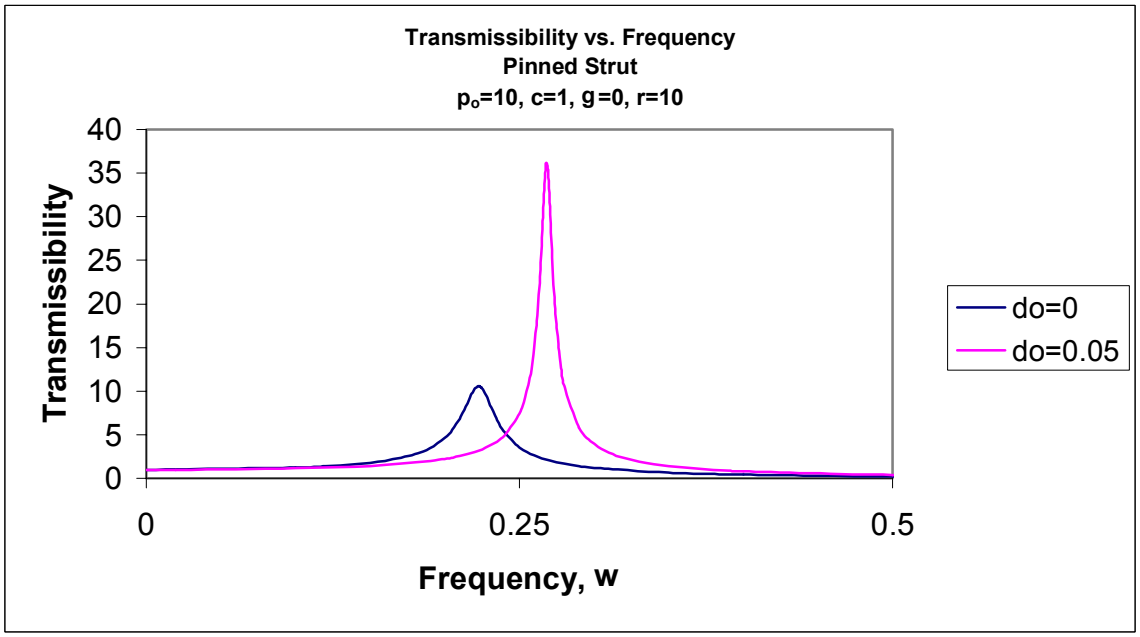

Figure C4.2: Transmissibility vs. Frequency for p_o=10, c=1, γ=0, r=10

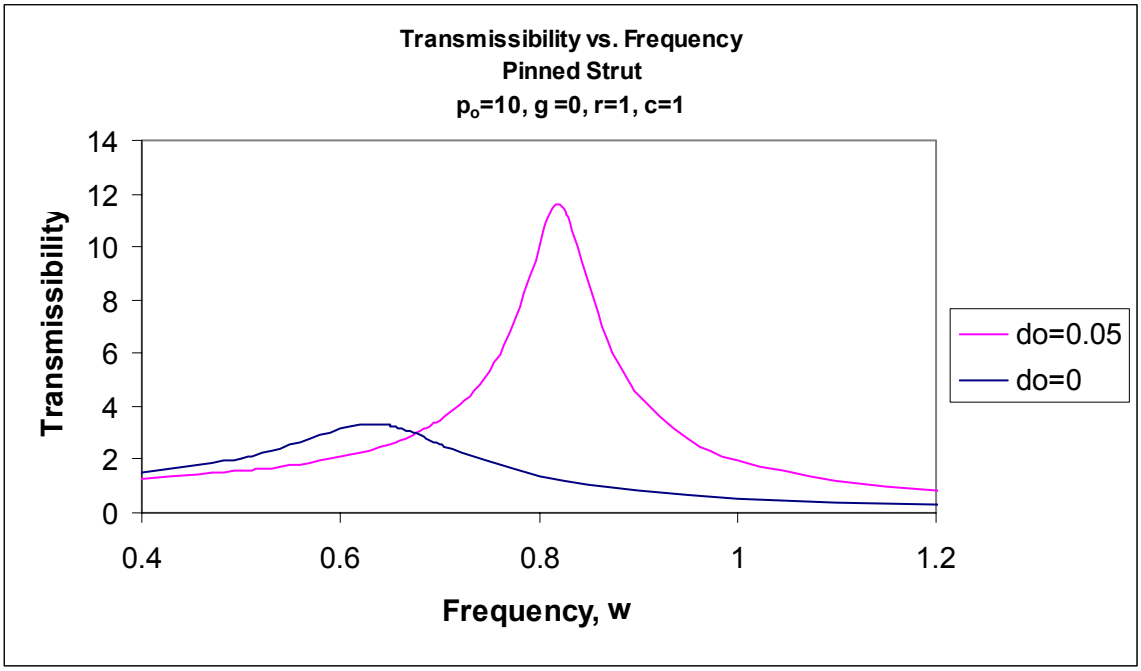

Figure C4.3: Transmissibility vs. Frequency for p_o=10, c=1, γ=0, r=1

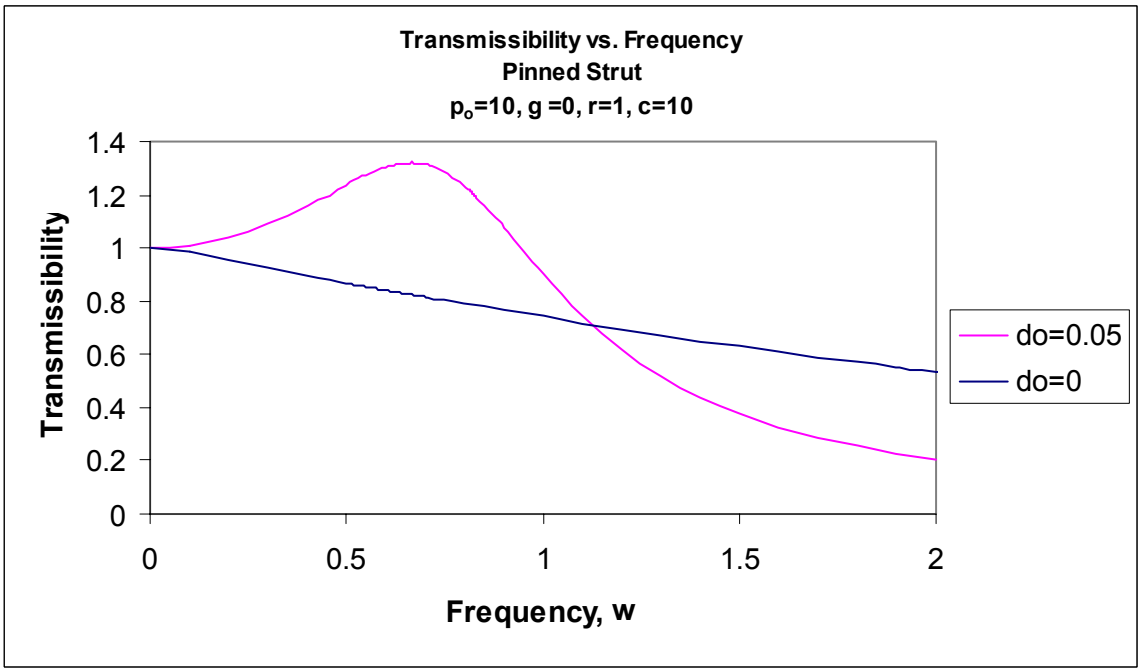

Figure C4.4: Transmissibility vs. Frequency for p_o=10, c=10, γ=0, r=1

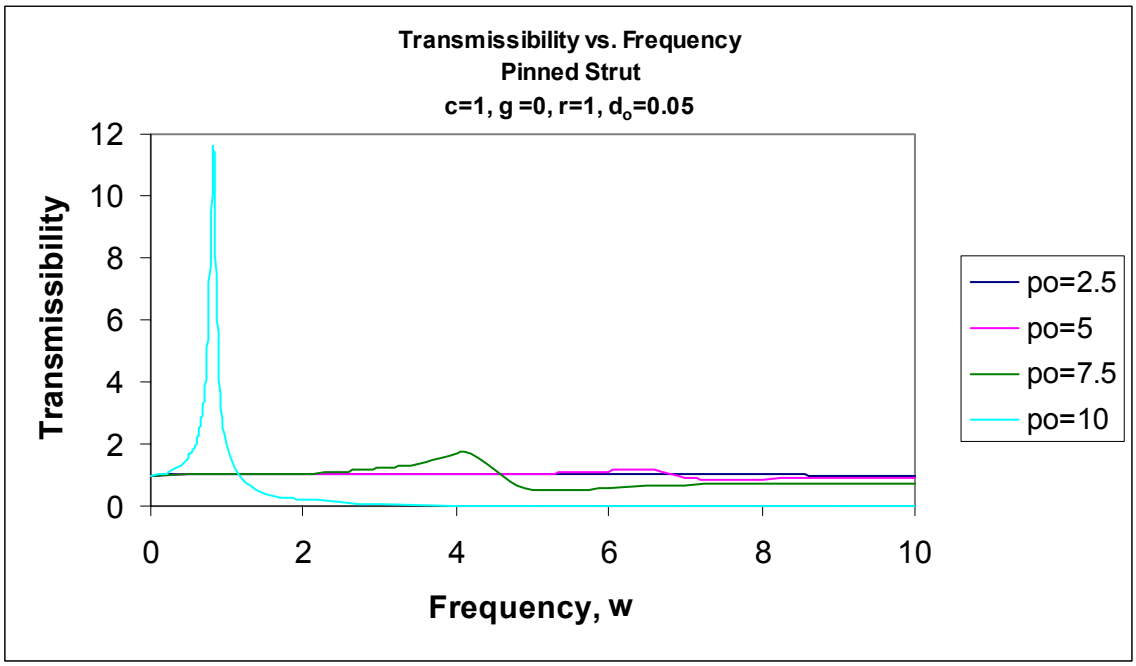

Figure C4.5: Transmissibility vs. Frequency for c=1, γ=0, r=1, d_o=0.05

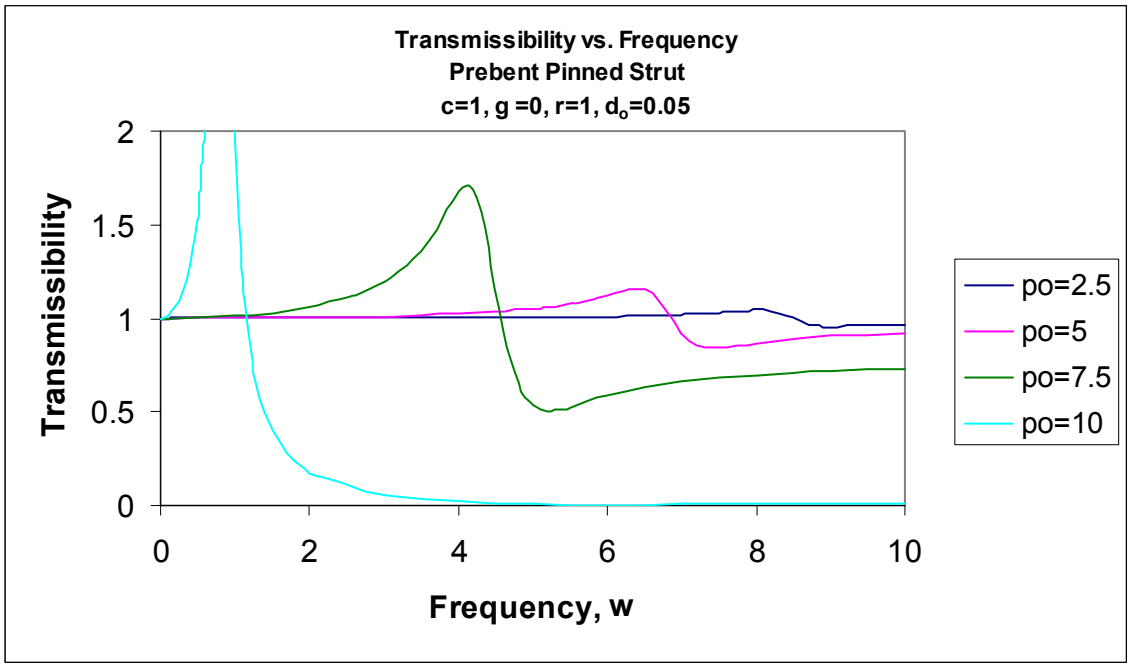

Figure C4.6: Transmissibility vs. Frequency for c=1, γ=0, r=1, d_o=0.05

Appendix D

D.1 Fixed-end Strut with Initial Curvature; Static Equilibrium

Mathematica code

```
Input and Initial Guesses
(*Equilibrium, clamped buckled strut,y1=x,y2=y,y3=theta,y4=moment,
  includes shear force q which is not zero; m in leftBC is theta at s=0,
  p=po (larger than 39.48 = 4*pi^2)*)

Clear[pi,gm,gq,m,q,po]
pi = N[\[Pi]];

po = 40;
ao=0.05;
gm = 2.04 ;
gq = -0.0000127;

Equations from equilibrium
de[y3_,y4_,q_]:={y1'[t]\[Equal]Cos[y3[t]],y2'[t]\[Equal]Sin[y3[t]],
   y3'[t]\[Equal]y4[t]+2*pi*ao*Cos[2*pi*t],
   y4'[t]\[Equal]-po*Sin[y3[t]]+q*Cos[y3[t]]}

Boundary conditions at s=0
leftBC[m_]:={y1[0]\[Equal]0,y2[0]\[Equal]0,y3[0]\[Equal]0,y4[0]\[Equal]m}

Numerical Solution
soln:=NDSolve[Flatten[Append[de[y3,y4,q],leftBC[m]]],{y1,y2,y3,y4},{t,0,1},
   MaxSteps\[Rule]2000]
endpt[m_,q_]:={y1[t],y2[t],y3[t],y4[t]}/.First[
        NDSolve[Flatten[Append[de[y3,y4,q],leftBC[m]]],{y1[t],y2[t],y3[t],
           y4[t]},{t,0,1},MaxSteps\[Rule]2000]]/.t\[Rule]1;
endpt[gm,gq]
{0.901959,0.38856,0.0362043,-1.84561}
Clear[m,q]

Solving for the moment and shear force
rts:=FindRoot[{endpt[m,q][[2]]\[Equal]0,
     endpt[m,q][[3]]\[Equal]0},{m,{gm,0.98*gm}},{q,{gq,0.98*gq}},
   AccuracyGoal\[Rule]4,MaxIterations\[Rule]2000]
endpt[m/.rts,q/.rts]
\!\({0.9988797498555153`, \(-3.602241896348731`*^-7\), \
```

\(-5.762522847939183`*^-7\), 0.10649620819124718`}\)
m=m/.rts
q=q/.rts
4.69001
0.0000515512

Plotting the Strut
{yy1[t_],yy2[t_],yy3[t_],yy4[t_]}={y1[t],y2[t],y3[t],y4[t]}/.First[soln];
ParametricPlot[Evaluate[{yy1[t],yy2[t]}/.soln/.rts],{t,0,1},
 PlotRange\[Rule]All,AspectRatio\[Rule]Automatic,PlotPoints\[Rule]100]

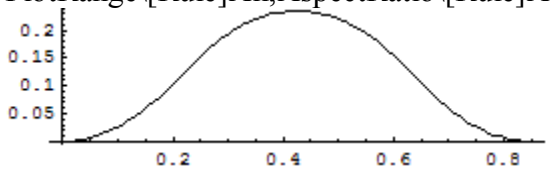

D.2 Deflected Shapes due to Load

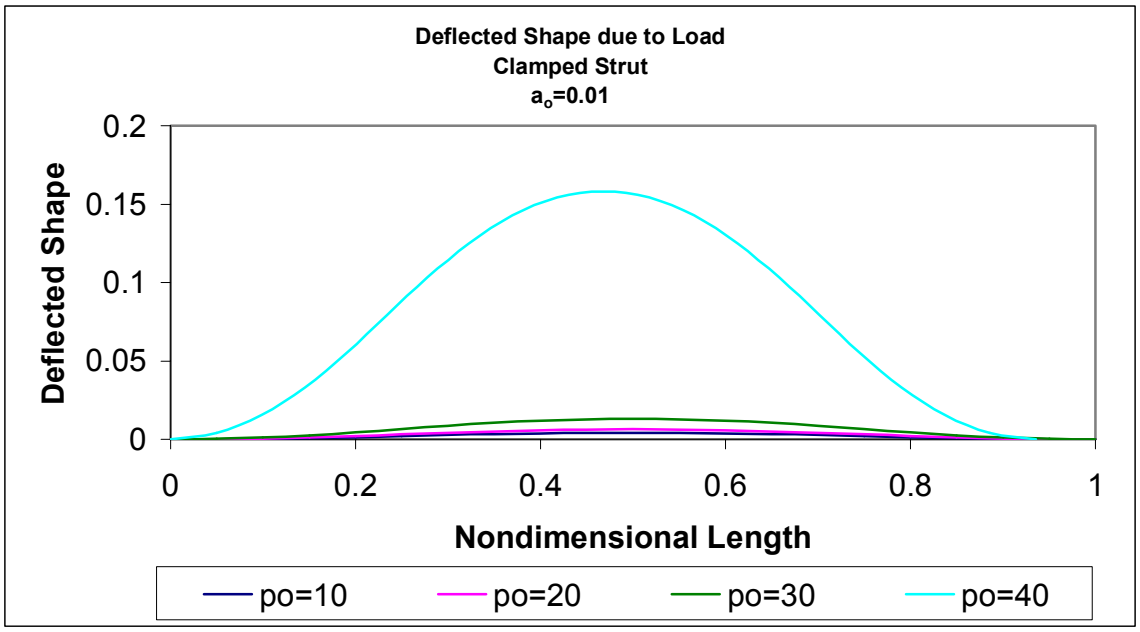

Figure D2.1: Deflected Shape due to Load for a_o=0.01

Table D2.1: Maximum Mid-span Deflection and End Shortening Values for a_o=0.1

po	max y	End Shortening
0	0.003183	0
10	0.004263	0.000045
20	0.006448	0.000103
30	0.013265	0.000434
40	0.15826	0.064392

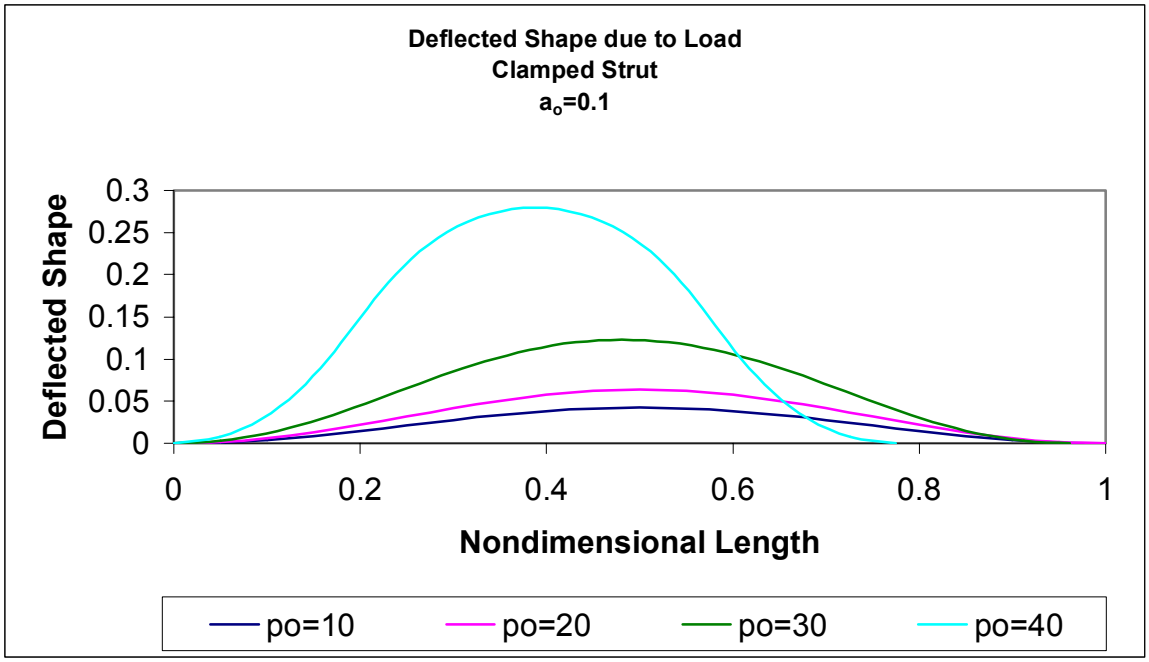

Figure D2.2: Deflected Shape due to Load for a_o=0.1

Table D2.2: Maximum Mid-span Deflection and End Shortening Values for a_o=0.01

po	max y	End Shortening
0	0.031796	0.002498
10	0.042512	0.004472
20	0.063892	0.010137
30	0.122903	0.038187
40	0.279734	0.224723

D.3 Fixed-end Strut with Initial Curvature; Dynamic Analysis

Mathematica Code

Input and Initial Guesses

```
(*Forced small vibrations about buckled equilibrium; clamped strut; y1=xe,
  y2=ye,y3=theta_e,y4=me, y5=xd,y6=yd,y7=theta_d,y8=md,y9=pd,y10=qd;
  given po and uo and frequency, and moment m from StrutEquilClamped,
  and q which is from StrutEquilClamped*)

Clear[pi,uo,po,m,c,\[Omega],q,gpd,gqd,gy8a]
  pi = N[\[Pi]];
  i=(-1)^0.5;
  uo=0.011;
  po=10;
  m=0.10650436498935865`;
  q=0;

  \[Omega]=287;
  c=.1;
  gpd=-941.9029632315893`+27.533937774251264` \[ImaginaryI];
  gqd=995.9602863375834`\[InvisibleSpace]+5.531734168208414` \[ImaginaryI];
  gy8a=-59.542186240032976`-0.29481774392484816` \[ImaginaryI];
  r=1;
  g=0;
  ao=0.05;
```

Equations from equilibrium

```
de[y3_,y4_,y5_,y6_,y7_,y8_,y9_,y10_] := {y1'[t]\[Equal]Cos[y3[t]],
    y2'[t]\[Equal]Sin[y3[t]],y3'[t]\[Equal]y4[t]+2*pi*ao*Cos[2*pi*t],
    y4'[t]\[Equal]-po*Sin[y3[t]]+q*Cos[y3[t]],y5'[t]\[Equal]-y7[t]*Sin[y3[t]],
    y6'[t]\[Equal]y7[t]*Cos[y3[t]],y7'[t]\[Equal]y8[t]/(1+i*\[Omega]*g),
    y8'[t]\[Equal](y10[t]-po*y7[t])*Cos[y3[t]]-(y9[t]+q*y7[t])*Sin[y3[t]],
    y9'[t]\[Equal](\[Omega]^2-i*\[Omega]*c)*y5[t],
    y10'[t]==(\[Omega]^2-i*\[Omega]*c)*y6[t]}
```

Boundary Conditions at s=0

```
leftBC[pd_,qd_,y8a_] := {y1[0]\[Equal]0,y2[0]\[Equal]0,y3[0]\[Equal]0,
    y4[0]\[Equal]m,y5[0]\[Equal]uo,y6[0]\[Equal]0,y7[0]\[Equal]0,
    y8[0]\[Equal]y8a,y9[0]\[Equal]pd,y10[0]\[Equal]qd}
```

Numerical Solution

```
soln:=NDSolve[
    Flatten[Append[de[y3,y4,y5,y6,y7,y8,y9,y10],leftBC[pd,qd,y8a]]],{y1,y2,y3,
      y4,y5,y6,y7,y8,y9,y10},{t,0,1}, MaxSteps\[Rule]2000]
```

```
endpt[pd_,qd_,
    y8a_]:={y1[t],y2[t],y3[t],y4[t],y5[t],y6[t],y7[t],y8[t],y9[t],
       y10[t]}/.First[
       NDSolve[Flatten[
          Append[de[y3,y4,y5,y6,y7,y8,y9,y10],leftBC[pd,qd,y8a]]],{y1[t],
          y2[t],y3[t],y4[t],y5[t],y6[t],y7[t],y8[t],y9[t],y10[t]},{t,0,1},
         MaxSteps\[Rule]1000]]/.t\[Rule]1;

Shooting for boundary conditions at s=1
endpt[gpd,gqd,gy8a];
Clear[pd,qd,y8a]
rts:=FindRoot[{endpt[pd,qd,y8a][[9]]\[Equal]-po*
        r*(\[Omega]^2)*(endpt[pd,qd,y8a][[5]]),
     endpt[pd,qd,y8a][[6]]\[Equal]0,
     endpt[pd,qd,y8a][[7]]\[Equal]0},{pd, {gpd,0.98*gpd}},{qd, {gqd,
      0.98*gqd}},{y8a, {gy8a,0.98*gy8a}},AccuracyGoal\[Rule]2,
   MaxIterations\[Rule]2000]

Solving for endpoint solution
endpt[pd/.rts,qd/.rts,y8a/.rts]
\!\({0.9988797766055644`, 9.68120232331078`*^-7, \(-3.101664744934506`*^-8\),
   0.10649468378703544`, \(-0.023934642637433733`\) -
     0.0007609563746889626`\ \[ImaginaryI], \(-4.918391475017871`*^-7\) -
     4.732804469258116`*^-9\ \[ImaginaryI], \(-0.000024219925502997092`\) -
     1.222005103279284`*^-8\ \[ImaginaryI], \(-299.7838283199751`\) -
     7.500544873097345`\ \[ImaginaryI], \(\(19714.727291111984`\)\(\
\[InvisibleSpace]\)\) +
     626.7920385324455`\ \[ImaginaryI], \(-5473.673006862414`\) -
     139.49743010656422`\ \[ImaginaryI]}\)

pd=pd/.rts
qd=qd/.rts
y8a=y8a/.rts
20245.5\[InvisibleSpace]+657.829 \[ImaginaryI]
5486.94\[InvisibleSpace]+140.266 \[ImaginaryI]
-300.024-7.51421 \[ImaginaryI]
```

Solving for the Transmissibility

```
{yy1[t_],yy2[t_],yy3[t_],yy4[t_],yy5[t_],yy6[t_],yy7[t_],yy8[t_],yy9[t_],
    yy10[t_]}={y1[t],y2[t],y3[t],y4[t],y5[t],y6[t],y7[t],y8[t],y9[t],
     y10[t]}/.First[soln];

TR=((((Re[N[yy5[1]]])^2+(Im[N[yy5[1]]])^2))^0.5)/uo
2.17698
```

D.4 Additional Results for Forced Vibrations of the Fixed-end Strut with Initial Curvature

The following plots support the conclusions made in Chapter 5. All of the plots were completed in Excel using data generated by Mathematica.

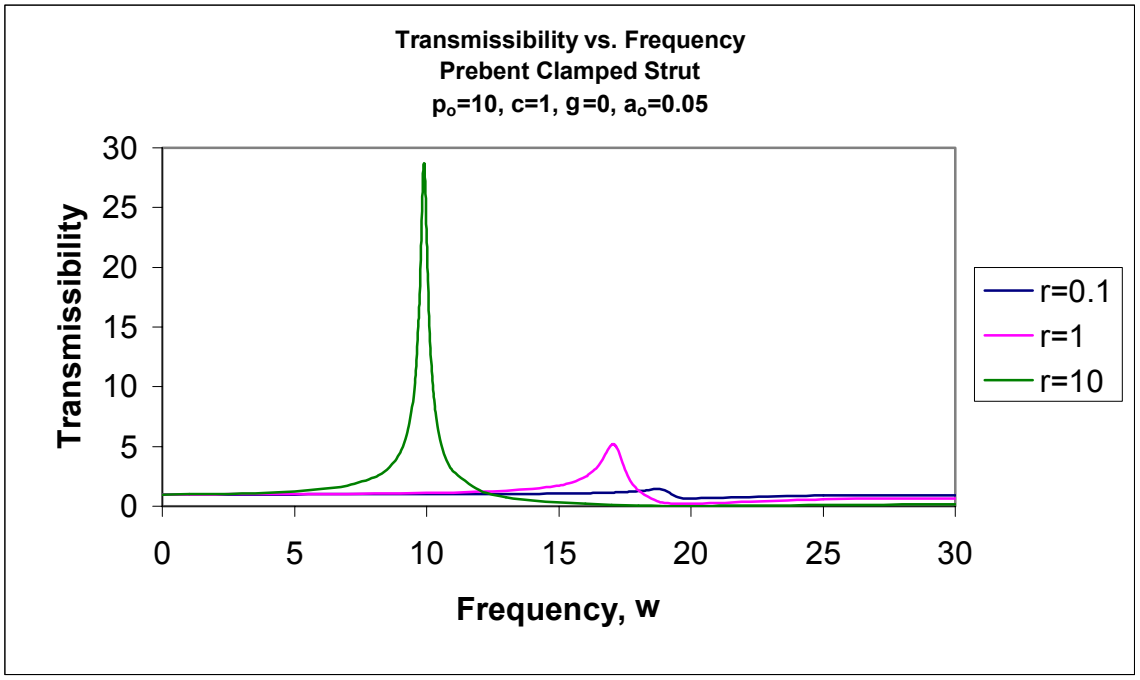

Figure D4.1: Transmissibility vs. Frequency for p_o=10, c=1, γ=0, a_o=0.05

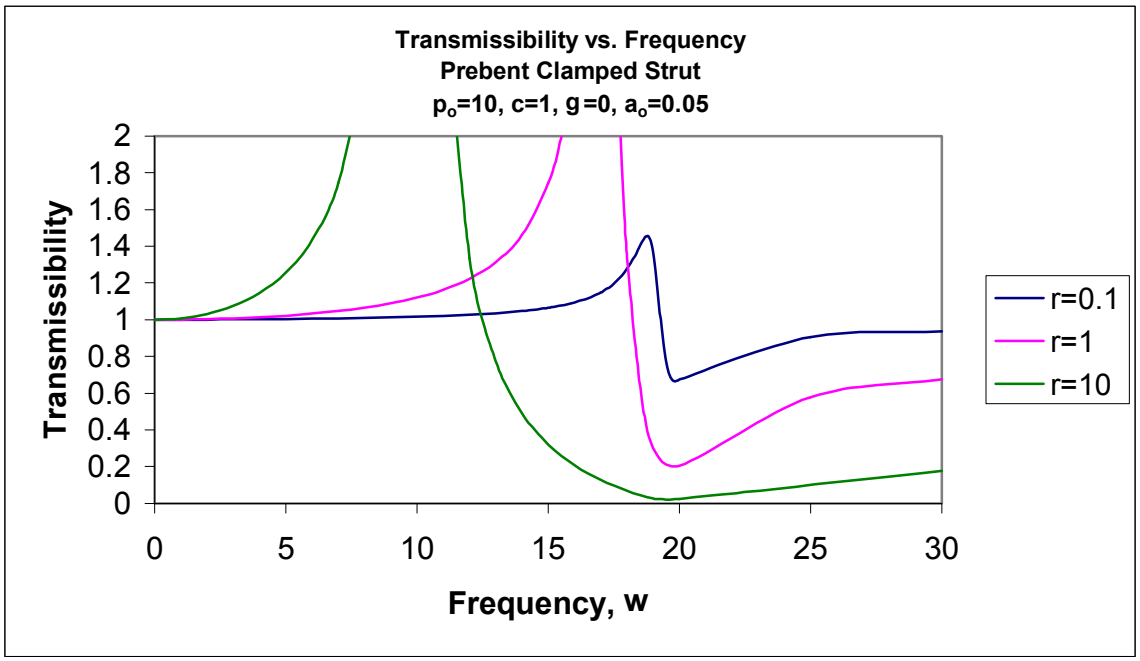

Figure D4.2: Transmissibility vs. Frequency for p_o=10, c=1, γ=0, a_o=0.05

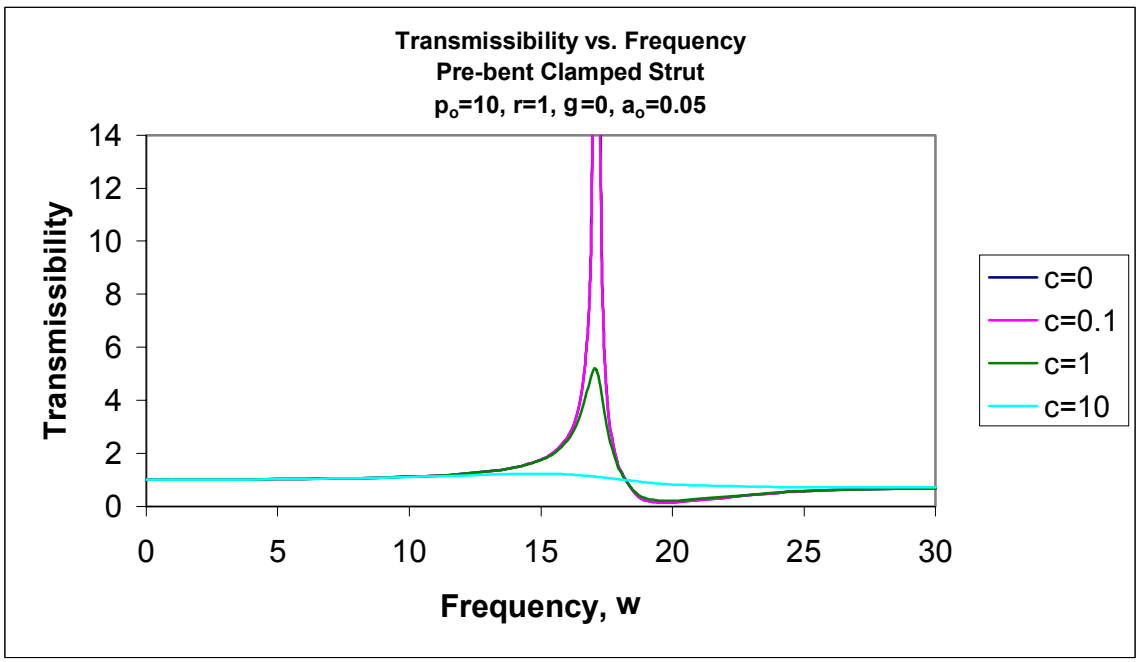

Figure D4.3: Transmissibility vs. Frequency for p_o=10, r=1, γ=0, a_o=0.05

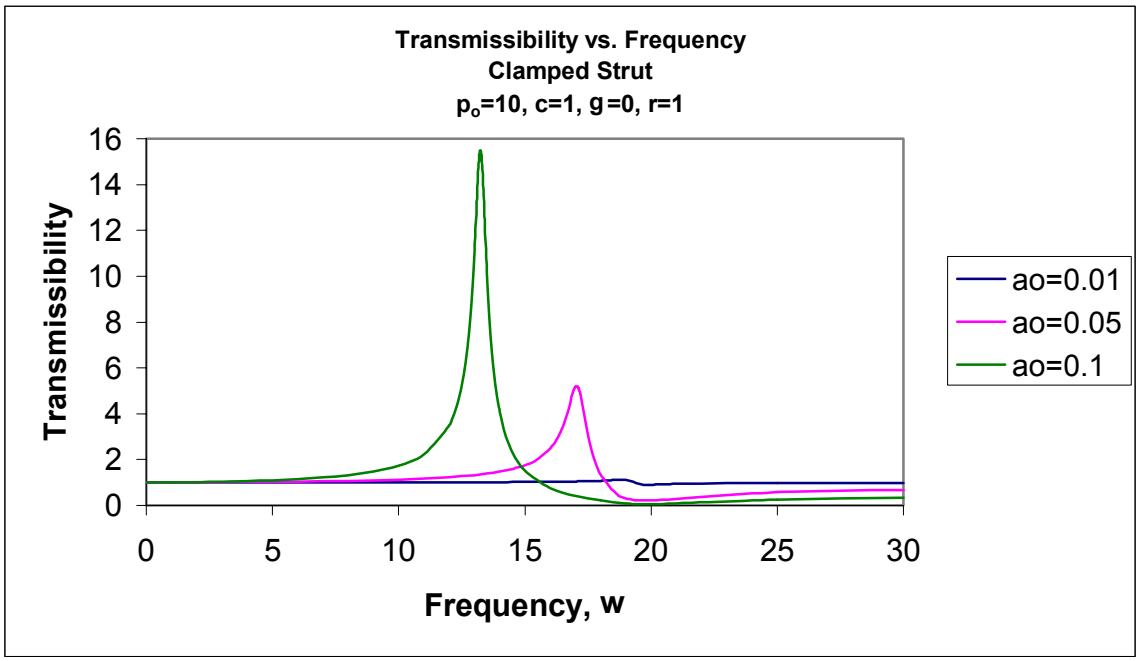

Figure D4.4: Transmissibility vs. Frequency for p_o=10, c=1, γ=0, r=1

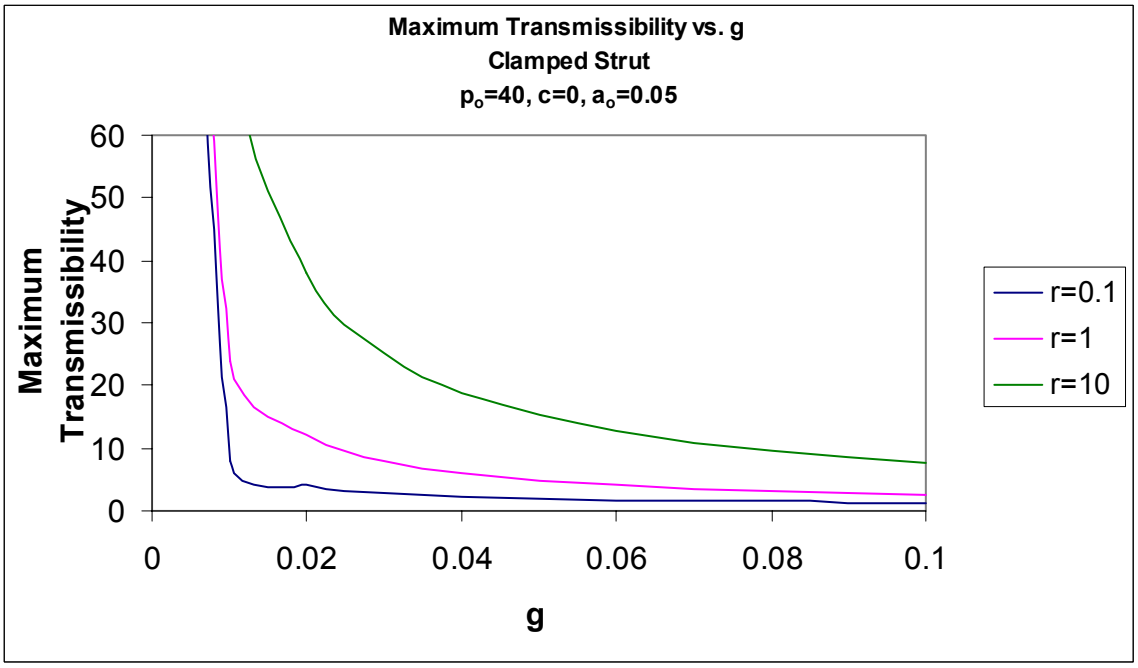

Figure D4.5: MaximumTransmissibility vs. γ for p_o=40, c=0, a_o=0.05

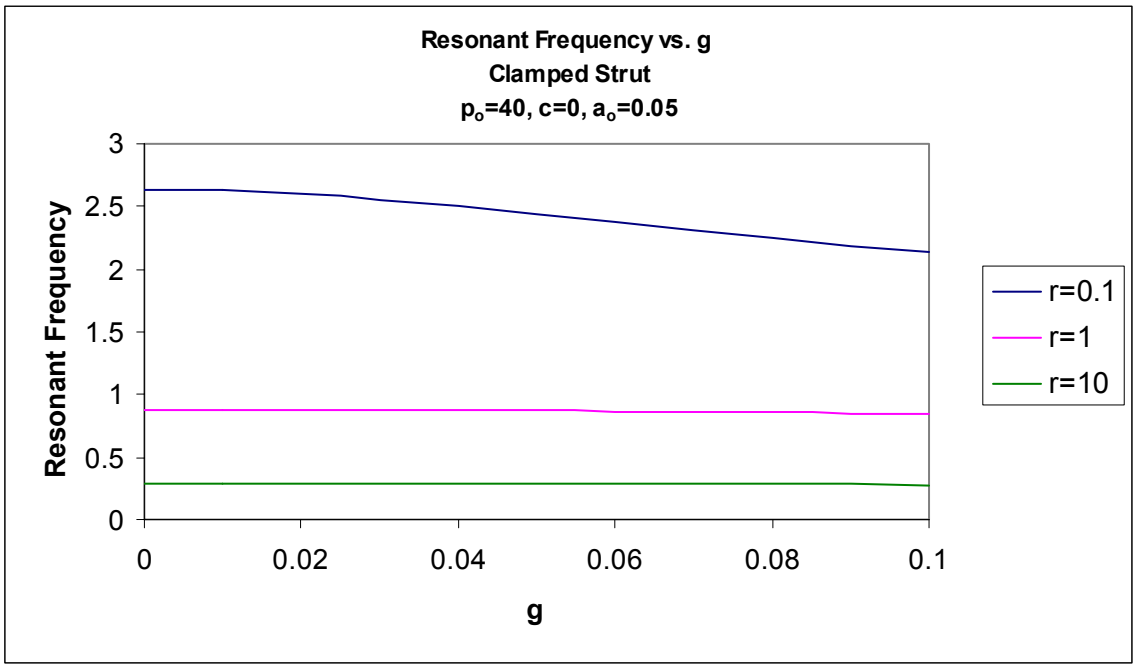

Figure D4.6: Resonant Frequency vs. γ for p_o=40, c=0, a_o=0.05

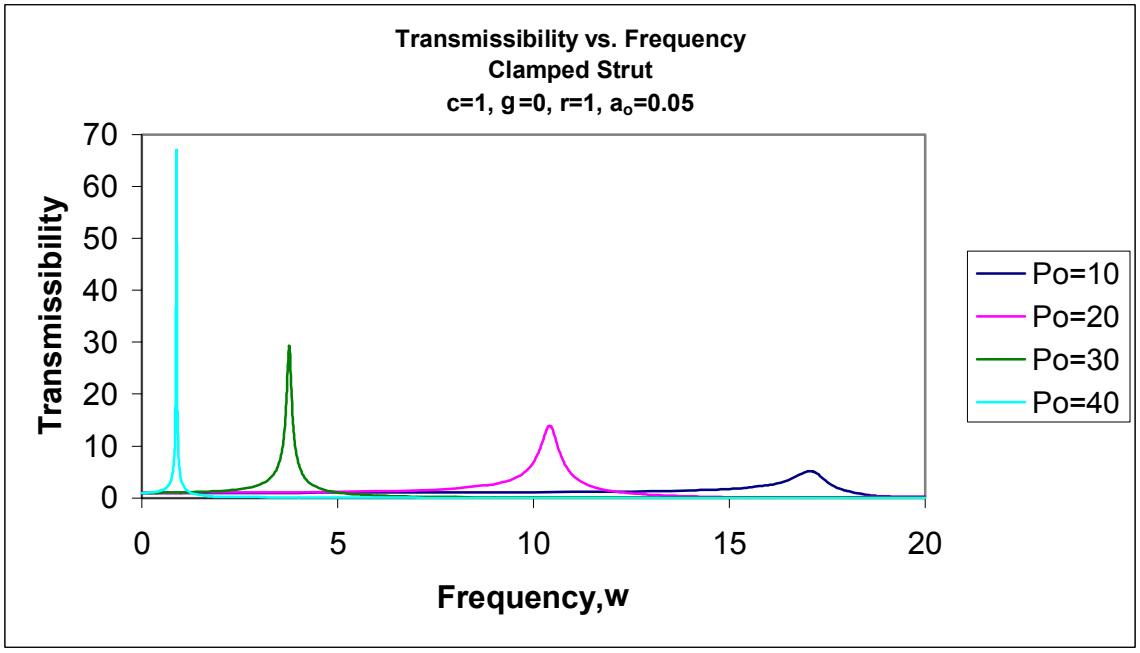

Figure D4.7: Transmissibility vs. Frequency for c=1, r=1, γ=0, a_o=0.05

Appendix E

E.1 Fixed-end Strut in Static Equilibrium

Mathematica Code

Input and Initial Guesses

```
(*Equilibrium, clamped buckled strut,y1=x,y2=y,y3=theta,y4=moment,
  includes shear force q which is not zero; m in leftBC is theta at s=0,
  p=po (larger than 39.48 = 4*pi^2)*)

Clear[pi,gm,gq,m,q,po]
pi = N[\[Pi]];

po = 40;
gm = 2.04;
gq = -0.00002;

Equations from equilibrium
de[y3_,y4_,q_]:={y1'[t]\[Equal]Cos[y3[t]],y2'[t]\[Equal]Sin[y3[t]],
   y3'[t]\[Equal]y4[t],y4'[t]\[Equal]-po*Sin[y3[t]]+q*Cos[y3[t]]}

Boundary conditions at s=0
leftBC[m_]:={y1[0]\[Equal]0,y2[0]\[Equal]0,y3[0]\[Equal]0,y4[0]\[Equal]m}

Numerical Solution
soln:=NDSolve[Flatten[Append[de[y3,y4,q],leftBC[m]]],{y1,y2,y3,y4},{t,0,1},
   MaxSteps\[Rule]2000]
endpt[m_,q_]:={y1[t],y2[t],y3[t],y4[t]}/.First[
        NDSolve[Flatten[Append[de[y3,y4,q],leftBC[m]]],{y1[t],y2[t],y3[t],
           y4[t]},{t,0,1},MaxSteps\[Rule]2000]]/.t\[Rule]1;
endpt[gm,gq]
\!\({0.9739042924518324`, \(-5.4737131136458815`*^-8\), \
\(-0.000029197552945157166`\), 2.039982711399395`}\)
Clear[m,q]

Solving for the moment and shear force
rts:=FindRoot[{endpt[m,q][[2]]\[Equal]0,
     endpt[m,q][[3]]\[Equal]0},{m,{gm,0.98*gm}},{q,{gq,0.98*gq}},
   AccuracyGoal\[Rule]8,MaxIterations\[Rule]1000]
endpt[m/.rts,q/.rts]
\!\({0.9739609773283532`, \(-1.5247386679445382`*^-14\),
   3.5765328536778025`*^-12, 2.0377877750502646`}\)
```

m=m/.rts
q=q/.rts
2.03781
-0.0000177529

Plotting strut
{yy1[t_],yy2[t_],yy3[t_],yy4[t_]}={y1[t],y2[t],y3[t],y4[t]}/.First[soln];
ParametricPlot[Evaluate[{yy1[t],yy2[t]}/.soln/.rts],{t,0,1},
  PlotRange\[Rule]All,AspectRatio\[Rule]Automatic,PlotPoints\[Rule]100]

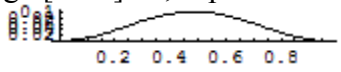

E.2 Fixed-end Strut; Dynamic Analysis for Two-frequency Axial Excitation

Input and Initial Guesses

```
(*Two-frequency forced small vibrations about buckled equilibrium;
  clamped strut; y1=xe,y2=ye,y3=theta_e,y4=me, y5=x1,y6=y1,y7=theta1,y8=m1,
  y9=p1,y10=q1,y11=x2,y12=y2,y13=theta2,y14=m2,y15=p2,y16=q2;
  given po and uo and frequency, and moment m from StrutEquilClamped,
  and q which is from StrutEquilClamped*)

Clear[pi,uo,po,m,c,\[Omega],q,gp1,gq1,gm1,gp2,gq2,gm2];
  pi = N[\[Pi]];
  i=(-1)^0.5;
  uo=0.011;
  po=40;
  m=2.0378050656886537`;
  q=0;

  \[Omega]=4;
  r=1;
  c=1;
  g=0;
  rf=2;
  ra=0.5;
  gp1=-29.211162010176693`+0.9102573207050219` \[ImaginaryI];
  gq1=-8.065008737265307`+0.16624126937603967` \[ImaginaryI];
  gm1=0.8421924069294446`\[InvisibleSpace]+0.0038278870395328387` \
\[ImaginaryI];
  gp2=-711.5914351986328`+635.2478911811554` \[ImaginaryI];
  gq2=-378.48784562081494`+348.4626974737764` \[ImaginaryI];
  gm2=34.581794936737644`\[InvisibleSpace]-31.911364193149826` \[ImaginaryI];
  \[Omega]1=\[Omega];
  \[Omega]2=rf*\[Omega];
```

```
Equations from equilibrium
de[y3_,y4_,y5_,y6_,y7_,y8_,y9_,y10_,y11_,y12_,y13_,y14_,y15_,
   y16_]:={y1'[t]\[Equal]Cos[y3[t]],y2'[t]\[Equal]Sin[y3[t]],
   y3'[t]\[Equal]y4[t],y4'[t]\[Equal]-po*Sin[y3[t]]+q*Cos[y3[t]],
   y5'[t]\[Equal]-y7[t]*Sin[y3[t]],y6'[t]\[Equal]y7[t]*Cos[y3[t]],
   y7'[t]\[Equal]y8[t]/(1+i*\[Omega]1*g),
   y8'[t]\[Equal](y10[t]-po*y7[t])*Cos[y3[t]]-(y9[t]+q*y7[t])*Sin[y3[t]],
   y9'[t]\[Equal](\[Omega]1^2-i*\[Omega]1*c)*y5[t],
   y10'[t]\[Equal](\[Omega]1^2-i*\[Omega]1*c)*y6[t],
   y11'[t]\[Equal] -y13[t]*Sin[y3[t]], y12'[t]\[Equal]y13[t]*Cos[y3[t]],
   y13'[t]\[Equal]y14[t]/(1+i*\[Omega]2*g),
   y14'[t]==(y16[t]-po*y13[t])*Cos[y3[t]]-(y15[t]+q*y13[t])*Sin[y3[t]],
   y15'[t]==(\[Omega]2^2-i*\[Omega]2*c)*y11[t],
   y16'[t]\[Equal](\[Omega]2^2-i*\[Omega]2*c)*y12[t]};

Boundary Conditions at s=0
leftBC[p1_,q1_,m1_, p2_, q2_, m2_]:={y1[0]\[Equal]0,y2[0]\[Equal]0,
    y3[0]\[Equal]0,y4[0]\[Equal]m,y5[0]\[Equal]uo,y6[0]\[Equal]0,
    y7[0]\[Equal]0,y8[0]\[Equal]m1,y9[0]\[Equal]p1,y10[0]\[Equal]q1,
    y11[0]\[Equal]ra*uo,y12[0]\[Equal]0,y13[0]\[Equal]0, y14[0]\[Equal]m2,
    y15[0]\[Equal]p2,y16[0]\[Equal]q2};

Numerical Solution
soln:=NDSolve[
    Flatten[Append[de[y3,y4,y5,y6,y7, y8, y9, y10,y11,y12,y13,y14,y15,y16],
       leftBC[p1,q1,m1, p2, q2,m2]]],{y1,y2,y3,y4,y5,y6,y7,y8,y9,y10,y11,
     y12,y13,y14,y15,y16},{t,0,1}, MaxSteps\[Rule]2000];
endpt[p1_,q1_,m1_,p2_,q2_,
    m2_]:={y1[t],y2[t],y3[t],y4[t],y5[t],y6[t],y7[t],y8[t],y9[t],y10[t],
       y11[t],y12[t],y13[t],y14[t], y15[t],y16[t]}/.First[
       NDSolve[Flatten[
          Append[de[y3,y4,y5,y6,y7,y8,y9,y10,y11,y12,y13,y14,y15,y16],
            leftBC[p1,q1,m1,p2,q2,m2]]],{y1[t],y2[t],y3[t],y4[t],y5[t],
          y6[t],y7[t],y8[t],y9[t],y10[t],y11[t],y12[t],y13[t],y14[t],
          y15[t],y16[t]},{t,0,1},MaxSteps\[Rule]1000]]/.t\[Rule]1;


Shooting for boundary conditions at s=1
endpt[gp1,gq1,gm1,gp2,gq2,gm2]
\!\({0.9739606504410063`,
   3.010822662906323`*^-9, \(-1.5785385346754582`*^-6\),
   2.0378049452557474`, \(-0.0390746730293957`\) +
     0.0007040075896852123`\ \[ImaginaryI], \(-0.1946828306626987`\) +
     0.0036359718946385247`\ \[ImaginaryI], \(-0.7622187241758941`\) +
     0.022688849952374 88`\ \[ImaginaryI], \(\(0.7996497172311896`\)\(\
\[InvisibleSpace]\)\) +
```

```
    0.014479021705833903`\ \[ImaginaryI], \(-29.23586785727498`\) +
    0.9176268797244804`\ \[ImaginaryI], \(-8.39120880748861`\) +
    0.252791292002893`\ \[ImaginaryI], \(-1.6284287818347645`\) +
    1.5003626001136239`\ \[ImaginaryI], \(-9.459607363252982`\) +
    8.787354386210538`\ \[ImaginaryI], \(-21.06740156289274`\) +
    19.550451508407033`\ \[ImaginaryI], \(\(21.262579490601045`\)\(\
\[InvisibleSpace]\)\) -
    15.914554658179743`\ \[ImaginaryI], \(-729.4358862587588`\) +
    656.4534480318142`\ \[ImaginaryI], \(-512.964578188737`\) +
    510.44427345827626`\ \[ImaginaryI]}\)
Clear[p1,q1,m1,p2,q2,m2]

Solving for endpoint solution
rts:=FindRoot[{endpt[p1,q1,m1,p2,q2,m2][[9]]\[Equal]-r*
       po*(\[Omega]1^2)*(endpt[p1,q1,m1,p2,q2,m2][[5]]),
    endpt[p1,q1,m1,p2,q2,m2][[6]]\[Equal]0,
    endpt[p1,q1,m1,p2,q2,m2][[7]]\[Equal]0,
    endpt[p1,q1,m1,p2,q2,m2][[15]]\[Equal]-r*
       po*(\[Omega]2^2)*(endpt[p1,q1,m1,p2,q2,m2][[11]]),
    endpt[p1,q1,m1,p2,q2,m2][[12]]\[Equal]0,
    endpt[p1,q1,m1,p2,q2,m2][[13]]\[Equal]0},{p1, {gp1,0.98*gp1}},{q1,{gq1,
      0.98*gq1}},{m1,{gm1,0.98*gm1}},{p2,{gp2,0.98*gp2}},{q2,{gq2,
      0.98*gq2}},{m2, {gm2,0.98*gm2}},AccuracyGoal\[Rule]3,
   MaxIterations\[Rule]2000]

endpt[p1/.rts,q1/.rts,m1/.rts,p2/.rts,q2/.rts,m2/.rts]
\!\({0.9739609586871885`,
   3.137542039221529`*^-7, \(-9.464783874699544`*^-7\),
   2.0377925155204943`, \(-8.990695948455368`*^-6\) -
    0.00008410896506263068`\ \[ImaginaryI], \(-6.899519244875681`*^-10\) -
    7.003398772401131`*^-12\ \[ImaginaryI],
   1.7092581627479858`*^-9 +
    3.382648513111064`*^-11\ \[ImaginaryI], \(\(0.44188334799399054`\)\(\
\[InvisibleSpace]\)\) +
    0.0016563118540822229`\ \[ImaginaryI], \(\(0.005753992662935137`\)\(\
\[InvisibleSpace]\)\) +
    0.05382974015533187`\ \[ImaginaryI], \(\(0.08164527992736582`\)\(\
\[InvisibleSpace]\)\) -
    0.0197508226961689 5`\ \[ImaginaryI], \(\(0.0001225053062939 4756`\)\(\
\[InvisibleSpace]\)\) -
    0.000020043666852226367`\ \[ImaginaryI], \(-3.3289199001872163`*^-10\) \
+ 2.5113437014311353`*^-12\ \[ImaginaryI],
   6.568083796479364`*^-10 +
    8.024124484037936`*^-11\ \[ImaginaryI], \(\(0.22602833428492153`\)\(\
\[InvisibleSpace]\)\) -
    0.0008796891598294524`\ \[ImaginaryI], \(-0.31361376683760683`\) +
```

```
    0.05131181101532038`\ \[ImaginaryI], \(\(0.1602140482114182`\)\(\
\[InvisibleSpace]\)\) - 0.019585055635103026`\ \[ImaginaryI]}\)

p1=p1/.rts
q1=q1/.rts
m1=m1/.rts
p2=p2/.rts
q2=q2/.rts
m2=m2/.rts
-0.0820331+0.0764995 \[ImaginaryI]
-0.0884601+0.021488 \[ImaginaryI]
0.440751\[InvisibleSpace]+0.00195344 \[ImaginaryI]
-0.493694+0.0745061 \[ImaginaryI]
-0.173691+0.0212347 \[ImaginaryI]
0.223609\[InvisibleSpace]-0.000551747 \[ImaginaryI]
{yy1[t_],yy2[t_],yy3[t_],yy4[t_],yy5[t_],yy6[t_],yy7[t_],yy8[t_],yy9[t_],
    yy10[t_],yy11[t_],yy12[t_],yy13[t_],yy14[t_],yy15[t_],
    yy16[t_]}={y1[t],y2[t],y3[t],y4[t],y5[t],y6[t],y7[t],y8[t],y9[t],y10[t],
      y11[t],y12[t],y13[t],y14[t],y15[t],y16[t]}/.First[soln];
Solving for the Transmissibility

Um1=Abs[uo*Cos[\[Omega]1*time]+ra*uo*Cos[\[Omega]2*time]];
R1=Abs[Re[yy5[1]]*Cos[\[Omega]1*time]+Re[yy11[1]]*Sin[\[Omega]2*time]-
      Im[yy5[1]]*Sin[\[Omega]1*time]-Im[yy11[1]]*Sin[\[Omega]2*time]];

numbers1=Table[
    Evaluate[Um1],{time,0,
      5000*(2*Pi)/(100*\[Omega]2),(2*Pi)/(100*\[Omega]2)}];
numbers2=Table[
    Evaluate[R1],{time,0,
      5000*(2*Pi)/(100*\[Omega]2),(2*Pi)/(100*\[Omega]2)}];
A1=(numbers2)^2;
B1=(numbers1)^2;

A=((1/Length[numbers2])*(Apply[Plus,A1]))^.5;
B=((1/Length[numbers1])*(Apply[Plus,B1]))^.5;
TR=A/B
0.0134731
```

Vita

Jenny Elizabeth Sidbury was born on December 11, 1979 in Pensacola, FL. She lived in Pensacola until the age of 12 when her family relocated to Coral Springs, FL. At the age of 15, Jenny moved again to Sarasota, FL where she graduated from Riverview High School in 1998. After graduation, Jenny commenced her studies at the University of Florida in the fall of 1998. She earned a Bachelor of Science degree in Civil Engineering when she graduated with honors in May of 2002. She was awarded her Engineering-In-Training certification in the state of Florida shortly after graduation. In August of 2002, Jenny began her graduate education at Virginia Polytechnic Institute and State University. She completed her Master of Science degree in the Structural Engineering and Materials program area of the Charles E. Via, Jr. Department of Civil and Environmental Engineering in December 2003.